



The
University
Of
Sheffield.

Modelling and optimisation of decentralised hybrid solar biogas system to power an organic Rankine cycle (ORC-Toluene) and air gap membrane distillation (AGMD) for desalination and electric power generation

Ismail AL-Arifi

*A thesis submitted in fulfilment of the requirements for the degree of
Doctor of Philosophy*

The University of Sheffield
Faculty of Engineering
Department of Mechanical Engineering
Energy 2050

September, 2022

DECLARATIONS

The candidate confirms that the work submitted is his own and that appropriate credit has been given where reference has been made to the work of others.

This copy has been supplied on the understanding that it is copyright material and that no quotation from the thesis may be published without proper acknowledgement.

©2021 The University of Sheffield

ACKNOWLEDGMENT

First of all, I would like to thank Almighty Allah for giving me the courage, determination, and guidance in conducting this research work successfully. I am immensely thankful to God for keeping me and my family in good health all through this period particularly, in the pandemic and for the deep insights and wisdom that sustained this research work.

I am extremely grateful to my supervisors; Professors Mohamed Pourkashanian, Derek Ingham and Lin Ma, and Dr. Kevin Hughes for their invaluable contributions, support, and guidance that were pivotal to the accomplishment of my Ph.D. In addition, I would like to thank Dr. Davide and Dr. Stavros for their support with several aspects of the modelling and documentation of the research and for providing very useful ideas and comments that helped in improving this work.

I am particularly, grateful to all my colleagues and brilliant friends in the Energy 2050 research group and in the department of Mechanical Engineering. Special thanks to my colleagues in the Energy Systems research group, Dr. Oscar, Dr. Godfrey, Dr. Ali, Dr. Bashar, Celal, Mohammed and all the newcomers, for the helpful feedback and informative presentations during the weekly meetings.

Furthermore, this research work would not have been possible without the valuable financial support provided by the Oman Ministry of Higher Education, Research & Education. Moreover, I would like to thank Oman Rural Areas Electricity Company and Solargis™ for providing the required data to this study for the inclusion in my PhD research work.

Finally, I would like to give special thanks to my lovely family, parents, beautiful wife and kids for their prayers, constant care and encouragement and moral support throughout my study. I could not have done my PhD without their unconditional support and love.

PUBLICATIONS FROM THIS THESIS

Publications in scientific journals

Chapter 3 contains the following publication:

B. Shboul, I. AL-Arfi, S. Michailos, D. Ingham, L. Ma, K.J. Hughes, and M. Pourkashanian, "A new ANN model for hourly solar radiation and wind speed prediction: A case study over the north & south of the Arabian Peninsula," *Sustainable Energy Technologies and Assessments*, vol. 46, Aug. 2021, doi: 10.1016/j.seta.2021.101248.

Chapter 4 contains the following publication:

I. AL-Arfi, B. Shboul, D. Poggio, D. Ingham, L. Ma, K. Hughes, and M. Pourkashanian, "Thermo-economic and design analysis of a solar thermal power combined with anaerobic biogas for the air gap membrane distillation process," *Energy Conversion and Management*, vol. 257, p. 115407, Oct. 2022, doi: 10.1016/j.enconman.2022.115407.

Publication in peer reviewed conference paper

Chapter 5 contains the following publication:

I. AL-Arfi, B. Shboul, S. Michailos, M. Alfaiakawi, GT Udeh, D. Ingham, L. Ma, K.J. Hughes, and M. Pourkashanian, *Multi-objective optimal sizing of a hybrid concentrated solar power-biogas for desalination and power generation*. The 14th International Conference on Applied Energy - ICAE2022, Aug. 8-11, 2022, Bochum, Germany.

ABSTRACT

The intensive use of fossil fuels to meet the world energy and water demand has caused several environmental issues, such as global warming, air pollution and ozone depletion. Therefore, the integration of stand-alone decentralised hybrid renewable energy systems is a promising solution to satisfy the global energy-water demands and minimize the effects of fossil fuels utilisation. Among these hybrid technologies, concentrated solar power (CSP) combined with waste-based biogas to power organic Rankine cycle for cogeneration provide the means to generate dispatchable, reliable, renewable electricity and water in high direct normal incidence (DNI) regions around the world. Due to the strong inverse correlation between DNI resources and freshwater availability, most of the best potential CSP regions also lack sufficient freshwater resources.

The current study proposes and applies a novel multi-dimensional modelling technique based on artificial neural networks (ANN) for hourly solar radiation and wind speed data forecasting over six locations in Oman. The developed model is the first attempt to integrate two ANN models simultaneously by using enormous meteorological data points for both solar radiation and wind speed prediction. The developed model requires only three parameters as inputs, and it can predict solar radiation and wind speed data simultaneously with high accuracy. As a result, the model provides a user-friendly interface that can be utilised in the energy systems design process. Consequently, this model facilitates the implementation of renewable energy technologies in remote areas in which gathering of weather data is challenging. Meanwhile, the accuracy of the model has been tested by calculating the mean absolute percentage error (*MAPE*) and the correlation coefficient (*R*). Therefore, the model developed in this study can provide accurate weather data and inform decision makers for future instalments of energy systems.

Furthermore, a novel proposed hybrid solar and biogas system for desalination and electric power generation using advanced modelling techniques to integrate the stand-alone off-grid system has been designed. The novelty emerges from some facts, which are centralised around the use of a hybrid electric generation via Concentrated Solar Power (CSP) and anaerobic digestion biogas to achieve higher stability and profitability. Meanwhile, the cogeneration through the waste heat of the ORC drives the AGMD, which benefits as well from the higher stability due to hybridisation. In addition, an innovative and user-friendly modelling approach has been applied, and this efficiently integrates the individual energy components, i.e. PTC, anaerobic biogas boiler, ORC and AGMD, which fosters the optimisation of the proposed system. The models have been developed in the

MATLAB/Simulink® software and have been used to investigate the system area, dimensions, and cost and to ensure that the electrical and water demand of the end-user are met. In addition, a new detailed thermo-economic assessment of the proposed hybrid solar biogas for cogeneration in off-grid applications has been investigated. An energy, exergy, and cost analysis has been performed and to fully utilise this, a sensitivity assessment on the developed model has been analysed to examine the effects of various design parameters on the thermo-economic performance. Finally, implementing an in-depth simulation testing of the system in a rural region in Oman is presented. The novel integrated solar and biogas system that has been designed through advanced modelling in the MATLAB/ Simulink® is integrated with a robust multi-objective optimisation technique to determine the best operating configuration. Three objective functions namely, maximising power and water production, and minimising the unit exergy product costs have been formulated. The turbine efficiency, top ORC vapor temperature and ORC condenser temperature has been selected as the decision variables. The non-dominated sorting genetic algorithm (NSGA-II) has been employed to solve the optimisation problem and produce a Pareto frontier of the optimal solutions. Further, the TOPSIS approach has been used to select the optimal solution from the Pareto set. The study constitutes the first attempt to holistically optimise such a hybrid off-grid cogeneration system in a robust manner.

TABLE OF CONTENTS

DECLARATIONS	ii
ACKNOWLEDGMENT	iii
PUBLICATIONS FROM THIS THESIS	iv
ABSTRACT	v
TABLE OF CONTENTS	vii
LIST OF FIGURES	xi
LIST OF TABLES	xiv
NOMENCLATURE	xvi
1. CHAPTER 1: INTRODUCTION	1
1.1 Energy crisis and water scarcity	1
1.2 Solar energy	3
1.3 Stand-alone solar energy	5
1.4 Hybrid solar energy technologies	6
1.4.1 Hybrid solar energy technologies with conventional sources.....	6
1.4.2 Hybrid solar energy technologies with non-conventional sources.....	7
1.5 Modelling method using artificial neural networks.....	9
1.6 Thesis Outline.....	10
1.6.1 Research proposal	10
1.6.2 Contribution of the Thesis	10
1.6.3 Structure of the Thesis.....	11
2. CHAPTER 2: LITERATURE REVIEW	13

2.1	Overview of CSP technologies	13
2.1.1	Parabolic trough collectors.....	16
2.1.2	Parabolic dish systems.....	16
2.1.3	Linear Fresnel reflectors unit.....	17
2.1.4	Solar thermal power towers.....	17
2.1.5	Comparison of CSP technologies	18
2.1.6	Economics of the CSP technologies.....	19
2.2	Waste-based biogas production	21
2.2.1	Anaerobic digestion technology	22
2.2.2	Hybrid CSP biogas plant.....	22
2.3	CSP-desalination technologies.....	24
2.3.1	Low energy desalination technologies	25
2.4	The ORC technology.....	28
2.4.1	Introduction to the ORC	28
2.4.2	Thermodynamics of the ORC.....	29
2.4.3	Comparison between ORCs and steam Rankine cycles.....	31
2.4.4	Organic fluids	32
2.4.5	Working fluids categories and selection criteria	34
2.4.6	Specific cost of an ORC system	38
2.5	Design integration of CSP-biogas for desalination and cogeneration.....	39
2.6	Design of ANN solar/wind prediction model.....	44
2.7	Optimisation methods for hybrid renewable energy systems	44
2.7.1	Classical methods.....	45
2.7.2	Artificial methods.....	45
2.7.3	Hybrid methods	45

2.7.4	Comparison between optimisation methods.....	46
2.8	Conclusion based on the literature review.....	47
3.	CHAPTER 3: HOURLY SOLAR RADIATION AND WIND SPEED PREDICTION MODEL USING ANN	50
3.1	Introduction	50
3.2	Locations of the study.....	53
3.3	Methodology.....	55
3.3.1	Meteorological data collection.....	56
3.3.2	The developed ANN prediction model	57
3.3.3	The Statistical Indicators.....	62
3.4	Results and Discussions.....	62
3.5	Conclusion of the chapter	77
4.	CHAPTER 4: THERMO-ECONOMIC AND DESIGN ANALYSIS OF THE HYBRID SOLAR BIOGAS SYSTEM FOR COGENERATION APPLICATION.....	78
4.1	Introduction	78
4.2	The Proposed System & Process Description	82
4.3	Mathematical Modelling, Simulation and Assumptions.....	84
4.3.1	The simulation model & assumptions	84
4.3.2	The Mathematical Model	87
4.3.3	The cost considerations	96
4.4	Results and Discussions.....	98
4.4.1	Mathematical model validation.....	98
4.4.2	Membrane distillation operating conditions.....	100
4.4.3	Solar/Biogas operating conditions.....	104
4.4.4	ORC operating conditions	106
4.4.5	Data results of the optimised hybrid cogeneration system	108

4.5	Design results under the real time mode: Case study	113
4.6	Conclusion of the chapter	116
5.	CHAPTER 5: MULTI-OBJECTIVE OPTIMAL SIZING OF A HYBRID CONCENTRATED SOLAR POWER-BIOGAS FOR DESALINATION AND POWER GENERATION.....	118
5.1	Introduction	118
5.2	Methodology and Procedure	124
5.2.1	Multi-objective optimisation	124
5.2.2	Decision making procedure	127
5.3	Results and Discussion	129
5.4	Conclusion of the chapter	136
6.	CHAPTER 6: CONCLUSIONS AND RECOMMENDATIONS FOR FUTURE WORK.....	137
6.1	Conclusion.....	137
6.2	Recommendations for future work	141
	REFERENCE.....	143

LIST OF FIGURES

Figure 1-1: Physical and economic water scarcity [6].....	2
Figure 1-2: Types of solar energy selected based on their availability in the global market [293]....	4
Figure 1-3: Configuration of general solar energy technologies [23].....	6
Figure 1-4: Concept of the CSP technology [25].....	6
Figure 2-1: The CSP main components [41].....	14
Figure 2-2: Main CSP technologies: (a) PTC; (b) LFR; (c) SPT; (d) PDS [42].....	14
Figure 2-3: Schematic diagram of the CSP technologies and their installed share [48].....	15
Figure 2-4: The PTC main parts and receiver details [49].....	16
Figure 2-5: The PDS main components [49].	16
Figure 2-6: The LFR main components [49].	17
Figure 2-7: The SPT main parts [49]	17
Figure 2-8: Impact of the DNI level of the location on the CSP LCOE [49]	19
Figure 2-9: Cost comparison between solar thermal energy against other energy sources [49].	20
Figure 2-10: Biogas plant schematic view [58].	21
Figure 2-11: Photographs of the hybrid CSP/Biogas plant in Spain [64].	23
Figure 2-12: Possible integrations of the RE with different desalination technologies [71].....	24
Figure 2-13: Schematic of the AD major components , illustrating the chilled and the potable water production using the available solar energy [84].....	26
Figure 2-14: Schematic of the working principle of the MD [91].	27
Figure 2-15: Schematic of the configuration of the basic ORC technology [15].....	29
Figure 2-16: T-s diagram of a typical ORC unit.	30
Figure 2-17: A possible working fluids integration with a different heat temperature source.	33
Figure 2-18: The slope diagram of the working fluid classifications: (a) isentropic, (b) wet and (c) dry.	34
Figure 2-19: Typical machine and installation costs of the ORC technology (€ per kW) [128].	38
Figure 2-20: Hybrid PTC-biomass system for cogeneration heat and power [129].	40
Figure 2-21: The integration of the stand-alone PTC-ORC-RO for water desalination.	42
Figure 2-22: Types of the optimisation methods used for hybrid renewable energy systems.....	44
Figure 3-1: Forecast locations map of Oman.....	54
Figure 3-2: A typical feed-forward artificial neural network.	57

Figure 3-3: The architecture structure of the developed FBANN-1 solar/wind prediction model. ..	58
Figure 3-4: The architecture structure of the developed FBANN-2 solar/wind prediction model. ..	59
Figure 3-5: Simulink diagram of the developed ANN model.	60
Figure 3-6: The nftool implementation steps in MATLAB/Simulink®.	61
Figure 3-7: Regression plot of training, validation, testing, and all for FBANN-1 at Al khuwaimah..	64
Figure 3-8: Regression plot of training, validation, testing, and all for FBANN-1 at Al Halaniyat.	64
Figure 3-9: Regression plot of training, validation, testing, and all for FBANN-1 at Al Mazyounah.	65
Figure 3-10: Regression plot of training, validation, testing, and all for FBANN-1 at Haitam.....	65
Figure 3-11: Regression plot of training, validation, testing, and all for FBANN-1 at Madha.	66
Figure 3-12: Regression plot of training, validation, testing, and all for FBANN-1 at Methane.....	66
Figure 3-13: Regression plot of training, validation, testing, and all for FBANN-2 at Al khuwaimah.	67
Figure 3-14: Regression plot of the training, validation, testing, and all for FBANN-2 at Al Halaniyat.	68
Figure 3-15: Regression plot of the training, validation, testing, and all for FBANN-2 at Al Mazyounah.	68
Figure 3-16: Regression plot of the training, validation, testing, and all for FBANN-2 at Haitam. ...	69
Figure 3-17: Regression plot of the training, validation, testing, and all for FBANN-2 at Madha.....	69
Figure 3-18: Regression plot of the training, validation, testing, and all for FBANN-2 at Methane.	70
Figure 3-19: Data signal entry for one year in the ANN model, which represents (a) days, (b) current time, and (c) month.	71
Figure 3-20: Hourly profile of GHI in Oman.	73
Figure 3-21: Hourly profile of DNI in Oman.	73
Figure 3-22: Hourly profile of the wind speed in Oman.	74
Figure 3-23: The MAPE for all selected locations regarding the GHI.....	76
Figure 3-24: The MAPE for all selected locations regarding the wind speed.	76
Figure 4-1: A schematic diagram of the proposed system.	83
Figure 4-2: The developed model browser in the MATLAB/Simulink® toolbox environment.	86
Figure 4-3: The stepwise procedures of the developed model in the MATLAB/Simulink®.	86
Figure 4-4: Comparison of the addressed types of MD related to the exergy destruction rate, kW, SPC, kWh/m ³ , and GOR parameters.	101
Figure 4-5: Data comparisons for all MD types related to the permeate flux and membrane area.	

.....	102
Figure 4-6 :Data comparison between the MD types related to the hourly costs.	102
Figure 4-7: Data results for the E-PH membrane distillation type based on the cold side temperature and productivity.....	103
Figure 4-8: Anaerobic digestion results based on the variations in the collection volume and retention time.....	105
Figure 4-9: PTC results based on the variations of the power generation and productivity.	105
Figure 4-10: (a) Toluene positive slope behavior regarding the T-S, and (b) T-H.....	106
Figure 4-11: The variation in the outlet turbine temperature, recuperator temperature and the ORC efficiencies based on the top vapor temperature and condenser temperature.	108
Figure 4-12: The Solar (PTC) ORC operating conditions on the T–S diagram.	109
Figure 4-13: Load and productivity fluctuations over one year (8760 epochs).	113
Figure 4-14: Data results of the proposed system over one year under a real time approach.	114
Figure 4-15: Daily data results related to a typical day in summertime (Al Khuwaimah rural region, Oman).	115
Figure 5-1: NSGA II algorithm flowchart.	126
Figure 5-2: Effects of the top vapor temperature and condenser temperature on the system cycle performance.	130
Figure 5-3: Effects of the top vapor temperature and condenser temperature on the AGMD permeate flux at different turbine efficiency.....	131
Figure 5-4:Pareto front for multi-objective optimisation result using TOPSIS with matrix judgment (A).....	132
Figure 5-5: Pareto front for multi-objective optimisation result using TOPSIS with matrix judgment (B).....	133
Figure 5-6: Pareto front for multi-objective optimisation result using TOPSIS with matrix judgment (C).....	134
Figure 5-7: Values of criteria A, B and C obtained by TOPSIS for the proposed system.	135

LIST OF TABLES

Table 1.1: Comparison between stand-alone renewable and conventional energy systems [35].	8
Table 2.1: A summary of the significant features of the main CSP technologies [1], [48].	18
Table 2.2: A review summary of the integration of hybrid solar-biomass ORC systems.	41
Table 2.3: Studies that deals with the integration of PTC-ORC for desalination and cogeneration.	43
Table 2.4: A summary of the artificial methods that used to size the hybrid energy systems.	46
Table 2.5: A summary of the disadvantages and advantages of each optimisation method.	47
Table 3.1: The geographical and meteorological information of the Omani’s locations [208], [209]	54
Table 3.2: Types of input meteorological parameters.....	55
Table 3.3: Characteristics of the database.....	56
Table 3.4: Geographical coordinates of the selected stations.	56
Table 3.5: Data validation results of the developed model.....	70
Table 3.6: Lowest and highest hourly average wind speed values of the selected stations.....	74
Table 3.7: Calculated annual average MAPE, % values.	75
Table 4.1: The main specifications of the PTC/LS-3 type [140], [234].	87
Table 4.2: IC and O&M costs for the solar organic Rankine cycle components.	97
Table 4.3: Design specifications of the 100 kW Solar ORC system [140].	98
Table 4.4: Data validation results of the Solar ORC model.....	99
Table 4.5: AGMD module properties and specifications [253].....	99
Table 4.6: Data validation results of the AGMD model.	100
Table 4.7: Data results of the air gap membrane distillation based on different membrane types.	101
Table 4.8: Data streams of the optimised proposed hybrid system.....	109
Table 4.9: Data results of the proposed system based on the optimised design indicators.	110
Table 5.1: Benefits and limitations of MCDM methods.	122
Table 5.2: Considered design variables and range of variations for the optimisation.....	125
Table 5.3: Specification of the GA operator.	125
Table 5.4: Decision matrix (A) for the TOPSIS analysis.	128
Table 5.5: Decision matrix (B) for the TOPSIS analysis.	128
Table 5.6: Decision matrix (C) for the TOPSIS analysis.	128

Table 5.7: Table 5.6: Decision matrix (C) for the TOPSIS analysis.....	128
Table 5.8: Values of decision variables using matrix judgment (A) for the hybrid concentrated solar power-biogas system.....	132
Table 5.9: Values of decision variables using matrix judgment (B) for the hybrid concentrated solar power-biogas system.....	133
Table 5.10: Values of decision variables using matrix judgment (C) for the hybrid concentrated solar power-biogas system.....	134

NOMENCLATURE

Acronyms:

ABGD	Anaerobic biogas digestion
AD	Anaerobic digester
AGMD	Air gap membrane distillation
ANN	Artificial neural networks
ANFIS	Adaptive neuro-fuzzy inference system
ARD	Automatic relevance determination
BP	Back-propagation
CNT	Carbon nanotubes
CSP	Concentrated solar power
CHP	Combined heat and power
CCHP	Combined cooling, heating and power
CFCs	Chlorofluorocarbons
DNI	Direct normal incidence
DCMD	Direct contact membrane distillation
DIF	diffuse horizontal irradiance
NNARX	Elman neural network, network auto-regressive
FBANN	Feed-forward back-propagation
FANN	Feed-forward artificial neural network
GA	Genetic algorithm
GSR	Global solar radiation
GWP	Global warming potential
GHG	Greenhouse gases
HTO	Heat transfer oil
HCs	Hydrocarbons
HFCs	Hydrofluorocarbons
HFOs	Hydrofluoroolefins
HCFCs	Hydrochlorofluorocarbons
IEA	International Energy Agency
LFR	linear Fresnel reflector

LM	Levenberg-Marquardt
LLR	Local Linear Regression
MAPE	Mean absolute percentage error
MCDM	Multi-criteria decision making
MD	Membrane distillation
MED	Multi-effect distillation
MENA	Middle East and North Africa
MSF	Multi-stage flash
NSGA-II	Non-dominated sorting genetic algorithm
ORC	Organic Rankine cycle
ODP	Ozone depletion potential
OMTS	Octamethyltrisiloxane
PV	Photovoltaic
PE	Polyethylene
PP	Polypropylene
PTC	Parabolic trough collector
PDS	Parabolic dish systems
PTFE	Hydrophobic polytetrafluoroethylene
PVDF	Polyvinylidene fluoride
PSO	Particle swarm optimisation
RE	Renewable energy
RES	Renewable energy system
R & D	Research and Development
RO	Reverse osmosis desalination
RMLP	Recurrent multilayer perception
SPT	Solar power tower
STE	Non-dispatchable solar thermal energy
SGMD	Sweeping gas membrane distillation
TOPSIS	Technique for order preferences by similarity to the ideal solution
TES	Thermal energy storage
WD	Wind direction
WT	Wind turbine

Symbols:

<i>ACC</i>	Annualised capital costs, \$/y
<i>A</i>	Cross-sectional area, m ²
<i>A_f</i>	Amortisation factor, 1/y
<i>C_i</i>	Concentration, g/L
<i>C_f</i>	Concentration factor
<i>CF</i>	Cost of biofuel, \$/m ³
<i>C_p</i>	Specific heat capacity, kJ/kg.K
<i>CV</i>	Calorific value, kJ/kg
<i>CO₂</i>	Carbon Dioxide
<i>C_w</i>	Overall mass transfer coefficient, m/s
<i>D</i>	Diameter, m
<i>DCC</i>	Direct capital cost, \$
<i>DL</i>	Digester loading, kg/m ³ /day
<i>D_{memb}</i>	Membrane thickness, m
<i>DNI</i>	Direct normal irradiation, W/m ²
<i>Ex</i>	Exergy rate, kW
<i>GR</i>	Gain ratio
<i>H</i>	Specific enthalpy, kJ/kg
<i>H_{fg}</i>	Latent heat of vaporization, kJ/kg
<i>I</i>	Exergy destruction rate, kW
<i>IC</i>	Investment costs, \$
<i>ICC</i>	Indirect capital costs, \$
<i>I_s</i>	Solar radiation, kW/m ²
<i>J_p</i>	The permeate flux, kg/m ² h
<i>K_m</i>	Mass transfer coefficient, kJ/m.s.K
<i>K</i>	Thermal conductivity, kW/m.K
<i>L</i>	Latent heat of vaporisation, kJ/kg, or length, m
<i>LEP</i>	Liquid entry pressure, kPa
<i>LF</i>	load factor
<i>LMTD</i>	Logarithmic mean temperature difference, K
<i>LCOE</i>	Levelised cost of energy, \$

\dot{m}	Mass flow rate, kg/s
M_b	Brine flow rate, kg/s
M_f	Feed flow rate, kg/s
M_p	Distillate product flow rate, kg/s
M_w	Molecular weight, kg/mol
N	Number
NOP	Number of pores
$O\&M$	Operating and maintenance costs, \$
ODM	organic dry matter, %
OH	Operating hour
P	Pressure, bar
$PDva$	Water-air diffusion coefficient
PR	Performance ratio
Pr	Pressure ratio
Q	Thermal power, kW, or influent in biogas, kg
R	Specific gas constant, J/mol.K
R	The correlation coefficient
r_{memb}	Membrane pore size, m
RT	Retention time, days
S	Salinity ratio
S	Specific entropy, kJ/kg.K
SC	Solid's concentrations, %
SCC	Specific capital cost, \$/m ³
SFC	Specific fuel consumption, kg/kWh
SPC	Specific power consumption, kWh/m ³
SR	Salt rejection, %
T	Temperature, °C
TAC	Total annual costs, \$/y
TCC	Total capital costs, \$
TD	Total discharge, kg
TS	Total solids, kg
TSC	Total solid concentration contents, %

T_{sun}	Sun temperature, °C
TWP	Total water price (whole system), \$/m ³
U	Overall heat transfer coefficient, kW/m ² .K
V	Velocity, m/s
V_{col}	Collection volume in biogas plant, m ³
V_{gd}	Working volume of the gas digestion, m ³
V_{sl}	Sludge layer volume, m ³
V_t	Total volume, m ³
W	Power, kW or width, m
WR	Water recovery ratio
Z	Hourly cost, \$/h

Greek symbols:

ε	Effectiveness, %, or membrane porosity
η	Efficiency, %
ρ	Density, kg/m ³
τ	Membrane tortuosity
Θ	Intrinsic advancing contact angle, degrees
γ_w	Water surface tension, kN/m
β	Number of particles
δ	Relative viscosity

Subscripts:

A	Air
Amb	Ambient
B	Brine
Bg	Biogas
C	Cold side through heat exchanger or condenser
C_i	Inlet collector state
C_o	Outlet collector state
Col	Solar collector
$Cond$	Condenser unit
Cw	Cooling water
D	Distillate

<i>Env</i>	Envelope related to PTC
<i>Ev</i>	Evaporator unit
<i>ex, exh</i>	Exergy, exhaust
<i>F</i>	Feed
<i>G</i>	Generator
<i>H</i>	Hot side through heat exchanger or condenser
<i>I</i>	Inlet stream or solute species
<i>LMTD</i>	Logarithmic mean temperature difference
<i>M</i>	Mean or mechanical
<i>Memb</i>	Membrane
<i>O</i>	Out
<i>Oil</i>	Oil stream
<i>Orc</i>	Organic Rankine cycle
<i>P</i>	Pump, product
<i>R</i>	Recycle stream
<i>Rec</i>	Recuperator
<i>S</i>	Steam, isentropic
<i>Sea</i>	Tend to sea
<i>T</i>	Turbine, tube
<i>U</i>	Useful, or user
<i>V</i>	Vapor
<i>W</i>	Exergy work

CHAPTER 1: INTRODUCTION

Summary

Water and energy are significant elements in the international development and environment level. The sustainable supply of energy and freshwater leads to better health and social economical life in the world. However, the nation's capability to provide energy and freshwater is being seriously confronted by several existing problems. This chapter provides a background of the worldwide energy crisis and water scarcity. In addition, the factors that drive solar thermal energy technologies to be integrated with the conventional and renewable energy technologies are discussed. Furthermore, the benefits and features of the integration of solar thermal energy technology with conventional and renewable energy sources are highlighted. Finally, a summary of the research objectives of the proposed research work and the description of the thesis structure are also presented in this section.

1.1 Energy crisis and water scarcity

In the next 40 years the world will require to double the installed energy capacity to meet the significant demands of the developing countries as reported by the International Energy Agency (IEA) [1]. In addition, the IEA has also estimated that in the remote areas in the developing countries, around 1.3 billion people have been excluded from using the grid electricity [2]. This option is uneconomically valid in these regions due to their high rate of investment and low energy requirements [3]. Therefore, to meet their energy demands, 80% of the people in these regions have conventionally utilised wood. As a result, deforestation has been reported to be one of the most severe environmental problems worldwide [4]. Furthermore, water scarcity is a worldwide problem affecting almost all continents, especially in countries where the demand for freshwater is higher than or near its accessibility. The water scarcity when the availability of freshwater is lower than the demand is called physical water scarcity. At present, water scarcity confronts approximately 2.8 billion people living in remote regions, where physical water scarcity effects around 1.2 billion and approaching 500 million from the total figure of 2.8 billion people [5]. The water scarcity when the water is available but not distributed uniformly due to financial reasons is called economic water scarcity. Figure 1.1 shows the physical and economic water scarcity that effects the planet projected by the International Water Management Institute [6].

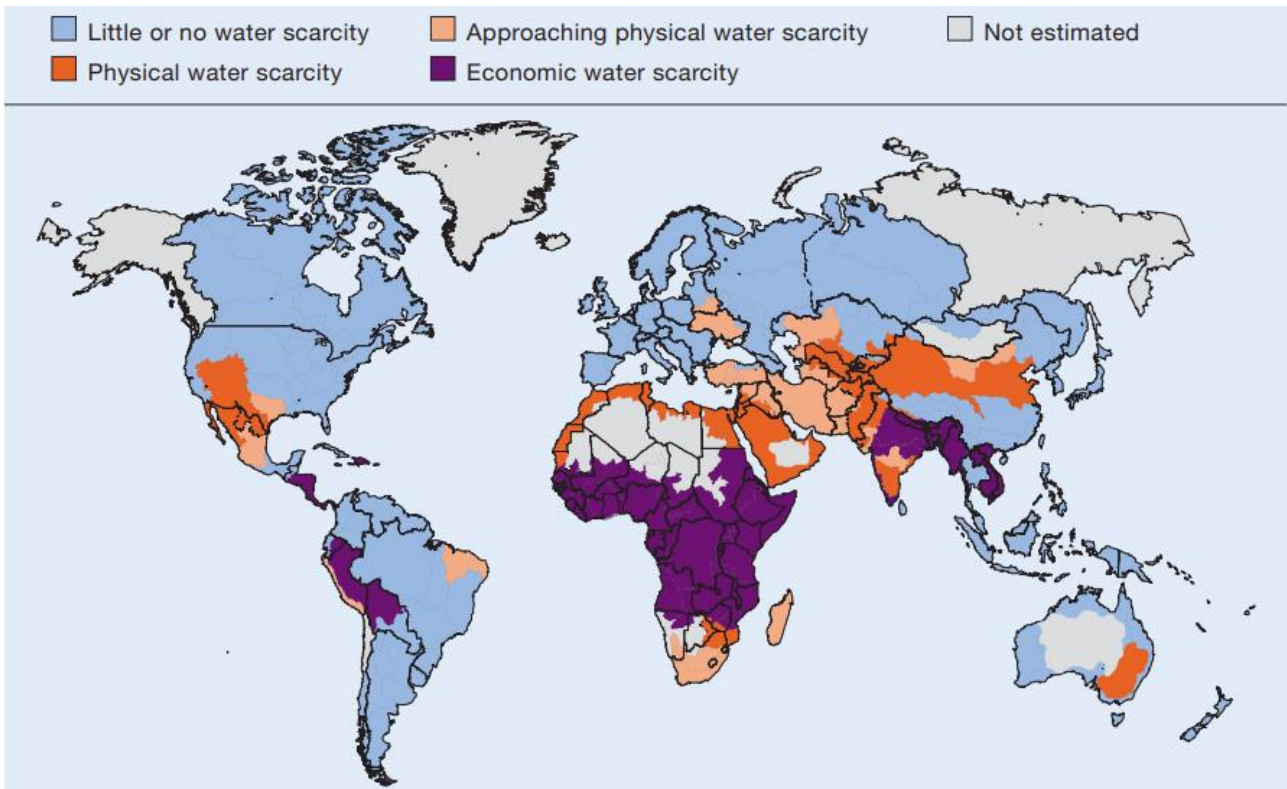


Figure 1-1: Physical and economic water scarcity [6].

The finite amount of fossil fuels, including crude oil, gas and coal, are currently the dominant energy sources internationally. The world cannot rely only on the fossil fuels because of the significant population growth, rapid urbanisation and the technological and industrial revolutions. Alternative Renewable Energy (RE) sources appear to be one of the best solutions to meet the significant future energy demand [7]. During the last decade, a considerable amount of attention has been given to the RE technology as a source for electrical and water production. This is because of the growing awareness of the global warming problems, the declining availability of fossil fuels, the unpredictable price of oil and the increasing demand for power generation. Although RE appears to be a promising alternative technology to replace the conventional fossil fuels, it still suffers from various disadvantages. This includes the high capital costs of the renewable technology and the unpredictable amount of the RE sources over time. The initial cost of the conventional system is much lower than that of the RE technology. In addition, due to the RE fluctuations over the daytime and year (e.g., solar, wind), it's difficult to provide a constant power supply to meet the energy consumption when compared to the fossil fuels systems. As a result, more than 80% of the world energy demand is covered currently by conventional sources, thus causing a significant environmental issue [8]. However, the drawbacks of the RE fluctuations can be overcome by integrating

solar energy with another energy system [9]. Hybrid energy systems are an attractive solution for the electrical generation to reduce both the growing fuel costs and costs of the grid propagation, especially in the rural regions. Hybrid RE sources with a conventional diesel generator or battery storage have been performing well in rural regions. Most of these hybrid energy sites have been utilising solar energy due to its potential ability for hybridisation and availability. Thus, solar radiation is intermittent in nature and this potential problem has been solved by the hybridisation. Several solar renewable energy systems have been constructed around the world in the rural regions, as hybrid energy systems or as stand-alone systems in the locations where the average monthly solar irradiation is approximately in the range 3 to 6 kWh/m² [10]. The implementation of hybrid solar technologies relies mainly on the availability of different energy resources at the designated location. The combined renewable source must be reliable and cost-effective to reduce the investment costs and meet the energy demand [11]. The next part of the review highlights the hybridisation of the RE systems, that is based on the potential solar energy for electrical production, especially for rural regions where the grid transmission becomes unpredictable, uneconomic and environmentally hazardous.

1.2 Solar energy

The quantity of energy reaching the Earth from the Sun at 1.7×10^{14} W is a very small fraction of the total sun radiation [12]. In addition, the total quantity of solar energy acquired by the Earth in a year is approximately ten times the available resources of the fossil fuels and the uranium in all of the Earth [12]. Moreover, in 2006 the solar energy reaching the Earth was recorded to be 5200 times more than the global energy demand in the same year [13]. Nevertheless, very often solar energy is categorised as a low and medium temperature grade, specifically, in the locations where solar intensity is relatively low, such as Europe. In the last few years, intensive research has been conducted in solar thermal applications for low and medium grades. Steam Rankine cycle technology appears to be more suitable to produce electricity for high temperature inlet sources compared to the low-grade temperature sources [14]. However, when heat source temperature drops below 370 °C, the thermal efficiency of the steam Rankine cycle will be relatively very low. Furthermore, the high capital cost and the low thermal efficiency in small-scale power generation systems (lower than 1 MW) imply that the conventional Rankine cycle is not suitable [15]. Steam power plants are mostly operated using fossil fuels with high temperature availability and large-scale productivity. This effects the evolution and the integration of low capability renewable energy resources using steam for small-scale applications. Thus, using low-grade heat resources to

improve the new energy conversion technologies is viable. The Organic Rankine Cycle (ORC) is among the well-proven technologies and one of the promising methods for power production. In this technology, organic working fluids with low boiling point temperatures are used instead of water to recover the low-grade heat sources. This capability enhances the system efficiency to produce electricity from a few KW up to few MW [15]. Several stand-alone renewable sources have been discussed in the literature that are combined with an ORC system, such as solar energy, biomass, geothermal, wind, industrial waste heat, etc. The reason is that this technology has a simple construction, low operating temperature and pressure, low maintenance, highly flexible, autonomous operation and low safety precautions [16–18]. Hence, a small-scale ORC that integrates with renewable energies appears to be an attractive method to satisfy the rural regions electrical needs and reduces the greenhouse gas emissions that are due to the intensive use of the fossil fuels [19]. On the other hand, the Sun is an abundant energy source that can be used indirectly or directly. In regard to the conventional fossil fuels pollution concern, solar energy plays an important role in reducing the environment hazards due to the gaseous emissions such as Carbon Dioxide (CO₂) that have been released from the conventional power generation plants. In addition, adopting solar energy in rural regions can also improve the life quality of the people and reduce the grid transmission costs without effecting the cultivated land [20]. The various types of solar technologies based on their availability in the market can be seen in Figure 1.2. The passive solar energy technology is referred to the system where the heat and light energy are directly utilised from the sun without changing the form status. On the other hand, the system where the energy is converted from one form to another is called the active solar energy technology [21].

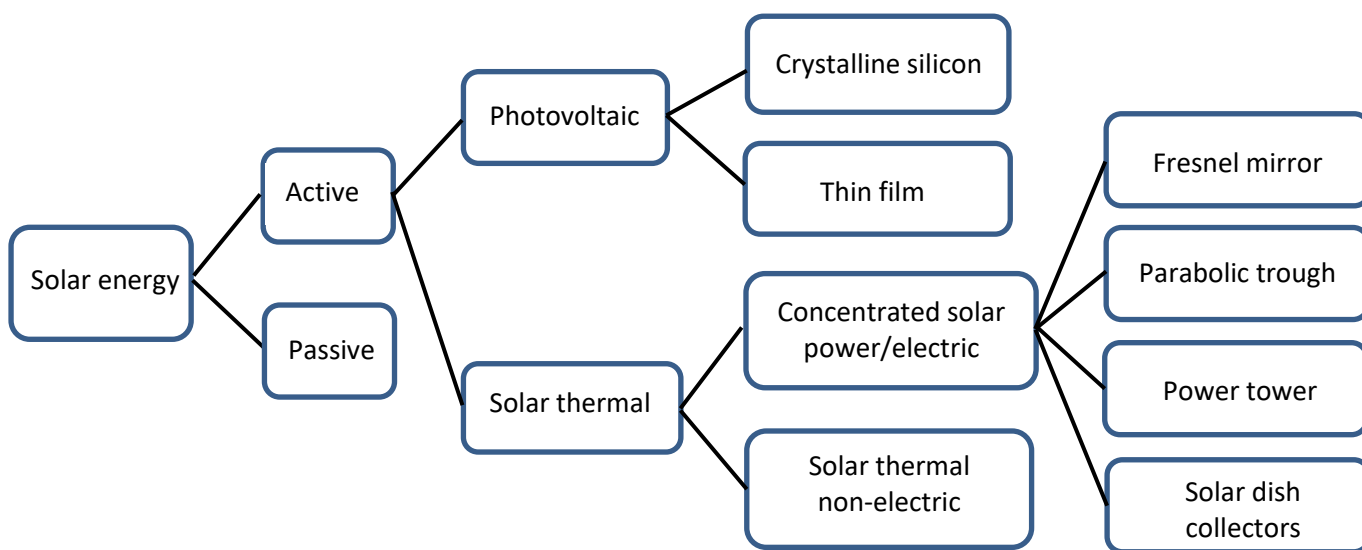


Figure 1-2: Types of solar energy selected based on their availability in the global market [293].

Concentrated solar power (CSP) has a unique feature as a RE source because of its capability to be integrated with an energy storage technology. The concentrated sunlight is used to increase the temperature of the working fluid. The high temperature working fluid is then utilised in the electrical power unit for electrical production. The operation of solar heat as an energy source in CSP makes low-cost energy storage feasible as heat can be readily stored with thermal energy storage (TES), which involves heating of a storage material and containing it in an insulated tank. More importantly, the ability of CSP to be hybridised with an alternative energy source or with a conventional power generation system, makes CSP technology an attractive option compared with other technologies. The hybridisation benefits are as follows:

- i. Reduces the capital costs through equipment sharing.
- ii. Increases the dispatchability.
- iii. Improves the profitability of the plant.
- iv. Enables a better exploration of the lowest solar radiation available.
- v. Increases the power generation capacity.
- vi. Increases the reliability.
- vii. Opportunity for flexible operation between the combined technologies.
- viii. Enhances the design and the operation optimisation.

1.3 Stand-alone solar energy

Stand-alone energy technology is the unit where electrical generation is produced independently from the utility grid. This technology is more suitable to use in remote regions, where the grid connection is not economically feasible. The most installed stand-alone energy units in remote regions around the world use the photovoltaic (PV) type of solar energy. This is because, PV technology is the most cost-effective option for the applications far away from the grid utility. The stand-alone solar energy systems are used in the auxiliary power units for military or emergency services, lighthouses, manufacturing facilities and remote power stations. However, these types of system suffer from many inherent disadvantages, such as excess battery costs and finite electrical storage capacity, thus forcing the throwing away of the excess power produced [22]. A general design of stand-alone solar energy systems is shown in Figure 1.3 [23].

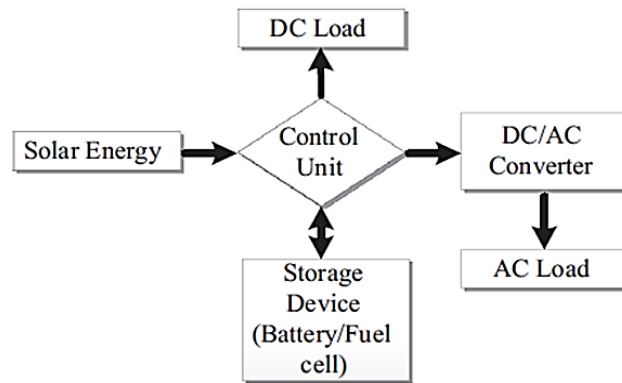


Figure 1-3: Configuration of general solar energy technologies [23].

In contrast, the ability of CSP to be hybridised with alternative energy sources or with a conventional power generation system, makes the CSP technology an attractive option compared with the other technologies. In addition, the use of Thermal Energy Storage (TES) in the CSP technology is much less costly than the chemical battery storage in the PV system [24]. Figure 1.4 shows the general concept of the stand-alone CSP technology [25].

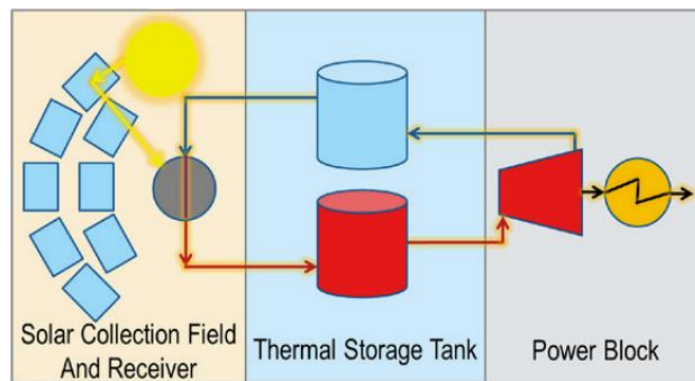


Figure 1-4: Concept of the CSP technology [25].

1.4 Hybrid solar energy technologies

1.4.1 Hybrid solar energy technologies with conventional sources

The hybridisation of CSP with coal plants has many advantages, such as low cost and abundant fuel, provides reliability and dispatchability and more efficiency. However, coal power plants are mostly old and if the plants are retrofitted with a solar CSP system then that will generate an equipment age

mismatch. Thus, the investment is appearing to be uneconomical in the CSP system combined with the coal plants because their plants are approaching their end of life. On the other hand, CSP hybridisation with natural gas has a lower carbon-to-hydrogen ratio compared to other fossil fuels. In addition, natural gas can easily be transported using pipelines due to its high energy density. Natural gas has a high potential to be integrated with CSP due to the rapid development of high effective TES technologies, and this allows the shifting of the operation from mostly being dependent on natural gas to be totally dependent on the solar thermal energy of the solar CSP and storage system. Therefore, power generation using natural gas is becoming relatively more popular and attractive around the world for the new constructed power plants. This strategy makes the hybrid system more flexible and very close to being carbon free and takes advantage of the natural gas ability to provide dispatchable energy.

Hybridisation has become an increasingly more attractive option recently due to the fact that solar thermal energy and feedstock costs continue to fall, while the conventional fossil fuel prices continue to increase. CSP appears to be an ideal technology to be integrated with other energy systems for the electrical production. In the following, the integration of CSP with the conventional sources as well as with the RE sources is reviewed.

1.4.2 *Hybrid solar energy technologies with non-conventional sources*

As the hybridisation of CSP with fossil fuels has been shown to have synergies, the hybridisation of CSP with biofuels demonstrate a similar advantage of improving flexibility and reliability. However, the additional advantage of the hybrid CSP biofuels systems over fossil fuel is to their ability to provide 100% renewable energy [26]. Miguel and Corona have performed a life cycle assessment on the impact of hybrid CSP with fossil fuels on the environment. The study concluded that the major impact is caused by fuel combustion, rather than in the plant construction. Therefore, replacing fossil fuel with the biogas as combined energy with the CSP can reduce most of the impact [27]. CSP technology can be hybrid with various biomass sources such as refuse-derived fuels, stubble, bagasse, wood waste and forestry residues [28]. In addition, solar CSP can be used in the hydrogen production as a supplemental heat source [28] or liquid biofuels for the transportation sector [30]. The use of solar thermal energy to produce syngas or liquid transportation fuels is considered as a type of storage device, which has many advantages. such as the capability to store energy for a long time when compared to the high temperature thermal energy storage [33]. It is worth mentioning that the hybrid solar CSP with biofuel have similar configurations to the hybrid solar CSP with natural gas.

In many studies, poly-generation systems have been proposed with different heat-injection points. The use of multi heat inputs is difficult, as it requires different heat sinks compared to solar energy (e.g industrial processes or buildings). On the other hand, the hybridisation of CSP with wind energy appears to be very much less discussed in the open literature.

This is because the CSP and wind systems are usually integrated at the level of the national grid. The hybridisation can improve the grid stability and better fits to the consumer demand [34]. The grid stability can be achieved due to the ability of the hybrid solar/wind systems to use TES to store energy at a low capital cost. The TES can be utilised in the CSP technology, thus allowing wind energy to stabilise the power outputs [34]. A detailed comparison between the stand-alone renewable energy system against the stand-alone conventional energy system and combined renewable energy with conventional energy system is shown in Table 1.1 [35].

Table 1.1: Comparison between stand-alone renewable and conventional energy systems [35].

Parameter	Conventional's	Renewable's	Hybrid system
Availability	Limited	Limited	Highly available
Capital cost	Low	High	Moderate
fossil fuel dependency	Highly dependent	Independent	Moderately dependent
Environmental effect	High	Low	Moderate
O&M costs	High	Low	Moderate
Maintenance	Frequent	Low- Frequent	Low- Frequent

The ability of CSP to be hybridised with alternative energy sources or with a conventional power generation system, makes the CSP technology an attractive option compared with the other technologies. The hybrid CSP with a biofuel source increases the system dispatchability and reliability, increases the operation flexibility, allows a better exploration of the lowest solar radiation available, overcomes the intermittency of the solar CSP source, improves plant profitability, enables a fully renewable solution and provides a secure energy supply. On the other hand, the Organic Rankine Cycle (ORC) unit appears to be a promising technology in small and medium scale power generation. This is because of its ability to utilise efficiently low-grade heat sources and to its capability to be used in remote regions where grid connection is not economically a viable option. However, the hybrid solar-biogas ORC for power production has various disadvantages, such as lack of research, low thermal efficiency and the high capital costs. A better

design optimisation will enhance the heat transfer processes and that will lead to a reduction in the final capital cost. Thus, extensive R & D is needed to enhance the system performance and reduce the system cost.

1.5 Modelling method using artificial neural networks

Forecasting meteorological conditions are critical for electrical energy system design and power production evaluations. Hence, academics and experts worldwide have developed several prediction techniques to understand the components of solar radiation to utilise solar energy effectively. For this purpose, traditional pyranometers are placed in strategic positions to measure the Global Solar Radiation (*GSR*). Notwithstanding, periodic maintenance and data recording are required to collect the *GSR* data and thus cause a rise in the cost of collecting the *GSR* data. Therefore, it is imperative to predict solar radiation using appropriate approaches. Similarly, wind speed forecasting assists in the reducing of the power supply irregularities and facilitates electricity grid connection [36]. Thus, the performance of solar or wind energy systems is defined by using an accurate solar radiation intensity and wind speed parameter.

Artificial Neural Networks (ANN) are a critical data processing technique that may be used to model complex input/output interactions. ANN exhibits excellent features such as mapping capabilities, high-speed information processing, fault tolerance, adaptiveness, robustness and generalisation [37]. An ANN would best describe the non-linear and discontinuous behaviour of solar radiation and wind speed [38]. Therefore, in this thesis, the data forecasting of ANN for hourly solar radiation and wind speed over Oman will be deployed.

ANN models are highly simplified representations of human brain systems. An ANN is made up of computational units that are equivalent to the neurons in the biological nervous system. These units are referred to as artificial neurons [39]. In general, ANN models have input and output layers and one or more hidden layers that include units referred to as neurons [39]. These neurons, or processing units, function as non-linear summing devices and are layered together and coupled via changeable connection weights, also called synaptic junctions [40]. In the next section a general outline of the thesis structure is illustrated.

1.6 Thesis Outline

The research objectives, contribution and outline of the thesis is presented in this section.

1.6.1 *Research proposal*

The research objectives of this thesis are as follows:

- To develop a new multi-dimensional forecasting model using the ANN technique for predicting the solar radiation and wind speed over six locations in Oman. The built model uses a large number of meteorological data points combined with two ANN models simultaneously to accurately predict the solar radiation and wind speed. Three input parameters are only required in the developed model to measure the solar radiation and wind speed with high accuracy simultaneously.
- To design the new proposed hybrid solar and biogas system for desalination and electric power generation using advanced modelling techniques to integrate the overall system components. The models have been developed with MATLAB/Simulink® and have been used to investigate the system area, dimensions, cost and to ensure that the electrical and water demand of the end-user are met. Moreover, a new detailed thermo-economic assessment of the proposed hybrid solar biogas for cogeneration in off-grid applications has been investigated. An energy, exergy, and cost analysis have been performed and to fully utilise this, a sensitivity assessment on the developed model has been analysed to examine the effects of various design parameters on the thermo-economic performance. Finally, implementing an in-depth simulation testing of the system in a rural region in Oman.
- To optimise the new hybrid solar biogas system for desalination and electric power using the non-dominated sorting genetic algorithm (NSGA-II) to solve the multi-objective optimisation problem and produce a Pareto frontier of the optimal solutions. Further, the TOPSIS approach has been used to select the optimal solution from the Pareto set. The aim of the multi-objective optimisation is to achieve maximum power and water production with minimum possible cost.

1.6.2 *Contribution of the Thesis*

Firstly, a novel Artificial Neural Network model has been developed based on the Feed-forward Back-propagation (FBANN) to simultaneously predict the hourly solar radiation and the wind speed. The developed model has been implemented over the six regions of Oman. The novelty of the new designed

model emerges from the following features: (a) two different FBANN configurations has been combined into a new integration, (b) the new developed model required only three input parameters, and (c) and both solar radiation and wind speed are calculated accurately and simultaneously. As a result, the model offers a user-friendly interface that can be integrated later in the process of designing the proposed cogeneration hybrid solar-biogas energy systems. Consequently, this model facilitates the implementation of renewable energy technologies, especially in the remote regions where the collection of weather data is very challenging. Meanwhile, the accuracy of the model has been tested by calculating the mean absolute percentage error (MAPE) and the correlation coefficient (R). Therefore, the model developed in this study can provide accurate weather data and inform decision makers for future instalments of energy systems.

Secondly, a new integrated solar and biogas model for desalination and electric power generation has been presented, investigated, and analysed in terms of the design, size and cost aspects. This study is the first attempt to integrate the off-grid hybrid model that contains PTC, anaerobic biogas boiler, ORC and AGMD for desalination and electric power generation. Accordingly, a comprehensive thermo-economic assessment has been conducted for the proposed novel integrated model and the modelling approach simultaneously solves the energy, exergy, and cost calculations and thus a new flexible model has been developed. Thus, the proposed assembly has not been studied before, and, typically, solar PTC linked with wind/thermal energy storage for combined heat and power is the most popular integration that has been investigated in the literature.

Finally, a robust multi-objective optimisation has not previously been performed for decentralised hybrid solar-biogas for power-water productions. First, a three objective optimisation is preformed using a non-dominated sorting genetic algorithm which present the results in terms of a Pareto set. Subsequently, a MCDM tool is deployed to select the optimal design parameter from the Pareto set. This robust optimisation can pave the way for further research on a scale up cases.

1.6.3 *Structure of the Thesis*

The thesis structure has been proposed to be arranged into six chapters as follows:

Chapter 1: Introduction. The research problem and motivation are presented in this chapter. Following that, a summary of the research objectives of the proposed research work and the description of the thesis structure are also presented in this section.

Chapter 2: Literature Review. In this chapter, a comprehensive review on what has been published in the open literature on the different solar CSP technologies, the economy of integrating CSP with thermal energy storage and backup systems, waste to biogas production and its potential hybridisation with the CSP, ORC technology and its attractive potential for a small scale production unit compared to the conventional systems, and the possibility of integrating low energy and innovative desalination processes to recover the waste heat from the ORC technology. The modelling and optimisation of solar driven cogeneration systems based on an ORC has been also reviewed. Finally, a highlight of the main Identified potential research gaps in the literature and the contribution to the original knowledge is also presented.

Chapter 3: Solar Radiation and Wind Speed Prediction model using ANN. A novel Artificial Neural Network model has been developed based on the Feed-forward Back-propagation (FBANN) to simultaneously predict the hourly solar radiation and the wind speed has been presented. In addition, the developed model has been implemented over the six rural regions of Oman and the accuracy of the results has been tested by calculating the MAPE and the R value. Finally, a comparison between the developed ANN model results and the typical meteorological correlations factors has been presented.

Chapter 4: Thermo-economic and design analysis of the hybrid solar biogas system. In this chapter, the design and the operation principle of the hybrid solar/biogas/ORC/AGMD technology using advanced modelling in the MATLAB/ Simulink® is presented. The overall mathematical thermodynamic equations of each of the sub-component of the proposed system have been described. Finally, the performance of the model has been tested in a rural region in Oman, and a thorough thermo-economic analysis of the combined system has been conducted. The selected area is a good example for the implementation of hybrid renewable energy systems since this region is very far from the main interconnected grid and the connection to the grid is not economically valid option.

Chapter 5: Multi-objective optimisation of the hybrid solar biogas system. In this chapter, the conducted parametric study in the previous chapters is utilised in defining the operating parameters that have the highest impact on the thermodynamic and economic performance of the cogeneration hybrid system. It is crucial to couple the overall simulation model with an appropriate optimisation technique to investigate the optimum operating parameters. The non-dominated sorting genetic algorithm (NSGA-II) approach will be utilised, and the obtained results will be discussed in this Chapter.

Chapter 6: Conclusions and future recommendations. In this chapter, a summary of the main findings drawn from the research work and the author's recommendations for possible future work is presented.

CHAPTER 2: LITERATURE REVIEW

Summary

This chapter presents a comprehensive critical review on the design and optimisation of solar-biogas systems for cogeneration applications. A critical literature review on the different solar CSP technologies, the challenges facing the integrations of CSP with thermal energy storage and backup systems, waste-based biogas production and its potential hybridisation with the CSP, ORC technology and its attractive potential for a mid- and low-scale production unit compared to the conventional systems, and the possibility of integrating low energy desalination processes to recover the waste heat from the ORC technology has been presented. In addition, the design integration of CSP-biogas systems for desalination and cogeneration has been elaborated. Furthermore, the recent optimisation methods that used for the optimisation of the hybrid renewable energy systems are discussed. Finally, a highlight of the main identification of the potential research gaps in the literature and the contribution to the original knowledge is also illustrated. Thus, the aim of this chapter is to trace the development progress that has been made so far in the design of sustainable, reliable, and cost-effective stand-alone solar energy systems and identifying the potential research gaps in this area.

2.1 Overview of CSP technologies

CSP is a power station that concentrates the sun's radiation on a small surface area using mirrors. A coolant fluid (e.g. molten salt) is then passed through the small surface area to be heated. This thermal energy is utilised to generate steam, which is then sent to a turbine to produce electricity or to be directly used in thermal desalination plants. The development of two innovative renewable technologies, thus allowing through a thermal energy storage system and back-up systems to solve the problem of the intermittent nature of solar energy. Generally, CSP power plants consist of several parts such as receiver, solar concentrators, steam turbine and electrical generator. The main components can be seen in Figure 2.1 [41].

Furthermore, there are four types of CSP technologies that has been developed up to now: solar power tower (SPT), linear Fresnel reflector (LFR), parabolic trough collector (PTC) and parabolic dish systems (PDS). Figure, 2.2 shows the main CSP technologies [42]. The United States and Spain are currently the two largest and most attractive markets for the medium to large-scale operation of CSP systems. They

also benefit from a very favourable regulatory context. Zhang et al. [43] stated that the second established CSP configuration after the parabolic trough collector (PTC) is the solar tower due to its attractive benefits. The different types of the configurations of the CSP and their advantages and disadvantages will be explained in the next section.

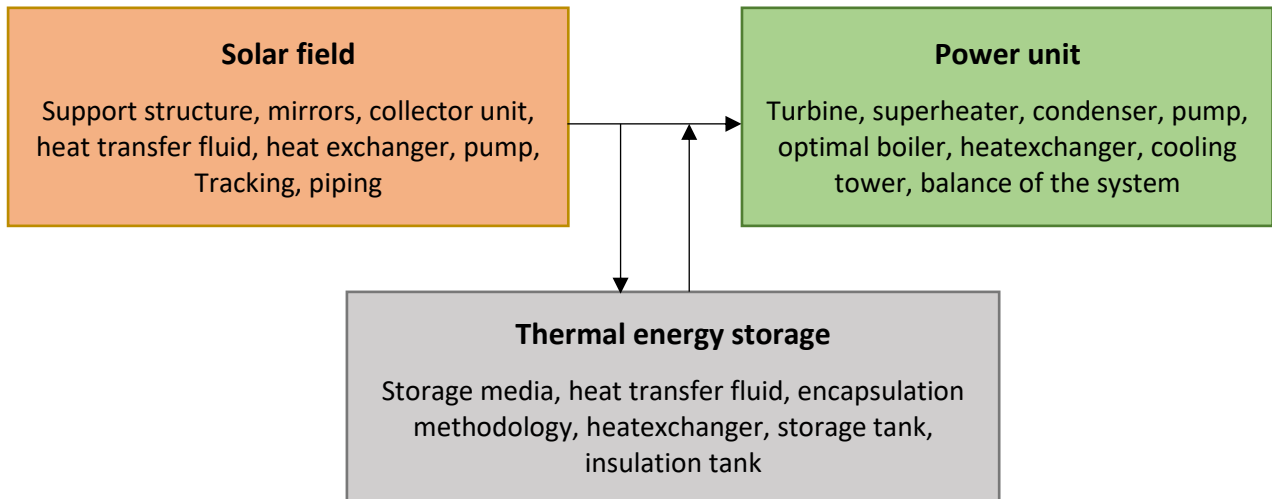


Figure 2-1: The CSP main components [41].

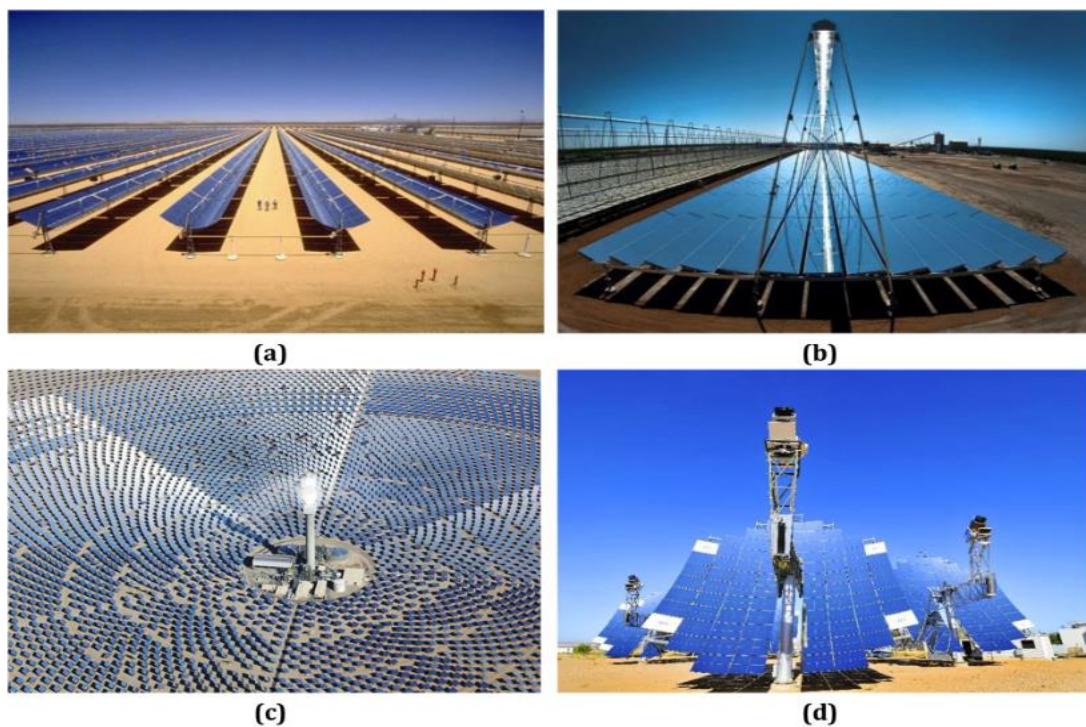


Figure 2-2: Main CSP technologies: (a) PTC; (b) LFR; (c) SPT; (d) PDS [42].

The CSP plants major challenges are the intermittency issues and the required cost [44]. Nevertheless, this can be solved by integrating the TES utilising such as molten salt. Therefore, the natural gas boiler can be replaced by the thermal storage to guarantee a backup power during times of no sunshine. Van Den Broek et al. [45] were not encouraged by the already high cost of the plant and the additional budget brought by the thermal storage feature. Any investor will not adopt any process or extension if the extra cost is higher than the expected benefit. Zhang et al. [46] disagreed with them and illustrated that, after a deep study, CSP plants are attracting more attention, especially when having the PTC feature even with the competition of SPT that have the advantages of lower operating costs, higher efficiency, and scale-up feature opportunity. Torresol joined Zhang et al. opinion when it successfully demonstrated that Large-scale CSP technology in the Spanish Gemasolar project [47]. It is worth noting that the Gemasolar CSP power plant was considered to be the first plant to effectively generate 19.9 MW of continuous electricity for 24 h. Figure 2.3 illustrates the worldwide utilised CSP technologies and their installed mix share [48].

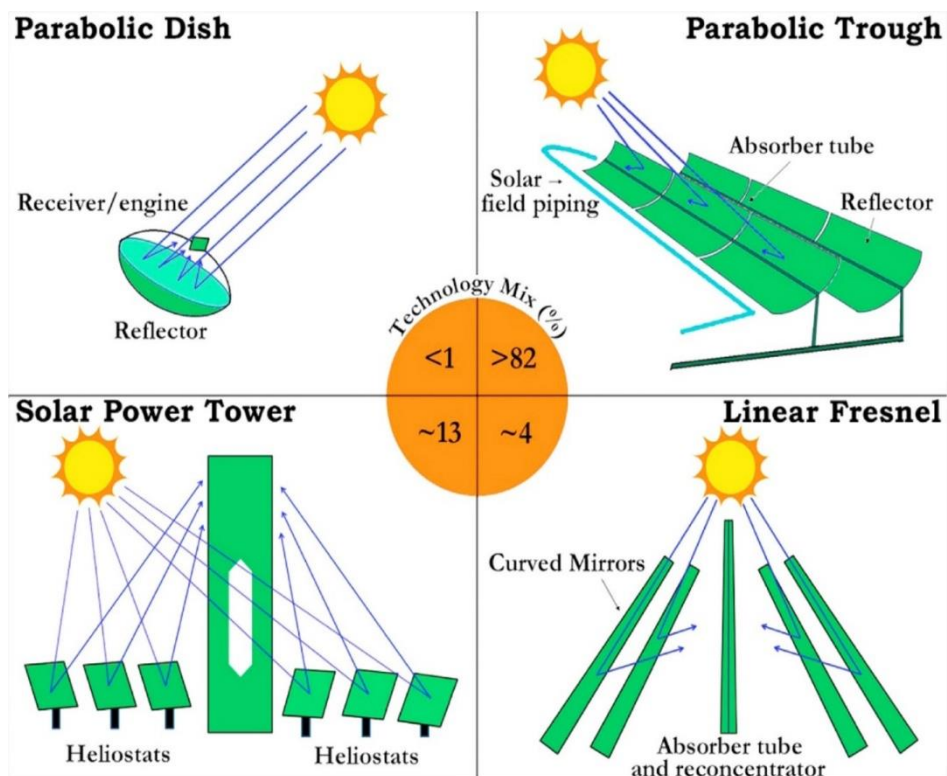


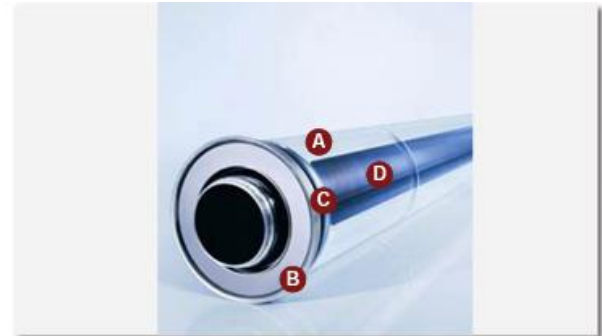
Figure 2-3: Schematic diagram of the CSP technologies and their installed share [48].

2.1.1 Parabolic trough collectors

The PTC focuses the sunlight on the focal line of the parabola and its mobile parts (reflectors and absorber) tracking the sun are synchronised. The absorber tube (Figure 2.3) is covered with a low thermal remittance and high selective solar irradiation absorbance materials. Zhang et al. [43] stated that covering the absorber tube with the glass metal seal is significantly important to reduce the heat losses. The PTC main parts and along with the receiver details are shown in Figure 2.4 [49].



- 1 Receiver
- 2 Parabolic shaped mirror
- 3 Ball joints
- 4 Support structure



- A External glass
- B Expansion bellow
- C Glass-to-metal seal
- D Internal pipe

Figure 2-4: The PTC main parts and receiver details [49].

2.1.2 Parabolic dish systems

PDSs allow the whole system to track motion of the Sun. Barlev et al. [50] stated that this solution is still expensive and not fully compatible with respect to hybridisation and thermal storage. However, the PDSs are still defended by people believing that their mass production will allow them to compete with larger solar thermal systems. Nowadays, the only existing PDS plant fully operational is in Arizona with a net capacity of 1.5 MW (Maricopa solar project). The PDS main components are shown in Figure 2.5.



- 1 Mirror facets
- 2 Support structure
- 3 Stirling engine

Figure 2-5: The PDS main components [49].

2.1.3 Linear Fresnel reflectors unit

The LFR in structure are similar to the parabolic trough systems. They reflect the sunlight to a downward facing linear receiver using the slightly curved or flat mirrors. The LFR main parts are shown in Figure 2.6. According to Barlev et al. [51], the LFR systems main advantage is their simple design of flexibly bent mirrors and fixed receivers that require lower investment costs and thus makes easier direct steam generation.



Figure 2-6: The LFR main components [49].

2.1.4 Solar thermal power towers

Solar towers guarantee producing high temperatures that enhance the heat generation efficiency to be converted into electricity or for thermal desalination. Solar towers offer a lower cost alternative for thermal storage in the power applications. The central receiver systems utilise a Sun tracking reflector called the heliostat field collector to focus the Sun's emissions onto the top of a fixed tower (central receiver), see Figure 2.7. Then, the heat will be absorbed and transferred to the heat exchangers to drive the steam/organic Rankine cycle using heat transfer fluid (HTF).



Figure 2-7: The SPT main parts [49] .

2.1.5 Comparison of CSP technologies

The CSP technology is the most advanced and widely used renewable energy system with almost zero carbon emissions. A summary of the significant features of the main CSP technologies is given in Table 2.1 [1], [48]. It can be noted that PTC is a desirable option for mid- and low-scale power plants with a very good conversion efficiency and low cost. In addition, the PTC is the most proven, reliable and mature technology worldwide. Thermal energy storage and backup systems can be integrated with the CSP in order to enhance the competitiveness of the CSP against the conventional technologies. The integration strategy provides a stable energy supply and offers the possibility of year-round operation to thermal power applications or electrical generation requirements [44].

Table 2.1: A summary of the significant features of the main CSP technologies [1], [48].

Parameter	SPT	PTC	PDS	LFR
Operating temperature (°C)	300-1200	150-400	300-1500	150-400
Capacity range (MW)	10-100	10-250	0.01-1	5-250
Annual Efficiency, (%)	10-22	10-16	16-29	8-12
Solar concentration ratio	600-1000	50-90	< 3000	35-170
Power cycle	Steam Rankine; Brayton Cycle	Steam Rankine; Organic Rankine	Stirling Engine; Rankine; Bryton cycle	Steam Rankine; Organic Rankine
Relative cost	High	Low	Very high	Low
LCOE, (\$/kWh)	Current:0.2-0.9 Future:0.06-0.08	Current:0.3-0.75 Future:0.06-0.08	Future: 0.05-0.08	Future: 0.06-0.08
Thermal storage suitability	Highly suitable	Suitable	Difficult	Suitable
Land requirement	Medium	Large	Small	Medium
Outlook for improvements	Very significant	Limited	High potential	Significant
Commercial development	Medium	High	Low	Medium

Furthermore, all CSP plants require water for both condensing and cooling processes. For instance, the PTC and LFR plants need 3000 L/MWh of water which is more than that needed for coal power applications and similar to a nuclear reactor [52]. Even though cooling using water appears to be more efficient, hybrid plants are increasingly using dry methods especially in the winter season where the cooling requirements are lower, whilst during summer, a combination of dry and wet cooling approaches are used [53]. For the new CSP development, the combination of CSP with desalination cogeneration

technology is an attractive alternative operation mode. The production of freshwater beside the power simultaneously can reduce the requirements of cooling water for CSP technology and provide freshwater to meet the peoples demand especially in the desert regions that faces water scarcity [54]. The MENA region has promising and attractive potential for the implementation of a CSP-desalination system due to the close access to the sea water for cogeneration application. In addition, the MENA region is considered one of the highest regions that is effected by the physical water scarcity around the world [55]. Despite the significant potential prospective, the CSP-desalination technology is still in an early stage of development [42].

2.1.6 Economics of the CSP technologies

The LCOE of the CSP plant is significantly influenced by the DNI level of the selected location as can be seen in Figure 2.8. It can be noticed that the LCOE is reduced by up to 4.5% for every additional 100 kWh/m²a. The locations, such as the MENA region or in California needs less than 25% of the minimum cost to breakeven compared to a similar project in Spain. Moreover, the variations of the labour and financing costs has also an important role in identifying the minimum LCOE. These facts show that the CSP technology has a significant potential to improve its competitiveness in the foreseeable future.

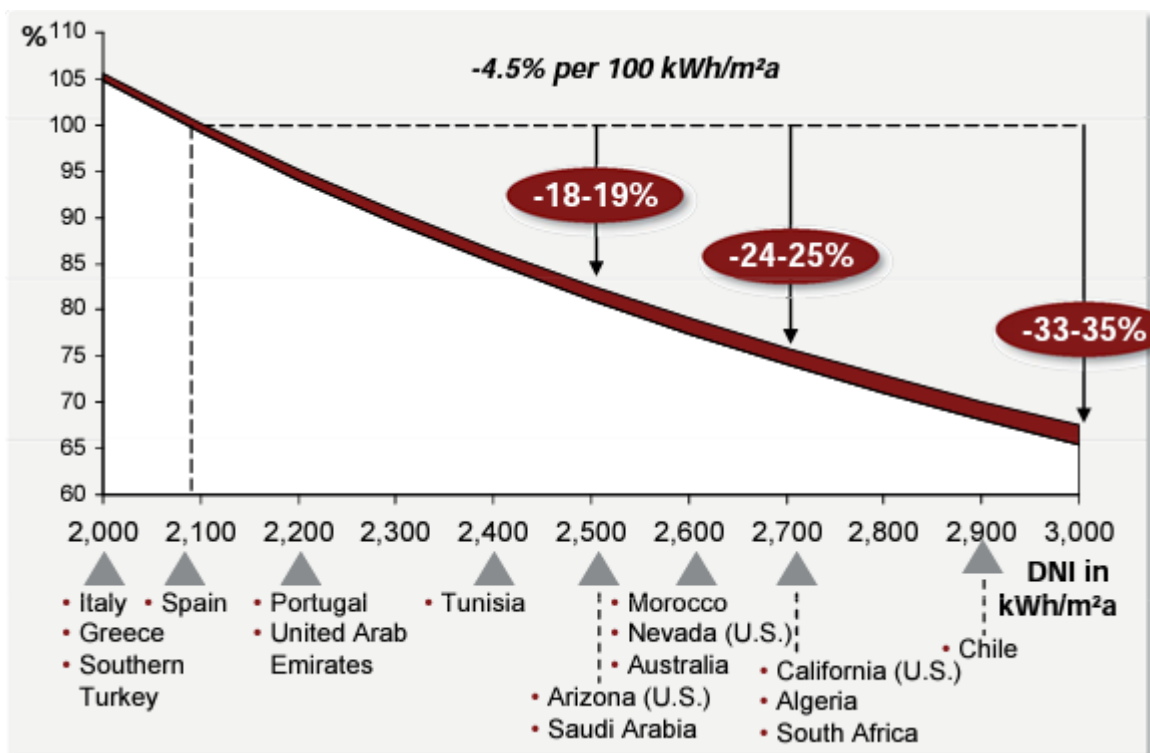


Figure 2-8: Impact of the DNI level of the location on the CSP LCOE [49].

Currently, the LCOE of the CSP technology is still not competitive against the conventional energy sources such as gas or coal. Nevertheless, the CSP is expected to compete against the conventional technologies, due to the projected cost increases of the gas and coal, along with the additional CO₂ penalties. Figure 2.9 shows the potential cost of the solar thermal energy against other energy sources.

Furthermore, the hybrid dispatchable CSP can substitute the combined cycle power plant technology in the end, as can be seen in Figure 2.9. Further, the competitiveness of the CSP can be increased by introducing additional CO₂-penalties in the future. In addition, it can be noticed on the right side of the Figure 2.9 that the non-dispatchable solar thermal energy (STE) can compete with the non-dispatchable renewable energy technologies such as PV. However, the STE is not estimated to compete with the wind technology because of the wind cost advantages. However, the availability of the solar and wind is generally complementary, regions that has high DNI, normally has low wind speed. In these regions, the cost of STE can compete with wind turbines technology.

The CSP system can offer additional grid advantages either its dispatchable or non-dispatchable technology, due to the operating temperature of the heat transfer fluid that do not cool down immediately that make it an alternative to consider compared to the PV technology.

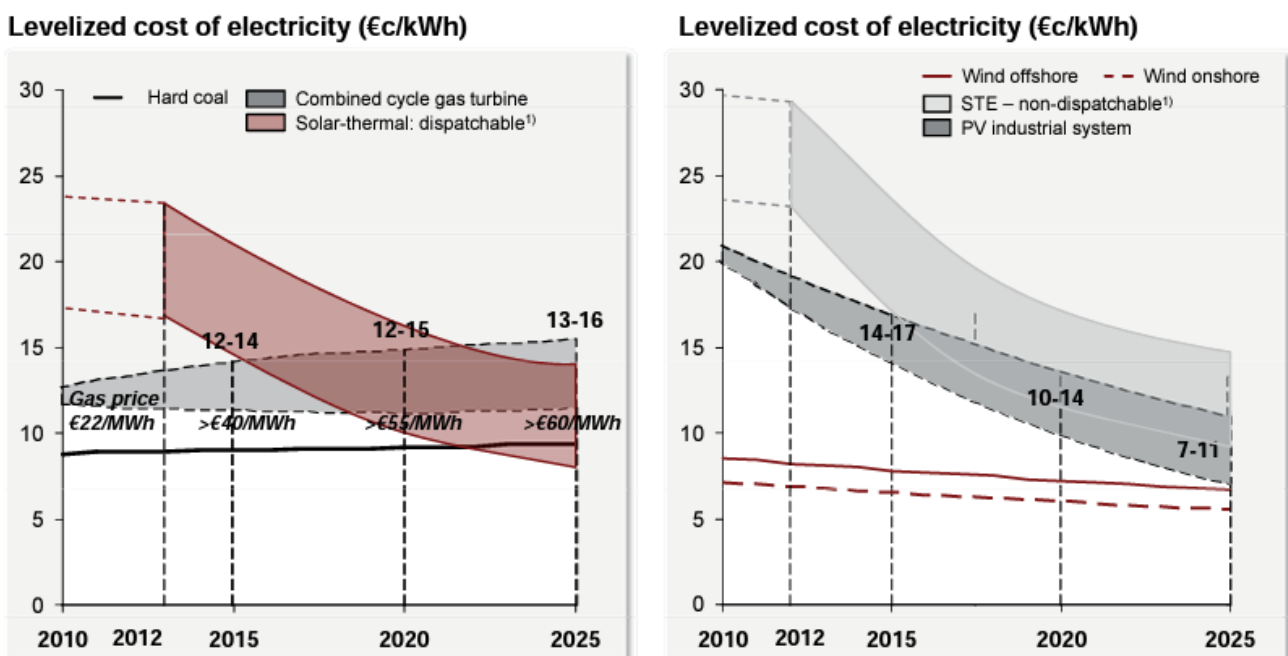


Figure 2-9: Cost comparison between solar thermal energy against other energy sources [49].

2.2 Waste-based biogas production

The energy security and the environmental concerns are the two main factors that have led to the huge developments in the utilising of alternative energy sources as a replacement to the conventional fossil fuels. Waste-based biogas appears to have potential as an alternative energy as a source of clean and sustainable energy. This technology has the advantages of utilising the waste and solving a serious international problem of generating unrestrained emissions of methane when dumped untreated. In addition, the rapid urbanisation and stringent legislations are restricting the disposal of degradable waste in the landfills. Therefore, utilising waste in producing biogas is an attractive alternative option. The methods that have been used to produce methane biogas from organic waste mainly includes pyrolysis, alcoholic fermentation, gasification, and the anaerobic digestion. In the last decade, anaerobic digestion technology is mostly used because it appears to be commercially feasible to produce biogas [56]. In addition, anaerobic digestion (AD) is a sustainable process for the generation of bioenergy and the management of organic waste worldwide due to its low energy demand [57]. Therefore, the AD process will be extensively reviewed in the next section. A schematic view of a biogas plant is shown in Figure 2.10 [58].

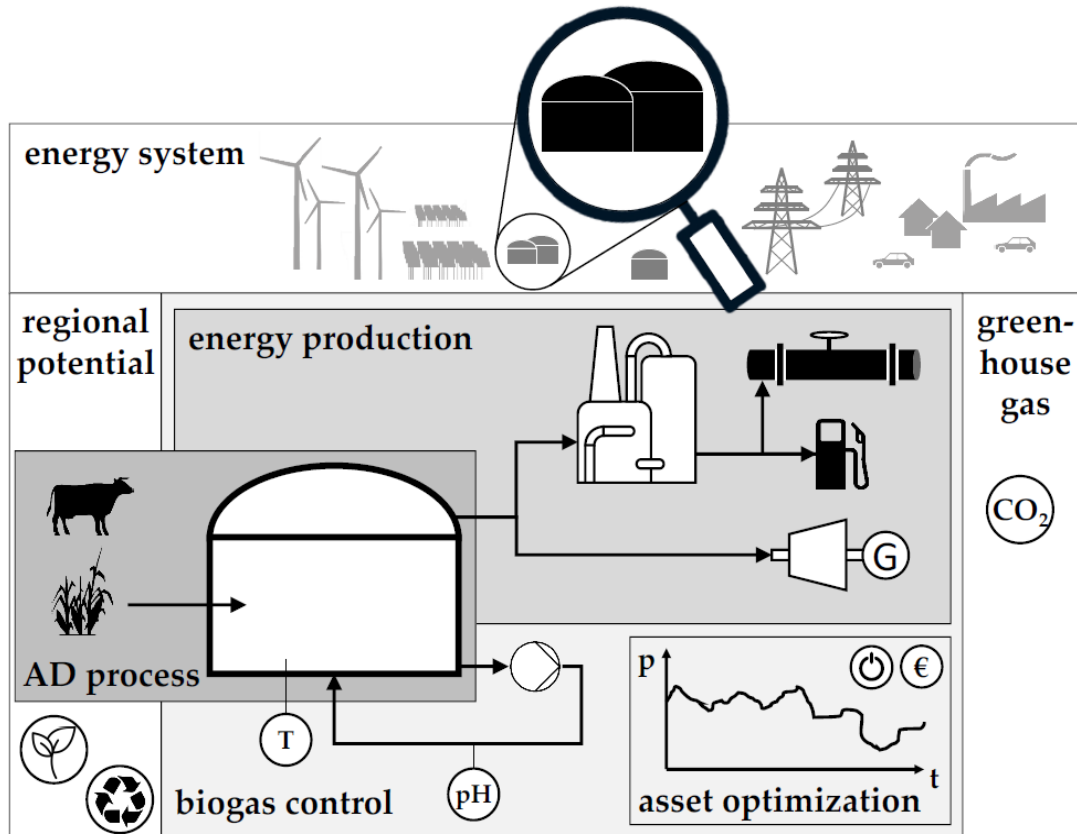


Figure 2-10: Biogas plant schematic view [58].

2.2.1 *Anaerobic digestion technology*

The AD process is the decomposition and stabilisation of organic matter in a series stage in the absence of Oxygen (O₂). A mixture of mostly methane (CH₄) and carbon dioxide (CO₂) can be produced using various types of organic matter that can be utilised to generate heat or electricity instead of the use of conventional fossil fuels [59]. By the end of 2014, more than 14,500 biogas plants had been established in Europe with a total capacity of 7857 MW_{el} [60]. The organic waste can be treated simultaneously in the biogas plants to reduce the environmental pollution and recover energy. These advantages can effectively alleviate the 21st century challenges of the environmental pollution and the energy insecurity [61]. However, AD technology suffers from instabilities [62], which has limited its applications in the energy production. For instance, in the 20 centralised biogas plants that have been investigated in Denmark [63], they have been shown to have periods of instability that continued for many weeks or months, where the generation was decreased by 20–30%. Therefore, the hybridisation of waste to biogas production with other RE, such as solar energy, is an interesting option to enhance the system stability and reliability.

2.2.2 *Hybrid CSP biogas plant*

In the past several years, the interest in the hybridisation of solar CSP/biogas power plants has been significantly increased. The first commercial hybrid solar CSP/ biogas power plant started to be operated in December 2012, in Spain (Figure 2.11). The \$210m power plant, produces 22.5 MW of electrical energy and 36 MW of thermal energy every year which has been calculated to be sufficient to meet the demand of approximately 27,000 households [64]. The solar block utilises parabolic troughs with thermal oil to generate power, while the biomass block uses biomass, agricultural waste and supplemental natural gas as fuel. The power plants run during the daytime using solar power and biogas during the night period. A PTC system has been utilised of with an area of about 180,000 m², and 2688 solar field parabolic collectors, with a diameter of approximately 5.5 m [64]. In addition, the steam Rankine cycle has been powered by two biogas boilers as a back-up. However, a water-based Rankine cycle is not economically feasible for small-scale power generation systems due to its inherent heat losses and high capital cost [65]. In the next section, the integration of RE powered desalination technologies will be discussed.



Figure 2-11: Photographs of the hybrid CSP/Biogas plant in Spain [64].

The hybridisation of CSP-Biogas systems solves the intermittence concern of the solar source and the shortage in the biogas feedstock. In the hybridised system both technologies share some common sub-components such as turbine, generator, air compressor and gas supplier which enhance the competitiveness cost with other technologies [66]. The areas of solar field and biogas fuel input decreased for a fixed plant size, offering a constant supply of biogas with the reduction in the logistical costs. The biogas consumption rate if compared with a typical biogas power plant is stated by Bai et al., to be reduced by 22.5% [67]. The LCOE of the hybrid solar CSP biogas technology is decreased to 0.077 \$/kWh differentiated to 0.192 \$/kWh for standalone CSP plant [67]. In addition, Sarkis and Zare reported that using direct steam generation further decreases the LCOE to 0.07495 \$/kWh [68]. The combination of solar biogas can reduce the total investment cost by 12% when compared to a standalone solar CSP system [69] and therefore the payback time is reduced. For the overall process cost, it is reported that the hybridisation of solar biogas can reduce up to 13%, by the removal of air separation units, gas cleaning system and the gas combustion [70]. The hybrid plant decreases the investment cost that is needed for each system, and developing a stable, high efficient and environmentally friendly system.

2.3 CSP-desalination technologies

The use of CSP to power desalination technologies is a promising and attractive mode to reduce the dependence on conventional resources, produce clean water to decrease water scarcity and lower greenhouse gas emissions. Many integrations of the desalination processes and CSP systems are already defined (see Figure 2.12 [71]) and they have a promising economic and technological potential. Some combinations are used for a large-scale desalination plant and some for low-scale applications. Multi-effect distillation (MED) plants are more flexible to operate at partial loads compared to Multi-stage flash (MSF) if combined with the solar CSP technology. In addition, the scaling issue does not affect MED considerably and appears to be more suitable for the limited capacity [54,55]. Furthermore, MED processes require a lower electrical demand compared to the Reverse Osmosis (RO) technologies [74]. However, MED remains to be an energy intensive technology [75] which negatively affects their hybridisation with CSP. The recent studies have shown a promising result in the integration of the CSP-driven Adsorption Desalination (AD) or the Membrane distillation (MD) processes. Therefore, many MD pilot plants have been installed utilising geothermal and solar energies [57–59] and due to their performance, they were proved to be better with many less operational issues over the conventional units. More descriptions of these desalination technologies that could be used for cogeneration application are explained in the next section.

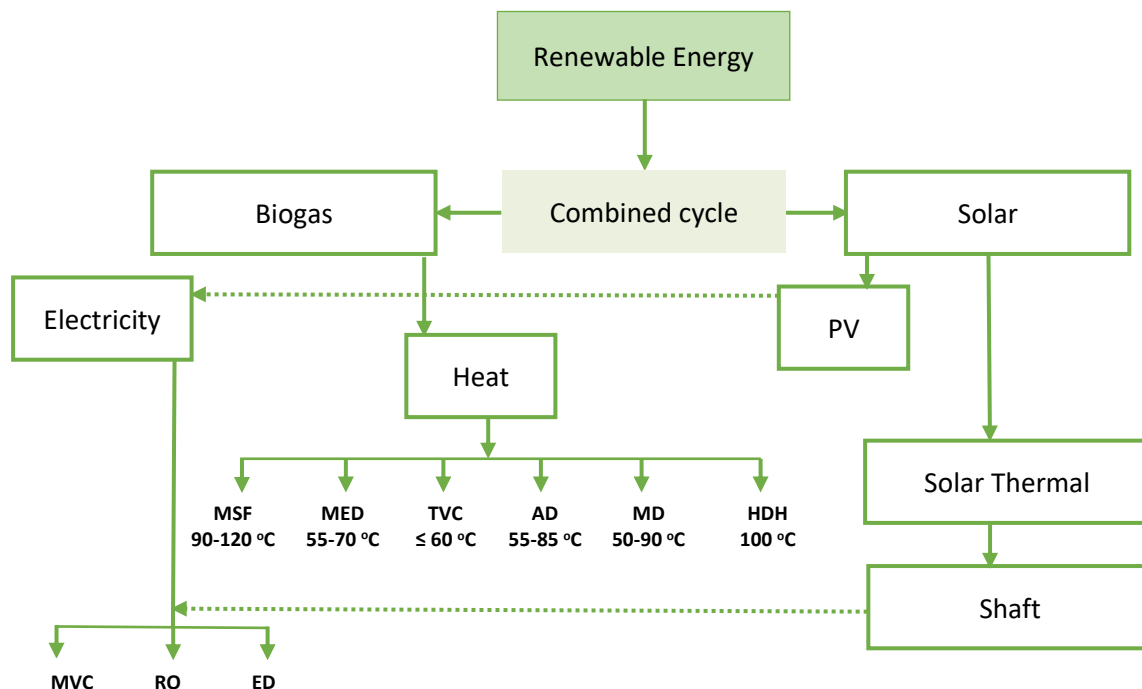


Figure 2-12: Possible integrations of the RE with different desalination technologies [71].

2.3.1 *Low energy desalination technologies*

The hybridisation of CSP to power the desalination technologies is mostly still under development. The AD and MD technologies will be covered in this review because of their significant potential to scale up. These two processes are much simpler, more compact, and more scalable if compared with the conventional desalination technologies. In addition, they can be operated at lower temperatures and at atmospheric pressure. Moreover, these processes can operate with an intermittent energy supply without any additional modifications. Therefore, they are a very attractive option for the intermittent CSP integration. Several studies have been reviewed the AD technology in [79], [80] and MD process in [81]–[83]. A summary of these two technologies will be discussed below to highlight their potential in the RE integration, especially with solar CSP energy because of the enormous availability of solar energy in regions where water scarcity is a serious problem.

2.3.1.1 *Adsorption desalination (AD)*

Recent research by Ng et al. [84] Ghazy et al. [85], Narasimhan et al. [86], Wang and Ng [79] and Sosnowski et al. [87] have led to the discovery of a new feature of the desalination cycle. This has a high and efficient heat adsorption capacity that matches twice that of the known thermodynamic limit in terms of kWh/m³. Further, this process involves the use of a low temperature heat source to enhance the sorption cycle, leading to the generation of two outputs from the one heat input, which are cooling and high-grade potable water. The plant core is a heat exchanger conducting hot water. The AD tubes are confined in a layer of an adsorbent such as silica gel. The vapour generated in the evaporator is sucked at very low temperature and pressure by the adsorbent. The applied envelop layer porosity ranges between 10 to 40 nm and the overall pore surface area ranges between 600 to 800 m²/g. The plant, supposedly treating raw water (e.g., seawater) at its ambient temperature leads to the dispense heating of the input water, unlike the other conventional thermal methods. When saturated, the adsorbent is heated to release the vapour (desorption) and is then condensed (Figure 2.13). This is achieved by recirculating the natural hot water which can be extracted from the RE systems. A study by Ng et al. [84], [88], [89], proved that the specific energy consumption of the solar AD pilot plant is unmatched by any other desalination technologies, thus giving a value of 1.5 kWh/m³. A hybrid solar AD pilot plant has been installed in Saudi Arabia to generate 8 m³/day of a high-quality water with less energy consumption [84], [90]. Moreover, the low evaporative temperatures, even at a concentration of 250 ppt, led to insignificant scaling on the surfaces of the equipment tubes [84], [89]. Also, another interesting advantage of this novel discovery is

that it is energy efficient, requires low maintenance cost and the design complexity and this is because it has almost no major moving components. The CO₂ emission estimation is at the level of 0.64 kg/m³ [84], [89], which is far lower than the conventional units. The AD major components can be seen in the Figure 2.13 [84].



Figure 2-13: Schematic of the AD major components , illustrating the chilled and the potable water production using the available solar energy [84].

2.3.1.2 Membrane distillation (MD)

The MD relies on using a microporous, hydrophobic membrane as a contractor in order to establish a liquid-vapour equilibrium state for the desired separation to occur. This phenomenon is defined as being a thermally driven process. The driving force in the membrane distillation operation is the partial vapour pressure difference at the two sides of the micro-porous membrane. This is unlike the other technologies that are handled by the concentration, pressure or an electrical potential gradient. The membrane allows only the vapour from the pre heated solution to go through the dry pores. On the other side (permeate side), it is condensed (coolant) (Figure 2.14 [91]). A temperature range of 7-10 °C between the two sides is theoretically enough to achieve a successful separation [83]. Convective and diffusive forces are responsible for this separation to occur, and this relies on the pure water vapours high volatility, compared with sodium chloride. This process is functional at low temperatures (50-90 °C) which makes it attractive option for treating the discharged waste brines. Also, corrosion is not an issue due to the low operating temperature and pressure and the no use of metallic materials. Also, membrane distillation is an efficient

and cost-effective way to obtain fresh water using RE or low-grade waste heat, such as solar or geothermal energies [92][90]. In order to achieve this, and considering that the waste heat is not payable, then the pumping of specific energy consumption should be as low as 1 kWh/m³, which is potentially possible. The AD and MD processes share the same trait of being unaffected by high feed salinity [92][90]. The challenge now remains on finding a newer membrane technology that offers better flux and lower wettability. In addition, the MD scale up and commercialization is being affected by the fact that existing membranes have insufficient water vapour flux, relatively high conductive losses leading to unstable flux over time, high temperature polarization, low thermal efficiency and potential pore wetting. These multiple difficulties make analysing the performance and researching possible solutions very complicated due to the significant variation in the operating conditions from the low-scale to the larger-scale modules. At the present, King Abdullah University of Science and Technology (KAUST) is planning to test solar multistage MD desalination technology with temperature modulating and heat recovery units using optimised experimental data [93]. The feed water will be the Red Sea water. A comprehensive analysis of the MD and solar power unit, including the amount of energy requirement to operate such a technology are covered by [93]. More description of various solar thermal-powered MD systems can be seen in [94], [95].

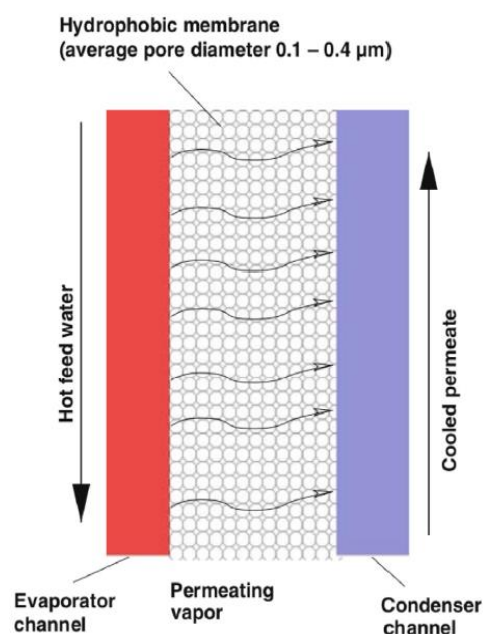


Figure 2-14: Schematic of the working principle of the MD [91].

2.4 The ORC technology

This section presents a comprehensive literature review on the ORC technology that has been conducted in the industrial and academia sector. The review highlights the advantages and disadvantages of ORC, the working fluids selection criteria, the recent theoretical and experimental conducted research, the various ORC design configurations and the ORC manufacturers and market evolution.

2.4.1 Introduction to the ORC

The conventional steam Rankine unit is a well-known technology on the large-scale power production to convert heat energy into mechanical energy. This system consists of four main components, namely pump, evaporator (steam generator), turbine and condenser. In addition to water being used as the working fluid in this cycle. The nature of the thermo-physical properties of the water in the Rankine cycle prevent its ability to recover low temperature heat sources. However, it is more economically suitable for high temperature applications, where water is heated to approximately 450 °C, which appears to be a very good compromise between the high performance and technical limits of the technology [96], [97]. In contrast, the water Rankine cycle is not economically feasible for small-scale electrical generation technology because of the inherent heat losses and high total capital cost [96], [97]. Therefore, the interest in utilizing alternative working fluids has been increasing recently as the interest of using alternative clean energy sources has been increasing rapidly. As a result, the research and development of the Organic Rankine Cycle (ORC) has been dramatically increased. The ORC consists of the same four main components (pump, evaporator (steam generator), turbine and condenser) of the steam Rankine cycle. The only difference is that the ORCs use organic fluids with low boiling temperatures that are typically between 80 °C and 350 °C as the driving element instead of water. This characteristic allows the utilisation of lower temperature heat sources to efficiently recover, and hence be convert into mechanical power. In addition, it offers an attractive performance over the conventional Rankine cycle in small-scale systems (from a few kW to several MW) [98]. Hence, there are various potential heat sources that can be considered to power ORCs, including solar energy [99], biomass/biogas energy [100], geothermal energy [101], industrial waste heat [102], gas turbine exhaust, internal combustion engine exhaust [103]. Moreover, ORCs can be applicable for use in several applications, such in the combined heat and power (CHP) applications [104], combined cooling, heating and power (CCHP) applications [105] and water desalination processes [106].

2.4.2 Thermodynamics of the ORC

The operation of the ORC technology is basically similar to the conventional steam Rankine cycle. The basic ORC configuration design is shown in Figure 2.15 [15], and the energy transfer cycles are plotted in a temperature-entropy (T-s) diagram as presented in Figure 2.16. The selected organic fluid is firstly pressurised (process 1 to 2, see Figure 2.15) using a pump. The pressurised fluid then passes through an evaporator to absorb the heat coming from a heat source in a constant pressure process. The temperature of the organic working fluid is gradually increased to its saturation temperature. In this process, the working fluid is fully evaporated and then, if necessary, superheated (process 2 to 3 see Figure 2.15). The high pressure and temperature vapour then flow across the turbine (expander) to produce mechanical energy which then, via a generator, converted into electricity. The expanded fluid then transfers into a condenser where the heat is rejected in a constant pressure process. During this process, the working fluid temperature is reduced gradually to the saturated vapour and then fully condensed (process 4 to 1, see Figure 2.15). The working liquid (fluid) is then pumped again to the same process cycle.

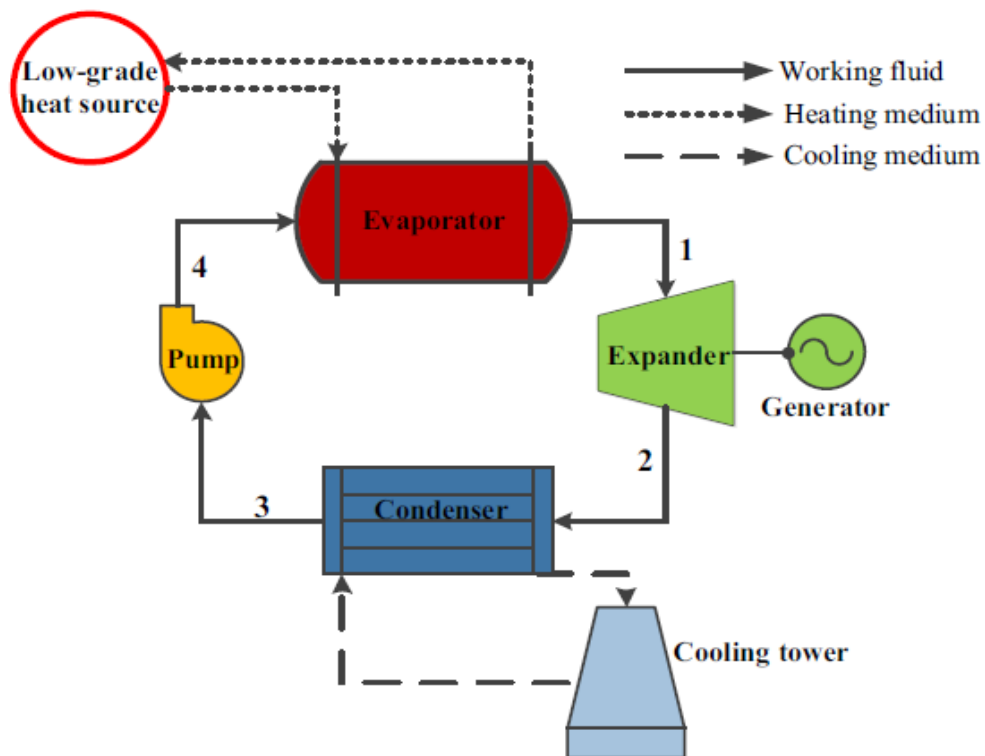


Figure 2-15: Schematic of the configuration of the basic ORC technology [15].

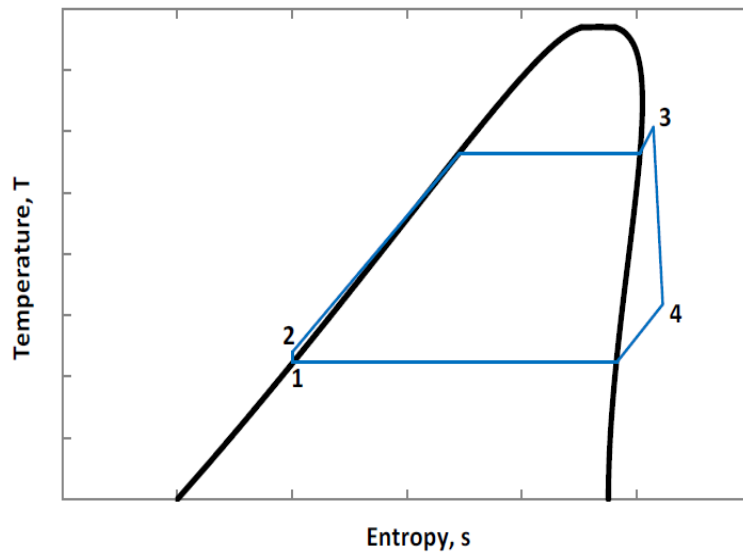


Figure 2-16: T-s diagram of a typical ORC unit.

The thermodynamic performance of the organic Rankine cycle depends mainly on the individual performance of the cycle components, the evaporation and condensation temperatures and the thermo-physical properties of the driving working fluid [107]. The available heat and sink sources define the evaporation and condensation temperatures, respectively. The cycle thermal efficiency is a critical indicator of the thermodynamic performance of the ORC unit. As it defines how much work can be generated to the relative amount of heat input to the system. Therefore, a higher system efficiency can be achieved by maximizing the evaporation temperature and minimising the condensation temperature [108]. On the other hand, the selection of the organic fluid plays an important role in the ORC performance. Therefore, the selection of the right organic fluid is essential to meet the targeted ORC thermodynamic performance as well as to be environmentally safe and chemically stable. The evaporation temperature of the organic fluid determines the evaporation pressure, while the condensation temperature of the organic fluid determines the condensation pressure. The higher differences between the condensation and evaporation pressure leads to a high pump power consumption, resulting in a similar power output and therefore a lower thermal efficiency. Thus, the higher efficiency of the individual system components leads to a better thermodynamic efficiency. In the next section, a detailed comparison between the ORC cycle and the conventional Rankine cycle will be discussed. The comparison will focus on the different working media, size and complexity of system components, operating conditions, costs and overall performance.

2.4.3 Comparison between ORCs and steam Rankine cycles

The ability of the ORC system to recover low class heat sources with low temperatures range between 80-150 °C makes it very interesting and a unique technology compared to the conventional Rankine cycle [109]. In addition, the system is applicable and flexible to any additional thermal energy system that has a temperature difference between the heat source and the heat sink varying from 30 to 500 °C [110]. This technology is therefore suitable for renewable energy conversion such as solar, biomass, geothermal, industrial waste heat and municipal solid waste. Thus, integrating renewable energy sources with the ORC system, result in a reduction in the climate change mitigation that caused by GHG emissions from the burning of conventional fossil fuels. In addition to the advantages stated above, several studies, such as [88,89], have described the benefits of using ORC over conventional Rankine cycles. A summary of these advantages are as follows:

- i. The ORC technology appears to be more economical in small-scale systems, up to a few MW, over the conventional Rankine cycle which only appears to be more economical at larger production capacity.
- ii. The superheating process is not required in the ORC technology compared to the steam Rankine cycle in order to avoid steam condensation in the expansion process. This is because of the ability of most organic fluids to remain in the wet region after the expansion process, thus preventing the turbine blades from erosion, damage and reducing the extra costs to the power cycle that is required only in the steam Rankine system.
- iii. The ORC system operates at lower evaporation pressure and temperature. Therefore, it has lower thermal stress, less safety precautions and a simple operating procedure which leads to lower equipment complexity and cost.
- iv. In the condensation process, the steam Rankine cycle operates at low pressure with typically less than 0.1 bar, which increase the possibility of the air leakage into the condenser. This increases the technical issues and therefore reduces the system performance. However, this phenomenon is unlikely to occur in the ORC technology as the condenser operates at a pressure higher than the atmospheric pressure due to the low critical temperatures of the organic fluids.
- v. The pressure ratio across the turbine is relatively low in the ORC technology and this permits single-stage turbines to be obtained. Whilst in the steam Rankine cycle, the pressure across the turbine is much higher and therefore the multistage turbine is commonly used.

- vi. The ORC organic fluid produces a lower enthalpy drop across the turbine with higher isentropic efficiencies and mass flow rates. In addition, the low enthalpy drop also produces a lower turbine speed, thus permitting a direct driving of the electrical generator without the need of a gear box.
- vii. Water treatment is not required in the ORC technology. In addition, the deaerator device that has been used to prevent the dissolved oxygen in the boiler feedwater is not required compared to the steam Rankine cycle.
- viii. In addition, the ORC system has low maintenance, simple construction, high flexibility and safety and autonomous operation compared to the steam Rankine cycle.

On the other hand, the studies [88,90] reported a few drawbacks of the ORC technology over the conventional Rankine cycle. A summary of these drawbacks are as follows:

- i. The current ORC technology has an efficiency up to 24%, which appears to be lower than steam Rankine cycles by about 30%.
- ii. The ORC requires higher pumping power relative to the turbine output power when compared to the steam cycle.
- iii. The typical water advantages over the organic fluids, and these include the high availability, being non-toxic, chemically stable, non-flammable, cheap, and environmentally friendly. Water also has a lower viscosity and that help to decrease the friction losses and pressure drops in the entire system.

In conclusion, the ORC technology appears to be more economical in small to medium-scale power generation systems and/or in the utilising of low temperature heat sources.

2.4.4 *Organic fluids*

The organic working fluids that have been used in the ORC technologies have low-temperature boiling points and high molecular weights. The low boiling point enables ORC systems to efficiently recover low grade heat sources and the higher molecular weights allow higher mass flow rates. As a result, a compact system with high expander isentropic efficiency can be designed (80-85%) [114]. There are a wide range of working fluids that cover several chemical groups, including hydrofluorocarbons (HFCs),

hydrofluoroolefins (HFOs), hydrochlorofluorocarbons (HCFCs), chlorofluorocarbons (CFCs), hydrocarbons (HCs) and fluid mixtures [102]. However, several working fluids have been already banned and many others in the future may be terminated by the international legislations due to their global environmental effects. For example, the CFCs have been phased out because of their massive ozone depletion potential (ODP) [115] and high global warming potential (GWP) [116]. As a result, HCFCs were developed to replace CFCs because of their similar interesting physiochemical characteristics [117]. However, the concern of the ODP is still present due to the availability of chlorine but at lower concentration rates. Therefore, the HCFCs are requested to be banned by the international legalisation in 2030 for the developing countries and in 2020 for the developed countries [116]. In addition, the PFCs appear to be a good alternative to the HCFCs because of their zero ODP and high thermal stability [118]. Nevertheless, it has been also scheduled to be voluntarily reduced according to the Kyoto Protocol due to their high GWP. Thus, it is essential to develop new alternative working fluids that have similar properties to CFCs, HCFCs and PFCs and have zero ODP and low GWP potentials. However, the application of the working fluids, such as in cooling, heating and power generation, will have a major effect on the selection of the appropriate working fluid. There are only few organic fluids that are currently being used for commercial ORC power plants despite the large number of the possible working fluids. The leading fluids obtained from a literature survey that categorised based on the heat source temperature and the organic fluids critical temperature, are listed in Figure 2.17.

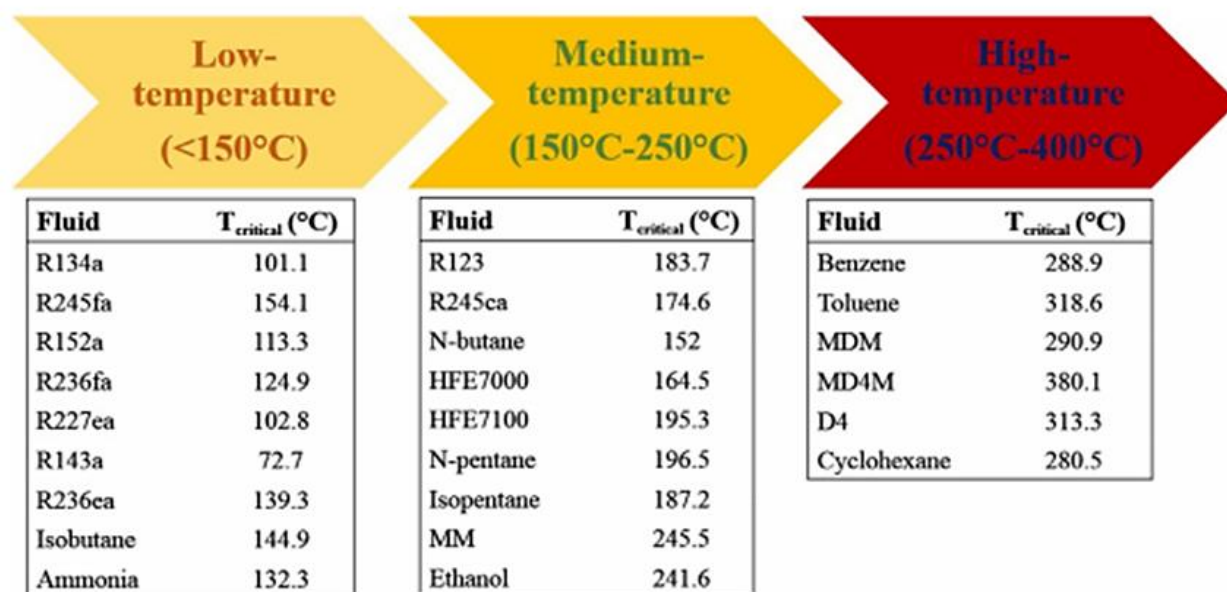


Figure 2-17: A possible working fluids integration with a different heat temperature source.

2.4.5 Working fluids categories and selection criteria

Dry, wet and isentropic are the three types of the organic working fluids. The differences between them can be described using the T-s slope diagram (see Figure 2.18). The isentropic type of organic fluids has infinitely large slope (nearly vertical), while the slope for the dry fluids is positive ($dT/ds > 0$) and for the wet fluids is negative ($dT/ds < 0$). This property affects the cycle efficiency, fluid quality and the arrangement of the operated equipment in the power production systems [119]. The utilisation of wet fluids may lead to the damage of the turbine blades due to the possibility of a liquid formation during the expansion process [120]. Therefore, to avoid this negative effect, a superheater with a large surface area is required in order to enhance the organic wet fluids temperature before entering the turbine. On the other hand, dry and isentropic fluids appear to be more applicable for the power generation cycle due to the fact that these types end in the superheated vapour region (dry region) [121]. In addition, the thermal heat of the dry and isentropic fluids at the turbine outlet can still be utilised in various applications, such as heating, cooling and water desalination. The higher the temperature difference between the pump exit and the turbine outlet, the greater the benefits from one of the above applications is achieved.

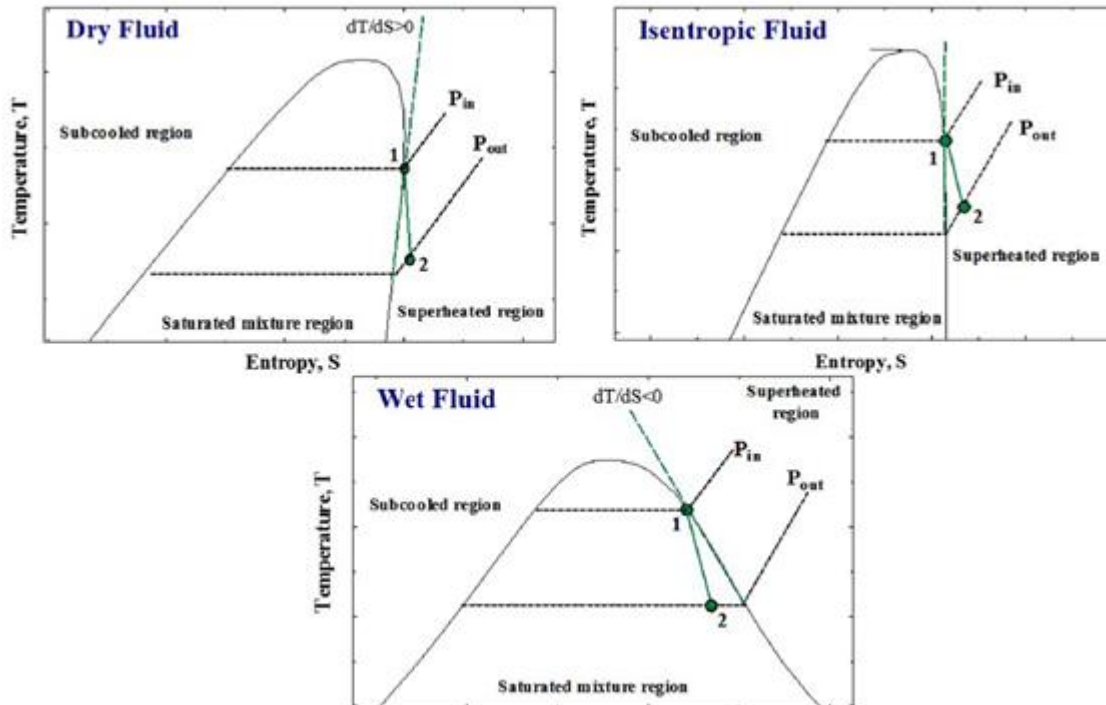


Figure 2-18: The slope diagram of the working fluid classifications: (a) isentropic, (b) wet and (c) dry.

On the other hand, the selection of an appropriate organic working fluid plays an important part in defining the entire ORC performance. It directly affects the design of the key components, operating conditions, cycle efficiency, environment and the economics of the ORC systems [122]. This explains the enormous attention on the selection of the proper organic fluids for various applications in the open literature. In general, the suitable organic working fluid should have the desirable chemical, economic, thermo-physical, safety and environmental characteristics. Additional important characteristics are as follows [88,100]:

- i. Thermodynamic performance: the selected organic fluids should provide a higher power output and high thermal efficiency.
- ii. Type of the organic fluid: the slope of the saturated vapour line showed that dry and isentropic fluids are more applicable to prevent turbine damage and avoid the additional cost of the superheating apparatus.
- iii. Molecular weight of the organic fluid: in the expansion process, a higher fluid molecular weight leads to a better mass flow rate and a low enthalpy drop. This results in a greater turbine isentropic efficiency with a smaller number of stages and a lower turbine speed.
- iv. Density of the organic fluid: a higher fluid density results in lower volume flow rates, and this is associated to the lower cost and compact system components.
- v. Thermal conductivity: a greater thermal conductivity enables high heat transfer coefficients. This results in high heat transfer in the heat exchangers at lower size and cost.
- vi. Organic fluid viscosity: the lower viscosity in the liquid and vapour phases reduces the friction losses and therefore decreases the pressure drop in the system components.
- vii. Operating pressures: the selected organic fluids should have an acceptable operating pressure. Generally, the high evaporating pressures increase the system component costs and complexity.
- viii. Chemical stability: organic fluids may decompose and deteriorate at higher temperatures. The selected organic fluid should have sufficient chemical stability within the considered temperature range.
- ix. Corrosiveness and compatibility: the working fluids should be compatible and non-corrosive with the system components.
- x. Safety: the fluid should be non-flammable and non-toxic.

- xi. Environmental concern: the environmental impact of the organic fluids, including ODP, GWP and ALT (Atmospheric Lifetime), should be considered.
- xii. Cost and availability: the fluid should have a low cost and be easily available.

Bao and Zhao have reviewed extensively the selection criteria of the working fluids and their ORC application based on the thermodynamic performance indicators, safety and environmental prospective [122]. There are several potential organic fluids which can be used in the ORC technology. However, a careful selection of the organic fluids is essential in order to obtain a higher thermal efficiency and a very good utilisation of the available heat sources. Specifically, in the biogas-based power generation, where the maximum temperature is high compared to the other ORC applications. Therefore, a thermal oil circuit is significantly important to prevent the local overheating and to avoid organic fluids from being chemically unstable [105]. The maximum operating temperature of the organic fluids is approximately 400 °C, given that the temperature of the fluid stability is considerably higher [120]. In addition, the condensation temperature is relatively high (80-120 °C) in order to allow cogeneration [75,78]. Octamethyltrisiloxane (OMTS) has been utilised in most biogas productions [14,81]. However, Drescher and Brüggemann argue that the global and the thermal efficiency of such a system is relatively low [105]. Therefore, more appropriate working fluids should be defined that take into account the availability of the high temperature heat source. In addition, it is important to consider the above-mentioned criteria other than just the thermal efficiency in the selection of the organic working fluid. There are various research studies, which have investigated the most appropriate organic working fluid. However, there is no single organic fluid have been recognised as the optimal option for all ORC technologies [124]. This is because of the characteristics, and nature of the different heat sources obtained [125], and the various cycle operating conditions assumed for evaluating the system performance [126]. Among the evaluating parameters that have been used to determine the performance of the ORC technology are, the exergy efficiency, thermal efficiency, net power output, expander outlet vapour quality and the mass flow rate.

The thermo-physical properties of the working fluid obtained has a significant influence on the system performance and economics. Therefore, appropriate criteria are required in order to select the optimal working fluid. The evaluation criteria of the selection procedure should consider the thermodynamic performance of the designed system, technical, cost, safety and environmental aspects. In the scientific literature, the most comment approach used for the fluid selection is the screening method. This approach requires building of a steady-state simulation model of an ORC system and run it with different working

fluids. The ORC working fluids can be classified into seven categories based on the chemical structure, as listed below, along with some advantages and disadvantages.

- i. The linear hydrocarbons (such as n-butane and n-pentane), hydrocarbons (such as isobutane, isopentane, toluene and benzene).
 - Attractive thermodynamic properties.
 - Flammability problems.
- ii. Perfluorocarbons fluids:
 - Inert and stable.
 - Undesirable thermodynamically.
 - Extreme molecular complexity.
- iii. Straight chain partially fluoro-substituted hydrocarbons:
 - Mostly have a zero ODP.
- iv. Siloxanes
 - Attractive thermal and physical properties (such as low flammability level, low toxicity, higher temperature heat carrier and high molecular mass).
 - Available as mixtures.
- v. Ethers:
 - Toxicity and flammability issues.
 - Undesirable thermodynamically.
- vi. Inorganics:
 - Inexpensive and extensive.
 - Less environmental impact.
 - Operational difficulties.
- vii. Alcohols:
 - Flammability problems.
 - Thermodynamically undesirable.
 - Soluble in water.

In conclusion, the advantage of isentropic and dry fluids to be in the vapour phase after the expansion process make them more attractive compared to wet fluids that can be found in the liquid–vapour mixture region after the expansion.

2.4.6 Specific cost of an ORC system

The cost of an ORC project relies on different parameters, including the scale and magnitude of the project, cost of land, cost and size of the ORC module, temperature of the heat source, labour, capital cost, cost of materials, storage/backup systems, etc. A cost of an ORC system changes relying on the technology nature, manufacturer and the capacity of the system [88,114]. The specific costs of the high temperature ORC technology that adopts toluene fluid and turbine are in the range between 1000–3000 €/kW (0.15–2 MWe). On the other hand, the low temperature ORC system using a scroll or screw usually generate a low power output production (≥ 400 kW) and appears to be more expensive, being in the range 1500–2500 €/kW (50–250 kW). Despite the massive attention that has been given currently to small-scale systems, it is still very expensive in comparison with large scale units of the MW size. Several studies are available in the literature that provide a cost indication [128], considering the extra costs because of the engineering and system hybridisation. The specific investment installation cost is calculated by multiplying the unit cost by a coefficient, namely $k=1.5-3$. A quick estimation of an ORC investment cost is illustrated in Figure 2.19 [128]. Quoilin et al. [111] argue that the k value would be higher for CHP technologies and lower for waste heat recovery units. However, it is worth noting that there has been no detailed analysis until now on the approach to reality. The available data of the installed systems and capacity in the literature varies from one author to another.

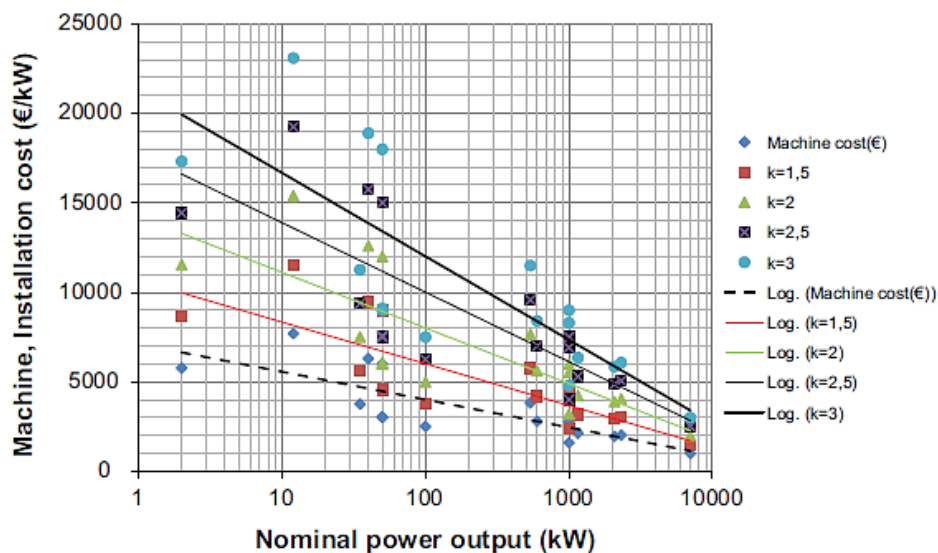


Figure 2-19: Typical machine and installation costs of the ORC technology (€ per kW) [128].

2.5 Design integration of CSP-biogas for desalination and cogeneration

A small number of studies that deals with the hybridisation of solar-biomass or biogas using the ORC technology exists in the literature. Zourellis et al. [129] designed a solar PTC-biomass system to power ORC technology for cogeneration applications (see Figure 2.20). The study concluded that the maximum generation of electrical energy was close to 15 MW using collector areas of 30 000 m². In addition, Karellas and Braimakis [130] analysed cogeneration of PTC-biomass system consisting a vapour compression unit and ORC technology. They found that the energy efficiency was approximately 5.5% and the exergy efficiency was around 7.5%. In another study, Patel et al. [131] examine a hybrid solar biomass to power ORC system for trigeneration application (cooling and heating). The analysis shows that DCS has the highest solar fraction followed by PTC and LFR. In addition to that, the minimum payback time of the system using biomass was recorded to be around 7.5 years. Yue et al. [132] developed a PTC-biomass system for cooling, heating and power production. The system was reported to be financially feasible after examining different design scenarios. Furthermore, Pantaleo et al. [133], [134] analysed a trigeneration hybrid PTC-biomass system using ORC as a bottom cycle. The studies found that the LCOE of the system lie between 100 €/MWh to 220 €/MWh. In another study, Bufi et al. [135] conducted thermodynamically optimisation of a hybrid PTC-biomass system. The study recommended using a Toluene as heat transfer fluid from the other fluid types. The maximum efficiency of the system using Toluene was recorded to reach 30.3%. In another investigation, Pantaleo et al. [136] conducted techno-economically analysis of hybrid PTC-biomass combined with ORC and Brayton power cycles. The system global efficiency noted to reach 25% with large PTC area and TES. Bellos et al. [137] developed PTC-biomass polygeneration system (cooling, heating and power). The system was optimised using steady-state conditions followed by a performance investigation during a typical year. The annual energy efficiency was recorded to reach approximately 51 %, while the annual exergy efficiency reaches close to 21.8%. Moreover, Morrone et al. [138], examined hybrid PTC-biomass for cogeneration application. They compared the operation of the system using solar-only and biomass-only. They concluded that the hybrid solar biomass allowed better energy utilisation of the low solar radiation and the system efficiency was recorded to reach 67%. In another study, Soares and Oliveira [139] analysed a hybrid PTC-biogas system for power generation application. The study concluded that the annual efficiency lies in 37.4% and the hybrid mode was the most efficient scenarios.

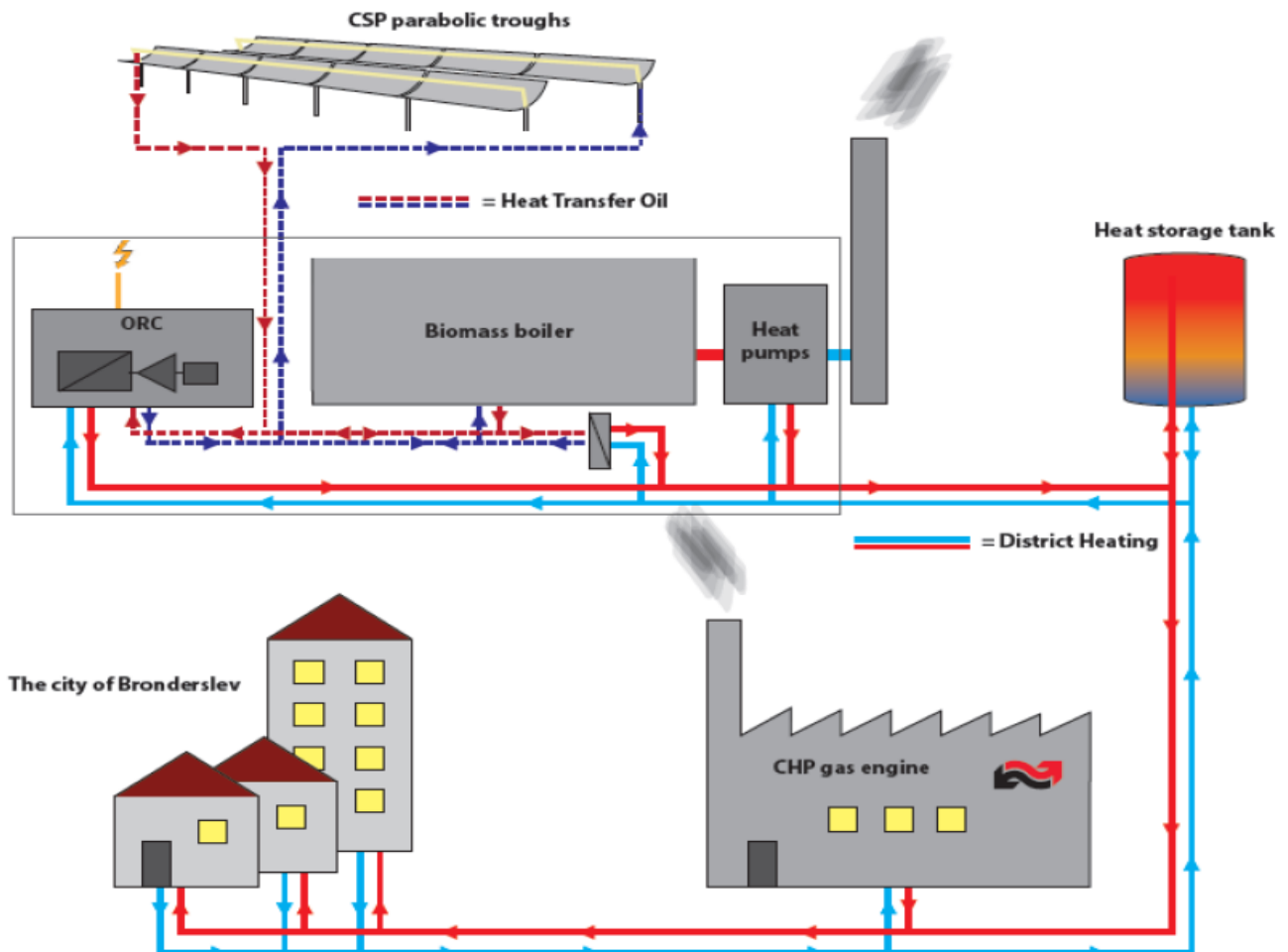


Figure 2-20: Hybrid PTC-biomass system for cogeneration heat and power [129].

For the integration PTC-ORCs for desalination application, a few numbers of study are exits in the literature that deal with this integration in terms of the design and optimisation. Delgado-Torres and García-Rodríguez [140], [141] developed PTC-ORCs for desalination application using several ORC working fluids. The study revealed that the system efficiency was recorded as 18.3%, 19.3%, and 22.3% using MM, D4 and toluene as heat transfer fluids, respectively. Delgado-Torres et al. [142] analyzed two different PTC units using ORC for three organic fluids. The freshwater production rate using toluene as fluid was calculated as 0.11 m³/h. Bruno et al. [143] investigated the integration of PTC, FPC and ETC with ORC to power desalination technology. The total system efficiency was examined for the different configurations using several heat transfer fluids. The PTC-ORC with isopentane configuration was determined to have the best performance. The system efficiency was stated to be 21%, with an ORC efficiency of 32%. Delgado-Torres and García-Rodríguez [99] used different working heat transfer fluids to study the aperture area of several solar types to drive an ORC system. The dry working fluids required the lower aperture area in compression to the wet working transfer fluids except for ammonia. In another study,

Nafey and Sharaf [144] developed solar powered desalination system using RO technology. Energy, exergy and cost analysis has been conducted to study different solar thermal collectors and heat transfer fluids. The results show that toluene and water were the best heat transfer fluids, and the PTC was the best solar collector. More specifically, PTC driven ORC and RO system using water as heat transfer media has an energy efficiency, exergy efficiency and cost of 30.47%, 22.52% and 0.95 \$/m³ respectively. More specifically, the overall efficiency, the exergy efficiency and specific capital cost of the ORC-RO with PTC and water as working fluid were 30.47%, 22.52% and 0.904 \$/m³ respectively. Furthermore, Li et al. [145], investigated the use of superheated status at the turbine inlet and the results reported that power and water production rate were at 200 kW and 40 m³/h, respectively.

Table 2.2: A review summary of the integration of hybrid solar-biomass ORC systems.

Authors	Title	Description	Ref.
Mosaffa et al. (2019)	Polygeneration system.	The energy efficiency was 70%, and exergy efficiency was around 63%.	[146]
Zourellis et al. (2018)	Cogeneration using PTC-WHR system.	The maximum generation of electrical energy was close to 15 MW.	[129]
Pantaleo et al. (2018)	Hybrid PTC-biogas system.	The total system efficiency was found at 25%.	[136]
Bellos et al. (2018)	Polygeneration using PTC-biomass system.	The annual energy was recorded at 51.3% with an exergy efficiency of 21.8%.	[137]
Morrone et al. (2018)	Cogeneration using PTC-biomass system.	The energy efficiency of the system recorded to be at 67%.	[138]
Pantaleo et al. (2017)	Trigeneration using PTC-biomass system.	The LCOE of the system lies between 100 €/MWh to above 220 €/MWh.	[134]
Pantaleo et al. (2017)	Trigeneration using PTC-biomass system.	The total investment was recorded to be financially viable.	[147]
Bufi et al. (2017)	Cogeneration using PTC-biomass system.	Employ toluene heat transfer fluid and the system efficiency was noted at 30.3%.	[135]
Karellas and Braimakis (2016)	Trigeneration using PTC-biomass system.	System energy and exergy efficiencies were 5.54% and 7.56% respectively	[130]

Table 2.3: Studies that deals with the integration of PTC-ORC for desalination and cogeneration.

Authors	Title	Description	Ref.
Delgado-Torres and García- Rodríguez (2007)	Integration of PTC-ORC system for desalination.	The system efficiency was recorded to be 18.3%, 19.3%, and 22.3% using MM, D4 and toluene as heat transfer fluids respectively.	[140], [141]
Delgado-Torres et al. (2007)	Integration of PTC driven RO system.	The freshwater production rate using toluene as fluid was calculated as 0.11 m ³ /h.	[142]
Bruno et al. (2008)	Integration of several thermal solar collectors with ORC-RO technology.	The system efficiency was stated to be 21% with an ORC efficiency of 32%.	[143]
Delgado-Torres and García- Rodríguez (2010)	Integration of solar- ORC using different working fluids.	The dry working fluids required the lower aperture area in compression to the wet working transfer fluids	[99]
Nafey and Sharaf (2010)	Energy, exergy, and cost analysis of solar-ORC-RO technology.	PTC driven ORC and RO system using water as heat transfer media has an energy, exergy and cost of 30.47%, 22.52% and 0.95 \$/m ³ respectively	[144]
Peñate and García-Rodríguez (2012)	Integration of solar-ORC system to power RO desalination.	For medium capacity, the ORC-RO systems are economically superior.	[106]
Li et al. (2013)	Integration of solar thermal collectors to power ORC-OR systems.	The results reported that power and water production rate were at 200 kW and 40 m ³ /h, respectively.	[145]
Ibarra et al. (2014)	Integration of solar thermal to power ORC-RO system.	The collector efficiency, water production capacity and the system efficiency were 60%, 1.2 m ³ /h and 7%, respectively.	[150]
Freeman et al. (2015)	Integration of solar-ORC system for the combined heat and power.	The electric power recorded at 776 kW and the capital costs lies between £2700 and £3900.	[148]
Rady et al. (2015)	Cogeneration using CSP technology.	The employment of LFR ensure a reduction in the annual operating hours of approximately 50%.	[149]
Borunda et al. (2016)	Integration of solar-ORC systems for cogeneration	The system electrical efficiency and the total system efficiency recorded as 7.5% and 60%, respectively.	[145]

2.6 Design of ANN solar/wind prediction model

Solar/wind forecasting models for renewable energy sources are usually utilised to manage stand-alone CSP systems. In many regions, such forecasting models are vital because of the high cost or even the absence of real-world data. In this context, different methods have been used in the literature to predict the solar radiation and wind speed data. In the recent years, the ANN method has been used over other statistical approaches such as non-linear correlations. This is due to the fact that ANN method has high potential to identify the relations that are not predefined and able to process large number of inputs effectively [151]. However, the integration of two ANN methods simultaneously using large meteorological data inputs for solar radiation and wind speed prediction has not really been discussed in the literature. A comprehensive literature review on the ANN methods that are used for the prediction of weather data will be presented in Chapter 3.

2.7 Optimisation methods for hybrid renewable energy systems

In the hybrid renewable energy systems, optimisation methods are used to optimise several objective functions such as sizing, control, management ...etc. In this review, the most employed optimisation techniques, which have been used in the recent years, is discussed. Figure 2.22 shows the types of the optimisation methods used for hybrid energy systems namely: classical methods, artificial methods, and hybrid methods.

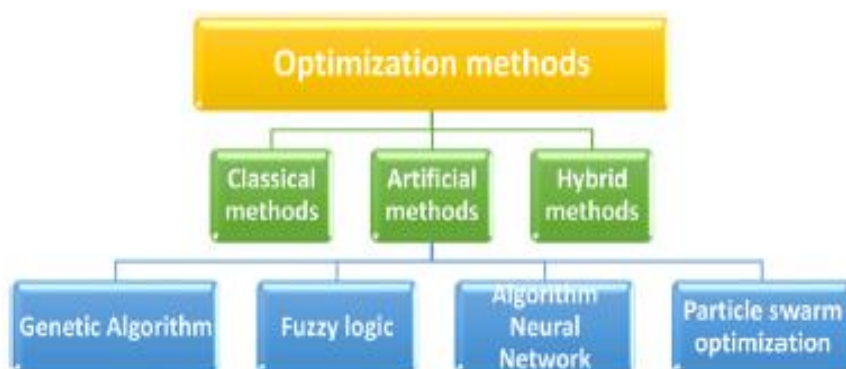


Figure 2-22: Types of the optimisation methods used for hybrid renewable energy systems.

2.7.1 *Classical methods*

In the classical methods, differential calculation is used to find the optimal solution [152]. These techniques have a limited optimisation space and rarely used in the open literature. Nevertheless, there are few studies that applied classical methods for the optimisation of the energy systems such as, multi choice goal programming [153], nonlinear programming [154], linear programming model [155], dynamic programming [156], multi-objective evolutionary algorithms [157], Mixed integer linear programming [158].

2.7.2 *Artificial methods*

In the literature several artificial methods have been implemented to size the hybrid energy systems (see Table 2.4). For example, the non-dominated sorting genetic algorithm (NSGA-II) has been utilised to optimise the hybrid PV/WT/Battery system aiming to minimise the overall costs and the power supply probability [159]. In another study, artificial neural network (ANN) has been implemented to minimise the overall life cycle costs of the hybrid PV/WT/hydrogen system [160]. In addition, fuzzy logic optimisation type has been deployed to minimize the overall system costs of the hybrid PV/WT/Battery system [161]. Particle swarm optimisation has been applied to minimise the life cycle costs of the hybrid PV/WT/Battery system [162]. Moreover, an analytical method has been used to minimise the levelized cost of energy (LCOE) of the PV/WT system [163]. An iterative approach has been used to optimise the loss of power supply probability of a PV/WT/Battery combined system [164]. A Generic algorithm has been implemented to minimise the LCOE and the initial investment of a PV/CSP system [165].

2.7.3 *Hybrid methods*

The combination of two or more algorithms is called a hybrid method. This integration offers a set of advantages to overcome the drawbacks of the single algorithm. Several hybrid optimisation methods have been used in the literature in the recent years. For example, improved harmony search-based chaotic simulated annealing [160], simulated annealing and chaotic Search, [166], harmony search-based simulated annealing [167], integration of particle swarm with genetic algorithm optimisation [168], and various other hybrid methods.

Table 2.4: A summary of the artificial methods that used to size the hybrid energy systems.

Sizing methods	System	Objective function	Ref.
Non-dominated sorting genetic algorithm (NSGA-II)	PV/WT/Battery	Minimise total cost and deficiency in power supply probability	[159]
Artificial neural network	PV/WT/hydrogen	Minimise total life cycle cost	[160]
Fuzzy logic optimisation	PV/WT/Battery	Minimise annualised cost of system	[161]
Particle swarm optimisation	PV/WT/Battery	Minimize LCC	[162]
Analytical method	PV/WT	Levelised cost of energy (LCOE)	[163]
Iterative approach	PV/WT/Battery	Loss of power supply probability	[164]
Generic algorithm optimisation	PV/CSP	Minimise LCOE and total initial investment, optimise capacity factor	[165]
Cuckoo search (CS)	PV/WT/Battery	Minimise the total costs	[169]
Artificial bee swarm algorithm	PV/WT/FC	Minimise the cost and Loss of power supply probability	[170]
A-Strong optimisation	PV/WT/Battery	Cost and reliability	[171]

2.7.4 Comparison between optimisation methods

The advantages of the optimisation methods include the ability to utilise multi objective functions and solve complex problems with high performance. On the other hand, the optimisation methods are time consuming and complex. Classical methods are useful in economical optimisation problems, however the limited space in optimisation parameters is the main concern in this type. The artificial method is a complex process and needs a high hardware performance system. The advantages of the artificial method are the high efficiency with a very good accuracy and speed. The hybrid methods using the integration of both classical and artificial methods required a complex design. However, these methods solve the optimisation problems with high speed and robustness. A summary of the disadvantages and advantages of each optimisation method can be seen in Table 2.5.

Table 2.5: A summary of the disadvantages and advantages of each optimisation method.

Methods	Disadvantages	Advantages
Classical method	Limited space in optimization parameters.	Solve multi-objective problems
	The relation to variables is linear.	Useful for investment decision
	Required discrete and continuous probabilities.	Requires less time
Artificial method	Complex process.	Maximum efficiency level
	Required memory space in long term.	Good calculation accuracy
	Required several changes.	High convergence speed
Hybrid method	Complex designing is required.	Require less time
	Solutions are extended.	Most robustness
	Code is difficult to write.	Quick convergence

In conclusion, the multi-objective optimisation of hybrid solar PTC-biogas for power and water production is rarely discussed in the literature. For the development and design of such attractive and promising integrations, multi-objective optimisation is required.

2.8 Conclusion based on the literature review

The use of renewable energy sources in power and water production is very promising in order to meet the tremendous increase in the global energy demand as well as to mitigate the harmful environmental impacts that have been caused by the immense consumption of the conventional fossil fuels. The free and abundant solar energy source makes concentrated solar power (CSP) to be a very attractive option to solve the energy crisis in the future. However, the intermittency is one of the biggest drawbacks of solar CSP power plants, but it can be compensated by utilising thermal energy storage (TES). However, the additional TES greatly increases the solar thermal power plant costs. Therefore, to solve such expensive costs and technical difficulties, hybridising solar thermal power with biogas energy is a very promising and attractive option. The hybridisation of solar CSP and biogas will not only reduce the investment and levelised cost of energy, but also enhances the power dispatchability and system reliability. Although, there are several types of solar thermal collectors, the parabolic trough collectors (PTC) appear to be the

best option due to their high performance and relatively low cost since complicated tracking technologies are not required. In addition, PTCs are also capable of achieving higher efficiency and higher solar collecting temperatures compared to flat plat collectors (FPCs). Whilst the anaerobic digestion process is widely used and is a commercially mature technology to convert waste to biogas energy. On the other hand, the Organic Rankine cycle (ORC) appears to be an interesting and flexible technology for cogeneration applications. The condensation temperature of the ORC is usually relatively high (80-120 °C), to allow cogeneration applications. Therefore, the use of integrated RE-driven low energy desalination technologies is interesting to produce portable water. Membrane distillation is an effective and cost-competitive desalination technology that can use the low-grade waste heat to produce clean water. This system is much simpler, more compact and more scalable if compared with the conventional desalination technologies. In addition, MD can operate at lower temperatures and at atmospheric pressure. Moreover, the MD technology can operate with an intermittent energy supply without any additional modifications. Therefore, the MD process does not require energy storage, which makes it more attractive for the intermittent RE sources. In addition, the ability of the ORC system to recover low-grade heat sources with low temperatures makes it a very interesting and unique technology compared to the conventional Rankine cycle. This technology is especially in demand in isolated regions where grid connection is not an economically viable option. Therefore, this system is very suitable for the renewable energy conversion, such as solar and biogas energy.

For the design of a successful and novel energy solution system, the research gaps in the literature have been identified and synthesised. The development of a novel solar/wind prediction model by integrating two different ANN methods is an attractive solution to provides a user-friendly interface that can be used efficiently in the new developed energy systems. In addition, the thermo-economics offer a powerful tool for primarily designing a stand-alone hybrid solar PTC-waste-based biogas to power ORC and AGMD for power generation and water desalination. Moreover, a thermo-economic analysis is an excellent tool to predict and optimise the performance of the sub-system components. It is clear that there exists a lack of in-depth studies on the modelling and thermo-economic design of the solar PTC, waste-based biogas, ORC, and AGMD integrated solution. Furthermore, the multi-objective optimisation procedure has not been implemented for decentralised hybrid CSP-biogas to drive the ORC and AGMD for power-water production integrated solutions. The present study aims at filling these very important knowledge gaps and adopts a comprehensive approach in assessing the feasibility of the proposed novel system. The main objectives of this thesis are as follows:

- Develop a new ANN solar radiation prediction model.
- Design of the hybrid solar PTC-biogas to power ORC and AGMD system through advanced modelling in order to efficiently integrate the system components in the MATLAB/Simulink®.
- Implement an energy, exergy, and cost analysis for the hybrid energy system.
- Construction of a sensitivity assessment on the developed system to investigate the effects of various design parameters on the thermo-economic performance.
- Conduct an in-depth simulation testing of the system in a rural region in Oman.
- Examine the detailed thermo-economic assessment of the proposed hybrid solar-waste-based biogas to power ORC and AGMD for cogeneration in off-grid applications.
- Implement a multi-objective optimisation technique using a non-dominated sorting genetic algorithm NASG-II and linking the produced results with a decision-making tool (TOPSIS) to find the best operation condition for the hybrid system to achieve the maximum power and water production with minimum possible cost.
- Assess the detailed multi-objective optimal sizing of a hybrid concentrated solar power-biogas for desalination and power generation.

CHAPTER 3: HOURLY SOLAR RADIATION AND WIND SPEED PREDICTION MODEL USING ANN

Summary

In this chapter, a novel Artificial Neural Network (ANN) model has been developed based on the Feed-forward Back-propagation (FBANN) to simultaneously predict the hourly solar radiation and the wind speed. In addition, the developed model has been implemented over the six rural regions of Oman and the accuracy of the results has been tested by calculating the mean absolute percentage error (MAPE) and the correlation coefficient (R). Finally, a comparison between the developed ANN model results and the typical meteorological correlations factors has been presented. The results shows that the R-value of the integrated ANN model for all the examined locations was higher than 0.96. On the other hand, the MAPE does not exceed 3%, which indicates that the developed ANN hybrid method has a high accuracy to predict the hourly solar radiation and wind speed. Therefore, the developed model can be further integrated with confidence with the proposed hybrid solar renewable energy system. The findings of this chapter have been published in the author's paper published in a peer reviewed journal.

3.1 Introduction

The development of the renewable energy technologies has been a vital goal in the recent years due to the energy depletion of fossil fuel, unpredictable costs and the environmental impact of the conventional fuels such as gas or coal [172]. The two main renewable energy resources projected in the literature to have the highest potential impact on the energy market share are solar and wind energy sources. To fulfill this potential, the availability of reliable weather data is essential. Nevertheless, in some remote regions, the weather data, such as the Global Solar Radiation (GSR) and wind speed does not exist. To solve such problems, where there is a lack of real-world weather data, sophisticated multivariate forecasting methods have been implemented. These technical methods are more suitable if compared with the conventional analytical forecasting methods [173]. The common and well-known multivariate method is the Artificial Neural Network (ANN). In several fields and science, ANN technology is implemented successfully [3,4]. The ANN networks consist of pattern classification, regression, prediction, recognition, approximation, optimisation, clustering, and automatic control [176]–[178].

Although the ANN approach was developed fifty years ago, only in the recent years has it been utilised to solve practical problems in software applications [179]. Researchers have shown that the ANN models, such as the Elman recurrent network and the adaptive neuro-fuzzy inference system (ANFIS) can be implemented effectively to forecast the hourly solar radiation [180]. The ANN models generally depend on two algorithms, i.e. the Levenberg-Marquardt (LM) and the back-propagation (BP) algorithms, to 'train' the models. The LM algorithm appears to obtain more accurate results when compared with the BP algorithm, this is because the LM algorithm has higher learning rate and lower estimated error between the expected and calculated values. Several ANN modeling studies have been conducted to forecast the solar radiation. For example, Ozgoren et al. [181] developed the Multi-Nonlinear Regression model and the results show that the correlation coefficient (R) was at 0.9936 with an error rate of 5.34% compared against a real data set of the adapted location in this study. In addition, Rahimikhoob [182] developed an ANN model to estimate the global solar radiation in a semi-arid environment in Iran. Moghaddamnia et al. [178], in a UK based study, developed a nonlinear model to predict the daily solar radiation. The developed model consists of the Local Linear Regression (LLR), Elman neural network, network auto-regressive (NNARX), adaptive neuro-fuzzy inference system (ANFIS), and multi-layer perceptron. However, the developed model required many trial-and-error processes. Several other studies that uses ANN to estimate the solar radiation can be found in [178], [183]–[185]. Furthermore, Kalogirou [186] investigated the feasibility of utilizing ANN in the design of renewable energy systems such as photovoltaic (PV), solar steam plant, solar/wind speed predictions and solar water heating systems. In other studies, Mellit et al. [16,17] developed the ANN model to predict the solar radiation in a period of 24 h ahead to be used later in the design of a PV solar system in Italy. The solar radiation prediction model consists of three parts: input, hidden and output layer. The findings revealed that the correlation coefficient was calculated to be higher on sunny days compared to hazy days. Wang et al. [189] developed the BP neural network to estimate the solar irradiance for a short-term by using 24-hour data. In another study, Alam et al. [190] conducted a feed-forward back-propagation network (FFBPN) Using an automatic relevance determination (ARD) approach under the Indian meteorological conditions. Moreover, López et al. [191] used ANN for predicting the hourly direct solar irradiance and reported that the relative air mass and clearness index were very useful variables. In another study, Bosch et al. [192] implemented the ARD technique successfully at high altitude locations to select the most suitable variables for the ANN model. Furthermore, the ANN methods have been also used in the past to predict the wind speed by considering the various factors that cause the speed variations [193], [194]. Despite the intermittence of the wind energy, ANN based models have proven to estimate the wind speed accurately compared to the statistical

approaches [195]. Mohandes et al. [196] used the ANN model considering ten minutes of data to implement multi-step forecasting. In another study, Flores et al. [197] utilised a back propagation technique for the ANN model as a control algorithm to determine the wind speed and estimate the active power. Paras Mandal et al. [198] used the hybrid intelligent algorithm ANN method to estimate the wind power based on the meteorological conditions. The predicted data are then optimised using the particle swarm optimisation (PSO). In another study, Carolin Mabel and Fernandez [199] used the generation hours, wind speed and the relative humidity as input variables to develop the ANN model. The study showed a satisfactory result compared to the obtained real data. Li [200] utilised a recurrent multilayer perceptron neural networks (RMLP) to predict the wind power generation and to train the network Kalman filter-based back-propagation algorithm was used. The results showed that the model performance was more suitable for long-term prediction compared to short terms. Barbounis and Theocharis [201] used an online 'learning' algorithm and found a better result accuracy in implementing the recurrent neural networks compared to the time-series and atmospheric models. A new method has been developed by Riahy and Abedi [202] using the linear prediction approach and the results show an improved outcomes but the model was less steady. In another study, Yayla and Harmanci [203] developed a novel ANN model for the wind speed prediction application by utilising the hourly wind speed data from two meteorological measurement stations in Turkey. Adedeji et al. [204] developed a hybrid model using the genetic algorithm and PSO to predict neurofuzzy wind power.

The literature shows that the ANN is an effective meteorological data forecasting tool, especially for solar and wind energy. The effective employment of any ANN model consists of the utilisation of the training data, the specification of the training method, the computational resources used for the algorithms, the low-cost and simple measuring system for the used study field. The current study proposes and applies a new multi-dimensional modelling approach using ANN for the hourly solar radiation and wind speed data prediction over the south of the Arabian Peninsula.

The proposed model is the first attempt to simultaneously combine two ANN models by using a large amount of meteorological input data for both the solar radiation and wind speed prediction. The constructed model requires only three input parameters, and it can estimate the solar radiation and the wind speed data simultaneously with a very high accuracy.

As a result, the model offers a user-friendly interface that can be integrated later in the process of designing the proposed cogeneration hybrid solar-biogas energy systems. Consequently, this model facilitates the implementation of renewable energy technologies, especially in the remote regions where the collection of weather data is very challenging. Meanwhile, the accuracy of the model has been tested

by calculating the mean absolute percentage error (MAPE) and the correlation coefficient (R). Therefore, the model developed in this study can provide accurate weather data and inform decision makers for future instalments of energy systems.

3.2 Locations of the study

The research aims to investigate the capability of a newly developed ANN based model to predict the hourly solar radiation and wind speed in Oman. This country is located at the southern part of the Arabian Peninsula bordering the Gulf of Oman, the Arabian Sea, the Arabian Gulf, as well as the United Arab Emirates, Yemen, and Saudi Arabia. This geographical location has granted Oman important access to one of the largest energy corridors in the world. The climate in Oman is hot and dry in the desert, and humid and hot along the long coastline. Yearly, a strong southwest summer monsoon is expected in Oman and that is usually from May to September. Oman's economy depends mostly on crude oil exploration and extraction as in most of the Arabian Gulf countries.

Oman has one of the highest solar radiation densities in the world. Solar energy has the potential to meet the entire Omani demand for electricity as well as being able to export part of it to the Cooperation Council for the Arab States of the Gulf, a political and economic union consisting of Bahrain, Kuwait, Oman, Qatar, Saudi Arabia, and the United Arab Emirates. Oman receives daily solar radiation between 5500 and 6000 Wh/m²/day in July and 2500 to 3000 Wh/m²/day in January [205]. Furthermore, Oman has a mean wind speed of 6m/s, which in theory is sufficient for clean energy generation [206].

The developed model has been used to predict the hourly wind and solar radiation in six sites in Oman, namely Al Khuwaimah, Al Halaniyat, Al Mazyounah, Haitam, Madha and Methane. These rural regions are suitable for the installation of off grid renewable energy systems as grid connection is not a viable option due to the great distances [207]. These rural regions can be seen in Figure 3.1. In addition, a detailed geographical and meteorological information of the selected regions is shown in Table 3.1.



Figure 3-1: Forecast locations map of Oman.

Table 3.1: The geographical and meteorological information of the Omani's locations [208], [209]

	Al khuwaimah	Al Halaniyat	Al Mazyounah	Haitam	Madha	Methane
Latitude	21.39 N	17.49 N	17.83 N	18.83 N	18.59 N	18.59 N
Longitude	59.20 E	55.97 E	52.62 E	56.92 E	56.33 E	52.45 E
Terrain form	Moderate to flat desert	Island (generally rugged and barren)	Moderate to flat desert	Flat, and desert, located in a coastal region	Mostly flat area located in a coastal region	Moderate to flat desert located near to the Yamen border
Terrain elevation	10 m	5 m	526 m	9 m	41 m	314 m
Geographical area	8.2 Km ²	56 Km ²	58 Km ²	86.1 Km ²	3.27 km ²	22.2 Km ²
Climate	Desert: Hot summer and warm winter	Hot, humid weather in summer and warm weather in winter.	Desert: Hot summer and warm winter	Desert: hot, humid weather in summer and cold weather in winter.	Hot summer and warm winter	Desert: hot, dry weather in summer and cold weather in winter.
Air temperature	13 to 45 °C	19 to 36 °C	12 to 44 °C	19 to 36 °C	20 to 38 °C	12 to 45 °C
Direct normal irradiation (DNI)	5.7 to 6 kWh/m ²	5.5 to 6.2 kWh/m ²	6.2 to 6.6 kWh/m ²	5.6 to 6.2 kWh/m ²	5 to 5.5 kWh/m ²	6.0 to 6.5 kWh/m ²
Global horizontal irradiation (GHI)	6.0 to 6.4 kWh/m ²	6.2 to 6.4 kWh/m ²	6.5 to 6.8 kWh/m ²	6 to 6.4 kWh/m ²	5.8 to 6.0 kWh/m ²	6.4 to 6.6 kWh/m ²
Diffuse horizontal irradiation (DIF)	1.6 to 1.8 kWh/m ²	1.7 to 1.9 kWh/m ²	1.3 to 1.5 kWh/m ²	1.67 to 1.88 kWh/m ²	1.75 to 1.99 kWh/m ²	1.35 to 1.55 kWh/m ²
Average wind speed at 10m	4.9 m/s	5.5 m/s	2.8 m/s	4.8 m/s	2.9 m/s	2.7 m/s

3.3 Methodology

The aim of this work is to investigate the capability of a developed meteorological forecasting model using ANN techniques to predict the hourly solar radiation and wind speed data. The estimated data are the global horizontal irradiation (GHI), the direct normal irradiation (DNI), the diffuse horizontal irradiance (DIF), the wind speed, and the wind direction (WD). The implemented model is a two-layer Feed-forward Back-propagation Artificial Neural Network (FBANN). The novelty of the work is the integration of two FBANN models. The first accepts as inputs the day, month and clock time and it is constructed to predict the necessary environmental parameters that subsequently serve as input to the second model to predict solar and wind data simultaneously. In this model, it is possible to accurately predict important solar/wind data by introducing only three parameters, i.e., day, month, and clock time (current time increment 1 to 24 hrs). In this study, the direct prediction method is used to model the solar and wind data. This technique makes the model more accurate by using previous measured data instead of meteorology factors. To obtain an accurate forecasting model, the input variables should be carefully selected. For solar data, the intensity of sunrays is mostly a function of the incident angle at the Earth's surface (altitude and azimuthal angles). In addition, the irradiance intensity at a given location depends on the terrain, latitude, season, time of the day, and atmospheric conditions such as cloud cover and water vapour. For the wind data, the local conditions may affect the wind profile. To illustrate this point, the wind speed is estimated by the pressure differences and boundary conditions, i.e., the terrain. These mostly occur due to the variations in some of the weather parameters such as air temperature, perceptible water, and relative humidity. Interestingly, the ANN model can include all the input parameters, including relevant and irrelevant parameters. Thus, the proposed model simultaneously integrates two ANN models for the solar radiation and wind speed prediction. In this regards, Table 3.2 shows the input meteorological parameters of the solar radiation and wind speed that issued in this study.

Table 3.2: Types of input meteorological parameters.

Input solar radiation parameters	Input wind speed parameters
Clock time	Clock time
Day	Day
Month	Month
Altitude angle	Air temperature
Azimuth angle	Relative humidity
Cloud identification quality	Atmospheric pressure
	Perceptible water

3.3.1 Meteorological data collection

The one-hour data resolution of the meteorological parameters (the day number, the month number, the current time, the cloud identification quality, the sun altitude angle, the sun azimuth angle, the air temperature at 2m, the relative humidity, the atmospheric pressure, and the perceptible water) of Oman for a wide time span of 20 years, i.e., from 1999 to 2019, have been introduced as inputs to the ANN model. This data was acquired from Solargis™ and it contains 182,617 samples from designated regions in Oman. The selected locations are Al khuwaimah, Al Halaniyat, Al Mazyounah, Haitam, Madha and Methane. Table 3.3 summarises the main features of the database. In addition, the geographical coordinates of the locations are indicated in Table 3.4.

Table 3.3: Characteristics of the database.

Description	Value
Weather database	Solargis™ company.
Weathers stations	Al khuwaimah, Al Halaniyat, Al Mazyounah, Haitam, Madha and Methane.
Period of measurement	01/01/1999 to 31/10/2019
Number of samples	Oman: 182617
Sampling period	1-hour
Measured variables	Day number, Month number, Current time, Cloud identification quality, Sun altitude angle Sun azimuth angle, Air temperature at 2 m, Relative humidity, Atmospheric pressure, Perceptible water.

Table 3.4: Geographical coordinates of the selected stations.

Station	Latitude	Longitude	Altitude (m)
Al khuwaimah	21.39	59.20	10
Al Halaniyat	17.49	55.97	5.0
Al Mazyounah	17.83	52.62	526
Haitam	18.83	56.92	9.0
Madha	25.29	56.33	56
Methane	18.59	52.45	314

3.3.2 The developed ANN prediction model

The successful implementation of any ANN model requires the specification of an optimal training method, high accuracy in the predictions which is typically achieved by using a vast amount of training data (as in the present study), and the utilisation of a wide range of computational resources for training algorithms. To this purpose, the FBANN model has been developed to correlate the future solar and wind indices with historical data of several meteorological parameters. The ANN's basic structure is made up of various interconnected fundamental processing units (known as neurons or nodes) that are usually grouped into three layers, i.e., input, hidden and output layers.

The computational capabilities are evaluated based on the connection weights, network architecture and training algorithm. Every node of an ANN takes input values, multiplies them by connection weights corresponding to each node and sums all the products plus a value of constant bias. Then, summation transmits a transfer function and generates the node output. The Feed-forward Artificial Neural Network (FANN) is the type of neural network that is most often implemented. In the two-layer FANN architecture, the processing of computations executes in the forward direction that is from input nodes to output nodes. Technically, the two-layer FANNs have input and output neuron layers along with one or more hidden layers. The primary role of the neurons in the hidden layers is to create functional connections between the inputs and the outputs of the network. The typical structure of a two-layer FANN is shown in Figure 3.2.

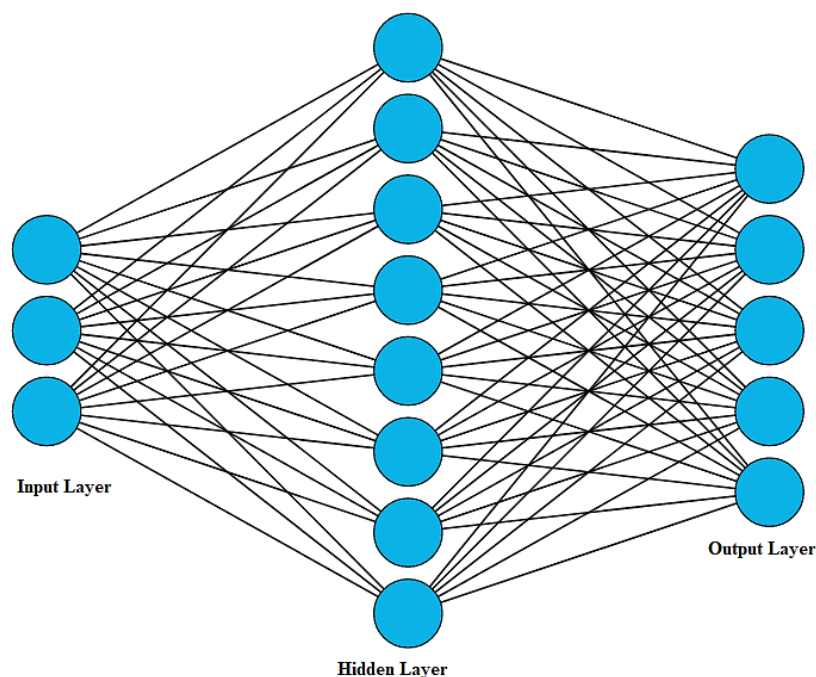


Figure 3-2: A typical feed-forward artificial neural network.

The BP techniques, such as the Levenberg– Marquardt and the Gradient descent, are well-known training algorithms and they are usually trained with FANN. BP training algorithms are considered ideal for two-layer FANNs. A BP algorithm is essential to reduce the mean square difference between the network and the needed output [210].

Two FBANN models, namely FBANN-1 and FBANN-2, have been built and integrated to evaluate the solar and wind data. In the FBANN-1 model, three parameters including day of the month, month of the year and clock time are introduced as input indices. The neurons/outputs (meteorological variables herein) of the FBANN-1 include the cloud identification quality, the sun altitude angle, the sun azimuthal angle, the air temperature at a height of 2 m, the relative humidity, the atmospheric pressure, and the perceptible water.

These outputs have been correlated with the weather data acquired from Solargis™. The general architecture structure of the proposed two-layer FBANN-1 is shown in Figure 3.3. In the FBANN-2 model, both the input and the output parameters of the FBANN-1 serve as input indices. Therefore, the total number of neurons in the input layer of the FBANN-2 is ten, as illustrated in Figure 3.4; the day, the month and the clock time are user defined while the remainder are calculated by the FBANN-1. The number of neurons of the output layer of the FBANN-2 is five, including the *GHI*, the *DNI*, the *DIF*, the wind speed and the *WD*. Accordingly, the purpose of this model is to provide a reliable tool that can forecast the hourly solar radiation and wind data with high accuracy.

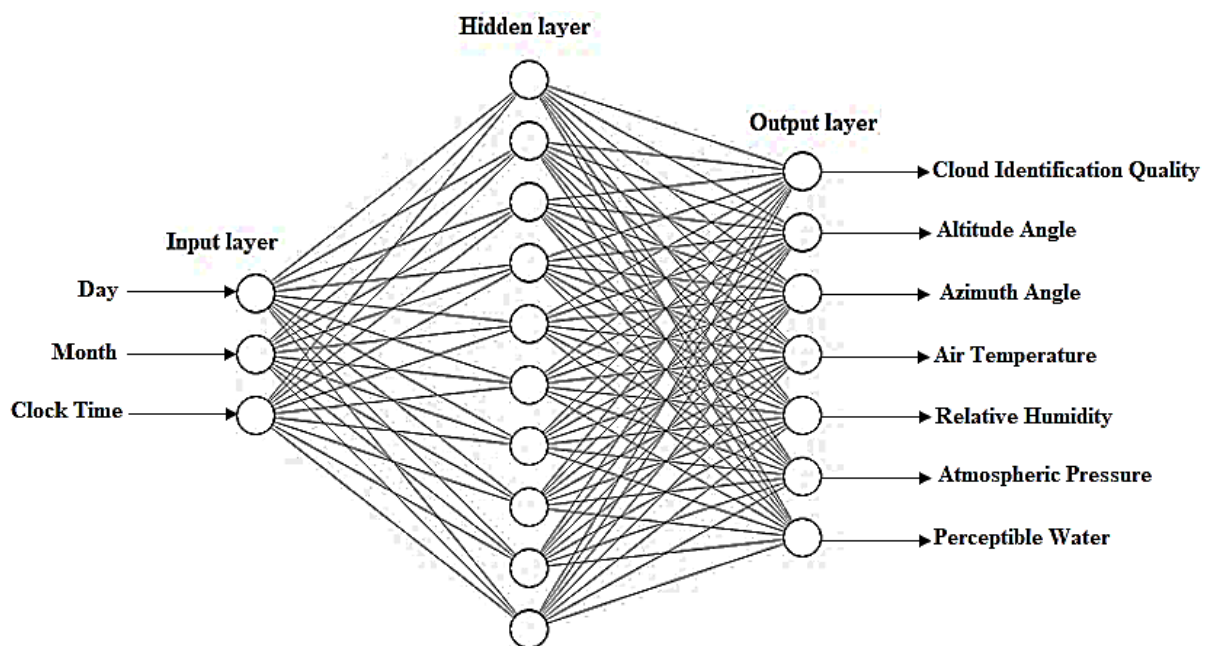


Figure 3-3: The architecture structure of the developed FBANN-1 solar/wind prediction model.

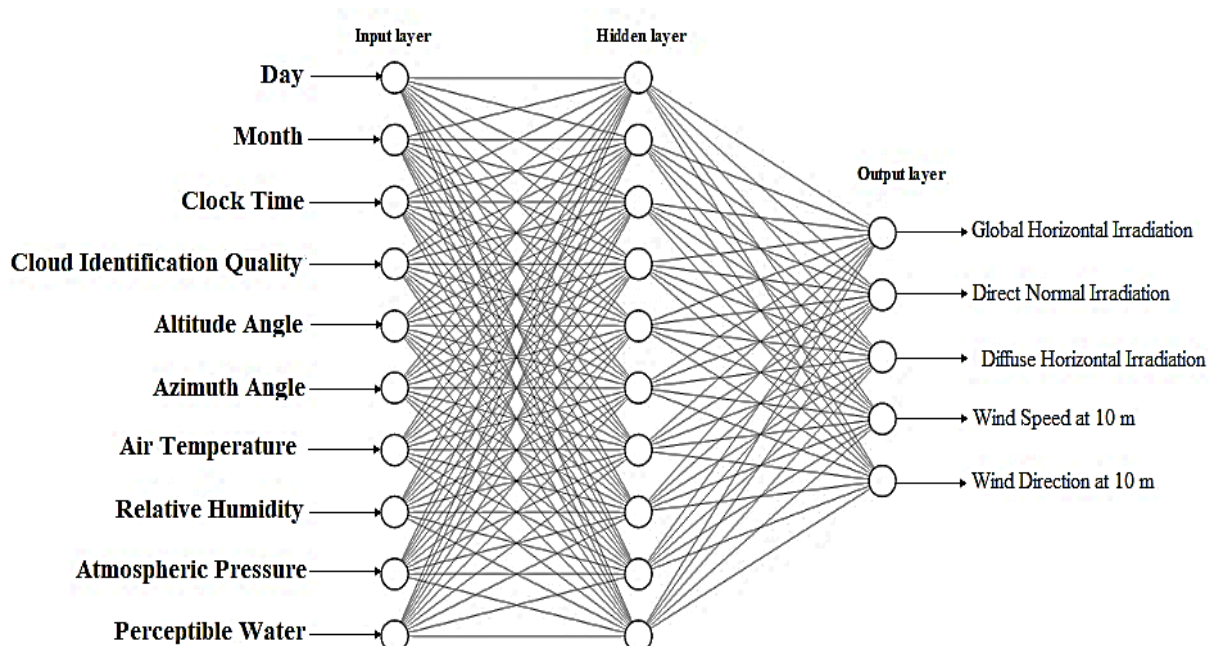


Figure 3-4: The architecture structure of the developed FBANN-2 solar/wind prediction model.

In this study, a two-layer of feed-forward back-propagation neural network with sigmoid hidden neurons and linear output neurons has been used to fit the examined multi-dimensional mapping problem; provided that the data used is consistent and enough neurons exist in the hidden layer, this technique can generate reliable results. The network has been trained with either the LM or the SCG back-propagation algorithm. The first step for developing the FBANN model is the selection of input parameters to correlate the future solar and wind indexes with historical data of these parameters. As mentioned previously, these parameters are the day number, the month number, the clock time, the cloud identification quality, the sun altitude angle, the sun azimuthal angle, the air temperature at a height of 2 m, the relative humidity, the atmospheric pressure, and the perceptible water. The second step is the training of the FBANN to determine the desired output.

The ANN solar/wind prediction model has been developed using the nested network fitting tool, i.e., *nftool*, in MATLAB/Simulink®. The *nftool* solves an input-output fitting problem using a two-layer feed-forward neural network trained with either the LM or the SCG algorithm. The input and target data are divided into 85% training, 10% validation, and 5% testing and is mapped in the range of -1 to 1. The testing data have no effect on the training process and provides an independent measure of network performance during and after training. The validation data identifies the potential of network generalisation and cease training when generalisation ends. The training data makes network weight adjustments according to the calculated error by training ANN models with either

the LM or the SCG algorithm. The Simulink diagram and stepwise procedures for implementation of the *nftool* are shown in Figures 3.5 and 3.6, respectively.

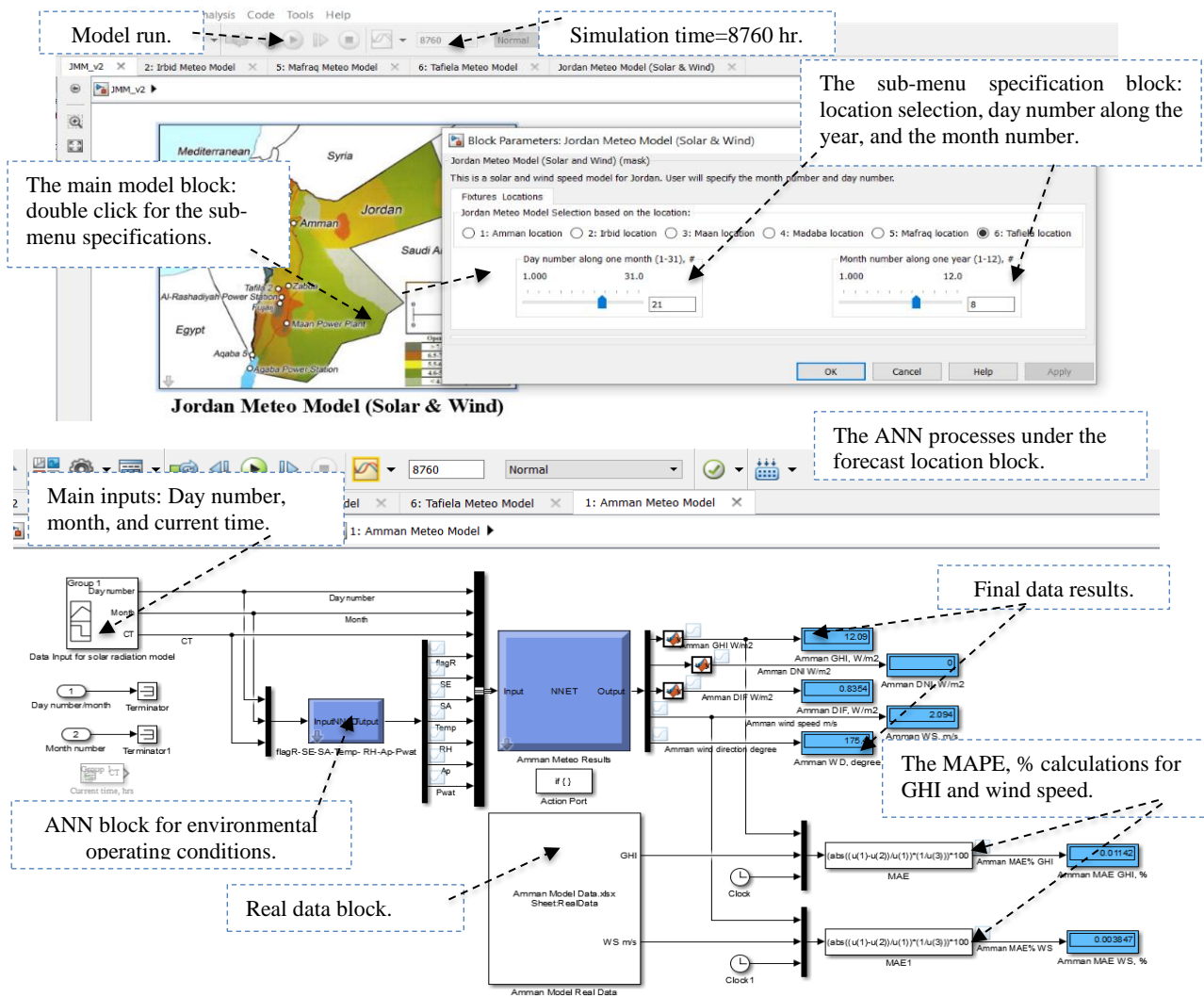


Figure 3-5: Simulink diagram of the developed ANN model.

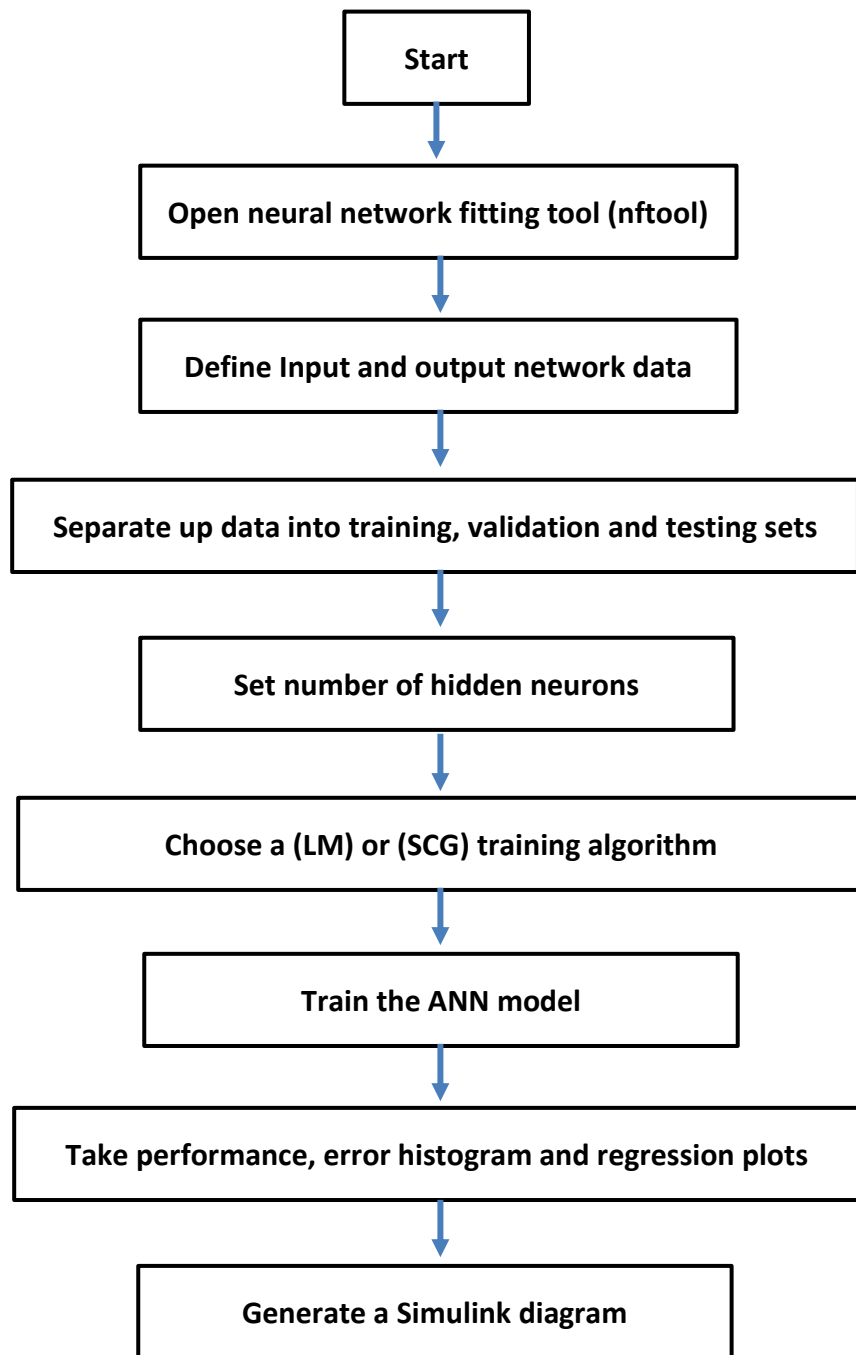


Figure 3-6: The nftool implementation steps in MATLAB/Simulink®.

3.3.3 The Statistical Indicators

It is of high importance to compare real data vs the ANN results in order to test the accuracy of the proposed model. Therefore, two types of statistical indicators have been used in this study. The first is the correlation coefficient which is presented in equation (3.1). The R has been used herein to measure the correlation between outputs and targets. An R value of 1 means a close relationship while a value of 0 signifies a random relationship. The R is defined as [211], [212]:

$$R = \frac{\sum_{i=1}^n (y_i - \bar{y}_i) (\hat{y}_i - \bar{\hat{y}}_i)}{\sqrt{\sum_{i=1}^n (y_i - \bar{y}_i)^2} \sqrt{\sum_{i=1}^n (\hat{y}_i - \bar{\hat{y}}_i)^2}} \quad (3-1)$$

where y_i and \hat{y}_i are the predicted and desired output values respectively, \bar{y}_i and $\bar{\hat{y}}_i$ are the mean of the predicted and desired output values, respectively and n is the number of data samples. The second statistical indicator is the *MAPE*. The *MAPE* is another index that measures the accuracy of a forecast model. It measures this accuracy as a percentage and can be calculated as the average absolute percentage error for each period minus the actual values divided by the actual values. The following equation represents the *MAPE* where n is the iteration number and represented as the simulation time domain (8760 h), X_n is the calculated data by the ANN and Y_n is the real data [213].

$$MAPE = \left(\frac{1}{n} \sum_{t=1}^n \left| \frac{X_n - Y_n}{X_n} \right| \right) \times 100 \quad (3-2)$$

3.4 Results and Discussions

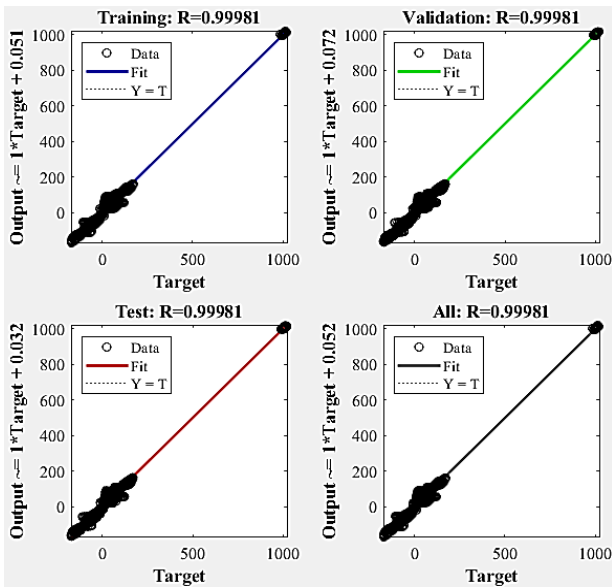
The input and target data are divided into three kinds of samples, namely, 85% training (155,223), 10% validation (18,262), and 5% testing (9131). The number of neurons in the fitting network's hidden layer is 10. As mentioned earlier, this study intends primarily to estimate the hourly, global horizontal, direct normal and diffuse solar radiation as well as the wind speed and direction. Therefore, the total number of neurons in the output layer has been assigned a value of 5. Generally, finding out the number of neurons in the fitting neural network's hidden layer as well as the number of hidden layers are not as simple as it is for the input and output layers. Herein, one hidden layer back-propagation neural network with ten neurons is adopted. By using 10 neurons both the computational speed and the accuracy of the results improve. Accordingly, the structure of the FBANN-1 and FBANN-2 model, as depicted earlier in Figures 3.3 and 3.4, are designed as 3-10-7 and 10-10-5, respectively. The inputs and outputs parameters of the FBANN-1 model are considered as the inputs to the FBANN-2, which is used to forecast the

solar/wind data. In principle, it is difficult to identify 10 parameters each time to estimate the solar and/or wind data. The main reason for using two ANNs is to reduce the number of inputs into the entire model to three, i.e., the current time, day number and month number, and thus to develop a user-friendly model. Consequently, the FBANN-1 is mainly utilised to evaluate the meteorological parameters with high degrees of accuracy.

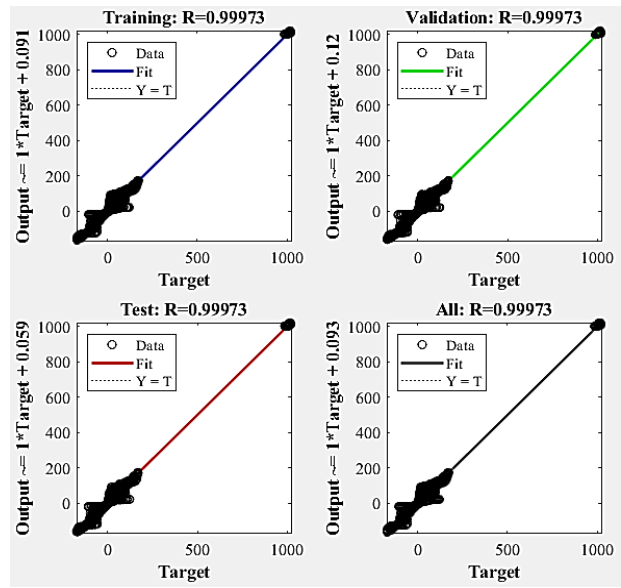
The R-value is calculated for training, validation, and testing results. The output acquired from the model should ideally match the targets, i.e., desired network output. Hence, a slope of 45° implies perfect fitting. In cases where the validation error no longer changes, the training ceases immediately. As shown in Figures 3.7 to 3.12, the FBANN-1 has achieved very high values of *R* and thus very accurate predictions. The regression plot for training, validation, testing, and all data are indicated in Figures 3.7 to 3.12. Within the main body of the chapter the results of selected six representative rural regions are presented, i.e., Al khuwaimah, Al Halaniyat, Al Mazyounah, Haitam, Madha, and Methane. The highest regression values (*R*) for training, validation, testing, and overall datasets using FBANN-1 with the LM back-propagation algorithm over all locations are above 0.999. The *R* values for training, validation, testing, and overall datasets using the FBANN-1 model based on the LM algorithm, which is obtained for all locations are above 0.999. It is observed that the FBANN-1 model predicts the meteorological parameters very closely to the measured values.

On comparing the LM algorithm results with that of the SCG algorithm, it can be observed that the FBANN-1 model with the LM algorithm gives slightly more accurate results than the SCG algorithm. As it can be seen from the scatter plots in Figures 3.7 to 3.12, the *R* values for training, validation, testing, and whole datasets using FBANN-1 based on the LM algorithm in Madha, for example, are 0.99983, 0.99983, 0.99983 and 0.99983, respectively and 0.99978, 0.99978, 0.99977, and 0.99978 when using FBANN-1 based on the SCG algorithm for training, validation, testing, and whole datasets, respectively.

Furthermore, most of the data input points of the SCG algorithm of the regression analysis fall closer to the fit line compared to the LM algorithm at all locations, as depicted in Figures 3.7 to 3.12. It can be seen from the scatter plot that all regression points for selected regions are located along the diagonal line, where some regression points deviate from the fitting line. The large sample for Oman may have contributed to the increase in the fitting accuracy. The FBANN-1 model has been analysed using three input parameters. From the Figures 3.7 to 3.12, it is demonstrated that a high agreement between the targets and output solar/wind data has been achieved. Furthermore, the *R*-value is remarkably high throughout the training, and this indicates a very good performance and strong correlation of the trained data.

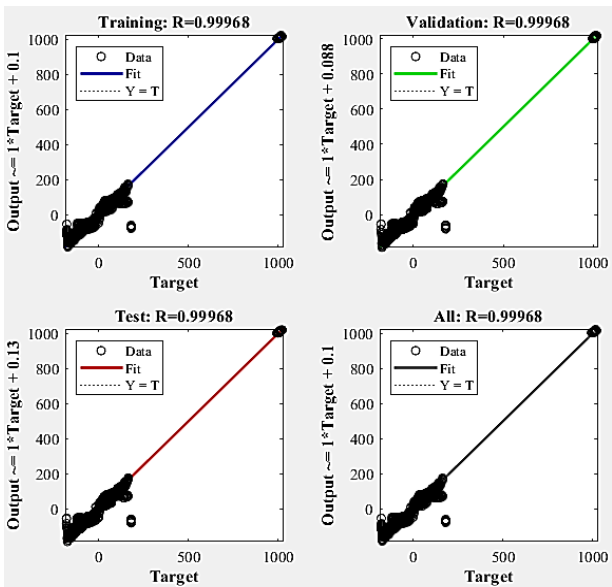


(a) LM regression plot.

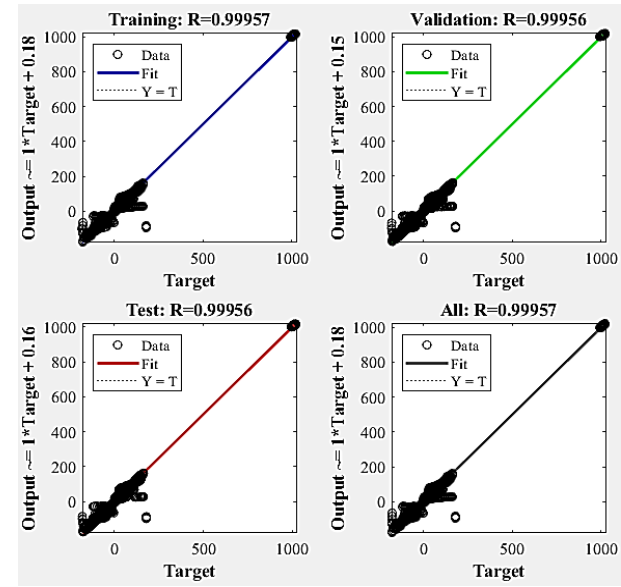


(b) SCG regression plot.

Figure 3-7: Regression plot of training, validation, testing, and all for FBANN-1 at Al khuwaimah.

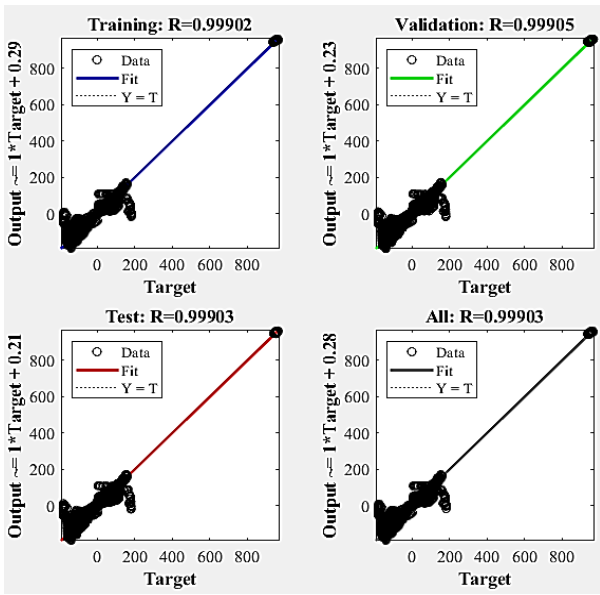


(a) LM regression plot.

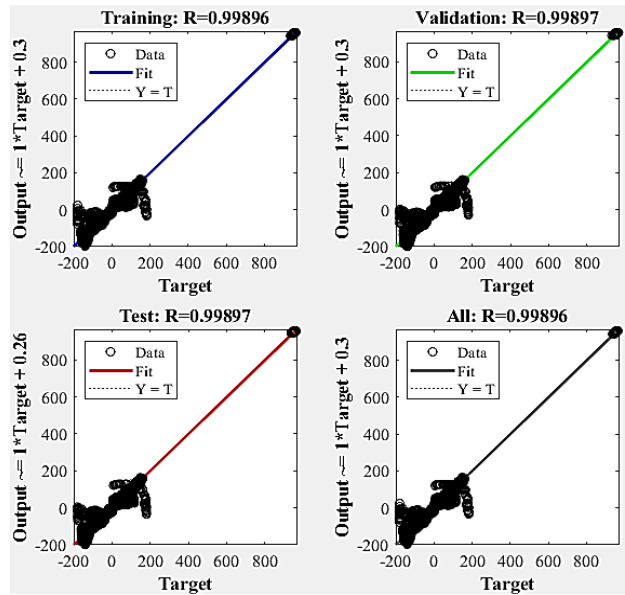


(b) SCG regression plot.

Figure 3-8: Regression plot of training, validation, testing, and all for FBANN-1 at Al Halaniyat.

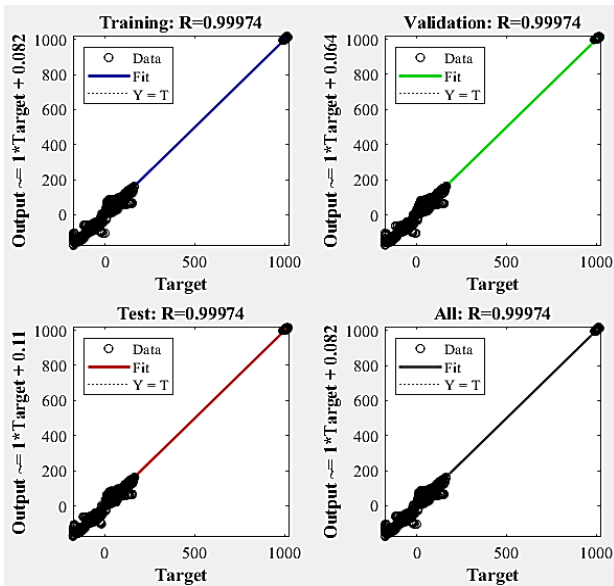


(a) LM regression plot.

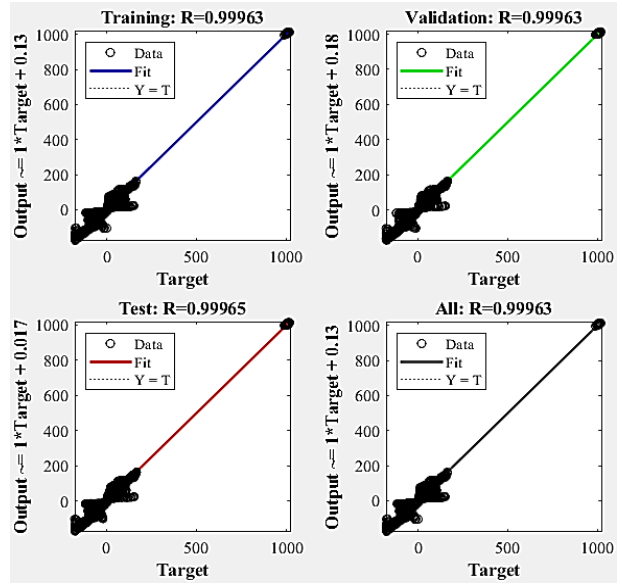


(b) SCG regression plot.

Figure 3-9: Regression plot of training, validation, testing, and all for FBANN-1 at Al Mazyounah.

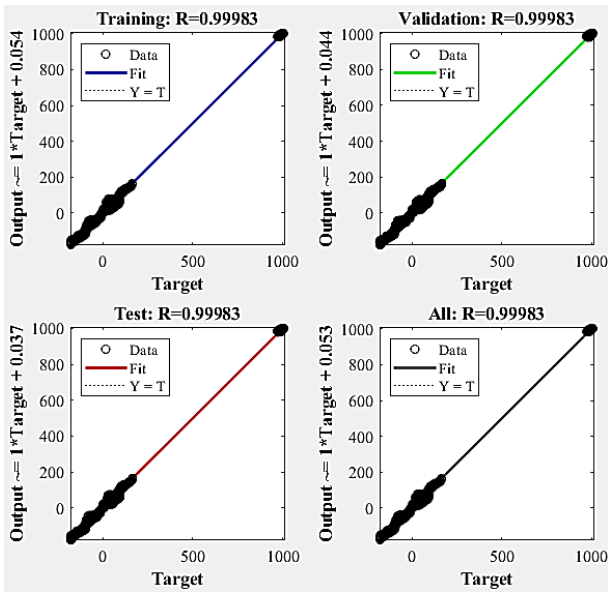


(a) LM regression plot.

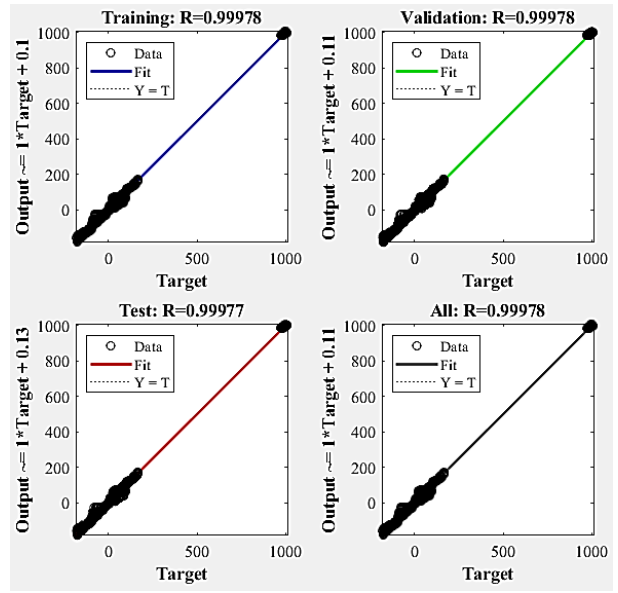


(b) SCG regression plot.

Figure 3-10: Regression plot of training, validation, testing, and all for FBANN-1 at Haitam.

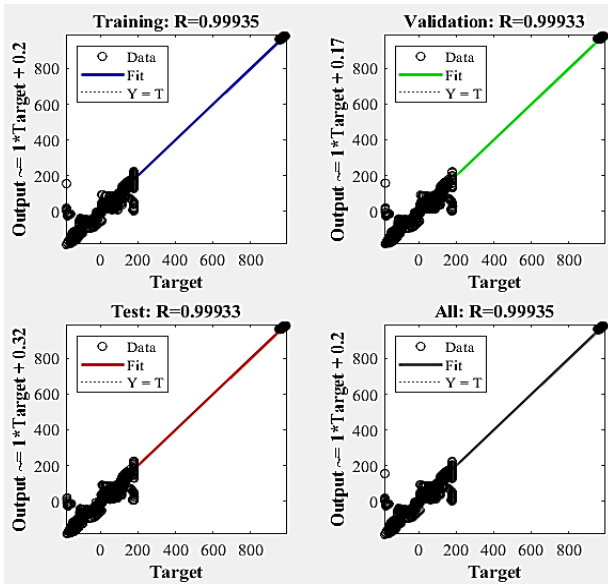


(a) LM regression plot.

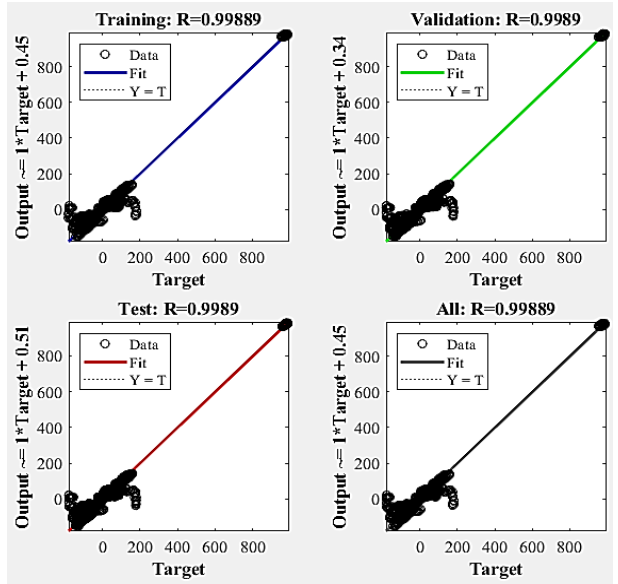


(b) SCG regression plot.

Figure 3-11: Regression plot of training, validation, testing, and all for FBANN-1 at Madha.



(a) LM regression plot.



(b) SCG regression plot.

Figure 3-12: Regression plot of training, validation, testing, and all for FBANN-1 at Methane.

The R values for the training, validation, testing, and overall datasets using FBANN-2 with LM and SCG back-propagation algorithm for all selected locations in Oman are depicted in Figures 3.13 to 3.18. Within the main body of the chapter, the results of selected six representative rural regions are presented, i.e., Al khuwaimah, Al Halaniyat, Al Mazyounah, Haitam, Madha, and Methane.

In Haitam, the remarkable R values are observed as 0.97478, 0.97542, 0.97445, and 0.97483, respectively. Based on the R values, it can be concluded that there is a very good match between real and simulated data. Al Mazyounah is the second-best rural regions with all datasets using the FBANN-2 with the LM back-propagation algorithm of 0.973472 R-value, while Al khuwaimah with the SCG algorithm of 0.9713 R-value. In addition, the Madha region was less accurate with all datasets with R- values of 0.96892. The R-values are for all rural regions are above 0.97 and this can be observed throughout the whole dataset. This demonstrates that the solar/wind outputs from the FBANN-2 model is close to the measured value, showing that the FBANN-2 model is accurate enough to be utilised with confidence for predicting the solar/wind data.

Comparison of the LM algorithm results with those of the SCG shows that the LM has relatively higher accuracy than the SCG. The most obvious finding to emerge from the simulations is that the FBANN with the LM is the most efficient model in the solar and wind prediction process.

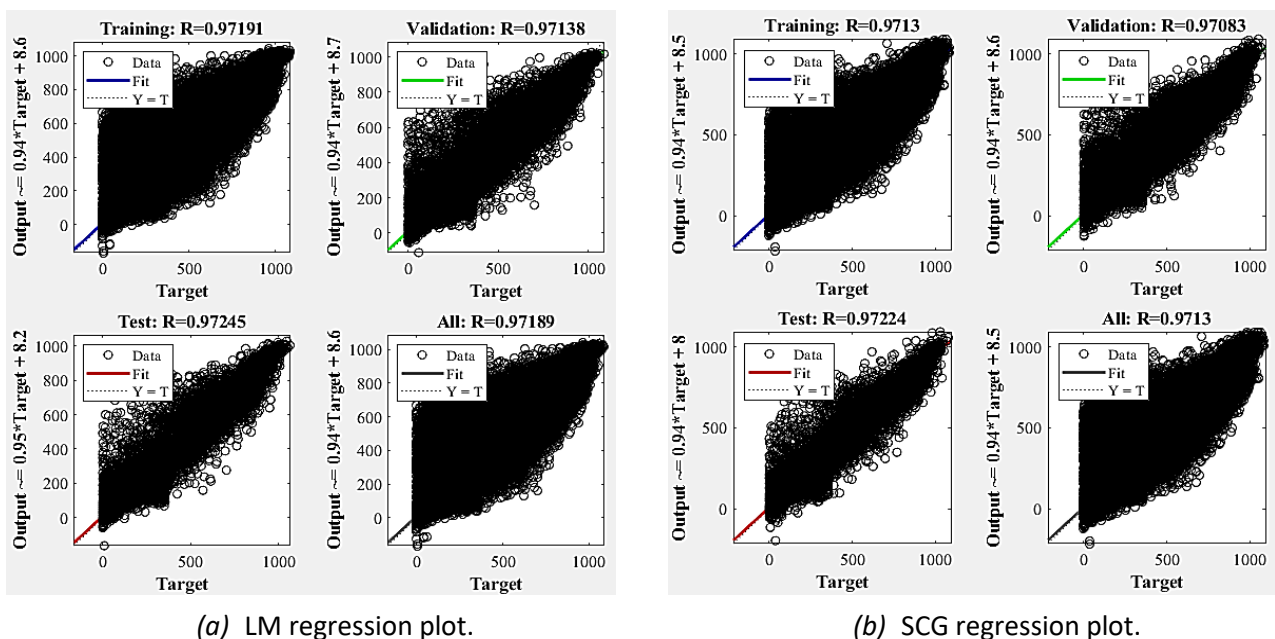
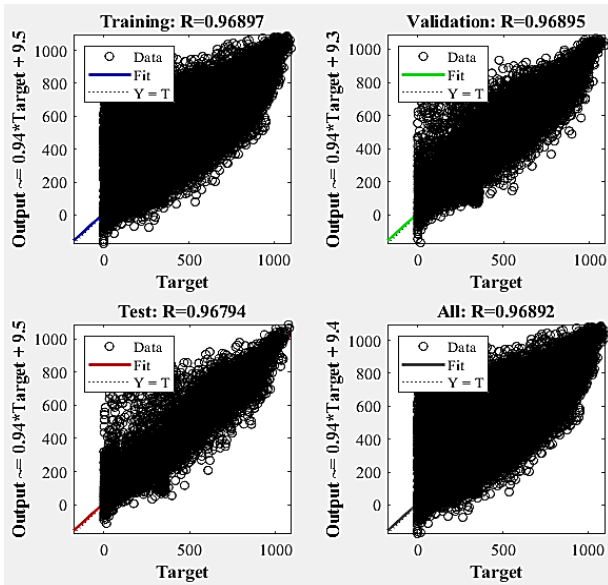
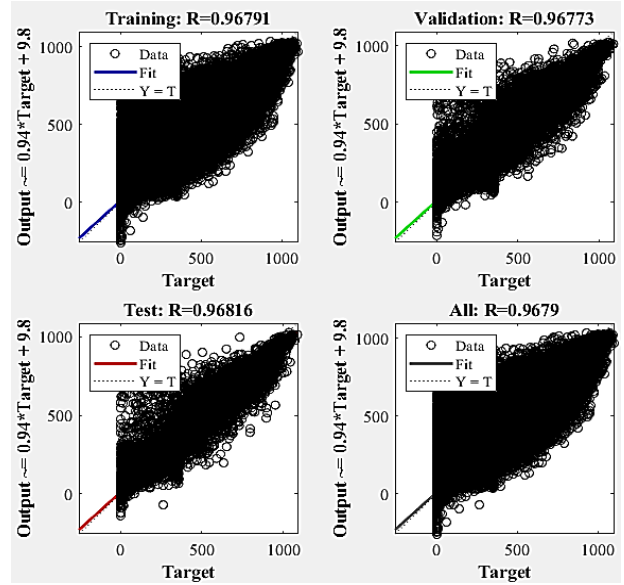


Figure 3-13: Regression plot of training, validation, testing, and all for FBANN-2 at Al khuwaimah.

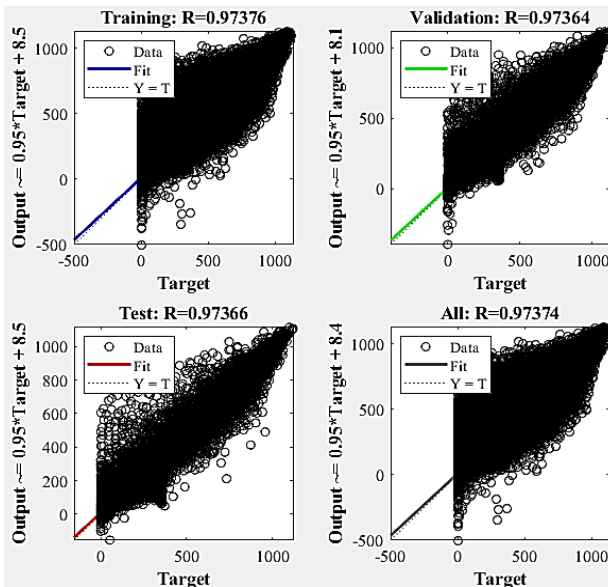


(a) LM regression plot.

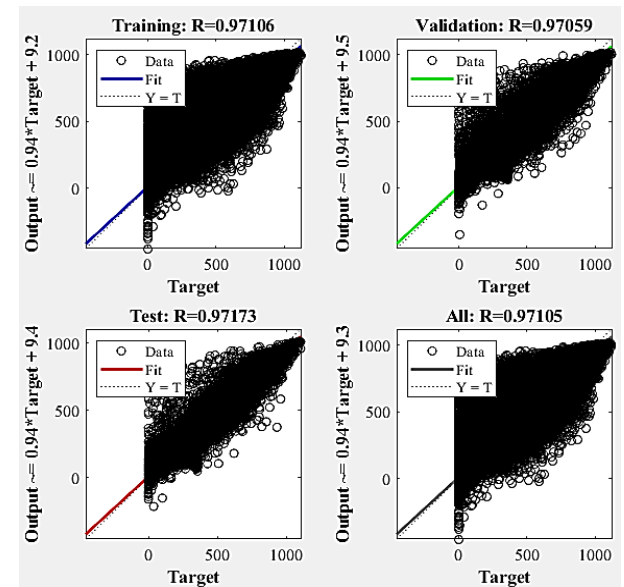


(b) SCG regression plot.

Figure 3-14: Regression plot of the training, validation, testing, and all for FBANN-2 at Al Halaniyat.

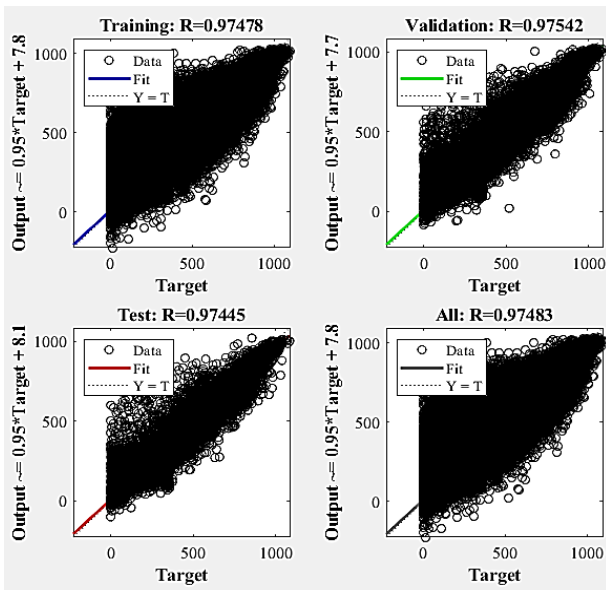


(a) LM regression plot.

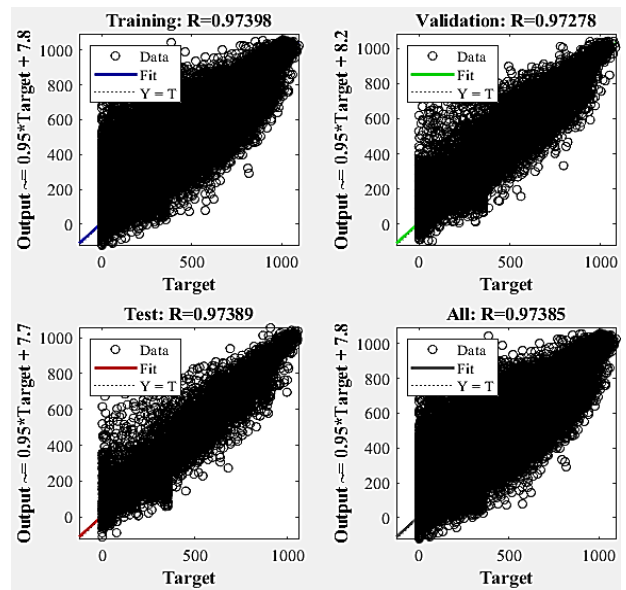


(b) SCG regression plot.

Figure 3-15: Regression plot of the training, validation, testing, and all for FBANN-2 at Al Mazyounah.

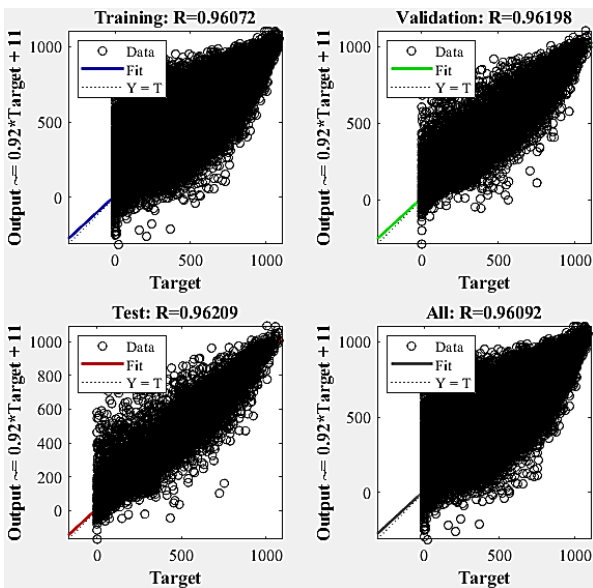


(a) LM regression plot.

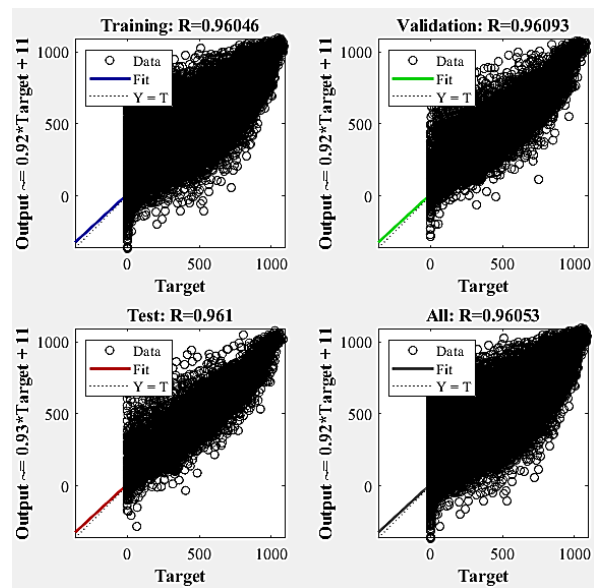


(b) SCG regression plot.

Figure 3-16: Regression plot of the training, validation, testing, and all for FBANN-2 at Haitam.

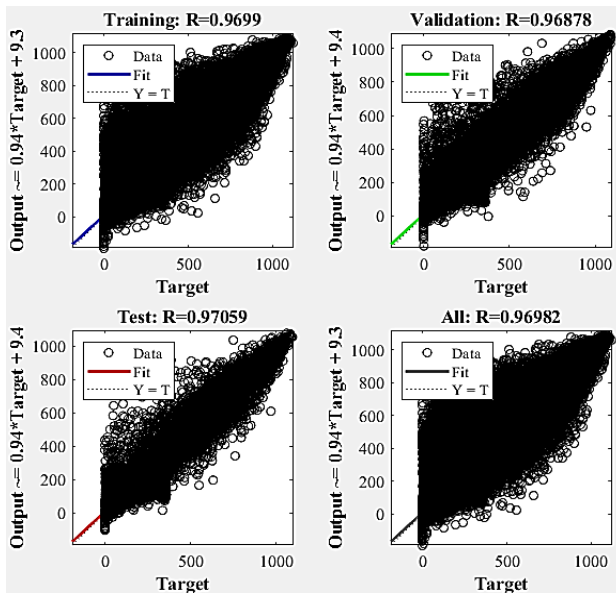


(a) LM regression plot.

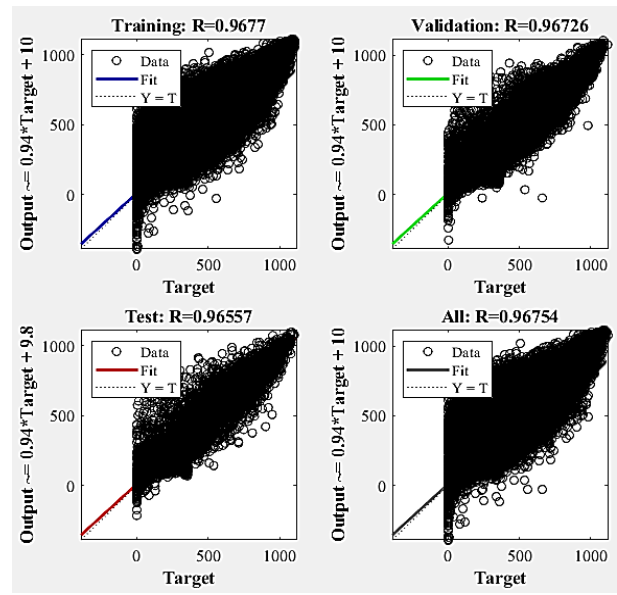


(b) SCG regression plot.

Figure 3-17: Regression plot of the training, validation, testing, and all for FBANN-2 at Madha.



(a) LM regression plot.



(b) SCG regression plot.

Figure 3-18: Regression plot of the training, validation, testing, and all for FBANN-2 at Methane.

The developed FBANN-2 model has been validated by comparing the results reported in [212], [214]. Table 3.5 provides a comparison of the present model with previous studies that have used similar models. Based on the R values, the developed model by Ramasamy et al. [214] demonstrates a higher performance for solar and wind data prediction compared to those of previous studies.

Table 3.5: Data validation results of the developed model.

Parameter	Present model	Xue [212]	Ramasamy et al. [214]
Model	FBANN-2	BPNN	Hamirpur ANN
Application	Solar radiation and wind speed	Diffuse solar radiation	Wind speed
Data resolution	1-hour	1-day	10-min
Time span	1999 to 2019	1995 to 2014	2012
Case study	Oman	China	India
R value	0.96 to 0.975	0.934	0.98

It is, therefore, recommended that this developed FBANN model should be adopted to estimate the wind speed and solar radiation in Oman. The developed model has several important implications for future practice by providing such a simple, low-cost wind speed and solar radiation measuring system for the study field. It does not require neighbouring station information for spatial interpolation, and it does not require costly data processing equipment. For that purpose, a MATLAB/Simulink[®] signal builder has been developed to evaluate the hourly GHI and wind speed profile at the adopted locations throughout the year. The purpose of these generated Figures is to understand how 1-hour values spread over the year. As a signal, each hour is represented as a 1 second signal in the signal builder block (see Figure 3.19). As a result, the hourly profiles of GHI, W/m² and wind speed in Oman are shown in Figures 20 to 23. A 1-hour GHI and wind speed timescale provides information on how GHI, W/m² and wind speed, m/s varies along the year. The maximum and minimum values are measured.

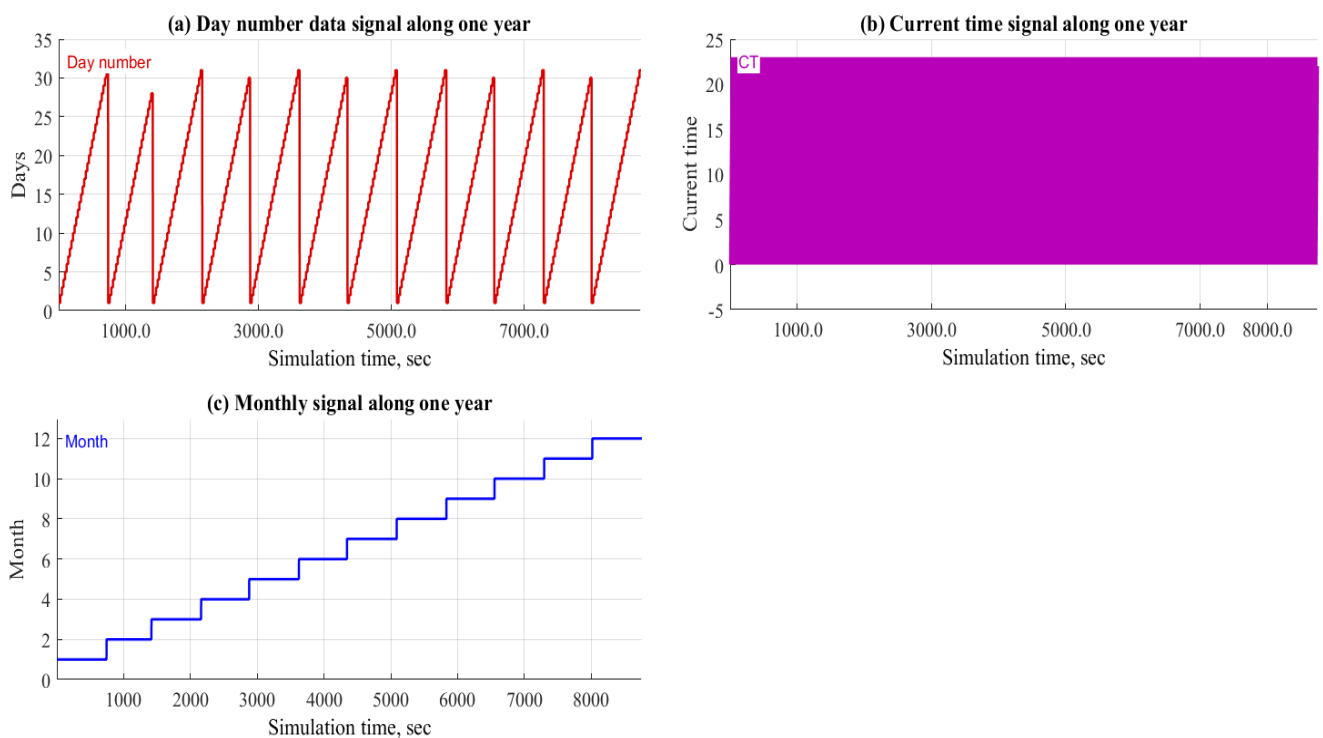


Figure 3-19: Data signal entry for one year in the ANN model, which represents (a) days, (b) current time, and (c) month.

As illustrated in Figure 3.20a, the hourly values of GHI in Al Khuwaimah are projected to reach about 960 W/m² as the highest value and 725 W/m² as the lowest value. The distribution profile in Al Khuwaimah is nearly stable and no sudden peaks occurred. Similarly, Al Halaniyat, Al Mazyounah, Haitam and Methane have stable GHI distribution profiles. Haitam region exhibited a similar distribution profile of hourly solar GHI that reveals maximum and minimum values of approximately 1005 W/m² and 840 W/m², respectively, as presented in Figure 3.20d.

The Al Halaniyat region exhibited a magnificent hourly solar GHI value, as shown in Figure 3.20b, with the highest and lowest solar GHI values of about 930 and 725 W/m², respectively. In addition, the maximum hourly value of hourly solar GHI was almost 985 W/m² with a minimum value of 840 W/m² in Al Mazyounah, Figure 3.20c. Moreover, the hourly solar GHI in Madha was predicted to reach about 920 W/m² as the highest value and 620 W/m² as the lowest value, Figure 3.20e. The hourly solar GHI highlighted the distribution profiles of Madha are fluctuating and changing substantially. The maximum and minimum hourly values of the hourly solar GHI in the Methane region is found to be approximately 980 and 780 W/m², respectively, as shown in Figure 3.20f.

For the design integration of hybrid CSP technology defining the hourly solar Direct Normal Irradiation (DNI) is crucial. Therefore, the generated DNI profile results from the developed ANN model can be seen in Figure 3.21. Based on the results presented in Figures 3.20 and 3.21, all regions in Oman exhibit extremely promising GHI/DNI potential. As a result, these regions can be very attractive for investments in solar energy applications. Consequently, significant opportunities exist to widen and decarbonise the electrical systems in Oman. In principle, the results of this analysis demonstrate that there are great incentives to move ahead with solar energy investments.

The hourly average wind speed has been predicted using the MATLAB/Simulink[®] signal builder. Al Halaniyat was predicted to achieve the highest hourly average wind speeds of approximately 12 m/s, as presented in Figures 3.22. Also, Table 3.6 exhibits the predicted minimum and maximum hourly average wind speeds of the selected stations in Oman.

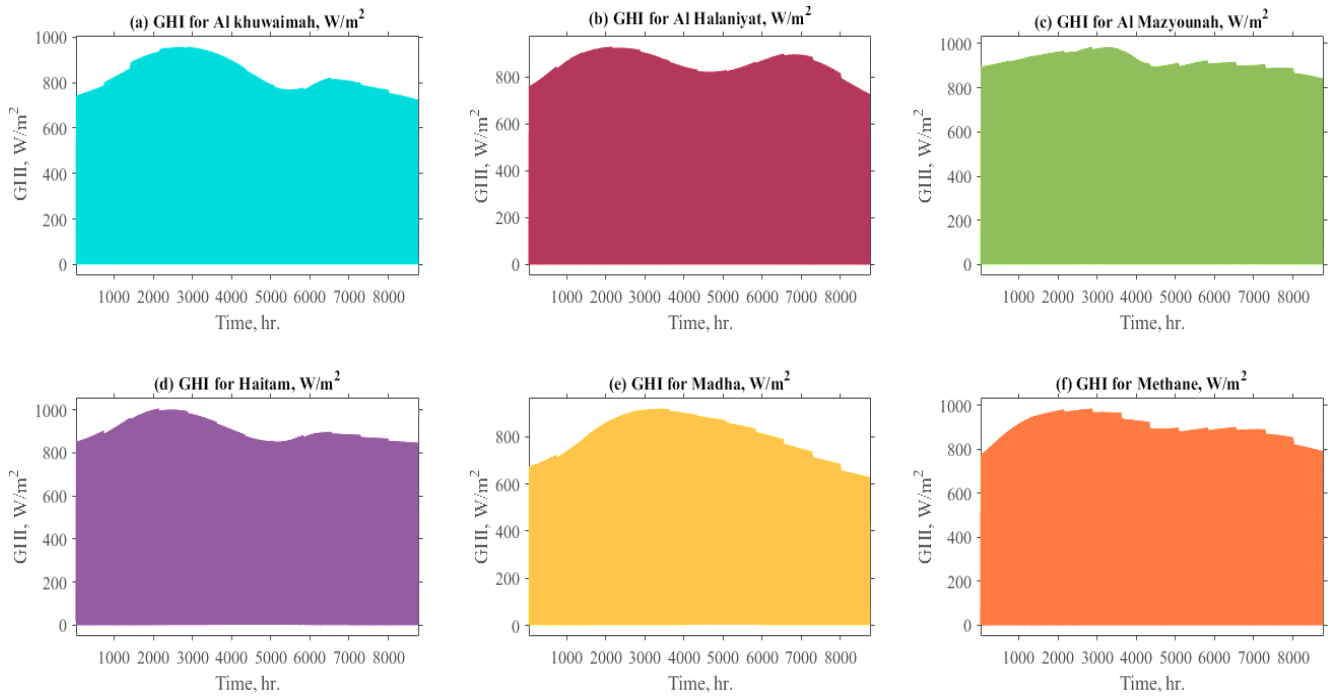


Figure 3-20: Hourly profile of GHI in Oman.

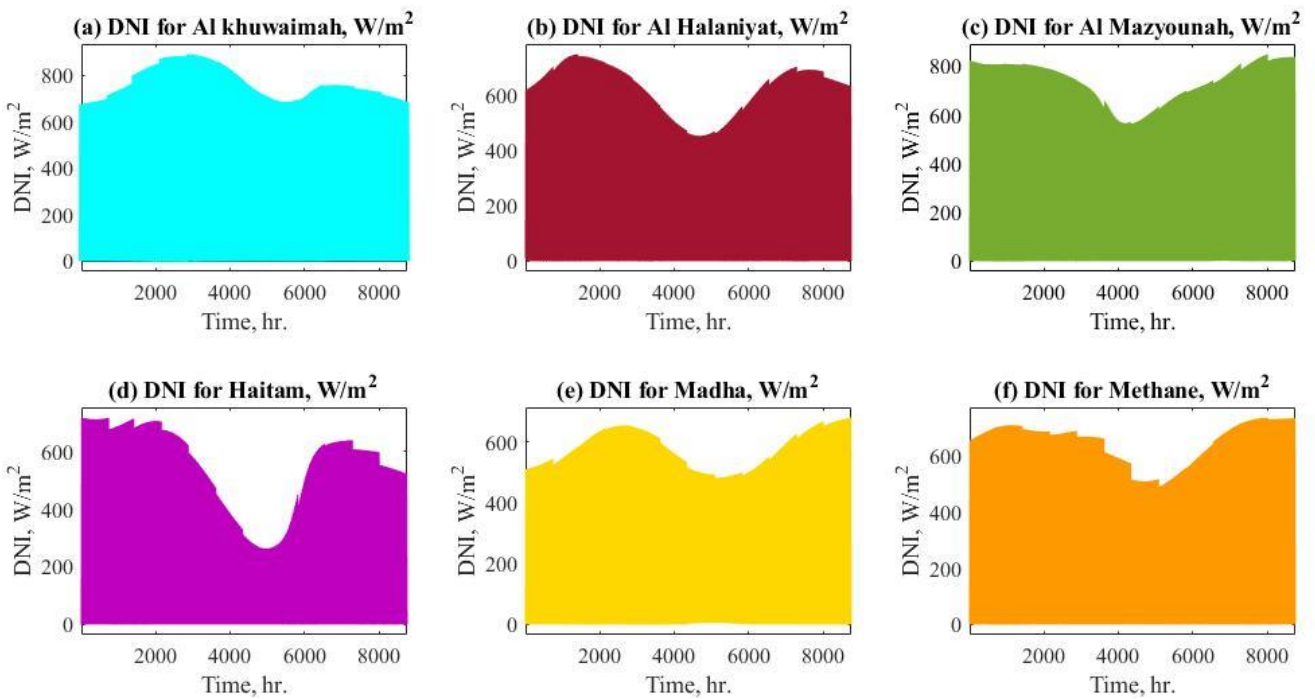


Figure 3-21: Hourly profile of DNI in Oman.

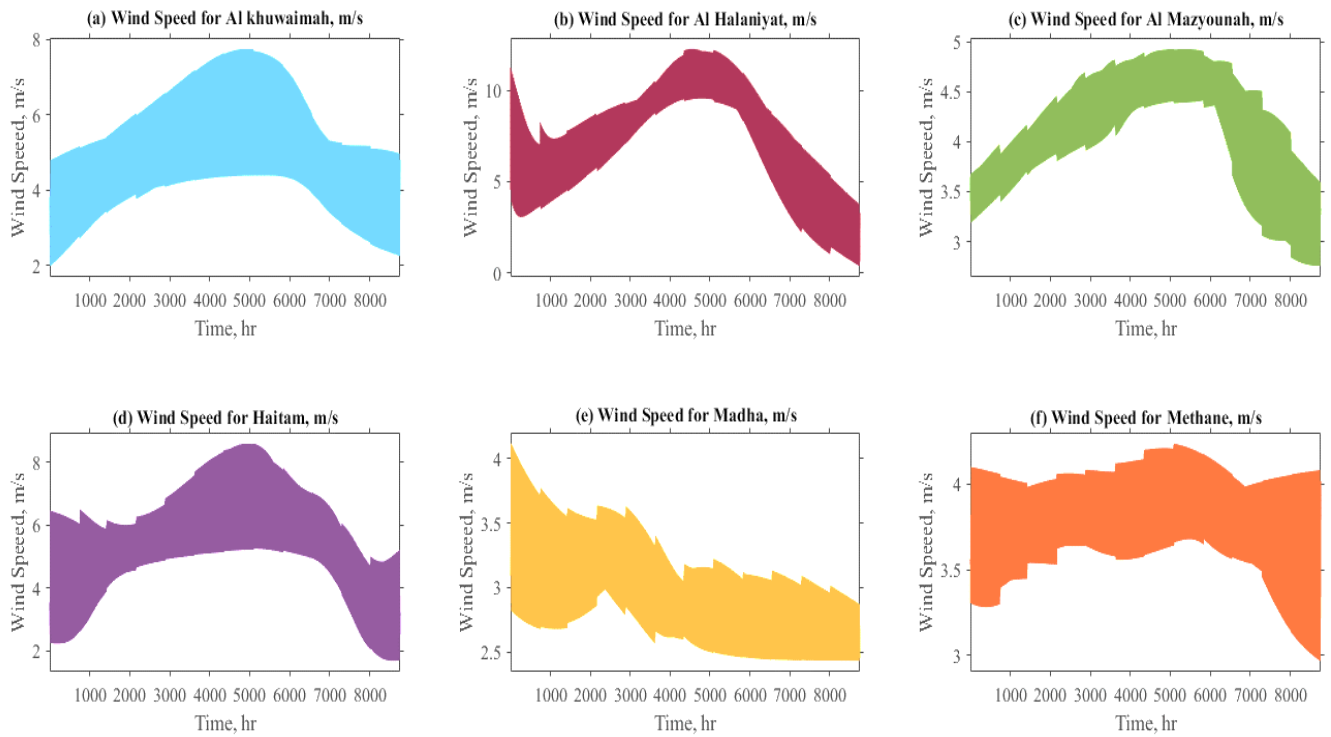


Figure 3-22: Hourly profile of the wind speed in Oman.

Table 3.6: Lowest and highest hourly average wind speed values of the selected stations.

Station	Maximum wind speed (m/s)	Minimum wind speed (m/s)
Al Khuwaimah	7.80	2.00
Al Halaniyat	12.00	0.35
Al Mazyounah	5.00	2.80
Haitam	8.50	1.70
Madha	4.10	2.40
Methane	4.20	2.30

Based on the ANN wind speed prediction analysis, Oman has suitable long-term wind energy resources and are appropriate for the installation of wind farms. Thus, wind farms could gain a great potential in that mentioned locations. For instance, Methane is found the best location for the hybrid solar and wind across the year. It should be noted that the wind energy varies much more than that the solar energy. Regarding the accuracy of the model, Table 3.7 presents the annual average values of MAPE while Figures 23-24 depict the behaviour of the MAPE for the GHI and wind speed along the whole year. For all locations, the average MAPE does not exceed 0.21% while at any time throughout the year the MAPE is below 3%, which typically signify great model accuracy. Figures 3.23 and 3.24 show the values of the MAPE based in Oman. Regarding the GHI, for all locations, the maximum percentage reported across one year is around 4%. Figure 3.24 shows the same general behaviour regarding the wind speed. The MAPE for wind speed in the Oman locations does not exceed 3%. Generally, the MAPE results indicate that the developed ANN model achieves a high accuracy over the addressed locations.

Table 3.7: Calculated annual average MAPE, % values.

Stations	GHI	Wind speed
Al Khuwaimah	0.0498	0.0549
Al Halaniyat	0.1592	0.0469
Al Mazyounah	0.0152	0.0450
Haitam	0.0289	0.0396
Madha	0.1037	0.0411
Methane	0.0816	0.0390

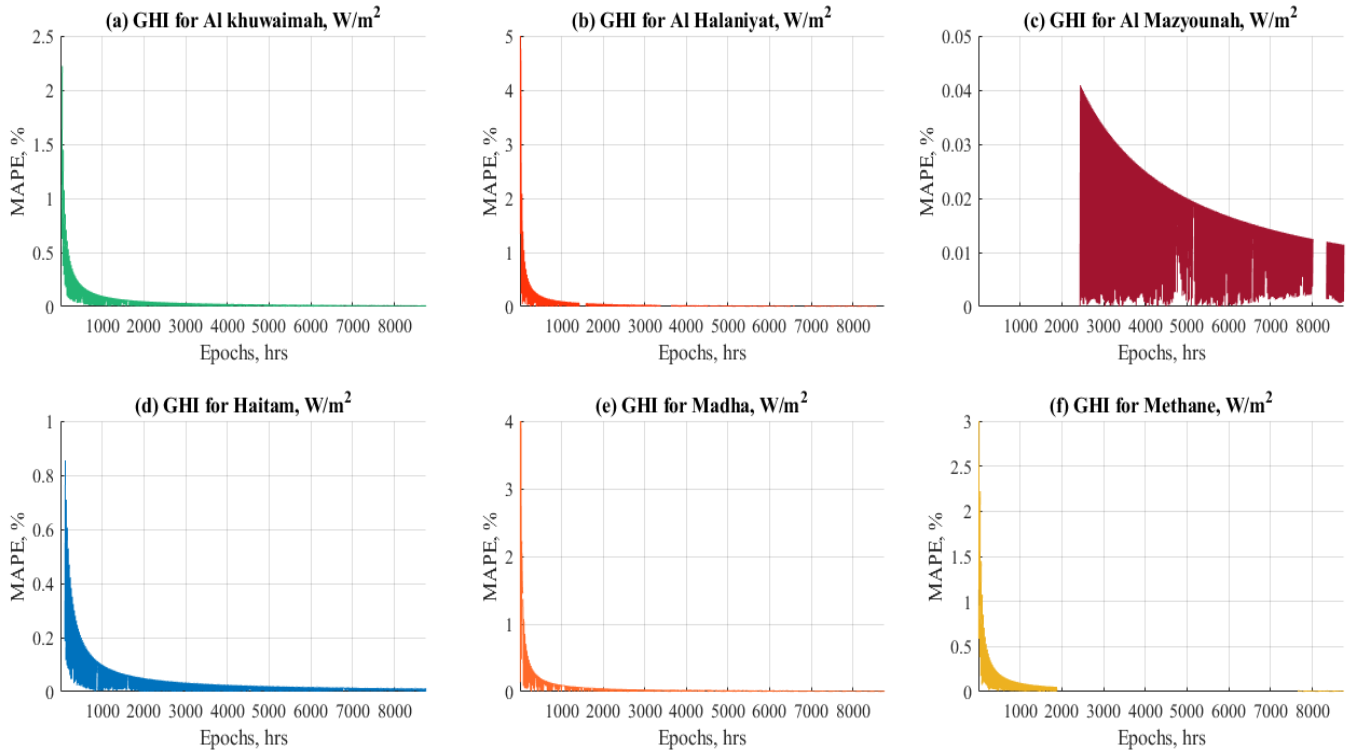


Figure 3-23: The MAPE for all selected locations regarding the GHI.

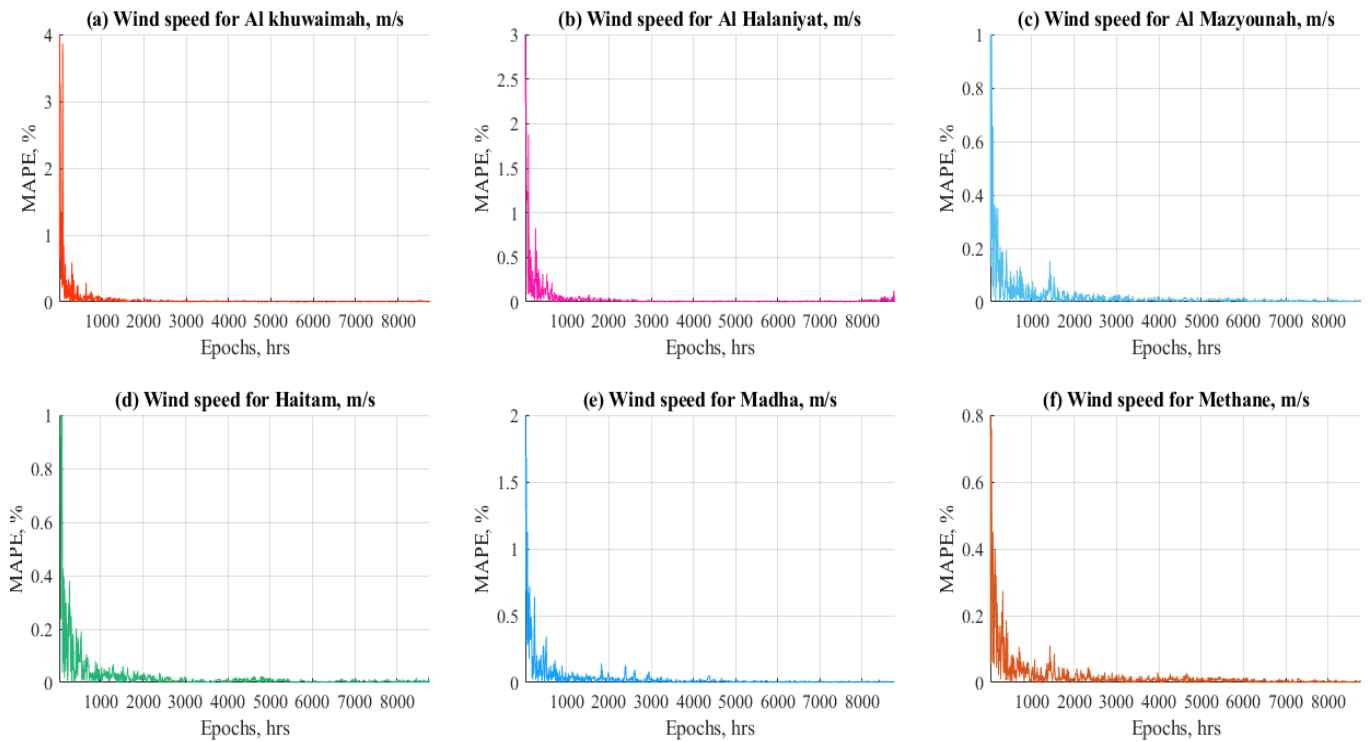


Figure 3-24: The MAPE for all selected locations regarding the wind speed.

3.5 Conclusion of the chapter

A new ANN technique has been developed and used for the Feed-forward Artificial Neural Network (FANN) model to predict the hourly solar radiation and wind speed data in 6 locations in Oman. The hourly-based data resolution was obtained from Solargis™ and covers a wide time span of 20 years. The fitting tool (*nftool*) in MATLAB/Simulink® solves an input-output fitting problem using a two-layer feed-forward neural network trained with the LM and SCG algorithms. A two stage ANN model comprising the FBANN-1 and the FBANN-2 solar/wind prediction models were designed and integrated to evaluate the solar and wind data. For the FBANN-1, the input parameters are the day number, month of the year and current time. The FBANN-2 receives as inputs the output parameters of the FBANN-1, i.e., the cloud identification quality, the sun altitude angle, the sun azimuthal angle, the air temperature, the relative humidity, the atmospheric pressure and the perceptible water, and thus the overall integrated model requires only three input parameters to run (those of the FBANN-1).

The R values for both the hourly solar radiation and the wind speed are higher than 0.96 for all the selected regions. This indicates that the proposed model can achieve high levels of accuracy and constitutes a powerful prediction tool. In addition, the obtained results indicate that the developed FBANN model with the LM algorithm has slightly higher accuracy than with the SCG algorithm.

Based on the results, Oman exhibit significant solar GHI potential and adequate wind speeds. In fact, the hourly solar GHI at all locations is mainly in the range of 620 W/m² to 1005 W/m². In addition, the wind speed varies from 0.35 m/s to 12 m/s. Moreover, Al Halaniyat has the greatest calculated hourly average wind speeds, namely 12 m/s. Haitam is the most promising region for the hourly solar GHI as it features the optimum hourly value of GHI, i.e., 1005 W/m². However, Methane has the most stable GHI and wind speed distribution profiles. As a result, Methane appears to be the best location for hybrid solar and wind applications across the year.

Regarding the model accuracy, the R-value was over 0.96 while the MAPE values did not exceed 3%, which indicates the high accuracy of the developed ANN model. According to the present research, Oman has great potential to augment their power systems due to a great potential of solar and wind energy resources. The developed prediction model can be utilised to design renewable energy systems.

In conclusion, the results showed that the proposed ANN model can achieve high levels of accuracy at predicting solar radiation and wind speed data. Finally, the results of this study can pave the way to move ahead with hybrid solar CSP energy investments and can inform decision making for future instalments of energy systems.

CHAPTER 4: THERMO-ECONOMIC AND DESIGN ANALYSIS OF THE HYBRID SOLAR BIOGAS SYSTEM FOR COGENERATION APPLICATION

Summary

In this chapter, a new layout of hybrid solar biogas system to power an Organic Rankine cycle (ORC-Toluene) and Air Gap Membrane Distillation (AGMD) for desalination and electric power generation is presented. The novelty emerges from some facts which are centralised around the use of a hybrid electric generation via Concentrated Solar Power (CSP) and anaerobic digestion biogas to achieve higher stability and profitability. Meanwhile, the cogeneration through the waste heat of the ORC drives the AGMD, which benefits as well from the higher stability due to hybridisation. The proposed system has been designed through advanced modelling in MATLAB/ Simulink® that facilitates the interaction of the individual energy technologies efficiently. To ensure reliability, the anaerobic digestion process has been used as a backup unit to compensate for the absence of solar energy and for the disposal of organic waste. A technical sensitivity analysis has been conducted for all the system units in order to reduce the respective design limits and identify optimum operational windows. The investigations are performed based on energy, exergy, and cost analyses to produce 100-1500 m³/day of freshwater. The results reveal that the total hourly costs are found within the range of 30-70\$/h which are considered to be remarkable results when comparisons are made with the conventional desalination processes. The range of total water price, \$/m³ was found to fluctuate between 0.5 and 1.45 \$/m³. The performance of the model has been tested in a rural area in Oman, and a thorough thermo-economic analysis of the integrated system has been conducted. Finally, the results of this study can pave the way for moving ahead with hybrid solar/anaerobic biogas energy investments and can inform decision makers for future installments of energy systems. The findings of this chapter have been published in the author's paper published in a peer reviewed journal.

4.1 Introduction

Among the major challenges facing a growing global population in the 21st century are the sustainability of energy and security of water supplies [215]. Water shortages represent serious challenges across continents, but particularly in the Middle East and Northern Africa. Potential solutions for water supplies include desalination of seawater and brackish water. One of the most productive as well as cost-effective

desalination solutions is Membrane Distillation (MD) due to its utilization of low-grade waste heat to produce clean water [216]. This is a much simpler, more compact, and more scalable solution than the traditional approaches, such as Multi-effect Distillation (MED), Multi-stage flash distillation (MSF) and Reverse Osmosis desalination (RO) [71]. In addition, MD can operate at lower temperatures (50-80 °C) and at lower atmospheric pressures [90]. In fact, a temperature difference range as low as 7-10 °C is theoretically sufficient to achieve a successful separation [217]. Moreover, the MD technology can be operated with intermittent energy supply without any additional modifications. However, having a constant operation will allow the achievement of a higher capacity factor of the MD and therefore a better return of investment. In addition, the problem of corrosion is minimised due to the low operating temperatures, pressure, and the characteristics of the utilized non-metallic membrane materials. Because of this, the MD process is not adversely affected by high feed salinity [88] and is an efficient and cost-effective means of utilising low-grade waste heat, such as solar and/or geothermal energies, to produce potable water. The MD relies on using a microporous, hydrophobic membrane as a contractor to achieve separation by liquid–vapor equilibrium. In recent years, preparing membranes has attracted much research attention, especially for the MD applications. Several membrane separation material types have been used for the MD technology, e.g., Polytetrafluoroethylene (PTFE), polypropylene (PP), polyvinylidene fluoride (PVDF), polyethylene (PE), polyvinylidene fluoride (C-PVDF), PH membrane type (E-PH), and new generations of carbon nanotubes (E-CNT).

Of the numerous MD configurations, air gap membrane distillation (AGMD) appears to be the best option due to its higher thermal efficiency than that of other configurations such as direct contact, vacuum, sweeping gas, permeating gap, material gap, and conductive gap MD [218]. In the sweeping gas membrane distillation (SGMD), gas such as nitrogen is presented in the permeate side of a membrane reactor to lower the partial pressure of the permeating species and increase the driving force. Nevertheless, MD is like other desalination processes in its requirement for thermal and/or electrical energy for its operation and this can have significant adverse environmental impacts. Consequently, a MD process that relies on solar power rather than on burning fossil fuels is immediately appealing. The driving force in the MD operation is the partial vapor pressure difference between the two sides of the microporous membrane, and unlike the other technologies that require concentration, pressure, or an electrical potential gradient. A number of MD pilot plants have been installed utilising geothermal and/or solar energies [78] and have proven to be more efficient with fewer operational issues than their conventional counterparts. Guillen-Burrieza et al. [219] presented an experimental analysis of a solar-powered AGMD technology using a flat sheet type PTFE membrane module. The results showed that the maximum specific

distillate flux was around $0.17 \text{ m}^3/\text{day}/\text{m}^2$ of membrane area. Kim et al. [93] have analyzed a direct contact membrane distillation (DCMD) desalination technology using solar energy and an auxiliary heater. A hollow fiber membrane PVDF module type was employed, and the results showed that the overall distillate production capacity was $31 \text{ m}^3/\text{day}$. Chen and Ho [220] presented a theoretical and experimental analysis of a solar-driven DCMD using lab-scale equipment to desalinate sea water. The results showed that the distillation ability was $0.14 \text{ m}^3/\text{day}/\text{m}^2$ with a high purity level.

Banat et al. [221] conducted an experimental study on a solar-powered MD plant in Jordan. The results revealed that the permeate water was in the range of 0.002 to $0.011 \text{ m}^3/\text{day}/\text{m}^2$ with specific energy consumption in the range of 200 – $300 \text{ kWh}/\text{m}^3$. Lee et al. [222] carried out a theoretical analysis of a solar-driven multi-stage DCMD desalination plant, focusing on the monthly average daily and hourly performances. The results showed that the water production increased from $0.37 \text{ m}^3/\text{day}$ to $0.4 \text{ m}^3/\text{day}$ with an increase in thermal efficiency from 31% to 45% . Banat [76] designed a stand-alone solar-driven AGMD desalination plant in a project funded by the European Commission. The permeate water was $0.12 \text{ m}^3/\text{day}$ when using a membrane area of 10 m^2 , and daily solar radiation of $7 \text{ kWh}/\text{m}^2$. The results showed a low specific distillate of approximately $0.01 \text{ m}^3/\text{day}/\text{m}^2$. Guopei et al. [223] designed and analyzed a solar-driven stand-alone sweeping gas membrane distillation (SGMD) desalination plant to supply a flexible fresh water supply for remote regions. The average daily water production was between $0.01 \text{ m}^3/\text{day}$ and $0.02 \text{ m}^3/\text{day}$, which was sufficient to meet the daily drinking water demand of a typical family. Bouguecha [224] conducted an experimental study of a solar-driven DCMD desalination system based on a hybrid solar collector and solar PV. The permeate water production was round 0.08 and $0.11 \text{ m}^3/\text{day}$, respectively for two different arrangements. Zhang [225] reported that the specific distillate production of a solar-powered SGMD plant was approximately $0.03 \text{ m}^3/\text{day}/\text{m}^2$ with a thermal efficiency of 80% . A hybrid solar MD pilot plant has been installed by Goosen et al. [92] in Saudi Arabia to generate $8 \text{ m}^3/\text{day}$ of high-quality potable water. This was achieved with less energy load while also generating power to supply cooling for air-conditioning.

A solar powered MD requires constancy throughout daily operations which can be achieved by augmenting solar radiation by means of a backup unit. It is, therefore, possible to integrate solar thermal power within the infrastructure of a conventional thermal power plant and this would allow constant and optimal operation of the MD. Therefore, potentially allowing better use of the capital (higher capacity factor) [88]. This integration of solar power with a more conventional system has the added advantage of reducing fossil fuel consumption, thus minimising the adverse environmental impacts due to lower CO_2 emissions. However, a hybrid solar and biogas boiler can generate a similar output of power and

temperature grade compared to hybrid solar fossil fuels and therefore is an attractive approach [226]. Combined solar and biogas could be one of the best solutions as a power supply for the MD operation. However, it is apparent that there is a lack of studies in the literature that deal with the integration of renewable energy technologies and only a few studies have focused on the hybrid solar and biogas utilizing waste as a heat source. In addition, an implementation of a hybrid PTC-biogas to power ORC and AGMD system in decentralised off-grid for desalination and electric power generation has not been previously studied in the literature. A small number of thermo-economic studies exist in the literature regarding PTC-biogas systems. One of these studies was conducted by Petrollese and Cocco [227] to investigate the hybrid solar biomass benefits in terms of system performance and economic efficiency, integrating anaerobic digestion processes with an existing solar Organic Rankine cycle (ORC) system for combined heat and power application at the Ottana solar facility in Italy. The power of the biogas boiler and its daily operating time have been used as the main design parameters to accurately size the biogas unit. The main annual performance of the hybrid CSP- biogas plant was examined by varying these two parameters. Starting with the expected performance for the current plant configuration of the Ottana solar facility (with only the CSP section), the results showed significant improvements in the plant's capacity factor and in the overall ORC efficiency that can be achieved by the hybridisation with biogas. Furthermore, Zhang et al. [228] investigated the thermal performance of the hybrid solar biogas for power generation using a steam turbine and found that hybridising solar energy with biogas energy improves the power stability and dispatchability. In addition, Soares and Oliveira [139] have analysed the hybridisation of PTCs biogas boiler for a mini ORC power plant (60 kW) as part of the renewable electricity cooperation project. The authors agreed that the hybridisation of CSP with biogas improves the technical performance of the plant by increasing the annual energy yield by 6.2%. The theoretical analysis conducted by Sterrer et al. [229] using the integration of parabolic trough collectors (PTCs) with a biomass for heat and power using ORC system was aimed at maintaining thermal stability. A thermodynamic model, based on a steam Rankine cycle, was constructed by Suresh et al. [230] in order to size a hybrid solar biogas power plant. The study concluded that to improve the power block efficiency, proper sizing of the specific solar field area and the amount of biomass consumed are essential dimensions to be considered. Peterseim et al. [28] studied the economic potential benefits of the hybridisation of CSP-biogas to produce 5-60 MW in regions in Australia that were characterised by high solar availability and using wood waste, bagasse, refuse-derived fuels, and forestry residues.

As aforementioned in the open literature, it is clear that there exists a lack in the literature of studies that deal, in depth, with the modeling and thermo-economic design of the solar PTC, anaerobic digestion

biogas, ORC, and AGMD integrated solution. The present study aims at filling this very important knowledge gap and adopts a comprehensive approach in assessing the feasibility of the proposed novel system. The new assembly configuration aims to achieve higher power stability and profitability using the ORC cycle. In the meantime, the waste heat of the ORC is utilized to drive the AGMD for cogeneration application, which benefits as well from the higher stability due to the hybridisation. The solar PTC is regarded as the prime mover, with the anaerobic digestion biogas serving as a backup energy source to compensate for the inconsistency of solar radiation during the day. Due to these features, the integration of PTC/biogas/ORC/AGMD has the potential to be economically attractive and this is thoroughly investigated within this study.

An innovative and user-friendly modelling approach has been applied that efficiently integrates the individual energy components, i.e. PTC, anaerobic biogas boiler, ORC and AGMD, which fosters the optimisation of the proposed system. The design procedure and the assessment performance of the off-grid have been exemplified in the rural region of Oman. The main objectives of this work are as follows:

- Design of the proposed system is through advanced modelling to integrate the hybrid solar biogas system. Models have been built in the MATLAB/Simulink[®] and have been utilised to analysis the system area, dimensions, and cost and to ensure that the electrical and water demand of the end-user are met.
- Perform an energy, exergy, and cost analysis for the proposed hybrid energy system.
- Construct of sensitivity assessment on the developed system to investigate the effects of various design parameters on the thermo-economic performance.
- Implement an in-depth simulation testing of the system in a rural area in Oman.
- Assess the detailed thermo-economic assessment of the proposed hybrid solar-anaerobic digestion biogas to power ORC and AGMD for cogeneration in off-grid applications.

4.2 The Proposed System & Process Description

Concentrated solar power (CSP) via PTC can generate enough thermal power to power thermal desalination technologies. A schematic diagram of the proposed hybrid solar biogas to power ORC and AGMD system for cogeneration application is illustrated in Figure 4.1.

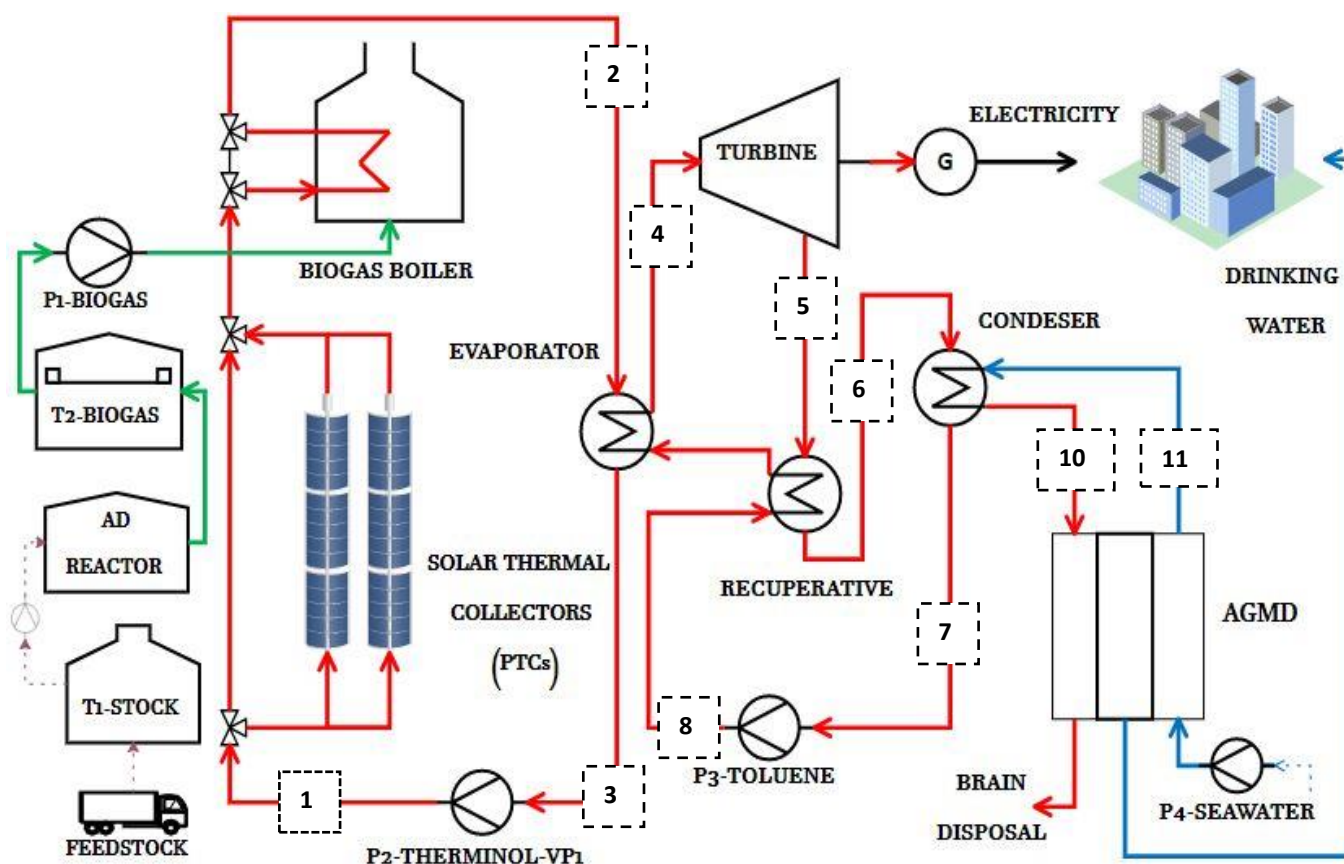


Figure 4-1: A schematic diagram of the proposed system.

The proposed system consists of three main cycles: the renewable energy heating cycle (solar and anaerobic biogas), the ORC system, and the AGMD desalination cycle. In the renewable energy heating cycle, thermophilic oil (THERMINOL-VP1) is used as a heat transfer oil (HTO) because of its ability to prevent the organic fluid from overheating and chemical instability [231]. The thermal oil is heated up in the renewable energy heating cycle (solar and biogas) using a PTC to the desired temperature. If the generated temperature in the outlet stream of the solar collector is lower than the set-point temperature, either due to cloudy weather or at night, the biogas boiler is utilised to maintain a constant hot thermophilic oil temperature supply. Anaerobic digestion (AD) reactor is used to supply sustainable biogas volume needed to fill the biogas tank. Different types of feedstocks, such as animal and fruit wastes, can be supplied to the anaerobic system. On the other hand, toluene is utilised in the ORC and circulated using the toluene pump. The high-pressure toluene then passes through the evaporator unit and is fully converted into vapor. Then, the high temperature vapor passes across the turbine, thus generating mechanical energy that is

converted into electricity using a generator. The working fluid then flows through the recuperator unit where the remaining heat is utilised to heat up the toluene at the end of the stream before returning it to repeat the cycle. Using the recuperator unit reduces the thermal power load on the CSP/biogas section leading to a reduction in the total area of the CSP/biogas [140]. After the regeneration through the recuperator unit, the high temperature toluene is again utilised in the condenser unit to heat the seawater stream. The heated water is then transferred into the AGMD plant. The driving force in the AGMD is the vapor pressure difference between the two sides of the micro-porous membrane. The membrane allows only the vapor from the pre heated solution to pass through the dry pores and on the other side (permeate side), the vapor is condensed. The generated electricity and power are then transferred to the end-user.

4.3 Mathematical Modelling, Simulation and Assumptions

4.3.1 The simulation model & assumptions

For the design of any desalination process, it becomes particularly important to specify the freshwater capacity, hence the thermal load is calculated through the condenser unit. In this work, it is assumed that the desired product capacity in m^3/day is specified as a known parameter to calculate the thermal load on the solar ORC turbine unit to serve the AGMD pump. Specifying the productivity allows the developed simulation model to calculate the electrical power of the AGMD pump. The main grid load from the end-user plus the AGMD pumping power will sequentially be set as an input to calculate the load power on the ORC turbine, i.e., $W_t=f$ (Main grid load+AGMD load). The unknown parameters are the areas, dimensions, mass flow rates, and the entire process temperatures or any other calculated physical properties. The following assumptions are made:

- The system operates under steady-state conditions and a dynamic real-time modelling is presented according to a specific case study located in the Al Khuwaimah rural region of Oman. This rural region is suitable for the installation of off-grid renewable energy systems as grid connection is not a viable option due to the great distances [232]. The average solar direct normal irradiation (DNI, W/m^2), value for the selected location is set at $666 \text{ W}/\text{m}^2$ which was obtained from the Solargis™ [233].
- Therminol-VP1 heat transfer oil is used through the CSP part, toluene is the main working fluid through the ORC and seawater is the main flow through the AGMD part.
- The system productivity is assumed to be in the range of $100\text{-}1500 \text{ m}^3/\text{day}$. This range of

production is most suitable for small scale communities, facilities, nomads' spots, tourist villages, rural areas, etc. and it can vary according to the consumption fluctuation in the case of dynamic modelling.

- The operating conditions, such as the temperature, °C or pressure, are kept constant and can be varied based on the case study. The top cycle pressure is assigned throughout the evaporator unit.
- The condenser and the heat exchangers' effectiveness are assigned to be 80%, while the pumps' efficiency is assigned to be in the range of 70%-75%.
- The obtained membrane types are PTFE, PP, PVDF, PE, C-PVDF, E-PH, E-CNT0.5, E-CNT1, E-CNT2, and E-CNT3 and the feed salinity is set to be 45,000 ppm which represents the seawater salinity.
- The product salinity ratio is set to be between 500-200 ppm, while the salt rejection is set at 0.99
- The inlet cold water temperature is set to be between 15 and 25 °C.
- The retention time of the anaerobic biogas unit varies between 40-50 days and cattle manure is used as the main source of biogas generation.

A robust modelling tool using the MATLAB/Simulink® software that uses actual weather data obtained from Solargis™ has been developed. The model components are fully and well-integrated with each other. Most importantly, all mathematical model equations are solved simultaneously, unlike other software that solves each subsystem separately. Moreover, the system runs based on an iterative loop solution with the forwarding and backwarding of the entire streams. The presented new model is developed based on a design approach, which is used to calculate and measure the system design, size and cost. The inlet system parameters are assigned by the user and then the entire design data (size, energy, exergy and cost) is calculated and easily appeared in the Simulink® display blocks. The new developed user-friendly model and its stepwise procedures are shown in Figure 4.2 and 4.3, respectively.

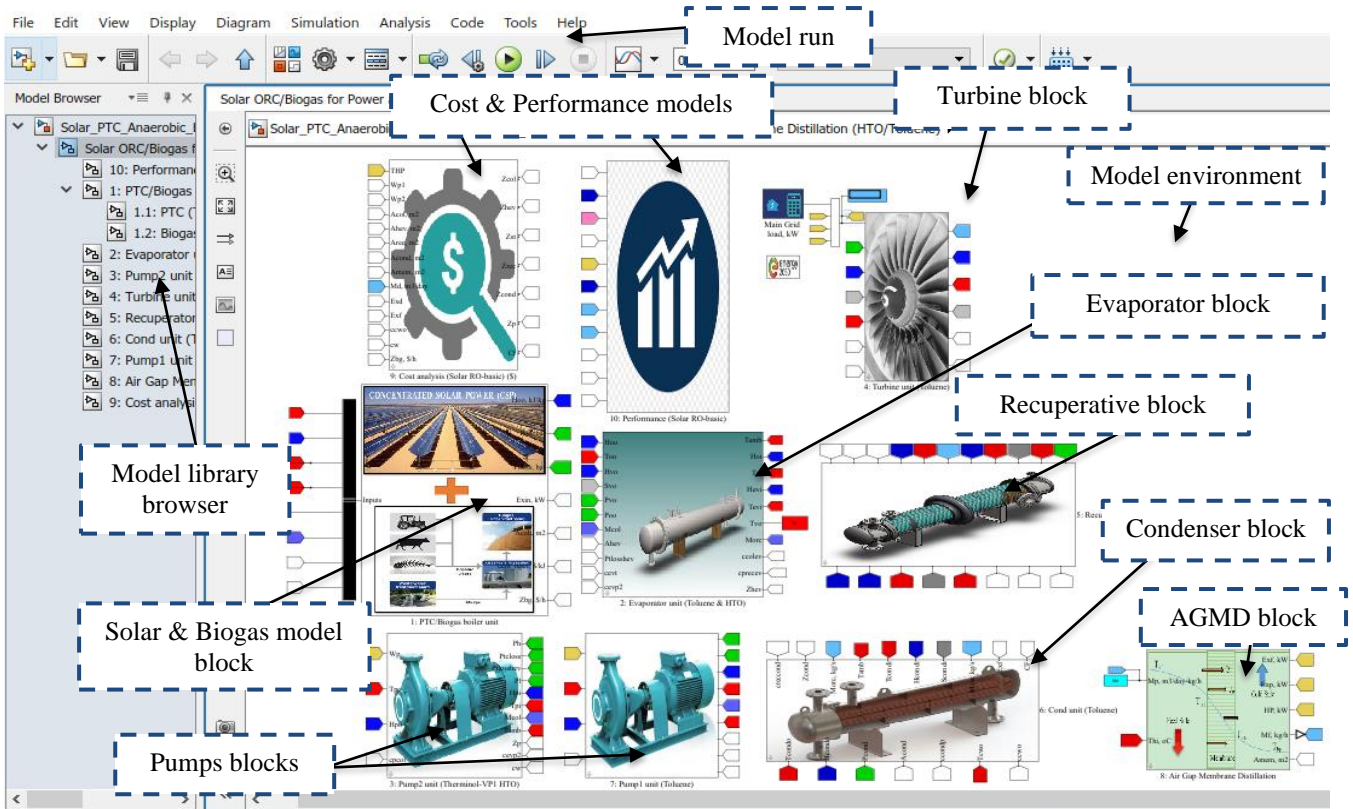


Figure 4-2: The developed model browser in the MATLAB/Simulink® toolbox environment.

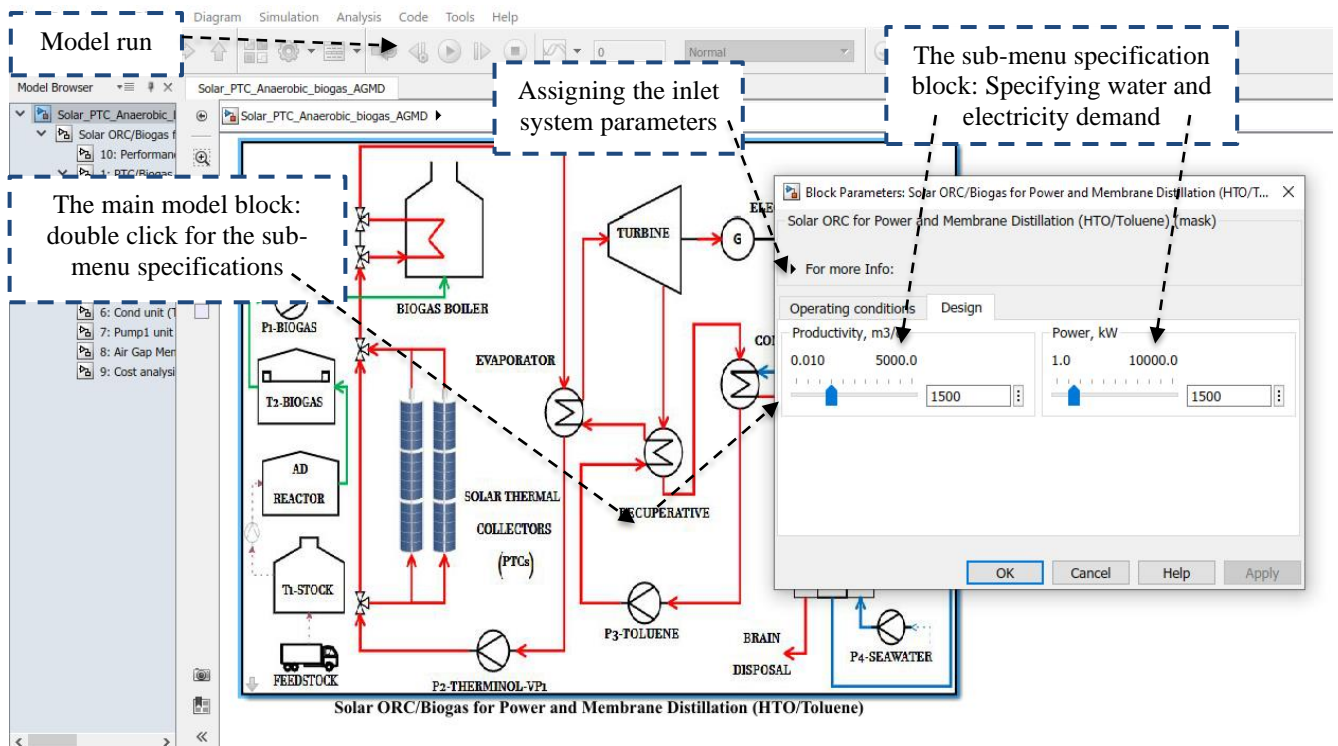


Figure 4-3: The stepwise procedures of the developed model in the MATLAB/Simulink®.

4.3.2 The Mathematical Model

The developed mathematical model that represents the simulation model is presented in the following subsections. The mathematical approach represents the solar PTC, anaerobic digestion biogas, ORC and AGMD parts.

4.3.2.1 Solar PTC

The solar collector is the heart of any solar energy system. The instantaneous efficiency of the solar collectors is defined by its characteristic curve using the solar irradiance, mean collector and ambient temperatures. The PTC configuration and design specifications are adjusted according to the LS-3 type [140], [234]. The LS-3 parabolic trough concentrator uses a glass mirror reflector supported by the truss system that provides its structural integrity. The glass mirrors, manufactured by Flabeg Solar International (FSI; formerly Pilkington Solar International, Koln, Germany), are made from a low-iron 4-mm float glass with a solar-weighted transmittance of 98%. Table 4.1 list some of the most important characteristics of the PTC/LS-3 type.

Table 4.1: The main specifications of the PTC/LS-3 type [140], [234].

Structure	Aperture width (m)	Focal length (m)	Length/ element (m)	Length/ collector (m)	Mirror area/ drive (m ²)	Receiver diameter (m)	Geometric concentration sun	Module weight/ m ² kg	Peak optical efficiency %
V-truss framework	5.76	1.71	12	99	545	0.07	82:1	33	80

The corresponding efficiency equation for the medium-high temperature parabolic trough collectors (PTC) [143] is given by (η_{col}):

$$\eta_{col} = \eta_o - a_{11}(T_{co} - T_{amb}) - a_{21} \left(\frac{T_{co} - T_{amb}}{I_s} \right) - a_{31} \left(\frac{T_{co} - T_{amb}}{I_s} \right)^2 \quad (4-1)$$

where, $a_{11}= 4.5e-6$ ($^{\circ}C^{-1}$), $a_{21}= 0.039$ ($W/m^2.^{\circ}C$), and $a_{31}=3e-4$ ($W^2/m^2.^{\circ}C^2$), $\eta_o = 0.75$.

The collector total area (A_{col}), in m², is estimated based on the collector energy balance equation as a function of collector efficiencies as follows:

$$A_{col} = \left(\frac{Q_u}{\eta_{col} \times I_s} \right) \quad (4-2)$$

where Q_u is the collector's useful thermal power, kW, I_s is the solar radiation over the collector area,

kW/m², and A_{col} represents the total area of the collector. The collector useful energy equation may exist according to the following expression:

$$Q_u = \dot{m}_{col} \times \Delta H \quad (4-3)$$

where ΔH is the enthalpy difference across the collector in kJ/kg, and \dot{m}_{col} is the mass flow rate of the solar collector. The overall length of the solar PTC (L_{col}) in m is calculated based on the collector width (W_{col}), in m , and tube glass cover envelope diameter, (D_{env}), in m as follows:

$$L_{col} = \frac{A_{col}}{(W_{col} - D_{env})} \quad (4-4)$$

Number of loops (N_{Loop}):

$$N_{Loop} = \frac{\dot{m}_{col}}{\text{Hydraulic mass flow rate per loop}} \quad (4-5)$$

Area of the loop (A_{Loop}):

$$A_{Loop} = \frac{A_{col}}{N_{Loop}} \quad (4-6)$$

Total number of PTC collectors (N_{col}), where W_{Loop} is the loop width:

$$N_{col} = \frac{A_{col}}{(L_{col} \times (W_{Loop} - D_{envloop}))} \quad (4-7)$$

In the physical behaviour, the solar radiation that reaches the solar collector is transformed into heat. This heat is partly absorbed by the heat transfer oil. The solar thermal exergy input rate to the solar powered system (I_{col}) is the exergy transferred from the sun to the heat transfer oil that is heated while crossing the solar collector. The exergy destruction rate (I_{col}), kW, in the solar collector is obtained from [235] as follows:

$$I_{col} = A_{col} \times I_s \times \left(1 - \frac{1}{3} \left(\frac{T_{amb}}{T_{sun}} \right)^4 - \frac{4}{3} \left(\frac{T_{amb}}{T_{sun}} \right) \right) + \dot{m}_{col} [h_i - h_o - T_{amb}(s_i - s_o)]_{col} \quad (4-8)$$

where $h_{i,o}$ represents the specific enthalpy of inlet and outlet cases, kJ/kg and $s_{i,o}$ represents the specific entropy of the inlet and outlet cases, kJ/kg°C, respectively. Bejan [236] has recommended $T_{sun} = 6,000$ K and this value is used in this study.

4.3.2.2 Pumps

The pump power (W_p) in kW is calculated as follows:

$$W_p = \frac{\dot{m} \Delta p}{\rho \eta_p} \quad (4-9)$$

where Δp is the pressure difference between the low pressure and the high pressure, \dot{m} is the mass flow rate in kg/s, and ρ is the density of the working fluid in kg/m^3 , and η_p is the pump efficiency. The pump outlet enthalpy (h_{out}), in kJ/kg is obtained via the following relation:

$$h_o = \frac{W_p}{\dot{m}} + h_i \quad (4-10)$$

By knowing the environmental conditions (T_{amb}), the exergy destruction rate (I_p), in kW may be obtained from the following relation [235]:

$$I_p = \dot{m}[h_i - h_o - T_{amb} \times (s_i - s_o)] + W_p \quad (4-11)$$

4.3.2.3 Evaporator & heat exchangers

The evaporator unit is responsible for the thermal power transfer from the CSP/Biogas to the ORC cycle. In the case of the thermal power transmission between the CSP and ORC, the contact becomes a liquid-to-liquid thermal power transition. In the case of biogas switching, the fired boiler is responsible for the thermal power delivery to the oil and therefore the contact remains as a liquid-to-liquid transition process (Therminol-VP1 vs Toluene). Generally, for such units, it is recommended (based on the design model) to assign the unit effectiveness. The following relations govern such units according to the energy, exergy, and thermo-economic approaches. The evaporator thermal power (Q), in kW is given by:

$$Q = \dot{m}_h \times \Delta h_h = \dot{m}_c \times \Delta h_c \quad (4-12)$$

where, $\dot{m}_{h,c}$ is the mass flow rates for the hot and cold sides, respectively, and $h_{hot,cold}$ is the enthalpy streams for the hot and cold sides respectively. The total heat transfer area (A), in m^2 for the counter current flow is calculated as follows:

$$A = \frac{Q}{U \times LMTD} \quad (4-13)$$

where,

$$LMTD = \frac{\Delta T_2 - \Delta T_1}{\ln(\Delta T_2 - \Delta T_1)} \quad (4-14)$$

where,

$$\Delta T_1 = T_{h_1} - T_{c_1} = T_{h_i} - T_{c_o} \quad (4-15)$$

$$\Delta T_2 = T_{h_2} - T_{c_2} = T_{h_o} - T_{c_i} \quad (4-16)$$

For simplification, the overall heat transfer coefficient U (in $\text{kW/m}^2 \cdot \text{K}$) for the evaporator, condenser,

and recuperative is calculated using two general equations as defined by El-Dessouky et al. [237]. For the evaporator:

$$U_{ev} = 1 \times 10^{-3}(1939.4 + 1.40562T - 0.0207525T^2 + 0.0023186T^3) \quad (4-17)$$

while for the condenser and the recuperative:

$$U_{cond \text{ or } recp} = 1 \times 10^{-3}(1617.5 + 0.1537T + 0.1825T^2 - 0.00008026T^3) \quad (4-18)$$

The evaporator effectiveness (ε) is assigned in the range of ~80% to calculate the outlet cooling water temperature in the case of the condenser unit, and/or the outlet stream to the solar field in the case of the evaporator operation:

$$T_{ho} = T_{hi} - (\varepsilon \times (T_{hi} - T_{ci})) \quad (4-19)$$

Based on an exergy analysis, the exergy destruction rate (I_{cond}) in kW is developed based on the following expression [238]:

$$I_{cond} = \dot{m}_h[h_i - h_o - T_{amb} \times (s_i - s_o)] + \dot{m}_c[h_i - h_o - T_{amb} - (s_i - s_o)] \quad (4-20)$$

4.3.2.4 Turbine unit

For models based on the design approach, it is particularly important to determine the mass flow rate through the turbine by knowing some of the parameters, such as the turbine efficiency, generator efficiency, and the developed power by the turbine (=AGMD pump load+Main grid load). The outlet enthalpy (h_{out}) of the turbine in kJ/kg is given as follows:

$$h_o = h_i - \eta_t \times (h_i - h_{o_s}) \quad (4-21)$$

where η_t is the turbine efficiency, the subscripts (s, t) represent the isentropic state and the turbine. The cycle flow rate (\dot{m}_t) in kg/s is given as follows:

$$\dot{m}_t = \frac{W_t}{\eta_t \times \eta_g \times (h_i - h_{o_s})} \quad (4-22)$$

where η_g is the generator efficiency. By calculating the ORC flow rate (\dot{m}_t), the CSP/biogas flow rate may then be calculated via the evaporator unit. Based on an exergy analysis, the exergy destruction rate of the turbine (I_t) in kW is calculated based on the following relation [238]:

$$I_t = \dot{m}_t[h_i - h_o - T_{amb} \times (s_i - s_o)] - W_t \quad (4-23)$$

4.3.2.5 AGMD unit

The mean temperature (T_m) of the solution that enters the feed side of the module is calculated in °C

using the following expression:

$$T_m = \frac{(T_{hi} + T_{ci})}{2} \quad (4-24)$$

where the T_{hi} and T_{ci} are the inlet and outlet feed side temperatures.

The mean vapor partial pressure (P_m) in kPa is calculated using the Antoine equation [239], [240]:

$$P_m = \exp \left(23.328 - \left(\frac{3841}{T_m - 45} \right) \right) \quad (4-25)$$

where the mean temperature T_m is expressed in K. The water surface tension (γ_w) in kN/m is determined thus [241]:

$$\gamma_w = (-0.1769 \times T_m + 76.58)^{-6} \quad (4-26)$$

The membrane tortuosity (τ) is the ratio of the length of the average pore to the membrane thickness or length and it can be expressed by:

$$\tau = \frac{(2 - \varepsilon)^2}{\varepsilon} \quad (4-27)$$

where ε , is the membrane porosity. The latent heat of vaporisation (H_{fg}) in kJ/kg, is calculated using

$$H_{fg} = (1.7535 \times T_m) + 2024.3 \quad (4-28)$$

The liquid entry pressure (LEP) kPa is then calculated [241];

$$LEP = \left(\frac{-2 \times \gamma_w}{r_{memb}} \right) \times \cos \theta \quad (4-29)$$

where, r_{memb} is the membrane pore size in m and θ is the intrinsic advancing contact angle between the liquid and the membrane material. The overall mass transfer coefficient (C_w) in m/s can be calculated using the following equation [242] if the T_m is > 50 ;

$$C_w = \left(\left(\frac{2 \times \varepsilon \times r_{memb}}{3 \times \tau \times D_{memb}} \right) \right) \sqrt{\left(\frac{8 \times M_{w_w}}{\pi \times R \times (T_m + 273)} \right)} \quad (4-30)$$

where, D_{memb} is the membrane thickness in m and R is the specific gas constant in ($J/mol K$). The M_{w_w} represent the molecular weight of the water in kg/mol . The overall mass transfer coefficient (C_w) when the T_m is < 50 is determined by [242]:

$$C_w = \frac{\varepsilon \times PD_{va} \times M_{w_w}}{\tau \times D_{mem} \times R(T_m + 273) \times P_m} \quad (4-31)$$

where the PD_{va} is the water-air diffusion coefficient and the average pressure of the air inside the membrane, which can be calculated using [242] as follows:

$$PD_{va} = 1.9851^{-5} \times (T_m^{2.072}) \quad (4-32)$$

The permeate flux (J_p) in kg/m²h is calculated by [242]:

$$J_p = C_w(T_{hi} - T_{ci}) \quad (4-33)$$

where T_{hi} and T_{ci} are the temperature at the feed side of the membrane, °C, and at the cold side of the condensation section.

The mass transfer coefficient (K_m) (in kJ/m.s.K) is determined by using

$$K_m = (J_p \times H_{fg}) / (T_{hi} - T_{ci}) \quad (4-34)$$

The membrane area (A_{memb}) in (m²) is calculated by

$$A_{memb} = \frac{M_p}{J_p} \quad (4-35)$$

The brine loss (M_b) in kg/h is expressed based on:

$$M_b = M_f - M_p \quad (4-36)$$

The salt rejection (SR) is calculated by:

$$SR = 1 - \left(\frac{S_p}{S_f} \right) \quad (4-37)$$

where S_p is the product salinity ratio and S_f is the feed salinity ratio. The brine loss salinity (S_b) is calculated by [239]:

$$S_b = \left((M_f \times S_f) - \left(\frac{M_p \times S_p}{M_b} \right) \right) \quad (4-38)$$

The concentration factor (C_f) is calculated based on the following equation [239]:

$$C_f = \frac{M_f}{M_f - M_p} \quad (4-39)$$

The water recovery ratio (WR) can be determined by [239]

$$WR = 100 \times \left(1 - \left(\frac{1}{C_f} \right) \right) \quad (4-40)$$

The energy transfer through the membrane (Q_{memb}) is expressed in kW by

$$Q_{memb} = Q_{conduction} + Q_{vaporization} \quad (4-41)$$

where,

$$Q_{vaporization} = \frac{J_p \times H_{fg} \times A_{memb}}{3600} \quad (4-42)$$

$$Q_{conduction} = \left(\frac{k_{memb}}{D_{memb}} \right) \times A_{memb} \times T_m \quad (4-43)$$

The thermal conductivity k_{memb} of the membrane in kW/mK varies for different membranes as follows:

$$k_{memb} = \varepsilon k_g + (1 - \varepsilon) \times K_p \quad (4-44)$$

where, k_g is the gas thermal conductivity, kW/mK in the pores of the membrane and is calculated as follows:

$$k_g = ((0.01383 \times \exp(0.005486 \times T_m)) + (3.344 \times 10^{17} \times \exp(0.0986 \times T_m))) \times 10^{-3} \quad (4-45)$$

The gain ratio (GOR) as a function of the specific feed flow rate in kg/m².h is calculated by

$$GOR = 6.467 \times \exp\left(-0.03327 \times \left(\frac{M_f}{A_{memb}}\right)\right) + 2.49 \times \exp\left(-0.002543 \times \left(\frac{M_f}{A_{memb}}\right)\right) \quad (4-46)$$

The thermal efficiency of the membrane (η_{memb}) is expressed as follows:

$$\eta_{memb} = \frac{Q_{vaporization}}{Q_{memb}} \quad (4-47)$$

The number of pores (NOP) is calculated using

$$\begin{aligned} NOP = & 247.3 - 198.1 \times \cos(r_{memb} \times 1.13 \times 10^7) + 237.2 \times \sin(r_{memb} \times 1.13 \times 10^7) \\ & - 31.65 \times \cos(2 \times r_{memb} \times 1.13 \times 10^7) \\ & - 69.25 \times \sin(2 \times r_{memb} \times 1.13 \times 10^7) \end{aligned} \quad (4-48)$$

The pump power (W_{pump}) is defined in kW by [243]:

$$W_{pump} = \frac{M_f \times \Delta P}{\rho_w \times \eta_{pump} \times 3600} \quad (4-49)$$

where ρ_w and η_{pump} are the water density and pump efficiency, respectively. ΔP is the net pressure difference across the membrane. The specific power consumption (SPC) in kWh/m³ is calculated as follows:

$$SPC = \frac{1000 \times W_{pump}}{M_p} \quad (4-50)$$

The exergy calculation models the seawater as a solution of various ionic species and calculates the exergy rates at the process stages under consideration using [244]–[246] as follows:

$$\dot{E} = \dot{m} \left(C_p \times (T - T_0) - C_p \times T_0 \ln\left(\frac{T}{T_0}\right) \right) + \frac{P - P_0}{\rho} - N_{solvent} R T_0 \ln x_{solvent} \quad (4-51)$$

where, \dot{m} is the mass flow rate (kg/h); C_p is the specific heat capacity (kJ/kg.K); T is the absolute temperature (K) at the process stage under consideration; T_0 is the absolute temperature (K) at the dead state; P and P_0 refer to the pressures (kPa) at the process stage and the dead state respectively; ρ is the density of the solution (kg/L). $N_{solvent}$ is the number of moles of the solvent per kilogram of the solution (mol/kg); R is the universal gas constant (kJ/mol.K); $x_{solvent}$ is the mole fraction of the solvent

(dimensionless).

The number of moles of the solvent ($N_{solvent}$) is calculated using equation (4-53), while the mole fraction of the solvent ($x_{solvent}$) is calculated using equation (4-54) as follows:

$$N_{solvent} = \frac{(1000 - \sum \frac{C_i}{\rho})}{Mw_{solvent}} \quad (4-52)$$

$$x_{solvent} = \frac{N_{solvent}}{(N_{solvent} + \sum (\frac{\beta_i C_i}{\rho M w_i}))} \quad (4-53)$$

where, C_i is the concentration in unit mass per litre (g/L) of solute species i ; $Mw_{solvent}$ is the molar mass of the solvent g/mol, pure water in this case; β_i is the number of particles of solute species i generated on dissociation and Mw_i is the molar mass ($\frac{g_i}{mol_i}$) of solute species i .

The exergy destruction rate in the air gap membrane distillation (I_{MD}) is calculated in kW using [247] as follows:

$$I_{MD} = \dot{E}_p + \dot{E}_f - \dot{E}_b - \dot{E}_x \quad (4-54)$$

where \dot{E}_f represents the chemical and physical exergy of the seawater feed stream to the air gap membrane distillation, \dot{E}_b is the exergy stream associated with the brine, while \dot{E}_x is the chemical and physical exergy stream of the permeate product, and \dot{E}_p is the exergy produced by the pump.

4.3.2.6 Biogas boiler unit

For the design technique in the modeling, it is very important to calculate the biogas mass flow rate in kg/s that is acquired from the anaerobic digestion process [235]:

$$\dot{M}_{bg} = \frac{(\dot{M}_{oil} \times (h_{oil_o} - h_{oil_i}))}{Cv} \times \eta_{bg} \quad (4-55)$$

Air mass flow rate kg/s:

$$\dot{M}_{air} = \frac{A}{F} \times \dot{M}_{bg} \quad (4-56)$$

where A/F is the air to fuel (gases) ratio. The exit exhaust temperature is given as follows:

$$T_{exh} = \frac{(\dot{M}_{bg} \times Cv) - (\dot{M}_{oil} \times (H_{oil_o} - H_{oil_i}))}{(\dot{M}_{bg} + \dot{M}_{air}) \times Cp_{bg}} \quad (4-57)$$

where Cv is the gases calorific value, kJ/kg, and Cp_{bg} is the specific heat capacity, kJ/kg.K of the waste gases, kJ/kg°C. The biogas power, kW, is given as follows:

$$Q_{bg} = \dot{M}_{bg} \times Cv \quad (4-58)$$

The specific fuel consumption, kg/kWh, is found using

$$SFC = \frac{3600 \times \dot{M}_{bg}}{Q_{bg}} \quad (4-59)$$

The biogas destruction rate can be calculated in kW using the following equation [235]:

$$I_{bg} = E_i + E_{oil_i} - E_{oil_o} \quad (4-60)$$

where E_i is the biogas boiler power; E_{oil_i} is the exergy oil stream inlet and E_{oil_o} exergy oil stream out.

4.3.2.7 Anaerobic digestion unit

Anaerobic digestion is a sequence of processes by which microorganisms break down biodegradable materials in the absence of oxygen. The process is used for industrial or domestic purposes to manage waste or to produce fuel. Much of the fermentation used industrially is to produce food and drink products, as well as home fermentation, using anaerobic digestion. As a part of an integrated waste management system, anaerobic digestion reduces the emission of landfill gas into the atmosphere.

The biogas volume is calculated based on the design analysis where the load from solar/ORC/MD section is calculated. As a result, the calculated volume is adequate for power maintenance. The following mathematical design model requires the calculation of the mass flow rate from the gas boiler. The production rate of the gas calculates the digestion design aspects such as volume, height, flow rate, area, load, etc. The total volume based on the collection volume, m^3 is given as follows [248][249]:

$$Vt = \frac{Vcol}{0.05} \quad (4-61)$$

where, $Vcol$, m^3 is the total biogas collection volume needed daily in the boiler when solar energy source is not available. The sludge layer volume (Vsl) based on the total volume, m^3 is then calculated based on the total volume as follows.

$$Vsl = 0.15 \times Vt \quad (4-62)$$

Working volume (Vgd) of the gas digestion in m^3 is given as follows:

$$Vgd = 0.8 \times Vt \quad (4-63)$$

Total influent required (Q) in kg is then calculated based on the retention time RT , days, is given as follows:

$$Q = \frac{Vgd \times 1000}{RT} \quad (4-64)$$

Total solids (TS) in kg needed for the gas production process is then calculated based on Q , kg, and the total solids concentrations SC , %.

$$TS = \frac{SC \times Q}{100} \quad (4-65)$$

The total discharge (TD) in kg, is found to be

$$TD = \frac{(100 \times TS)}{TSC} \quad (4-66)$$

where, TSC is the total solid concentration contents, %. The water mass (WM) to be added, kg is then calculated as $WM=Q-TD$.

The digester loading (DL), in $\text{kg}/\text{m}^3\text{day}$ is calculated based on the organic dry matter (ODM) parameter, total volume (Vt) and total influent (Q) needed as follows:

$$DL = \frac{ODM \times Q}{Vt \times 100} \quad (4-67)$$

4.3.3 The cost considerations

In this part, cost analysis is presented to calculate the total water price TWP in $\$/\text{m}^3$, and the hourly costs, $\$/\text{h}$ indicators. Since the total freshwater productivity and the user load are the main causes of the electric power load on the ORC turbine via an AGMD pump and being the thermal load on the ORC via the ORC condenser, the TWP, $\$/\text{m}^3$ is a very important indicator in this study. For membrane distillation, the direct capital costs, $\$$, is calculated based on the membrane area A_{mem} , m^2 , as follows [250]:

$$DCC = \frac{A_{mem} \times 150000}{800} \quad (4-68)$$

The indirect capital costs ICC , is found to be 27% of the direct capital cost,

$$ICC = 0.27 \times DCC \quad (4-69)$$

Hence, the total capital costs TCC , $\$$ is calculated as

$$TCC_{md} = ICC \times DCC \quad (4-70)$$

The Annualised capital costs are calculated based on the amortisation factor, $1/y$, as follows:

$$A_f = \left(\frac{ir \times ((1 + ir)^{LT_p})}{((1 + ir)^{LT_p}) - 1} \right) \quad (4-71)$$

where ir is the interest rate, ($\sim 5\%$) and LT_p is the plant lifetime.

The annualised capital cost $\$/\text{year}$ becomes as

$$ACC_{md} = TCC_{md} \times A_f \quad (4-72)$$

The hourly costs, $\$/\text{h}$ of the membrane distillation is then calculated based on the operating hours per year as

$$Z_{md} = \frac{ACC_{md}}{OH \times 365} \quad (4-73)$$

where OH is the Operating Hours. For solar ORC, the following steps are considered as listed in Table 4.2 [144], [251].

Table 4.2: IC and O&M costs for the solar organic Rankine cycle components.

Parameter	IC, \$	O&M, \$	TCC, \$/year	Z ^{IC&OM} , \$/h	Ref
Solar field	$639.5 \times (A_{col})^{0.95}$	$15\% \times IC_{col}$	$A_f \times (IC + O\&M)_{col}$	$TCC_{col}/8760$	
Turbine	$4750 \times (W_t)^{0.75}$	$25\% \times IC_{st}$	$A_f \times (IC + O\&M)_{st}$	$TCC_{st}/8760$	
Recuperator	$150 \times (A_{rec})^{0.8}$	$25\% \times IC_{rec}$	$A_f \times (IC + O\&M)_{rec}$	$TCC_{rec}/8760$	[144],
Condenser	$150 \times (A_{cond})^{0.8}$	$25\% \times IC_{cond}$	$A_f \times (IC + O\&M)_{cond}$	$TCC_{cond}/8760$	[251]
Pump	$3500 \times (W_p)^{0.47}$	$25\% \times IC_{pump}$	$A_f \times (IC + O\&M)_{pump}$	$TCC_{pump}/8760$	

For the anaerobic biogas cost analysis, the following steps are considered [252]. The specific capital cost, SCC, \$/m³ is calculated based on the total biogas collection volume as follows:

$$SCC = \begin{cases} 155.1 & \dots Vcol < 150 \text{ m}^3 \\ 141.04 & \dots Vcol > 150 \text{ m}^3 \\ 127 & \dots Vcol > 550 \text{ m}^3 \end{cases} \quad (4-74)$$

The total capital cost, \$+variable costs=7% of total capital costs:

$$TCC_{bg} = (SCC \times Vcol) + (0.07 \times SCC \times Vcol) \quad (4-75)$$

Hence, the total annual costs, TAC, \$/y becomes:

$$TAC_{bg} = TCC_{bg} \times A_f \quad (4-76)$$

Then the hourly costs, \$/h become

$$Z_{bg} = \frac{TAC_{bg}}{365 \times 24} \quad (4-77)$$

For the fired biogas boiler, the hourly cost is calculated based on the cost of biofuel (CF) and mass flow rate from the anaerobic digestion system and it is calculated as follows:

$$Z_{bgb} = CF \times M_{bg} \times 3.6 \quad (4-78)$$

Then, the total hourly costs in \$/h is calculated as the summation of all units, namely,

$$Z_{tot} = Z_{md} + Z_{col} + Z_{bg} + Z_{bgb} + Z_{ev} + Z_{st} + Z_{rec} + Z_{cond} + Z_p \quad (4-79)$$

Then, the total water price, \$/m³ is calculated based on the plant productivity in m³/h, and the load factor, LF as follows:

$$TWP = \frac{Z_{tot}}{M_p \times LF} \quad (4-80)$$

where, the LF is the load factor of the plant, and it is set to be 0.9.

4.4 Results and Discussions

To obtain the design results, the most appropriate operating conditions should be assigned. As it is performed in this new system model, the total plant productivity takes all the design aspects which are calculated in this work. For instance, a high rate of productivity would result in a large plant area, and a high rate of cost. Therefore, the system units with the greatest influence are optimised for the best operating conditions.

4.4.1 Mathematical model validation

The main concern in the numerical modelling in predicting the physical behaviour of the real system is the accuracy of the utilised model. In this section, the obtained simulation results are validated against theoretical and real data that is available in the open literature. Due to lack of data for the integrated system, each component is validated individually and therefore it is reasonable to assume that the model for the integrated microgrid is reliable.

4.4.1.1 Solar ORC model validation

The simulation results of the Solar ORC system are validated under the same conditions as the findings from Torres et al. [140]. Table 4.3 lists the main specifications of the solar ORC model used for validation. The comparison reveals a very good agreement between the two results, as depicted in Table 4.4. For example, the Rankine efficiency value has errors of approximately 4.06% compared to the reference study. Thus, this model may be used with confidence for further investigations to improve the overall performance of the proposed system.

Table 4.3: Design specifications of the 100 kW Solar ORC system [140].

Specifications	Unit	Quantity
PTC type	-	LS-3
Working fluid	-	Toluene
Power	kW	100
Solar radiation	W/m ²	850
Recuperator effectiveness	%	80
Evaporation temperature	°C	300
Turbine efficiency	%	75
Pump efficiency	%	75
Superheating temperature	°C	380

Table 4.4: Data validation results of the Solar ORC model.

Description	The developed model	Ref [140]	Error (%)
Evaporation pressure, bar	32.75	33.737	2.926
Condenser pressure, bar	0.06214	0.0624	0.417
Working fluid mass flow rate, kg/s	0.4515	0.442	2.149
Thermal power rejected, kW	209	209.8	0.381
Rankine efficiency, %	30.49	31.78	4.059
PTC area, m ²	503	514.3	2.197

4.4.1.2 AGMD model validation

The reliability of the AGMD model was tested under the same operating conditions against the experimental data obtained from the pilot solar thermal AGMD plant located in Port Said City, Egypt [253]. The main specifications and the operational condition of the pilot plant are given in Tables 4.5. The comparison reveals a very good agreement between the developed model and real plant data as seen in Table 4.6. It is found that the area of the developed AGMD model has a deviation of approximately 4.86% compared to the Port Said pilot plant. Therefore, this new integrated model may be used with confidence for further investigations to improve the overall performance of the proposed system.

Table 4.5: AGMD module properties and specifications [253].

Description	Parameters	Port Said plant
Specifications	Materials	Polyethylene (PE)
	Total net Membrane surface area	14.4 m ²
	Diameter	0.4 m
	Air gap thickness	1 mm
	Porosity of membrane sheet	85%
	Tortuosity of membrane sheet	1.56
	Thermal conductivity of membrane sheet	1.35 W/m K
	Mean pore size diameter	0.3 μm
The spacer characteristics	Channel thickness	2.01 mm
	Spacer filament thickness	1.005 mm
	Spacer angle (0-90)	60 deg
Operating data	Feed flow rate	10 L/min
	Inlet hot water temperature	64.81 °C
	Inlet cold water temperature	34.66 °C
	Salinity of hot flow	40-60 g/kg
	Salinity of cold flow	35 g/kg

Table 4.6: Data validation results of the AGMD model.

Parameters	The developed model	Experiment study [253]	Error (%)
Outlet cold water temperature, °C	62.2	60.7	2.47
Outlet hot water temperature, °C	40.45	39.67	1.97
Permeate flux, kg/h	18.62	18.01	3.39
Area, m ²	15.1	14.4	4.86

4.4.2 Membrane distillation operating conditions

For membrane distillation, the selection of the membrane type has a significant influence on the system design and performance. Therefore, to select the best-operating conditions, it is vital to investigate the performance of different membrane material types to identify the one with the most striking results. For that purpose, all the input data was set to be the same for all membrane types in order to ensure a fair comparison between each type. Table 4.7 and Figures 4.4-4.6 illustrate the data comparison between all the addressed types. The permeate flux of all the types vary from approximately 2-6, kg/m²/h, which is in the expected range compared to [254], [255]. The exergy destruction rate was recorded as being almost the same for all the types, as shown in Figure 4.4. The range of the exergy destruction rate was found to be between 5.5 and 5.6 kW. The SPC ranges between 1 and 2.6 kWh/m³ which is considered to be quite low and remarkable if compared to the Reverse Osmosis desalination where it has been calculated in the range of 2.5 to 4 kWh/m³ in [256]. The SPC in kWh/m³ was recorded to be lower in the C-PVDF, E-PH, E-CNT0.5, E-CNT1, E-CNT2, and E-CNT3 membrane types if compared against the PTFE and PP. The liquid entry pressure is recorded to be above 100 kPa for all membrane distillation types except for the PVDF. This means that the AGMD using the PVDF type needs to be run under a partial vacuum to avoid “wetting” of the membrane. The PE type yielded the largest membrane area among the remaining membrane types by 10.7~11 m² followed by the PTEE type with 9.5~10 m². A larger area yields a higher hourly cost rate. Therefore, the types of C-PVDF, E-PH, E-CNT0.5, E-CNT1, E-CNT2, and E-CNT3 were recorded to be the lowest in terms of the hourly costs in \$/h. Generally, the hourly costs are found to be in the range of 0.01 to 0.035 \$/h which is considered exceptionally low when compared with the costs of the reverse osmosis or nanofiltration processes. On the other hand, the GOR parameter was recorded in the range of 1.8 to 3.7. The highest and lowest values were recorded for the E-PH and E-CNT2, respectively. It is significantly found that the higher values of the GOR harvest larger membrane areas, hence, higher values of the hourly costs. Based on the analysis that has been presented in Table 4.7 and Figures 4.4-4.6, the E-PH membrane type was selected for this study. Its permeated flux is in an acceptable range and also gives a remarkable result for the hourly costs in \$/h.

Table 4.7: Data results of the air gap membrane distillation based on different membrane types.

Parameter:	PTFE	PP	PVDF	PE	C-PVDF	E-PH	E-CNT0.5	E-CNT1	E-CNT2	E-CNT3
Exergy destruction, kW	5.584	5.608	5.545	5.592	5.567	5.570	5.570	5.565	5.565	5.55
SPC, kWh/m ³	2.217	3.365	0.334	2.618	1.400	1.547	1.480	1.300	1.330	0.900
GOR	3.438	2.885	3.280	3.740	3.288	1.923	1.976	1.900	1.850	1.920
Permeate flux, kg/m ² .h	2.205	2.847	2.360	1.944	2.355	5.503	5.230	5.616	6.000	5.520
Liquid entry pressure, kPa	274	416	41.360	324	172	191	183	160	164	110
Permeability coefficient	0.105	0.135	0.1123	0.0924	0.112	0.261	0.250	0.267	0.282	0.262
Area, m ²	9.448	7.318	8.818	10.720	8.847	3.786	4.000	3.710	3.500	3.770
No. of pores	25	608	321	608	25	82	302	630	631	28
Hourly costs, \$/h	0.035	0.027	0.033	0.040	0.033	0.014	0.015	0.0138	0.0131	0.0141

Productivity, m³/day=500

Product salinity, ppm=500

Inlet cold water temperature, °C=20

Inlet hot water temperature, °C=52.4

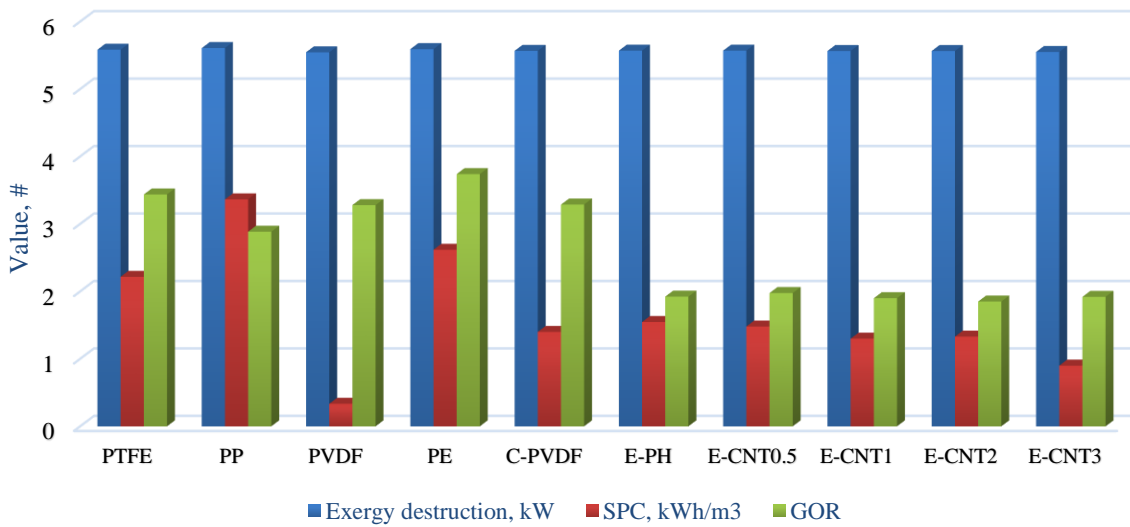


Figure 4-4: Comparison of the addressed types of MD related to the exergy destruction rate, kW, SPC, kWh/m³, and GOR parameters.

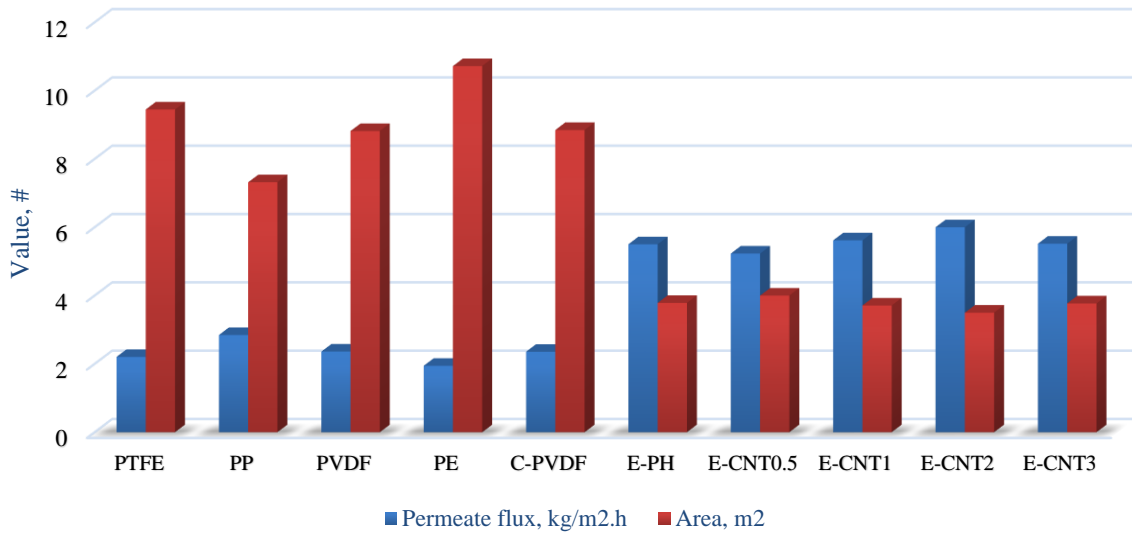


Figure 4-5: Data comparisons for all MD types related to the permeate flux and membrane area.

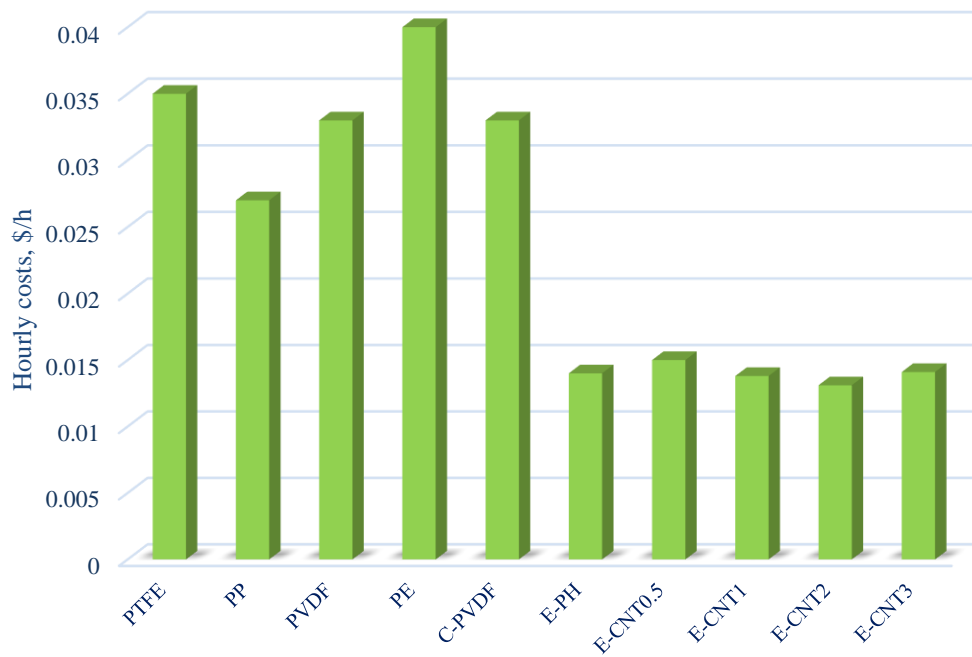


Figure 4-6 :Data comparison between the MD types related to the hourly costs.

Figure 4.7 shows the optimised results according to some of the most important indicators, such as SPC in kWh/m³, GOR, membrane area in m², and hourly cost in \$/h. All these indicators are performed for the optimised E-PH membrane type only. Figure 4.7-a shows that the SPC is recorded to be high at lower rates of system productivity. Increasing the productivity led to a reduction in the SPC from 1.8 to 1.5kWh/m³. While the cold side temperature variation has no significant effect on the SPC. However, Figure 4.7-b shows that the cold side temperature has a remarkable influence on the GOR. Increasing the inlet fluid temperature could lead to a significant increase in the GOR from 2 @ 15°C up to 4.5 @ 35°C. The productivity variation was found to have only a slight effect on the GOR. Figure 4.7-c shows that increasing productivity and temperature has a direct effect on the membrane area. However, a notable effect is observed in the variation of the system productivity compared to the temperature recorded to have a slight effect on the membrane area. The area has been increased from 5m² @ (15°C, 100m³/day) up to 35m² @ (35°C, 1500m³/day). On the other hand, Figure 4.7-d is a direct reflection to Figure 4.7-c. Increasing the membrane area result in a direct increase in the hourly costs, as shown in Figure 4.7-d. Similarly, the hourly costs increase from 0.05\$/h @ (15°C, 100m³/day) up to 0.25\$/h @ (35°C, 1500m³/day). In general, the hourly costs are strikingly low and can compete against reverse osmosis technology. Moreover, to obtain better results, it is very highly recommended to increase the inlet feed temperature into the condenser unit to over 35°C.

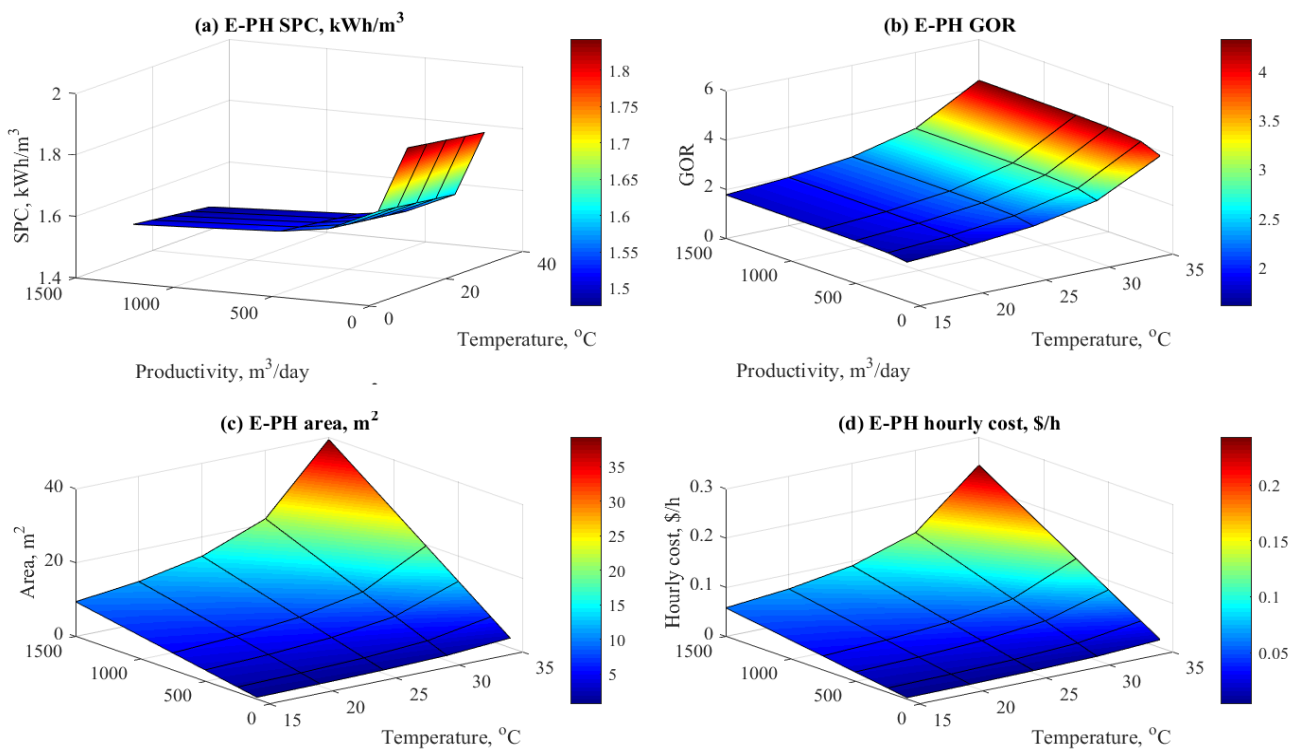


Figure 4-7: Data results for the E-PH membrane distillation type based on the cold side temperature and productivity.

4.4.3 Solar/Biogas operating conditions

In this section, the influence of the operating conditions on the hybrid connection has been addressed. For the anaerobic digestion design model, the collection volume is assigned by the user and then all the design aspects of the biogas plant, such as volume, height, flow rate, area, load, etc. are calculated. Therefore, to select the best operating conditions, it is important to study the effect of the collection volume variations between 100 and 500 m³ at different retention times of 25-50 days on five different parameters, such as, the quantity of water that needed to be added in the digestion process (kg), the total influent required (kg), the total solid (kg), the total discharge (kg) and the biogas cost \$/h. In this investigation, cattle manure properties have been used. Figure 4.8 shows the obtained biogas anaerobic digestion design results based on the variations of the collection volume and retention time. It is indicated that the amount of water needed in the anaerobic digestion using cattle manure is increased at higher collection volume demand, especially at the lower retention time of 25 days compared to 50 days due to the increased demand for biogas production. Similar results are observed for the total amount of influent required, the total solid, and the total discharge, see Figures 4.8-b, 4.8-c and 4.8-d. For instance, at a collection volume of 300 m³, the total influent required at 50 days of retention time is found to be 1x10⁵ kg, while at 25 days of retention time the total amount of influent is 2x10⁵ kg. Moreover, the hourly costs are increased with respect to the collection volume but are not affected by the variation of the retention time. This is because the hourly costs are a function of the collection volume regardless of the retention time of the process. It is observed that at a collection volume of 200 m³, the obtained biogas cost is approximately 0.3 \$/h, and it reaches 0.8 \$/h at 500 m³. The fluctuation in the hourly costs is due to the fact that the specific capital cost, SCC, \$/m³ is calculated based on the total digestion volume as described in the cost consideration.

For the solar part, it is considered vital to investigate the effect of the variations in power generation and water production on the PTC mass flow rate of kg/s, specific solar area (SSA, m²/m³/day), PTC collectors' hourly cost of \$/h, and total water price, TWP, \$/m³. Figure 4.9 shows the obtained PTC results based on the variations of the power generation (load on the ORC) and productivity ranges (freshwater from AGMD). As expected, the PTC flow rate will increase gradually as the power generation increases. On the other hand, the water productivity appears to have a slight effect on the PTC flow rate.

For instance, at a 3000 kW power load and 100 m³/day, the PTC flow rate increases from 18 kg/s to just over 20 kg/s at 5000 m³/day as indicated in Figure 4.9-a. This leads to a remarkably similar behaviour as that obtained from the collector's hourly cost (see Figure 4.9-c). However, it is found that there is a huge

effect of the variation of the water productivity on the SSA and TWP as seen in Figures 4.9-b and 4.9-d. This was because, at high productivity values, such as at 5000 m³/day, the water cost price was reduced as anticipated when compared to 100 m³/day.

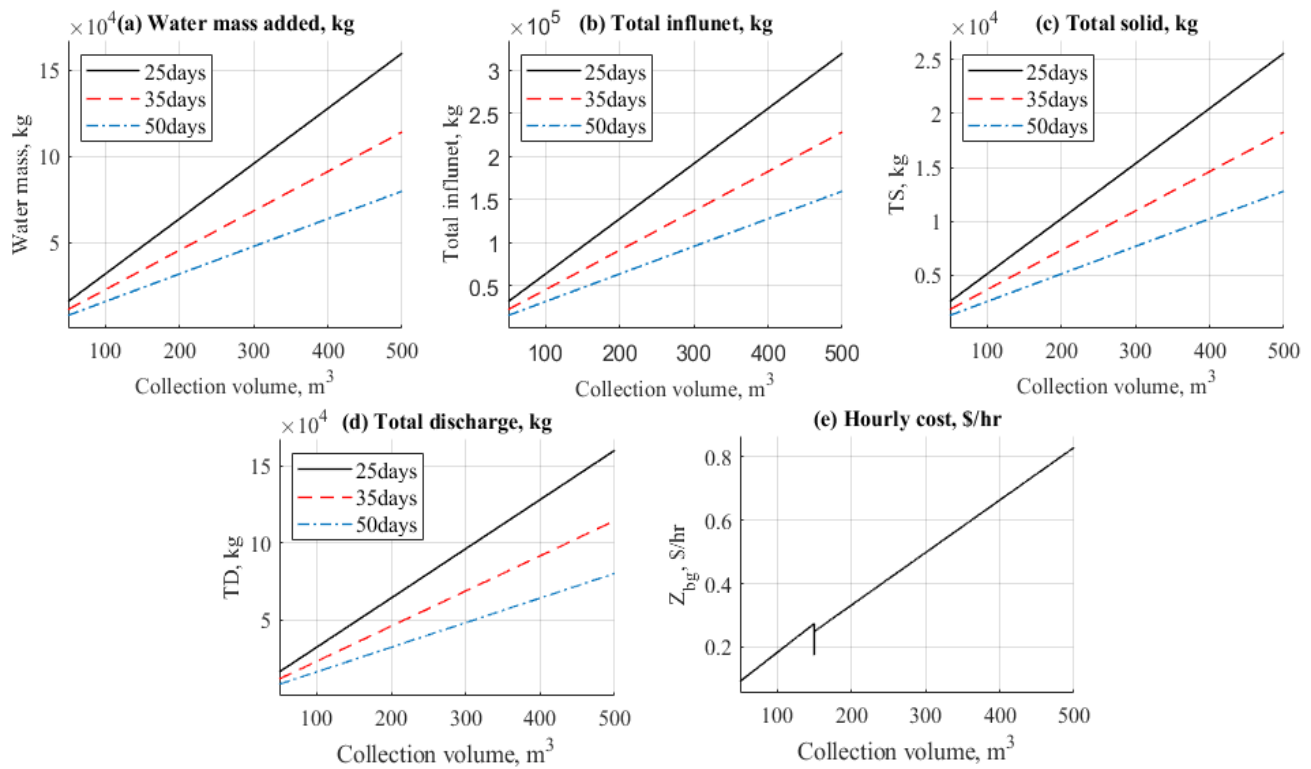


Figure 4-8: Anaerobic digestion results based on the variations in the collection volume and retention time.

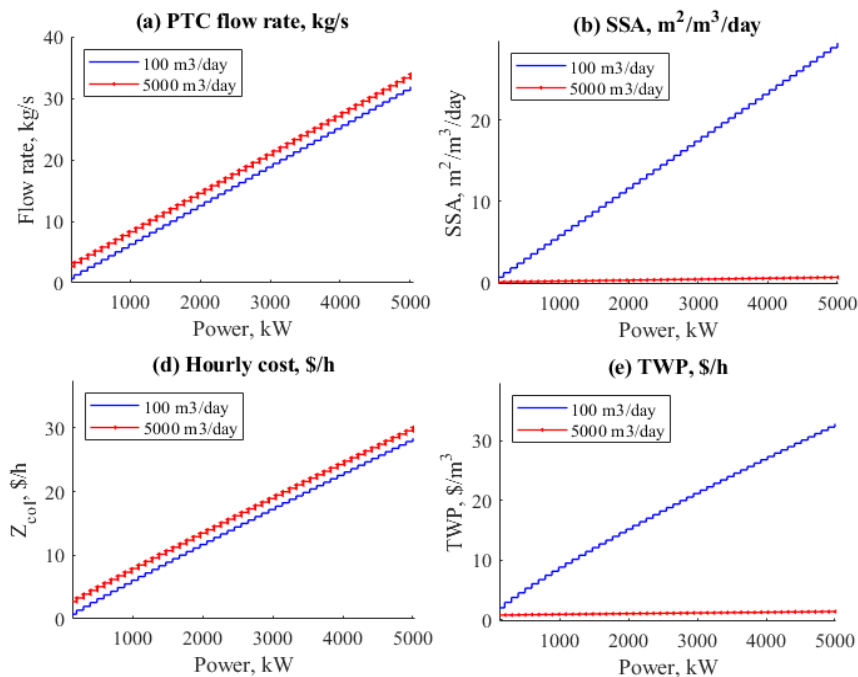


Figure 4-9: PTC results based on the variations of the power generation and productivity.

4.4.4 ORC operating conditions

In the last decade, the ORC has attracted considerable attention because of its great potential, especially for the use of positive slope working fluids such as Toluene and Pentane. Positive slope organic fluids can be used for direct and indirect vapor generation through the solar fields. In this study, Therminol-VP1 is very suitable for PTC because its top temperature can be reached at 450~500°C without any severe stresses on the absorber tube of the PTC combined with a maximum pressure of no more than 15 bar. Moreover, Toluene is used in ORC because it has a positive slope on the T-S diagram, i.e. there is no need for superheating conditions. The selection of Toluene was performed and studied previously by Nafey et al. [242]. Figures 4.10-a, b shows the positive slope behavior of Toluene in relation to the temperature and enthalpy when compared with water. It is pinpointed from the figure that using a recuperator is particularly important because the outlet turbine condition is still in the superheated region. The selection of Toluene depends on many criteria and the most important recognised criteria is the maximum operating temperature of the cycle. The following criteria are achieved by the Toluene working fluid [242]:

- High molecular weight to reduce the turbine nozzle velocity and reasonable pressure corresponding to the boiling temperature of the fluid (high pressure requires careful sealing to avoid leakage).
- Dry expansion, i.e., the positive slope of the vapor saturation curve on the T-S diagram, to ensure that all expansion states in the turbine exist in the superheated region (see Figure 4.10).
- Regeneration can increase the inlet exergy stream or decrease the total exergy destruction rate for the whole cycle.
- The critical temperature is substantially above the maximum operating temperature of the cycle.
- Reasonable pressure at condensing temperature (usually about 30-50°C).

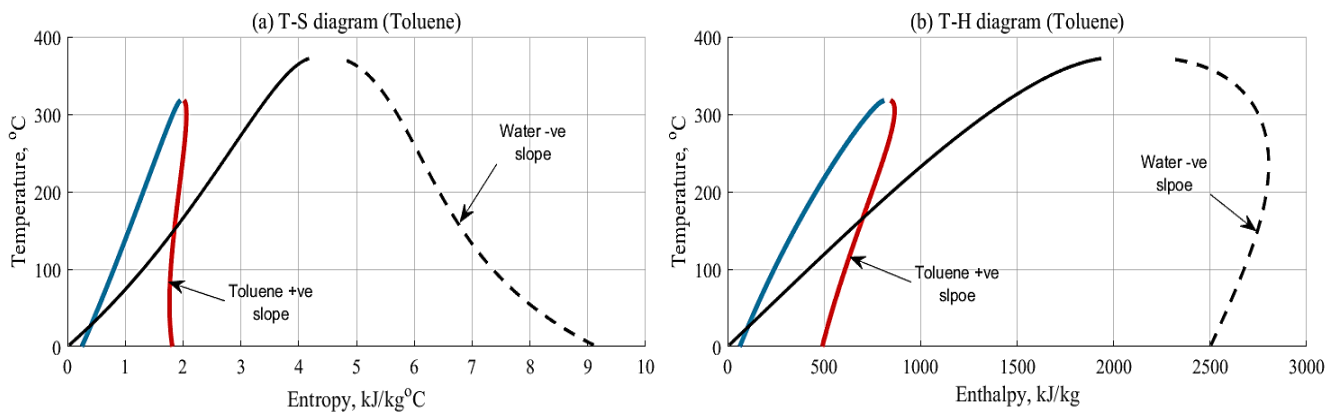


Figure 4-10: (a) Toluene positive slope behavior regarding the T-S, and (b) T-H.

In the ORC section, it is important to study the effects of the top vapor temperature in the evaporator and the condenser temperature on the outlet turbine temperature, recuperator temperatures, and the ORC efficiencies. Figure 4.11-a shows that by increasing the vapor temperature, T_{vo} , °C, the outlet turbine temperature increases. However, the condenser temperature, T_{cond} , °C, has a minor effect on the outlet turbine temperature. For instance, at 250 °C for the vapor temperature and 35 °C for the condenser temperature, the outlet turbine temperature is recorded to lie between 110 °C and 115 °C. Figure 4.11-b shows that the outlet recuperator temperature is affected by variations of the vapor temperature and condenser temperature. For instance, at a vapor temperature of 250 °C, and condenser temperature of 35°C, the recuperator temperature is recorded between 50 °C and 55 °C. Increasing the vapor temperature and condenser temperature increases the outlet recuperator temperature and which means that there is more steam for regeneration.

Figure 4.11-c shows the variation of the ORC thermal efficiency, and the maximum effect is noticed by the increase of the top vapor temperature. For instance, at vapor temperatures close to 300 °C, the range of the Rankine efficiency lies between 28 and 30% which is reasonably noticeable for ORC when compared to [140], [257]. Therefore, it is significant to operate the ORC at high values of the vapor temperature. On the other hand, the condenser temperature plays a minor role in Rankine efficiency.

Figure 4.11-d shows the ORC exergy efficiency based on the variation of the top vapor temperature and condenser temperatures. It should be noted that the condenser temperature has a great influence on the exergy efficiency term. For instance, the exergy efficiency of the ORC is in an increasing mode while the condenser temperature is in the range of 30 °C and 35 °C. Moreover, the optimised top vapor temperature for significant values of the exergy efficiency is in the range of 250 °C to 275 °C. Generally, the condenser temperature value of 35 °C and vapor temperature value of 275~300 °C are quite suitable for achieving better system performance.

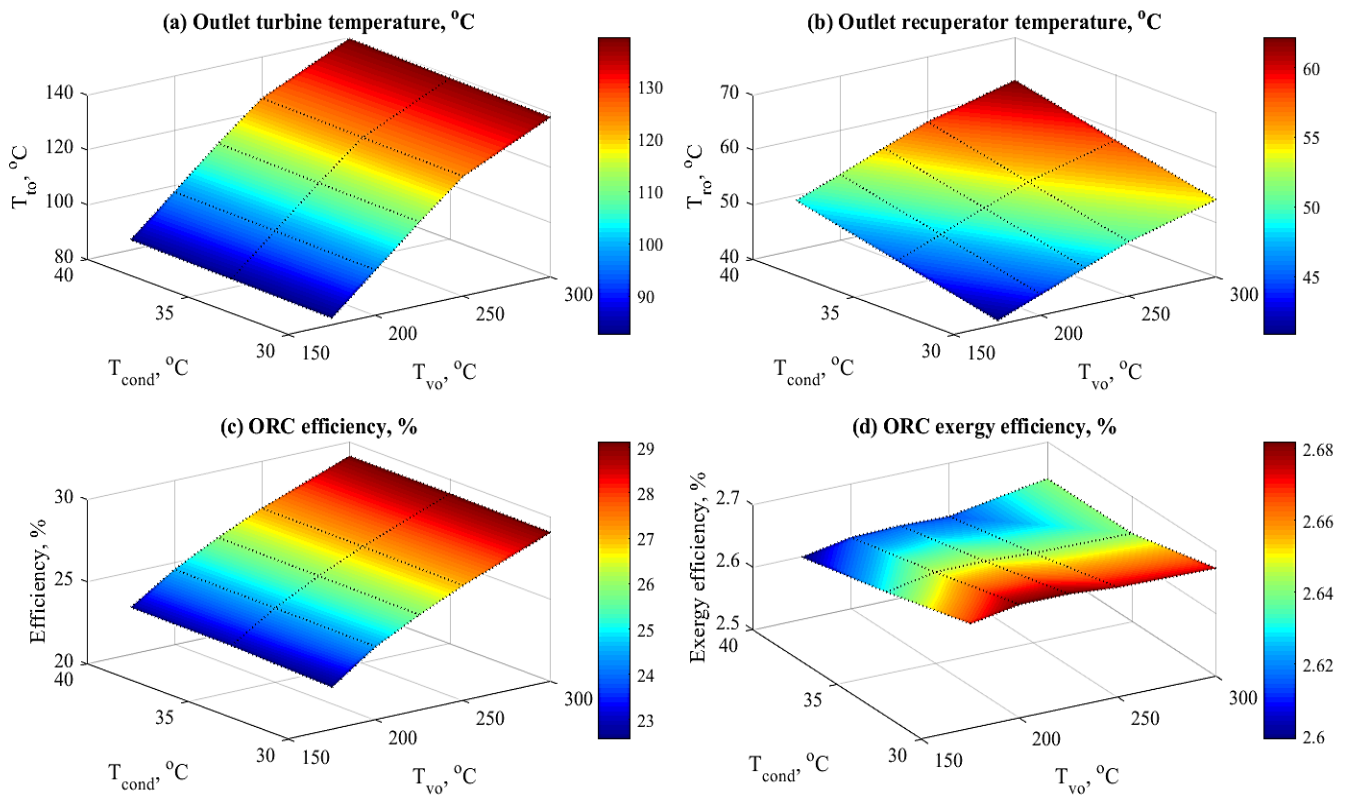


Figure 4-11: The variation in the outlet turbine temperature, recuperator temperature and the ORC efficiencies based on the top vapor temperature and condenser temperature.

4.4.5 Data results of the optimised hybrid cogeneration system

In this section, the results of the cogeneration hybrid system based on the optimised design indicators are presented. The thermodynamic parameters of the optimised proposed system such as temperature, specific enthalpy and pressure of each indicated stream in Figure 4.1, are shown in Table 4.8. Figure 4.12 shows the Solar (PTC) ORC operating conditions on the T–S diagram. The results illustrate the importance of utilising the organic Rankine concept instead of steam to decrease the degree of risks of using water steam and molten salt as operating conditions. Moreover, the outlet turbine condition at 140 °C, as indicated in Figure 4.12, is still remained in the superheated region which allows the benefit of adding a recuperative section for the regeneration stage before using the energy of the solar-biogas field. Utilising a recuperator unit will reduce the thermal power load on the CSP/biogas, which leads to a reduction in the total area of the CSP/biogas and therefore the reduction in the total cost of the technology. Furthermore, the vapor outlet temperature of the toluene after the regeneration of the recuperative at

62 °C can be utilised in the condenser to heat up the seawater stream (heat sink cooling water) that enters at 25 °C and leaves at 52 °C. The heated water can then be transferred to the AGMD desalination.

Table 4.8: Data streams of the optimised proposed hybrid system.

Streams	1	2	3	4	5	6	7	8	9	10	11
Temperature, °C	165	400	163.1	300	140	62.17	40	42.84	103.9	52.73	25
Specific enthalpy, KJ/kg	264.2	800.7	262.7	860.91	675.6	561.5	130.3	135.4	249.5	-	-
Pressure, bar	10.88	10.88	0.067	32.75	0.0784	0.0784	0.0784	32.75	32.75	-	-

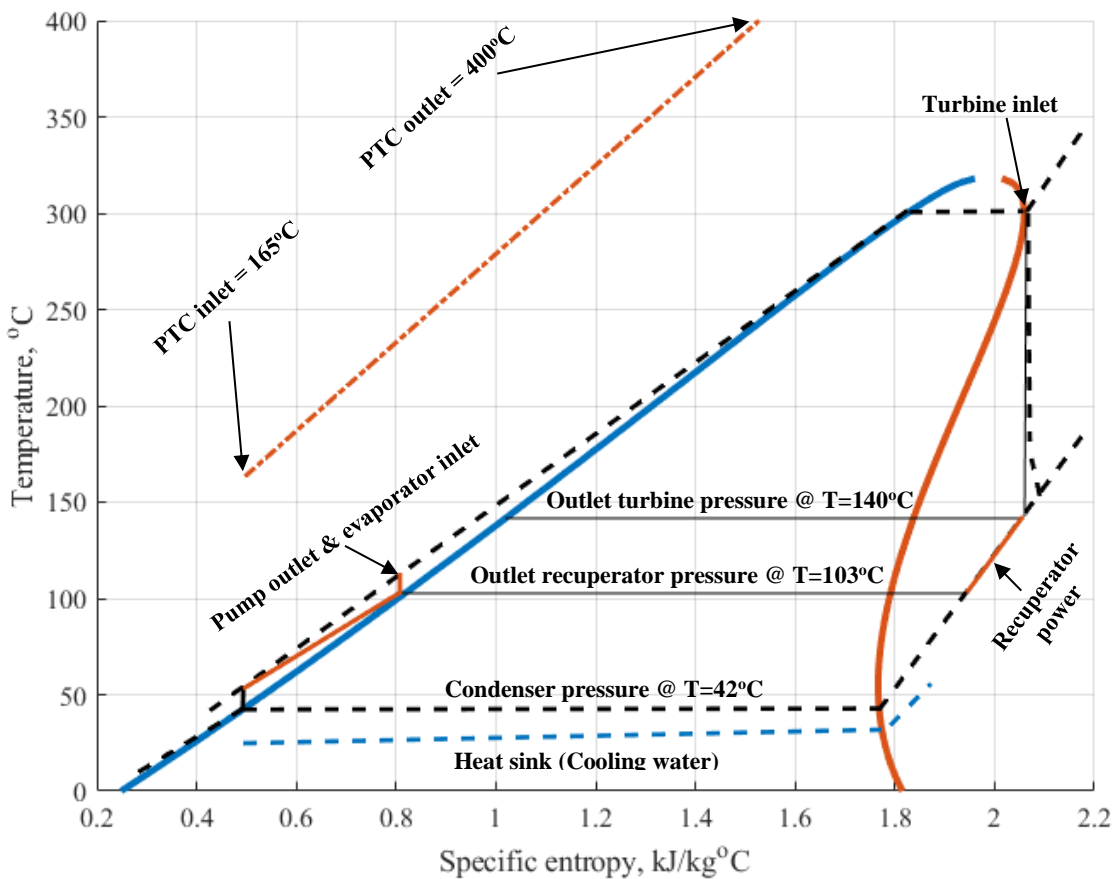


Figure 4-12: The Solar (PTC) ORC operating conditions on the T–S diagram.

Table 4.9 illustrates the results that the hybrid system undergoes while desalination and power are operating. If more power is requested from the ORC, then this increases the total load on the ORC turbine, i.e., increasing the total mass flow rate through the ORC units. Furthermore, increasing the load on the ORC requires a larger area for the energy required by the PTC or a larger volume from the anaerobic biogas

digestion (ABGD) plant. Table 4.9 shows that to generate 1500 kW of power, as well as producing 1500 m³/day of freshwater, the total PTC area increases to 11280 m². In addition, the mass flow rate through the solar field and/or the biogas plant was also increased up to 10 kg/s. Furthermore, the total ABGD required in terms of total volume for the power and desalination was increased to 1.122e5m³. The ORC efficiency is found to be 29.2% which is considered an attractive and remarkable outcome. As shown in Table 4.9, the effect of the optimised indicators on the cost and performance is also observed. The total water price, \$/m³ was found to be 0.6 and 0.7 \$/m³ if PTC or ABGD are used, respectively. Furthermore, the unit product cost is almost 12.24 \$/GJ).

Table 4.9: Data results of the proposed system based on the optimised design indicators.

PTC results:	
Outlet temperature, °C	400
Inlet temperature, °C	165
Pressure, bar	10.88
Total area, m ²	11280
Exergy efficiency, %	44.67
Exergy destruction rate, kW	4300
Mass flow rate, kg/s	10.17
Number of loops, #	20
Anaerobic Biogas boiler results:	
Feedstock type	Cattle manure
Retention time, days	50
Collection volume, m ³	5611
Biogas Digester load kg/m ³ /day	0.3328
Total influent required, kg	1.8e6
Total discharge, kg	8.978e5
Water mass to be added, kg	8.978e5
The total volume, m ³	1.122e5
The sludge layer volume, m ³	1.683e4
Working volume of digestion, m ³	8.978e4
Dimeter of the cylindrical part, m	63
The volume of the cylindrical part, m ³	7.887e4
Height of the cylindrical portion, m	25
Biogases flow rate, kg/s	0.1624
Boiler air mass flow rate, kg/s	2.03
Boiler useful energy, kW	5455
Exhaust gas temperature, °C	311
Boiler Specific fuel consumption, kg/kWh	0.1071
Boiler number of tubes, #	300
Evaporator (ORC) results:	

Top cycle temperature, °C	300
Inlet temperature, °C	104
Mass flow rate, kg/s	8.948
Outlet oil temperature (Therminol-VP1), °C	163.1
Vapor pressure, bar	32.75
Exergy destruction rate, kW	530
Number of tubes, #	1550
Effectiveness, %	0.8
Pump (Therminol-VP1) results:	
Power, Kw	15.5
Outlet/inlet temperature, °C	164/163
Exergy destruction rate, kW	10.2
Turbine (ORC) results:	
Total power, kW	1660
Mass flow rate, kg/s	8.948~9
Outlet temperature, °C	139.5~140
Exergy destruction, kW	327~330
Recuperator (ORC) results:	
Inlet steam temperature, °C	140
Outlet steam temperature, °C	62.17
Inlet liquid temperature, °C	42.84
Outlet liquid temperature, °C	103.9~104
Mass flow rate, kg/s	8.948~9
Exergy destruction rate, kW	103.4
Thermal power, kW	1021
Condenser (ORC) results:	
Inlet steam temperature, °C	62.17
Outlet temperature, °C	40
Mass flow rate, kg/s	8.948~9
Inlet cooling water temperature, °C	25
Outlet cooling water temperature, °C	52.74
Thermal power, kW	5.875e4
Area, m ²	1573
Exergy destruction rate, kW	475
Pump (ORC) results:	
Power, kW	46
Outlet/inlet temperature, °C	43/40
Exergy destruction rate, kW	42.84
AGMD results:	
Membrane type	E-PH
Feed salinity, ppm	45,000
Product salinity ratio, ppm	250
Pump efficiency, %	75
Inlet temperature, °C	25

Feed exergy, kW	6.43e4
Brine exergy, kW	4.175e4
Product exergy, kW	2043
Exergy destruction, kW	2.062e4
Pumping power, kW	97~100
Specific power consumption, kWh/m ³	1.55
Membrane energy, kW	1.17e5
Thermal efficiency, %	31.05
GOR	1.721
Feed flow rate, kg/h	1.34e6
Brine loss flow, kg/h	1.278e6
Brine loss salinity ratio, kg/kg	0.0472
Salt rejection	0.9944
Liquid entry pressure, kPa	187.1
Mass transfer coefficient kg/m ² .s.Pa	552.1
Permeate flux, kg/m ² .h	7.185
Permeability coefficient	0.2638
Total membrane area, m ²	8699
Cost results:	
AGMD direct capital costs, \$	1.631e6
Biogas hourly costs \$/h	8.76
Evaporator hourly costs \$/h	0.022
Turbine hourly costs, \$/h	19.38~20
Recuperator hourly costs, \$/h	0.01521
AGMD hourly costs \$/h	32.53
Pumps hourly costs \$/h	0.38
PTC hourly costs, \$/h	19.16~20
Total hourly costs (PTC), \$/h	72.34
Total hourly costs (Biogas), \$/h	62
Total Water Price, \$/m ³ (PTC)	0.7502
Total Water Price, \$/m ³ (Biogas)	0.6423
Unit product cost, \$/GJ	12.24
Performance results:	
Specific solar area, SSA m ² /(m ³ /day)	0.3133
Rankine efficiency, %	29.2
Total exergy efficiency, %	2.861
Total exergy destruction, kW	7e4

4.5 Design results under the real time mode: Case study

To examine the design aspects over a large time span, a real-time mode is created to measure the fluctuations in the system design and performance results over a period of one year. The data input is used over one year (8760 epochs) and a specific location (Al Khuwaimah rural region, Oman, 21°39' N 59°20' E) is selected for this study. The selected area is a good example for the implementation of hybrid renewable energy systems since this region is very far from the main interconnected grid and the connection to the grid is not economically valid option [258]. In addition, the Al Khuwaimah village is located in a coastal region, thus allowing cogeneration application by utilising seawater and up to now, diesel fuel power plants are used in electrical and water production. Solar and meteorological data (DNI, W/m^2) are obtained from ANN developed model over the duration of one year (2019). Figure 4.13 shows the data input into the dynamic model over one year of operation in relation to the system productivity and power load from the user. The following parameters have been considered as the main input within the following ranges:

- Time, $h=8760$
- Power load, $kW=500:2000$
- Productivity, $m^3/day=1000:1500$

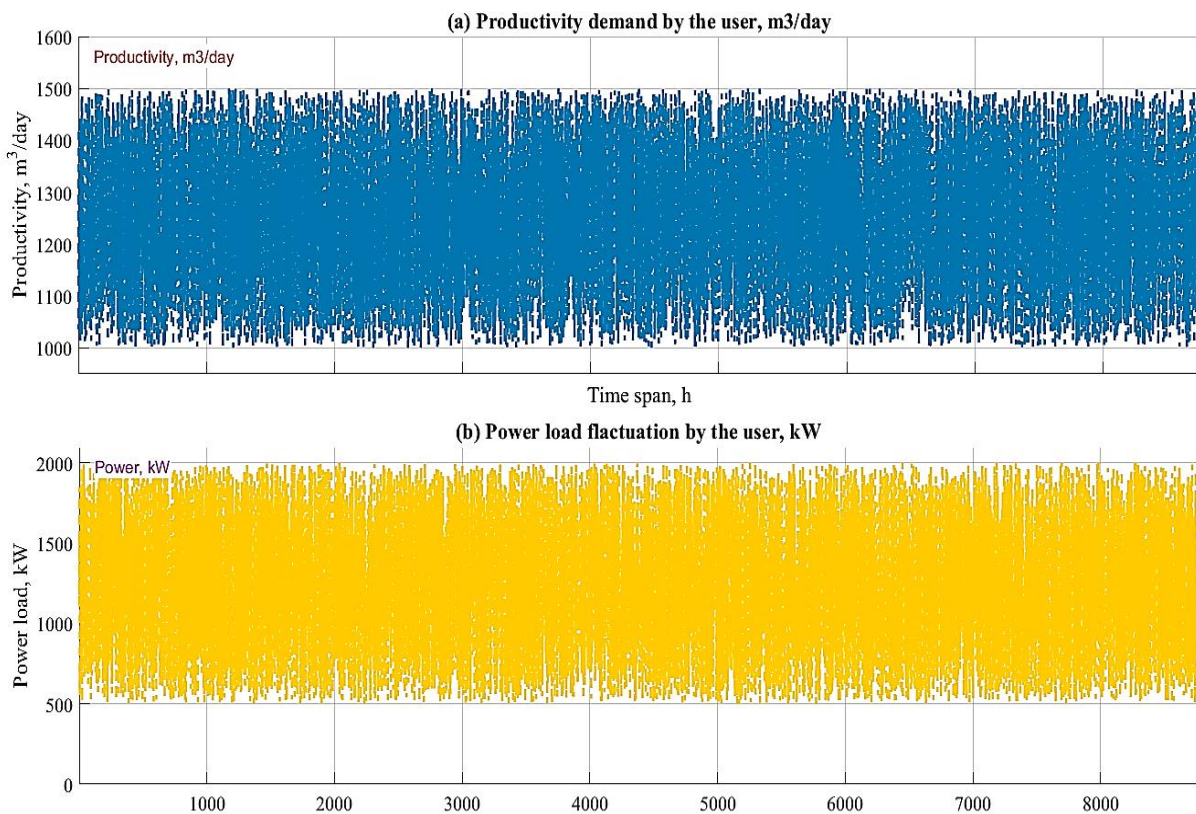


Figure 4-13: Load and productivity fluctuations over one year (8760 epochs).

Figure 4.14 shows the data variations over one year of operation depending on the location and meteorological conditions (DNI, W/m^2), productivity and load power fluctuations. Figure 4.14-a shows the variation in DNI over the year at the location of operation and it shows that the DNI ranges between $300 W/m^2$ and $900 W/m^2$. The solar radiation limit for the solar part (PTC) was set as $400 W/m^2$ and below this value, the biogas system will operate automatically. Figure 4.14-b shows that the total area of the PTC would be in the range of 8000 to $25,000 m^2$. The designers should bear in mind that the excessive area of the PTC would be most helpful in winter operating conditions. Figures 4.14-c and d show the variations in the flow rates. The solar field flow rate is considered to be slightly greater than the ORC and biogas flow rates. The range of the solar field flow rate was recorded between 10 and $12 kg/s$. However, the ORC and biogas flow rates were recorded as between 5 and $10 kg/s$ and between 0.06 and $0.2 kg/s$, respectively. Based on the cattle manure feedstock, the anaerobic biogas digestion volume will range between 5×10^4 and $1.5 \times 10^5 m^3$ (see Figure 14-e). For cost and exergy, Figure 4.14-f shows a striking result related to the unit exergy product cost, $\$/GJ$. The range over one year was recorded between 10 and $17 \$/GJ$ which is very interesting. Such values are quite remarkable and demonstrate that it can compete against the other energy resources. Figure 4.14-g shows the variations in the total system exergy destruction rate. The range of exergy destruction rate ($50,000$ to $70,000 kW$) is quite normal according to the current specifications. Figure 4.14-h, i shows that the total hourly costs are recorded as in the range of 50 - $100 \$/h$ and that the total water price was recorded as 0.5 - $1.45 \$/m^3$. Such values can compete against the operation of solar ORC assisted reverse osmosis desalination process.

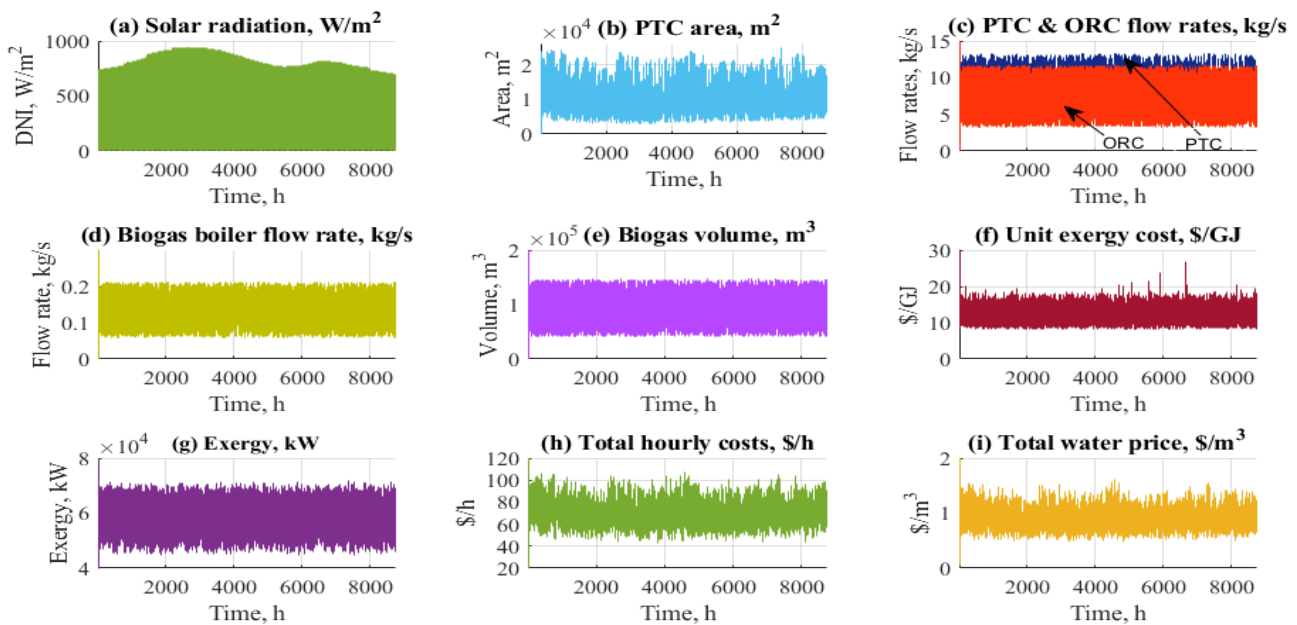


Figure 4-14: Data results of the proposed system over one year under a real time approach.

For daily operation, and for a typical day in summertime, Figure 4.15 shows the variation of some design and cost aspects. Figure 4.15-a shows the variation of solar radiation on that typical day (21 Aug. 2019) as an input example. Figures 4.15-b, c show the variation of the total mass flow rates for PTC, ORC and biogas fired boiler. It shows from the figure that the operating hours of the PTC were from 09:00 until 16:00 hours. The hourly measurements of the day were recorded for the operation of the biogas system. Figure 4.15-d shows the fluctuations in thermal Rankine efficiency. The range of the efficiency was recorded as lying between 25% and 33% which is quite remarkable and an attractive outcome. Figure 4.15-e shows the fluctuations in the load power which was required to be delivered by the turbine unit bearing in mind the load from the user, the load of AGMD pump, the solar filed pump and ORC pump. Figures 4.15-f, g show the data results related to the hourly costs, and the total water price throughout the day. The hourly costs did not exceed the value of 80 \$/h and the total water price was recorded as between 0.5 and 1 \$/m³. It has been noticed that maximum values are centralised around the middle of the day. Figure 4.15-h shows the fluctuations of the specific solar area, m²/m³/day. The range was between 0.2 and 0.4 m²/m³/day.

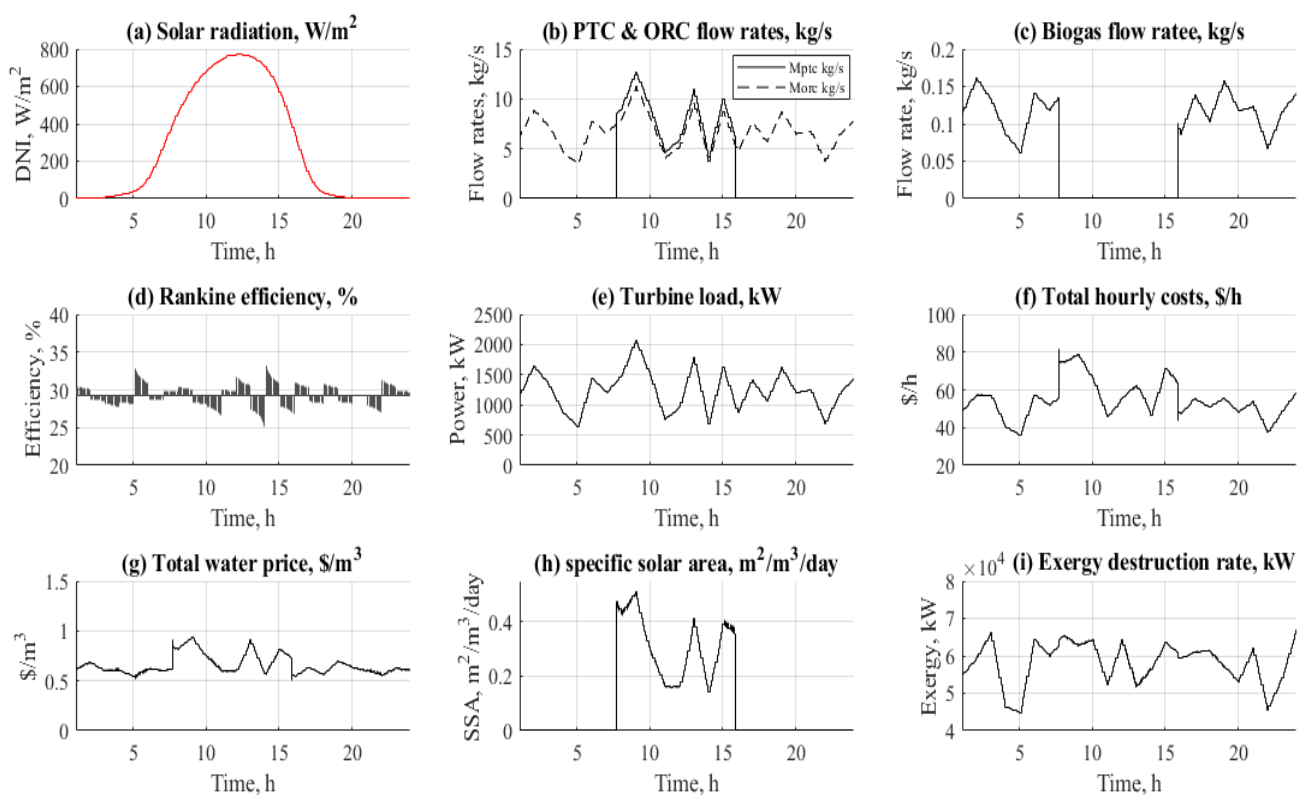


Figure 4-15: Daily data results related to a typical day in summertime (Al Khuwaimah rural region, Oman).

4.6 Conclusion of the chapter

A novel integrated solar and biogas for desalination and electric power generation has been presented, investigated and analysed in terms of the design, size and cost aspects. The system comprises a parabolic trough collector, anaerobic biogas digestion and organic Rankine cycle coupled with air gap membrane distillation for cogeneration application. The parabolic trough collector is considered the prime mover and the biogas is utilised as a backup energy source during the periods of no or limited sunlight to achieve higher stability and reliability. The system is modelled and simulated in order to measure and calculate some of the most important indicators, such as total water price, hourly costs, thermal energy, temperature, brine loss, solar field area and membrane areas. These mentioned indicators are performed based on controlling some of the most important parameters, such as the total system productivity, top vapor temperature, and load power from the user. Furthermore, a real-time dynamic model is considered to predict the system's performance over one year. The location of the study was in the Al Khuwaimah rural area, Oman, 21°39' N 59°20' E. Based on the analysis performed in this work, the following conclusions can be drawn:

- The plant's productivity should be in the range of 100-1500 m³/day.
- The load power from the user is in the range of 1000-2000 kW.
- 10 types of air gap membrane distillation are compared, and these are related to the best operating conditions and minimum design aspects. The E-PH type is considered to be the most appropriate for this study.
- For the ORC, Toluene has been selected as the main working fluid. The top steam temperature should not exceed 275~300 °C. However, the condensation temperature of the steam should be in the range of 30~40 °C.
- The feed salinity should be in the range of 40,000-45,000 ppm.
- The total hourly costs are within the range of 30-70 \$/h which is considered a remarkable result when comparisons are made with the conventional desalination processes. The range of the total water price, \$/m³ was found to fluctuate between 0.5 and 1.45 \$/m³. Such values can, with advantage, compete against the operation of a solar ORC-assisted reverse osmosis desalination process under the same production category.
- Based on cattle manure, the anaerobic biogas digestion volume ranged between 5x10⁴ and 1.5x10⁵ m³. For cost and exergy, a remarkable result related to the unit exergy product cost, \$/GJ has been obtained. The range over one year was recorded as lying between 10 and 17 \$/GJ which is very

interesting, and such values are quite remarkable and can compete against the other energy resources. Two biogas production tanks should be operated alternatively. The 1st is for gas support and the 2nd for gas production depending on the retention days. This is due to the fact that anaerobic digestion is a biological process and cannot be switched on and off quickly.

In conclusion, it is possible to combine solar ORC with membrane distillation for moderate scale desalination plants, taking into consideration the location space area, solar field area and volume of the supply biogas system. Finally, the results of this study can pave the way for moving ahead with hybrid solar/anaerobic biogas energy investments and can inform decision makers for future installments of energy systems.

CHAPTER 5: MULTI-OBJECTIVE OPTIMAL SIZING OF A HYBRID CONCENTRATED SOLAR POWER-BIOGAS FOR DESALINATION AND POWER GENERATION

Summary

The use of a fully renewable energy system (RES) to power mid- and low-scale off-grid systems is an attractive alternative solution to replace fossil fuel technologies in order to meet the ever-growing demand and tackle environmental problems. In this chapter, the design optimisation of a hybrid solar biogas, Organic Rankine Cycle (ORC-Toluene) and Air Gap Membrane Distillation (AGMD) for desalination and electric power generation system is presented. Three objective functions namely, maximising power and water production, and minimising the unit exergy product costs has been formulated. The turbine efficiency, top ORC vapor temperature and ORC condenser temperature has been selected as the decision variables. The non-dominated sorting genetic algorithm (NSGA-II) has been employed to solve the optimisation problem and produce a Pareto frontier of the optimal solutions. Further, the TOPSIS approach has been used to select the optimal solution from the Pareto set. The study constitutes the first attempt to holistically optimise such a hybrid off-grid cogeneration system in a robust manner. The key findings of this results chapter have been published in the Energy Proceedings Conference Journal.

5.1 Introduction

The intensive use of the fossil fuels to meet the world energy and water demand has caused several environmental issues, such as global warming, air pollution and ozone depletion. Therefore, the use of a fully renewable energy system to operate water and power plants have become one of the most important research topics in energy systems.

The free and abundant solar energy source makes concentrated solar power (CSP) an attractive option to solve the energy crisis in the future. The intermittency is the biggest drawback of solar CSP power plants, but this problem can be compensated by utilising thermal energy storage (TES). However, the additional TES greatly increases the solar thermal power system costs. Therefore, to overcome such expensive costs and technical difficulties, hybridising solar thermal power with biogas energy is a promising and attractive option. The hybridisation of solar CSP and biogas from waste will not only reduce the investment and Levelised Cost of Energy but enhance the power dispatchability and system reliability [259]. Such systems

have some advantages, such as (i) utilising the human, animal, and agriculture wastes, (ii) reducing the greenhouse gas emissions and (iii) overcoming the uncertainty of the solar thermal systems.

The cogeneration of power-water using thermal power plants are typically constructed on large sale rate which is not a valid option for rural areas with scattered population. For these areas, building close and low-capacity power plants to produce the required electricity and water to the consumer is an efficient option, which eliminates the cost of the power grid, cost of water pipelines and the energy loss due to the power transmission systems. The recommended solution is the mid- and low-scale off-grid cogeneration systems.

Recently, the use of waste heat in the seawater desalination industry has been reviewed by Elsaid et al. [260], they concluded that this topic still requires more efforts on the R&D section to meet the significant demand of clean water.

In the literature, the optimisation techniques have been divided into single-objective and multi-objectives optimisation, where a single solution leads to a single-objective, and multi-objective offers a set of solutions called a “Pareto front” [261].

Different optimisation algorithms have been examined, with different objectives for the optimisation of RES (off-grid/grid-connected). For example, Acuna et al. used NSGA II to performed multi-objective optimisation to improve the reliability of RES derived from the minimum hourly energy achieved by the RE [262].

For the hybrid system example that comprises of CSP and wind, there have been several attempts to optimise the hybrid CSP/wind system that would importantly minimise power supply curtailment as wind and solar usually do not peak simultaneously. To illustrate this process, Yang et al. [263] proposed a new hybrid system that includes CSP/wind/electric heater being employed with the thermal energy storage. This hybrid system is designed to optimise the profit under technical limitations as a mixed-integer linear programming problem. The proposed method has enormously reduced the wind curtailment by more than 90% over 151 days. Zeyu Ding et al. [264] have developed an optimisation technique based on the PSO algorithm to find the optimal design of the hybrid CSP/wind system coupled to thermal storage. Such CSP/wind hybridisations are also seen in a recent study in the literature by Keyif et al. [265] who performed a non-linear optimisation model to measure the critical component investment costs and operational flexibility in the plant configuration.

For solar thermal energy optimisation, Guo and Huai [266] utilised a GA approach to optimise multiparameter in a parabolic trough solar receiver. The results show that the obtained heat by the working fluid increases when the thermal efficiency is taken as the objective function while the average

temperature of the working fluid and wall temperatures of the solar receiver decrease. On the other hand, when exergy efficiency is taken as the objective function, the average temperature of the working fluid and the wall temperature of the solar receiver increase while the heat obtained by the working fluid decreases. Toghiani et al. [267] developed a multi-optimisation GA approach to maximise the exergy efficiency of a PTC-ORC power plant. The investigation showed that the optimal nano-fluids choice to be used in the PTC system between the four utilised ones (SiO_2 , TiO_2 , CuO and Al_2O_3) was CuO . Rajanna and Saini [268] developed the hybrid system using genetic algorithms. The genetic algorithm was used to achieve the energy needs of various load sections inside the villages of Chamarianagar, in the Southern State of Karnataka, India. Chauhan and Saini [269] proposed a sizing-based hybrid renewable energy system to provide uninterrupted power supply to fulfil the energy demands within the region under study. Chauhan and Saini [270] also presented a comparative study of the demand side management (DSM) based hybrid energy system through a load shifting strategy. They suggested that the demand side management strategy to be the most suitable solution without the demand side management strategy. Different configurations of hybrid energy systems were developed in six geographic zones of Nigeria by Olatomiwa et al. [271] and it can determine the economic feasibility solution using the HOMER software with sensitivity cases of \$1.1–\$1.3 based NPC and COE. Based on the availability of meteorological data, Olatomiwa et al. [272] presented a statistical analysis of the wind and solar energies' potentials for rural areas in Nigeria. It employs design and sizing of the optimal technical and economic hybrid energy system components using the HOMER software. Mohamed et al. [273] presented a bi-level system employing decision analysis and multi-objective optimisation method for the design and analysis of a rural micro grid for developing nations with a perception of sustainable development. Zhang et al. [160] proposed a new hybrid optimisation algorithm for the optimal sizing of a standalone hybrid energy system based on three algorithms such as chaotic search, harmony search and simulated annealing. These are used for reviewing the feasibility study of the proposed system with reliability. From this literature, the multi-optimisation algorithms are the most utilised optimisation techniques because of its ability to overcome all preceding difficulties for which the single-objective algorithms failed to provide. Also, multi-optimisation algorithms are less sensitive to the objective function characteristics and the number of the design variables. The Genetic Algorithm (GA) optimisation is the most used type of the evolutionary algorithms which has an excellent performance to the solving of many engineering problems. However, like most memetic algorithms, it does not converge at the global optimal [271]. This problem can be overcome by combining the GA with other classical optimisation tools.

The optimisation of the fully renewable decentralised systems is crucial as this will result in more efficient designs and will eventually assist to phase out existing fossil fuel technologies. To implement and fully utilise the hybrid solar biogas system a combination of multi-objective optimisation and multi-criteria decision making (MCDM) tools have been employed. There are several MCDM tools that have been used to evaluate RES. Table 5.1 shows the benefits and limitations of MCDM methods that are utilised in the RES.

Of the numerous MCDM tools, TOPSIS appears to be the best option because of the following characteristics: (i) this method has a rational and comprehensible logic, (ii) the concept is in a quite simple mathematical form, (iii) the computation process is straightforward, and (iv) the results are obtained quickly. In addition, TOPSIS is one of the most popular MCDM methods that has been used for solving energy sector issues in the literature.

Several studies have been conducted to optimise the design of hybrid CSP plants using the single and multi-objective optimisation approach [165], [263], [265], [274]–[276]. However, none of these studies consider the integration of the CSP-biogas to power ORC and AGMD for desalination and power generation. Typically, solar PTC linked with wind/thermal energy storage for combined heat and power is the most popular integration approach that has been investigated in the literature [274], [277]–[279].

As it can be observed from the literature review and to the best of the author's knowledge, multi-objective optimisation has not been performed for decentralised hybrid CSP-biogas to drive ORC and AGMD for power-water productions integrated solution, and this forms the basis for this study. This study constitutes the first attempt to holistically optimise such a hybrid off-grid system in a robust manner. The integrated solar and biogas system that has been designed through advanced modelling in the MATLAB/Simulink® in the previous chapter is combined with the multi-objective optimisation technique to determine the best operating parameters. The developed system aims to achieve higher stability and profitability. Meanwhile, the cogeneration through the waste heat of the ORC power the AGMD, which benefits as well from the higher stability due to hybridisation. Due to these advantages, the system has the potential to be economically attractive. Therefore, the integration of the new developed model with multi-objective optimisation technique is crucial to determine the optimal operating configuration and this study investigates the results.

Table 5.1: Benefits and limitations of MCDM methods.

Method	Benefits	Limitations	Source
PROMETHEE	<ul style="list-style-type: none"> • Very useful when there are alternatives that are hard to harmonize. • Works well with qualitative and quantitative information. • Fuzzy and uncertain information can be included into the calculations. 	<ul style="list-style-type: none"> • Compared with other methods, the computation process is quite long, and the calculation process is very completed. 	[280], [281]
AHP	<ul style="list-style-type: none"> • Compared with other methods, the computation process is quite simple, the calculation can be easily applied, and the results are obtained quite quickly. • Has a better focus on each criterion used in the calculations. 	<ul style="list-style-type: none"> • Interdependence between alternatives and objectives can lead an inaccurate result. • Additional analysis is needed to verify the results. • Requires data collected based on experience. 	[282]– [284]
WSM	<ul style="list-style-type: none"> • Has simple computation process • Good for managing single-objective problems. 	<ul style="list-style-type: none"> • Calculate only one dimension. • Can not integrate multiple preferences. 	[285], [286]
TOPSIS	<ul style="list-style-type: none"> • The method completely uses allocated information and works with a fundamental ranking. • Compared with other methods, the computation process is quite simple, the calculation can be easily applied, and the results are obtained quite quickly. 	<ul style="list-style-type: none"> • The method is suitable when the indicators of alternatives do not vary very strongly. 	[287]– [289]
CRITIC	<ul style="list-style-type: none"> • Not required for decision-maker’s intervention. • The method has simple calculations process. 	<ul style="list-style-type: none"> • Does not articulate the importance of achieving decision-makers’ goals. • The method indicates only some properties of the initial data. 	[290], [291]

Of the numerous MCDM tools, TOPSIS appears to be the best option because of the following characteristics: (i) this method appears to have more rational and comprehensible logic, (ii) the concept is in a quite simple mathematical form, (iii) the computation process is straightforward, and (iv) the results

are obtained quickly if compared with other MCDM tools. In addition, TOPSIS is one of the most popular MCDM methods that has been used for solving energy sector issues in the literature.

Several studies have been conducted to optimise the design of hybrid CSP plants using the single and multi-objective optimisation approach [165], [263], [265], [274]–[276]. However, none of these studies consider the integration of the CSP-biogas to power ORC and AGMD for desalination and power generation. Typically, solar PTC linked with wind/thermal energy storage for combined heat and power is the most popular integration approach that has been investigated in the literature [274], [277]–[279].

As it can be observed from the literature review and to the best of the author's knowledge, multi-objective optimisation has not been performed for decentralised hybrid CSP-biogas to drive ORC and AGMD for power-water productions integrated solution, and this forms the basis for this study. This study constitutes the first attempt to holistically optimise such a hybrid off-grid system in a robust manner. The integrated solar and biogas system that has been designed through advanced modelling in the MATLAB/Simulink® in the previous chapter is combined with the multi-objective optimisation technique to determine the best operating parameters. The developed system aims to achieve higher stability and profitability. Meanwhile, the cogeneration through the waste heat of the ORC power the AGMD, which benefits as well from the higher stability due to hybridisation. Due to these advantages, the system has the potential to be economically attractive. Therefore, the integration of the new developed model with multi-objective optimisation technique is crucial to determine the optimal operating configuration and this study investigates the results.

A robust multi-optimisation approach has been used and linked with a decision-making tool to find the optimal solution from the set of the produced results. The hybrid system consisted of PTC, anaerobic biogas boiler, ORC and AGMD system. The main objectives of this work are as follows:

- Construction of a sensitivity assessment on the developed system to investigate the effects of various design parameters on the thermo-economic performance.
- Implement a multi-objective optimisation technique using a non-dominated sorting genetic algorithm NSGA-II and linking the produced results with a decision-making tool (TOPSIS) to find the best operation condition for the hybrid system to achieve the maximum power and water production with minimum possible cost.
- Assess the detailed multi-objective optimal sizing of a hybrid concentrated solar power-biogas for desalination and power generation.

5.2 Methodology and Procedure

The obtained procedure of multi-objective optimisation and the decision-making tool is described in this section.

5.2.1 Multi-objective optimisation

The key aim of the multi-objective optimisation of the integrated PTC-AD-ORC-AGMD systems is to achieve maximum power and water production with minimum possible cost. The three selected objective functions are: maximise the net output work (W_{net}) (Eq. (5.1, 5.2 and 5.3)), maximise the total amount of distilled water (Eq. (5.4)) and minimise the unit exergy product costs (Eq. (5.5)). The design variables and their range of variations that have been considered for the multi-objective optimisation of the hybrid system are given in Table 5.2. The non-dominated sorting genetic algorithm (NSGA-II) [292] is used as the multi-objective optimisation method for optimising the objective functions.

The net output work of the ORC system in kW is defined as follows:

$$W_{net} = (W_{turbine} - W_{pump}) \quad (5-1)$$

$$W_{pump} = \frac{\dot{m}\Delta p}{\rho\mu_p} \quad (5-2)$$

$$W_{turbine} = \dot{m}(h_i - h_{os})\mu_t \times \mu_g \quad (5-3)$$

The total amount of distilled water in kg/m^2h is calculated by:

$$J_p = C_w(T_{hi} - T_{ci}) \quad (5-4)$$

where T_{hi} and T_{ci} are the temperature at the feed side of the membrane, °C, and at the cold side of the condensation section, and C_w is the overall mass transfer coefficient in m/s.

The unit exergy product costs (C_p) in \$/GJ are calculated based on the overall thermo-economic equation:

$$C_p = 1000000 \left(\left(\text{Cooling feed cost} \left(\frac{\$}{\text{kJ}} \right) \times \text{Feed exergy (kW)} \right) + \left(\text{Cost of power} \left(\frac{\$}{\text{kJ}} \right) \times \text{Power output (kW)} \right) + \left(\frac{\text{IC\&OM Costs}}{3600} \left(\frac{\$}{\text{h}} \right) \right) / \text{Distilled exergy from AGMD (kW)} \right) \quad (5-5)$$

Table 5.2: Considered design variables and range of variations for the optimisation.

Decision variables	Range of variation
$\mu_{turbine}$	[0.7, 0.95]
$T_{vo}, ^\circ\text{C}$	[200, 300]
$T_{cond}, ^\circ\text{C}$	[30, 70]

The elitist Pareto front NSGA-II combined with a classical optimisation search tool was developed in solving the multi-objectives optimisation problem. The NSGA-II optimisation algorithm has been implemented in MATLAB. The NSGA-II flowchart and the details of the GA operators to obtain a set of potential solutions called a Pareto front are presented in Figure 5.1 and Table 5.3, respectively.

Table 5.3: Specification of the GA operator.

Parameter	Value
Population size	50
Population type	Double vector
Pareto fraction	0.5
Max. generation	200
Cross-over operator	Intermediate
Cross-over fraction	0.8
Hybrid function	fgoalattain

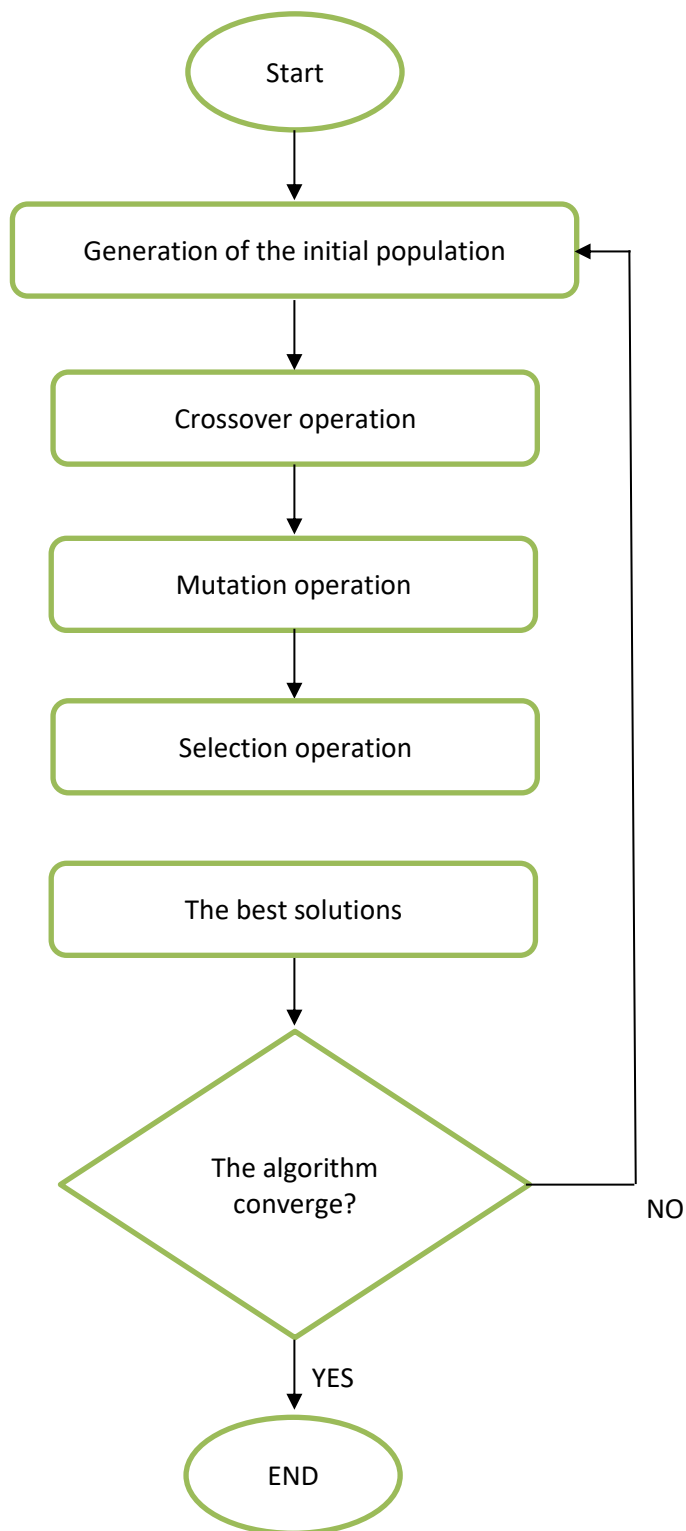


Figure 5-1: NSGA II algorithm flowchart.

5.2.2 Decision making procedure

The decision-making method is used in selecting the optimal solution from the Pareto fronts. The Pareto front in multi objective optimisation contains a set of optimal solutions which means there is not a single optimal solution. Therefore, to select the optimal solution, a technique for order preferences by similarity to the ideal solution (TOPSIS) is used in this study.

The TOPSIS method was developed based on the concept that the best solution is that which is closest to the ideal solution [287]. The TOPSIS method measures a distance to the positive ideal solution and the distance from the negative ideal solution. The alternative closest value is selected as the best alternative. It is anticipated that each attribute has an increasing or decreasing utility. The following steps are the implementation process of the TOPSIS:

- i. Calculate the weighted normalised optimised results. The weighted normalised data u_{ij} is given as:

$$u_{ij} = w_j \times \frac{x_{ij}}{\sqrt{\sum_{i=1}^n x_{ij}^2}} \quad i = 1, 2 \dots n; j = 1, 2 \dots m \quad (5-6)$$

where w_j is the weight obtained from the criteria of the decision matrix and x_{ij} are the optimised results.

- ii. Compute the separation of each of the weighted normalised results from the negative and positive ideal solutions, NIS and PIS, respectively. The Euclidean distance between an alternative and the PIS, NIS are calculated using equation (7) and (8), respectively:

$$D_i^+ = \sqrt{\sum_{j=1}^n (u_{ij} - u_j^+)^2} \quad i = 1, 2 \dots n \quad (5-7)$$

$$D_i^- = \sqrt{\sum_{j=1}^n (u_{ij} - u_j^-)^2} \quad i = 1, 2 \dots n \quad (5-8)$$

where the positive ideal solution is $u_j^+ = \max_{\forall i} u_{ij}$ and negative ideal solution is $u_j^- = \min_{\forall i} u_{ij}$.

- iii. Compute and order the ranking index in a descending order. The ranking index is calculated using:

$$RI_i = \frac{D_i^-}{D_i^- + D_i^+} \quad i = 1, 2 \dots n \quad (5-9)$$

Based on this approach, the alternative with the highest RI_i is selected. In this study, to gain a better insight into the optimal solution, different decision criteria have been used to calculate the weight for each of the alternatives. Tables 5.4, 5.5 and 5.6 show the utilised decision matrixes, while Table 5.7 shows the judgement criteria for the different selected decision matrixes.

Table 5.4: Decision matrix (A) for the TOPSIS analysis.

	Power	Water	Costs
Power	1	1/4	1/3
Water	4	1	3
Costs	3	1/3	1

Table 5.5: Decision matrix (B) for the TOPSIS analysis.

	Power	Water	Costs
Power	1	3	4
Water	1/3	1	2
Costs	1/4	1/2	1

Table 5.6: Decision matrix (C) for the TOPSIS analysis.

	Power	Water	Costs
Power	1	1	1/3
Water	1	1	1/3
Costs	3	3	1

Table 5.7: Table 5.6: Decision matrix (C) for the TOPSIS analysis.

Intensity of importance	Definition
1	Equal importance
3	Moderate importance
5	Strong importance
7	Demonstrated importance
9	Extreme importance
2,4,6,8	Intermediate values

5.3 Results and Discussion

The performance of the hybrid ORC system is influenced by several operating parameters. In Chapter 4, a comprehensive parametric analysis is conducted to investigate the effect of six different operating parameters on the system performance. However, to examine the significant of the selected design variables for the optimisation a further detailed sensitivity analysis is conducted.

In the ORC system, it is significant to investigate the effect of the top vapor temperature in the evaporator and the condenser temperature on the cycle and system performance. Figure 5.2 (a-d) illustrates the effect of the top vapor temperature and condenser temperature on the system cycle performance.

Figure 5.2-a, shows the effect of the top vapor temperature (T_{vo}) and condenser temperature (T_{cond}) on the outlet turbine temperature (T_{to}). From the Figure 5.2-a, as expected, it can be seen that the top vapor temperature has higher impact than the condenser temperature on the outlet turbine temperature. For example, at 250 °C for the vapor temperature and 35 °C for the condenser temperature, the outlet turbine temperature has been recorded between 120 °C and 125 °C.

Figure 5.2-b, shows that the outlet recuperator temperature is affected by variations of the top vapor temperature and condenser temperature. For instance, at a vapor temperature of 250 °C, and condenser temperature of 35 °C, the recuperator temperature is noted to lie between 50 °C and 55 °C. Increasing the vapor temperature and condenser temperature increases the outlet recuperator temperature and which means that there is more steam for regeneration.

Figure 5.2-c, shows the variation of the ORC thermal efficiency and the maximum effect is noticed by the increase of the top vapor temperature. For instance, at vapor temperatures close to 300 °C, the range of the Rankine efficiency lies between 28 and 30% which is reasonably noticeable for ORC when compared to [257]. Therefore, it is significant to operate the ORC at high values of the vapor temperature. On the other hand, the condenser temperature plays a minor role in Rankine efficiency.

Figure 5.2-d shows the ORC exergy efficiency based on the variation of the top vapor temperature and condenser temperatures. It should be noted that the condenser temperature has a great influence on the exergy efficiency term. For instance, the exergy efficiency of the ORC is in an increasing mode while the condenser temperature is in the range of 30 °C and 35 °C. Moreover, the optimised top vapor temperature for significant values of the exergy efficiency is in the range of 250 °C to 275 °C. It is worth mentioning that, the condenser temperature value of 35 °C and vapor temperature value of 280 °C are quite suitable for achieving better system performance.

Figure 5.3 (a-b), illustrates the effects of the top vapor temperature and condenser temperature on the AGMD permeate flux at 70% and 95% turbine efficiency. Figure 5.3-a, shows the effects of the variation of top vapor temperature and condenser temperature on the AGMD permeate flux at 70% turbine efficiency. Increasing the vapor temperature and condenser temperature increases the AGMD permeate flux. However, the condenser temperature has the highest impact on the permeate flux of the AGMD. For example, at a vapor temperature of 250 °C, and condenser temperature of 35 °C, the AGMD permeate flux is noted to be around 6.6 kg/m²h. Figure 5.3-b, shows the effects of the variation of top vapor temperature and condenser temperature on the AGMD permeate flux at 95%. Increasing the top vapor temperature and condenser temperature decreases the overall system unit product costs. For example, at 250 °C for the vapor temperature and 35 °C for the condenser temperature, the overall system unit product costs is lies between 4.9 kg/m²h.

It is noteworthy to note that at higher turbine efficiency the freshwater amount is reduced due to the fact that at higher turbine efficiency more heat is utilised for the generation of electricity while at lower turbine efficiency more heat concentration will be given for the desalination purpose. Therefore, it is crucial to couple the developed hybrid model with multi-optimisation method to find the best operating configuration that generates the maximum electricity and water at the lowest cost possible.

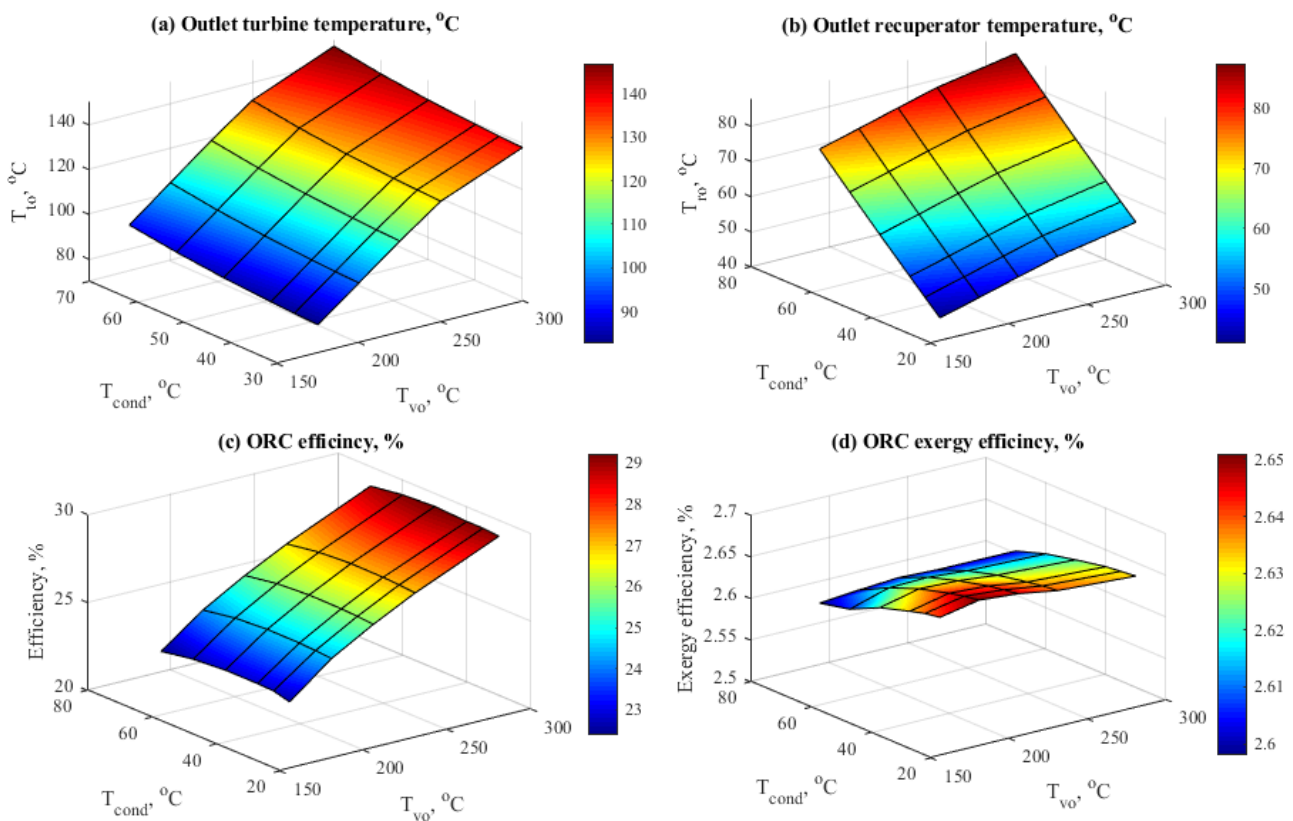


Figure 5-2: Effects of the top vapor temperature and condenser temperature on the system cycle performance.

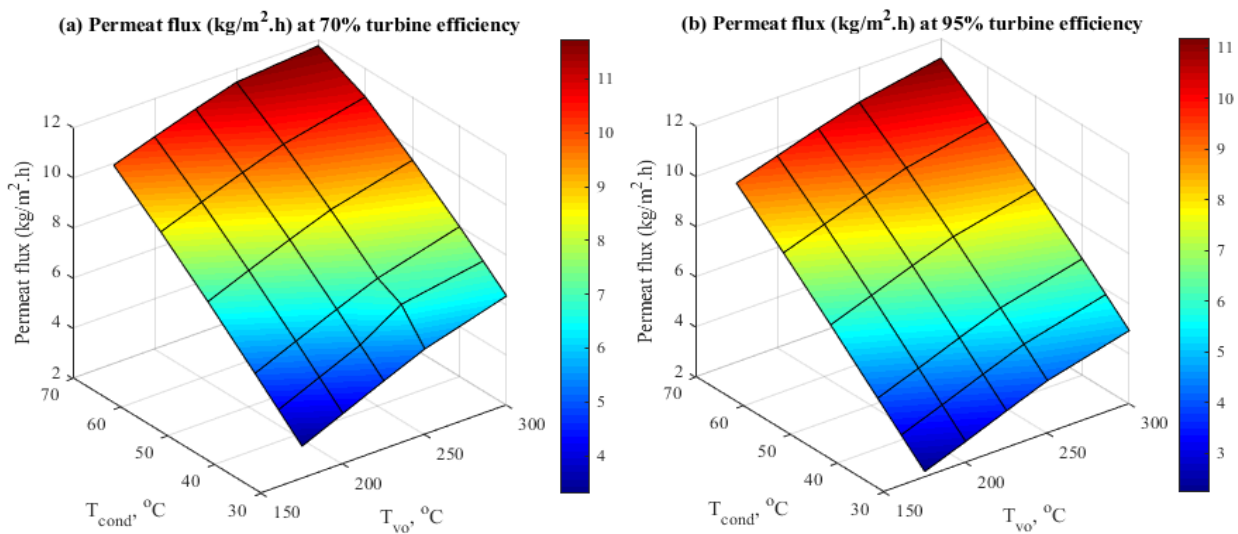


Figure 5-3: Effects of the top vapor temperature and condenser temperature on the AGMD permeate flux at different turbine efficiency.

For the multi-objective optimisation, Figure. 5.2 shows the Pareto frontier of the multi-objective optimisation and this is presented in three-dimensional space. The conflict in the objectives function is evidenced by the spread in the optimised data. As seen in Figure. 5.2, the optimal data present both dominated and non-dominated solutions. It is also evident that there is no single solution that maximises all the objectives; hence, in order to select an optimal solution TOPSIS MCDM tool need to be applied.

To have a better insight of the optimal solution different matrix judgment have been developed. Therefore, the optimum solutions for the decision-making tool (TOPSIS) using three different matrix judgment (A), (B) and (C) are obtained and indicated in Figure 5.2, Figure 5.3 and Figure 5.4 and the corresponding decision variables for the selected solutions are presented in Tables 5.8, Tables 5.9 and Tables 5.10.

Figure 5.2. using matrix judgment (A) for selecting the optimal value, shows that the Hybrid PTC-AD-ORC-AGMD system is capable of delivering 1960 kW (1.96 MW) of electricity and 8 kg/m²h of distilled fresh water at unit exergy product costs of 11 \$/GJ. The values were observed for the decision variables; turbine efficiency = 0.83 (-), top ORC vapor temperature = 283 (°C) and ORC condenser temperature = 37 (°C), as indicated in Table 5.8.

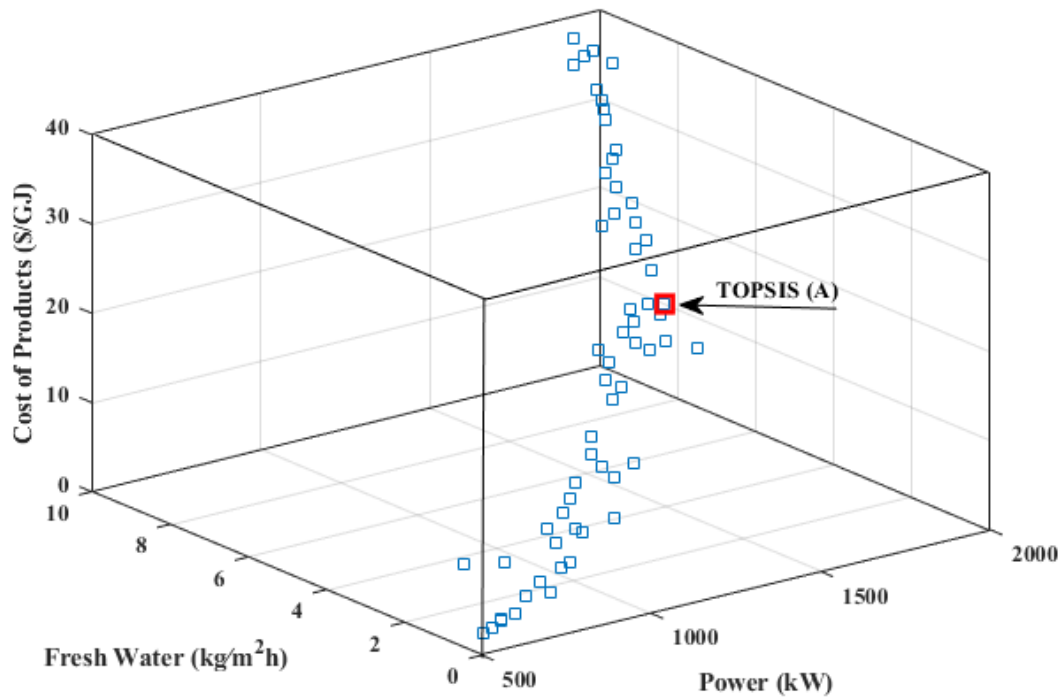


Figure 5-4: Pareto front for multi-objective optimisation result using TOPSIS with matrix judgment (A).

Table 5.8: Values of decision variables using matrix judgment (A) for the hybrid concentrated solar power-biogas system.

Decision variables	TOPSIS
$\mu_{turbine}$	0.83
$T_{vo}, ^\circ\text{C}$	283
$T_{cond}, ^\circ\text{C}$	37

To gain a better insight of the optimal solution different TOPSIS ranking have been utilised. The produced results using matrix judgment (B) is shown in Figure 5.3 and Table 5.9. It can be noticed that the Hybrid system is capable of generating 1940 kW (1.94 MW) of electricity and 7.8 kg/(m² h) of distilled freshwater at unit exergy product costs of 7.9 \$/GJ. The values were observed for the decision variables; turbine efficiency = 0.82 (-), top ORC vapor temperature = 282 °C and ORC condenser temperature = 36 °C, as indicated in Table 5.9.

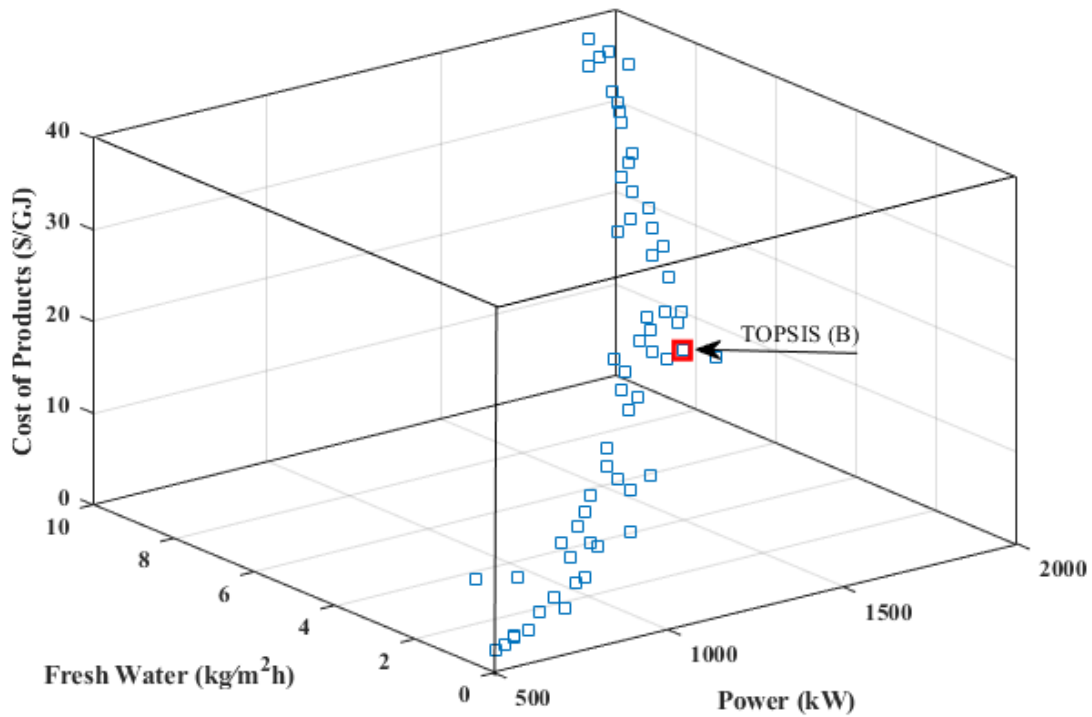


Figure 5-5: Pareto front for multi-objective optimisation result using TOPSIS with matrix judgment (B).

Table 5.9: Values of decision variables using matrix judgment (B) for the hybrid concentrated solar power-biogas system.

Decision variables	TOPSIS
$\mu_{turbine}$	0.82
$T_{vo}, ^\circ\text{C}$	282
$T_{cond}, ^\circ\text{C}$	36

The generated results using matrix judgment (C) is illustrated in Figure 5.4 and Table 5.10. It can be seen that the system is able to generate 1990 kW (1.99 MW) of electricity and 8.65 kg/(m² h) of freshwater at unit exergy product costs of approximately 13.37.9 \$/GJ. The values were produced by the decision variables; turbine efficiency = 0.81 (-), top ORC vapor temperature = 276 °C and ORC condenser temperature = 35.5 °C, as indicated in Table 5.9.

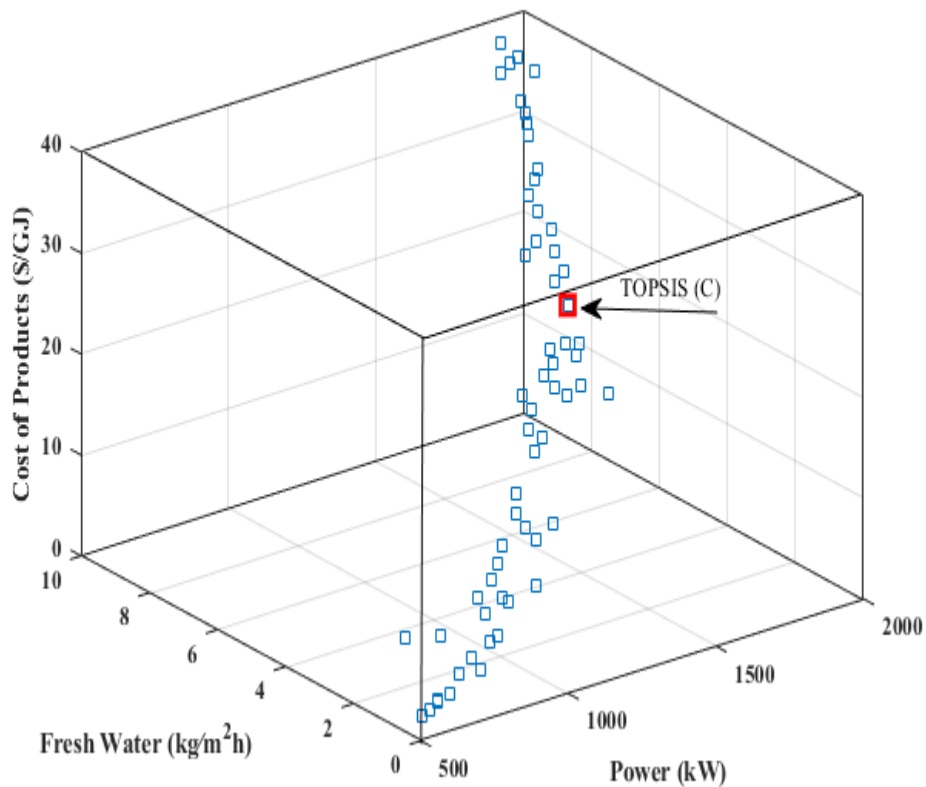


Figure 5-6: Pareto front for multi-objective optimisation result using TOPSIS with matrix judgment (C).

Table 5.10: Values of decision variables using matrix judgment (C) for the hybrid concentrated solar power-biogas system.

Decision variables	TOPSIS
$\mu_{turbine}$	0.81
$T_{vo}, ^\circ\text{C}$	276
$T_{cond}, ^\circ\text{C}$	35.5

As can be seen that the current optimum value relies on the matrix judgment (TOPSIS ranking) as decided by the authors and different results will be obtained for different rankings. Hence, the main objective of the hybridising multi-objective optimisation with MCDM is to showcase a method that can lead to a single

optimum based on the practitioner's preferences. A comparison between all three criteria that have been obtained by TOPSIS for the proposed system can be seen in Figure 5.7.

The results show that using criteria (C) produces lower unit exergy product costs in comparison to other configurations. The system is capable of producing 1940 kW (1.94 MW) of electricity and 7.8 kg/(m² h) of freshwater at unit exergy product costs of 7.9 \$/GJ.

In conclusion, the findings approved that the hybrid CSP-Biogas system is an efficient and economically feasible option for mid- and low-scale production of power and water in remote and rural areas. In addition, the used optimisation can pave the way for further investigate on scale up cases.

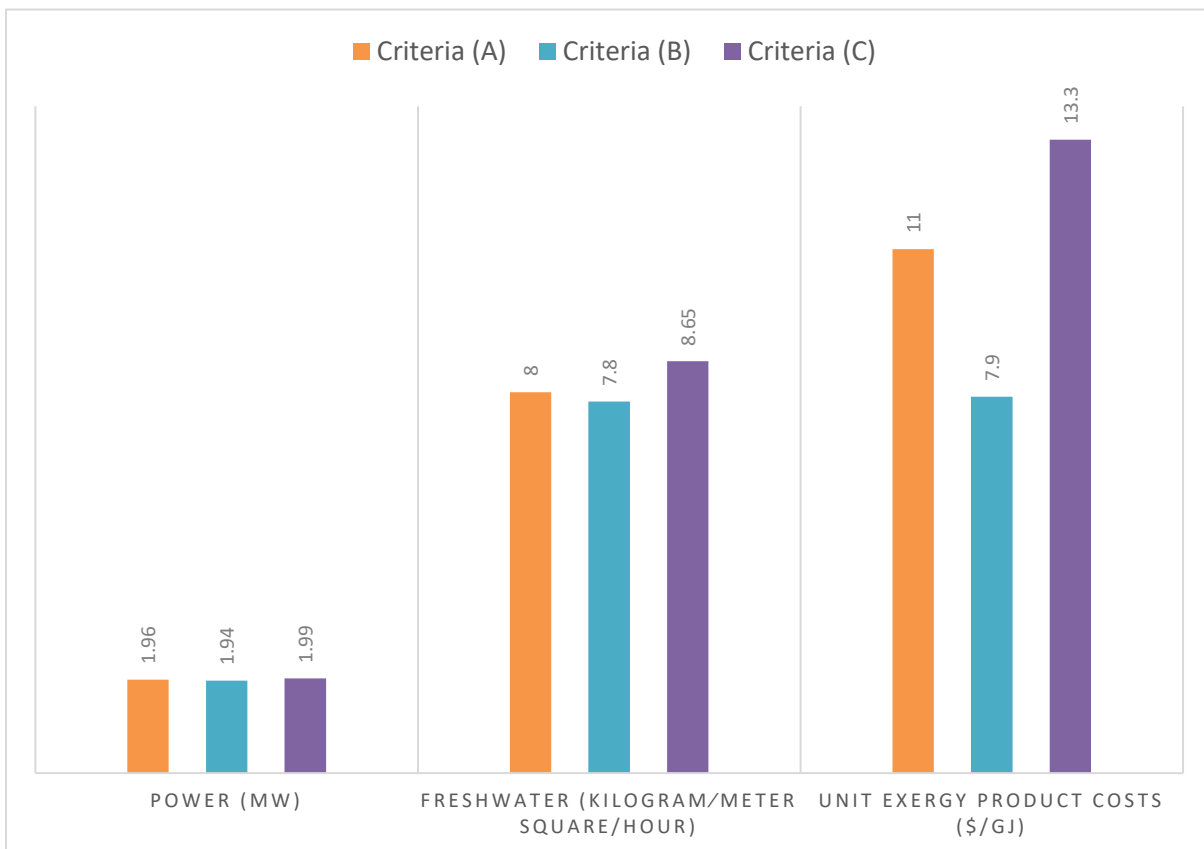


Figure 5-7: Values of criteria A, B and C obtained by TOPSIS for the proposed system.

5.4 Conclusion of the chapter

This study constitutes the first attempt to holistically optimise such a hybrid off-grid system in a robust manner. The novel integrated solar and biogas system that has been designed through advanced modelling in the MATLAB/ Simulink® in the previous chapters is integrated with a multi-objective optimisation technique to determine the best operating configuration. The feature of the new developed configuration aims to achieve higher power stability and profitability using the ORC cycle. In the meantime, the waste heat of the ORC is utilised to power the AGMD for cogeneration application, which benefits as well from the higher stability due to the hybridisation. The solar PTC is regarded as the prime mover, with the anaerobic digestion biogas serving as a backup energy source to compensate for the inconsistency of solar radiation during the day. Due to these advantages, the integration of the new developed model with the multi-objective optimisation technique is crucial to finding the best operating condition and this study thoroughly investigates the optimisation results. A sensitivity analysis has been conducted to examine the significance of the selected design variables for the optimisation problem and to reduce the respective design limits and identify the optimum operational windows. A combination of the NSGA-II multi-objective optimisation and multi-criteria decision-making techniques (TOPSIS) were employed to solve the optimisation problem and select the best configuration. To have a better insight of the optimal solution, three different matrix judgments have been developed and the generated optimal results have been analysed and compared. Based on the analysis performed in this work, the following conclusions can be drawn:

- The results show that using criteria (C) produces lower unit exergy product costs in comparison to other configurations. The system is capable of producing 1940 kW (1.94 MW) of electricity and 7.8 kg/ (m² h) of freshwater at unit exergy product costs of 7.9 \$/GJ. This amount of produced electricity-water can fulfill the electrical and water demands of small-scale communities, facilities, nomads' spots, tourist villages, rural regions, etc.
- The multi-optimisation is performed in order to find the optimum design points where the system performance is maximised, and the unit exergy product costs is minimised. The main aim of hybridising multi-objective optimisation with MCDM is to showcase a method that can lead to a single optimum based on the practitioner's preferences.

In conclusion, the findings proved that the hybrid CSP-Biogas system is an efficient and economically viable option for mid- and low-scale production of power and water in remote and rural areas. The utilised robust optimisation can pave the way for further research on scale up cases.

CHAPTER 6: CONCLUSIONS AND RECOMMENDATIONS FOR FUTURE WORK

Summary

The development of a sustainable and clean energy-based solution is a promising and attractive pathway to overcome the existing world energy and environmental crisis. Therefore, new integrations of sustainable and clean energy systems are required, and this has become a hot topic in the scientific community. In this PhD thesis, a new hybrid sustainable and clean energy system is proposed. The main focus of this thesis is based on the modelling, optimisation, simulation and control of the proposed integrated energy systems. This chapter outlines the main findings, original contributions to existing knowledge and along with recommendations for future enhancements to the developed integrated energy systems.

6.1 Conclusion

The key objective of this work is to design and optimize the hybrid solar PTC waste-based biogas to power ORC and AGMD system through advanced modelling in order to combine efficiently the system components in the MATLAB/Simulink®. The thermo-economic performance analysis of the proposed hybrid system is employed to evaluate the system performance. The capacity of the developed energy system is set to meet the electrical and water demand of rural regions.

The integration of the PTC/waste-based biogas/ORC/AGMD has the potential to be economically attractive and this is thoroughly investigated within this study.

The novelties, importance and main contributions of this study are outlined as follows:

- A new user-friendly multi-dimensional forecasting model using the ANN technique for predicting the solar radiation and wind speed over six locations in Oman has been developed. The built model uses an enormous number of meteorological data points, and it is combined with two ANN models simultaneously to accurately predict the solar radiation and wind speed. Three input parameters are only required in the developed model to measure the solar radiation and wind speed with high accuracy simultaneously. In addition, the developed model can be integrated with the proposed sustainable and clean energy system to provide the necessary solar data at the addressed location.

- A novel proposed hybrid solar and biogas system for desalination and electric power generation using advanced modelling techniques to integrate the stand-alone off-grid system has been designed. The novelty emerges from some facts, which are centralised around the use of a hybrid electric generation via Concentrated Solar Power (CSP) and anaerobic digestion biogas to achieve higher stability and profitability. Meanwhile, the cogeneration through the waste heat of the ORC drives the AGMD, which benefits as well from the higher stability due to hybridisation. In addition, an innovative and user-friendly modelling approach has been applied, and the efficiently integrates the individual energy components, i.e. PTC, anaerobic biogas boiler, ORC and AGMD, which fosters the optimisation of the proposed system. The models have been developed in the MATLAB/Simulink® software and have been used to investigate the system area, dimensions, and cost and to ensure that the electrical and water demand of the end-user are met. In addition, a new detailed thermo-economic assessment of the proposed hybrid solar biogas for cogeneration in off-grid applications has been investigated. An energy, exergy, and cost analysis has been performed and to fully utilise this, a sensitivity assessment on the developed model has been analysed to examine the effects of various design parameters on the thermo-economic performance. Finally, implementing an in-depth simulation testing of the system in a rural region in Oman.
- The novel integrated solar and biogas system that has been designed through advanced modelling in the MATLAB/ Simulink® is integrated with a robust multi-objective optimisation technique to determine the best operating configuration. Three objective functions namely, maximising power and water production, and minimising the unit exergy product costs has been formulated. The turbine efficiency, top ORC vapor temperature and ORC condenser temperature has been selected as the decision variables. The non-dominated sorting genetic algorithm (NSGA-II) has been employed to solve the optimisation problem and produce a Pareto frontier of the optimal solutions. Further, the TOPSIS approach has been used to select the optimal solution from the Pareto set. The study constitutes the first attempt to holistically optimise such a hybrid off-grid cogeneration system in a robust manner.

In this work, advanced, innovative and user-friendly integration of ten different models have been developed using MATLAB/Simulink®. The integrated models are used to predicate the weather condition, investigate the performance and optimisation of the hybrid solar biogas system to meet the electrical and water demand of rural regions.

Firstly, a novel Artificial Neural Network model has been developed based on the Feed-forward Back-propagation (FBANN) to simultaneously predict the hourly solar radiation. The developed model has been implemented over the six regions in Oman. The novelty of the new designed model emerges from the following features: (a) two different FBANN configurations has been combined into a new integration, (b) the new developed model required only three input parameters, and (c) and both solar radiation and wind speed are calculated accurately and simultaneously.

Secondly, a new integrated solar and biogas for desalination and electric power generation has been presented, investigated and analysed in terms of the design, size and cost aspects. This study is the first attempt to integrate the off-grid hybrid model that contains PTC, anaerobic biogas boiler, ORC and AGMD for desalination and electric power generation. Accordingly, a comprehensive thermo-economic assessment has been conducted for the proposed novel integrated model, and the modeling approach simultaneously solves the energy, exergy and cost calculations and thus a new flexible model has been developed. Thus, the proposed assembly has not been studied before, and, typically, solar PTC linked with wind/thermal energy storage for combined heat and power is the most popular integration that has been investigated in the literature.

Finally, an integration of the new developed model with multi-objective optimisation technique to determine the optimal operating configuration has been conducted. A robust multi-objective optimisation technique using a non-dominated sorting genetic algorithm NASG-II has been developed. The produced results are linked with a decision-making tool (TOPSIS) to find the best operation condition for the hybrid system to achieve the maximum power and water production with minimum possible cost.

The following conclusions can be drawn from the current research:

- Investigation of the existing literature reveals that solar PTC to power large-scale ORCs are at early stages and not fully commercialised, and at the same time as the small-scale solar CSP ORC technology is still at the development phase. Moreover, the integration of two renewable energy sources to drive an ORC system has not been extensively and well investigated. These findings highlighted the importance of developing an accurate comprehensive simulation model with a capability to predict the thermo-economic performance, equipment sizing and economic feasibility of the low- medium temperature hybrid solar CSP-ORC system for a wide range of working fluids and operating conditions.

- The new developed ANN model to predict the hourly solar radiation and wind speed showed a high level of accuracy at predicting solar radiation and wind speed data. The R-value was over 0.96 while the MAPE values did not exceed 3%, which indicates the high accuracy of the developed ANN model. This paves the way to integrate the ANN predication model with the proposed stand-alone hybrid solar CSP energy system.
- The mathematical model of each component of the hybrid solar PTC with waste-based biogas to power ORC, and AGMD system has been developed based on the energy, exergy and cost analysis. The obtained simulation results are validated against theoretical and real data available in the open literature and due to lack of data for the integrated system, each component is validated individually. The comparison reveals a very good agreement between the presented results and the literature results with maximum deviation of 4.86% in the AGMD component. Therefore, this new integrated model may be used with confidence for further investigations to improve the overall performance of the stand-alone hybrid solar CSP/ biogas system.
- Adding 10 different types of air gap membrane distillations to select the best design configurations, which are related to the operating conditions and minimum design aspects, have further improved the developed and validated model. The conducted analysis shows that the E-PH type is considered to be the most appropriate for this study due to its permeated flux that is found to be in an acceptable range and with a remarkable hourly cost in \$/h.
- For the ORC model, the toluene heat transfer fluid has been selected as the main working fluid. The selection of toluene depends on many criteria and the most important recognised criteria is the maximum operating temperature of the cycle. In the ORC, the results show that, the top steam temperature should not exceed 275~300°C, and the condensation temperature of the steam should be in the range of 30~40°C.
- The economic analysis of the desalination unit indicates that; the total hourly costs are within the range of 30-70\$/h which is considered a remarkable result when comparisons are made with the conventional desalination processes. The range of the total water price, \$/m³ was found to fluctuate between 0.5 and 1.45\$/m³. Such values can, with advantage, compete against the operation of a solar ORC-assisted reverse osmosis desalination process under the same production category.
- For the anaerobic biogas digestion volume (based on cattle manure), ranged between 0.5e5 and 1.5e5m³. For cost and exergy, a remarkable result related to the unit exergy product cost, \$/GJ has been obtained. The range over one year was recorded as lying between 10 and 17\$/GJ which is

very interesting, and such values are quite remarkable and can compete against the other energy resources.

- The integration of the new developed model with the multi-objective optimisation technique to find the best operating conditions using non-sorting genetic algorithm shows that the system is capable of producing 1940 kW (1.94 MW) of electricity and 7.8 kg/ (m² h) of freshwater at unit exergy product costs of 7.9 \$/GJ. This amount of produced electricity-water can fulfill the electrical and water demands of small-scale communities, facilities, nomads' spots, tourist villages, rural regions, etc.
- The economic analysis of the hybrid solar biogas ORC with membrane distillation for moderate scale desalination plants is economically an attractive solution, taking into consideration the location space area, solar field area and volume of the supply biogas system. Finally, the results of this study can pave the way for moving ahead with hybrid solar/anaerobic biogas energy investments and can inform decision makers for future installments of energy systems.

6.2 Recommendations for future work

The newly developed models in this study could be effectively utilised for designing and predicting the dynamic performance and optimisation of the hybrid solar CSP with waste-based biogas for cogeneration application to meet the demand of end users under different weather conditions. Furthermore, a number of improvements can be employed in future work as follows:

- In this study, toluene and thermal oil heat transfer fluids have been used in the ORC and in the solar-biogas heating cycle. However, further fluids could be investigated to enhance the overall system performance and to select the best suitable working fluid that produce the maximum output power and water production with lower possible costs.
- Several types of concentrated solar collectors with wide operating temperatures could be employed to compare the thermo-economic performance. For example, solar power tower (SPT), linear Fresnel reflector (LFR), and parabolic dish systems (PDS) etc., could be integrated with the developed hybrid energy system. Therefore, the library tool of the solar collectors in the MATLAB/Simulink[®] software could be extended, and continuously updated.
- The Organic Rankine system has been implemented for the cogeneration application, a number of cycles could be utilised and thermo-economically compared with the produced ORC results such

as steam Rankine cycle and Bryton cycle.

- In this investigation, the air gap membrane distillation technology has been employed as the integration for the cogeneration application in ORC system. Several conventional and non-conventional desalination technologies can be further implemented in the integration of the CSP-driven desalination technologies, and included into the developed modelling program.
- In waste-based biogas production, cattle manure properties have been used as the feed raw materials in this study. However, different types of feedstocks, such as animal and fruit wastes, etc., can be supplied to the anaerobic system, and included in the developed modelling tool.
- Experimental studies are required to calibrate the performance of the developed hybrid energy system in this thesis, while further studies may consider expanding the scope of work done in the parametric analysis and optimisation by calculating the effect of other key variables on its performance.
- The work done on the energy management of the hybrid solar biogas system is limited because the biogas unit in this thesis is used as back up source when the solar radiation is lower than 400 W/m^2 . The biogas below this value will operate automatically and fully replace the solar PTC system. For further improvement, the operation and control strategy should be improved to distribute the load between the system units to enhance the hybridisation benefits.
- In this thesis, the non-sorting genetic algorithm has been implemented for the multi-optimisation problem of the hybrid solar biogas system. However, other optimisation algorithms could be examined and with different objectives.
- A modified TOPSIS has been used to select the best solution from the Pareto set of optimal solutions. Other decision-making tools, such as Fuzzy-logic and linear programming techniques for multi-dimensional analysis of preference could be explored to compare results.
- The proposed hybrid system offers clean, sustainable energy solution. However, an environmental assessment could be performed to determine the magnitude of the savings of carbon emission compared to conventional fossil fuel energy systems.

REFERENCE

- [1] M. S. Raboaca *et al.*, “Concentrating solar power technologies,” *Energies*, vol. 12, no. 6, pp. 1–17, 2019.
- [2] B. K. Sovacool and I. M. Drupady, *Energy Access, Poverty, and Development*. 2016.
- [3] M. M. kamal, I. Ashraf, and E. Fernandez, “Sustainable electrification planning of rural microgrid using renewable resources and its environmental impact assessment,” *Environ. Sci. Pollut. Res.*, no. 0123456789, 2022.
- [4] A. Rahman, O. Farrok, and M. M. Haque, “Environmental impact of renewable energy source based electrical power plants: Solar, wind, hydroelectric, biomass, geothermal, tidal, ocean, and osmotic,” *Renew. Sustain. Energy Rev.*, vol. 161, no. February, p. 112279, 2022.
- [5] M. Shengo Lutandula and F. Ilunga Mpanga, “Review of Wastewater Treatment Technologies in View of their Application in the DR Congo Mining Industry,” *Glob. Environ. Eng.*, vol. 8, no. October, pp. 14–26, 2021.
- [6] D. Molden, *Water for food water for life: A Comprehensive assessment of water management in agriculture*. 2013.
- [7] R. Vakulchuk, I. Overland, and D. Scholten, “Renewable energy and geopolitics: A review,” *Renew. Sustain. Energy Rev.*, vol. 122, no. October 2019, p. 109547, 2020.
- [8] M. Mele, A. R. Gurrieri, G. Morelli, and C. Magazzino, “Nature and climate change effects on economic growth: an LSTM experiment on renewable energy resources,” *Environ. Sci. Pollut. Res.*, vol. 28, no. 30, pp. 41127–41134, 2021.
- [9] R. Milani, A. Szklo, and B. S. Hoffmann, “Hybridization of concentrated solar power with biomass gasification in Brazil’s semiarid region,” *Energy Convers. Manag.*, vol. 143, pp. 522–537, 2017.
- [10] A. Pandey, P. Pandey, and J. S. Tumuluru, “Solar Energy Production in India and Commonly Used Technologies—An Overview,” *Energies*, vol. 15, no. 2, pp. 1–26, 2022.
- [11] Erdiwansyah, Mahidin, H. Husin, Nasaruddin, M. Zaki, and Muhibbuddin, “A critical review of the integration of renewable energy sources with various technologies,” *Prot. Control Mod. Power Syst.*, vol. 6, no. 1, 2021.
- [12] G. Nasti and A. Abate, “Tin Halide Perovskite (ASnX3) Solar Cells: A Comprehensive Guide toward the Highest Power Conversion Efficiency,” *Adv. Energy Mater.*, vol. 10, no. 13, pp. 1–16, 2020.
- [13] H. Z. Hassan, A. Mohamad, and R. Bennacer, “Simulation of an adsorption solar cooling system,” *Energy*, vol. 36, no. 1, pp. 530–537, 2011.

- [14] O. Konur, C. O. Colpan, and O. Y. Saatcioglu, "A comprehensive review on organic Rankine cycle systems used as waste heat recovery technologies for marine applications," *Energy Sources, Part A Recover. Util. Environ. Eff.*, vol. 44, no. 2, pp. 4083–4122, 2022.
- [15] K. Rahbar, S. Mahmoud, R. K. Al-Dadah, N. Moazami, and S. A. Mirhadizadeh, "Review of organic Rankine cycle for small-scale applications," *Energy Convers. Manag.*, vol. 134, pp. 135–155, 2017.
- [16] D. Wei, X. Lu, Z. Lu, and J. Gu, "Performance analysis and optimization of organic Rankine cycle (ORC) for waste heat recovery," *Energy Convers. Manag.*, vol. 48, no. 4, pp. 1113–1119, 2007.
- [17] S. Lecompte, S. Lemmens, H. Huisseune, M. Van Den Broek, and M. De Paepe, "Multi-objective thermo-economic optimization strategy for ORCs applied to subcritical and transcritical cycles for waste heat recovery," *Energies*, vol. 8, no. 4, pp. 2714–2741, 2015.
- [18] Y. Feng, Y. Zhang, B. Li, J. Yang, and Y. Shi, "Sensitivity analysis and thermoeconomic comparison of ORCs (organic Rankine cycles) for low temperature waste heat recovery," *Energy*, vol. 82, pp. 664–677, 2015.
- [19] M. Imran, B. S. Park, H. J. Kim, D. H. Lee, and M. Usman, "Economic assessment of greenhouse gas reduction through low-grade waste heat recovery using organic Rankine cycle (ORC)," *J. Mech. Sci. Technol.*, vol. 29, no. 2, pp. 835–843, 2015.
- [20] A. Bahadori and C. Nwaoha, "A review on solar energy utilisation in Australia," *Renew. Sustain. Energy Rev.*, vol. 18, pp. 1–5, 2013.
- [21] M. Zeyghami, D. Y. Goswami, and E. Stefanakos, "A review of solar thermo-mechanical refrigeration and cooling methods," *Renew. Sustain. Energy Rev.*, vol. 51, pp. 1428–1445, 2015.
- [22] R. K. Akikur, R. Saidur, H. W. Ping, and K. R. Ullah, "Comparative study of stand-alone and hybrid solar energy systems suitable for off-grid rural electrification: A review," *Renew. Sustain. Energy Rev.*, vol. 27, pp. 738–752, 2013.
- [23] C. Oko, E. . Diemuodeke, E. . Omunakwe, and E. Nnamdi, "Design and Economic Analysis of a Photovoltaic System: A Case Study," *Int. J. Renew. Energy Dev.*, vol. 1, no. 3, p. 65, 2012.
- [24] W. Cole, A. W. Frazier, W. Cole, and A. W. Frazier, "Cost Projections for Utility-Scale Battery Storage : 2020 Update Cost Projections for Utility-Scale Battery Storage : 2020 Update," *Nat. Renew. Energy Lab.*, no. June, 2020.
- [25] M. Mehos, J. Jorgenson, P. Denholm, and C. Turchi, "An Assessment of the Net Value of CSP Systems Integrated with Thermal Energy Storage," *Energy Procedia*, vol. 69, pp. 2060–2071, 2015.
- [26] R. Domínguez, A. J. Conejo, and M. Carrión, "Operation of a fully renewable electric energy system with CSP plants," *Appl. Energy*, vol. 119, pp. 417–430, 2014.

- [27] G. San Miguel and B. Corona, "Hybridizing concentrated solar power (CSP) with biogas and biomethane as an alternative to natural gas: Analysis of environmental performance using LCA," *Renew. Energy*, vol. 66, pp. 580–587, 2014.
- [28] J. H. Peterseim, A. Herr, S. Miller, S. White, and D. A. O'Connell, "Concentrating solar power/alternative fuel hybrid plants: Annual electricity potential and ideal areas in Australia," *Energy*, vol. 68, pp. 698–711, 2014.
- [29] Y. Lu, L. Zhao, and L. Guo, "Technical and economic evaluation of solar hydrogen production by supercritical water gasification of biomass in China," *Int. J. Hydrogen Energy*, vol. 36, no. 22, pp. 14349–14359, 2011.
- [30] B. Liao and L. J. Guo, "Concentrating Solar Thermochemical Hydrogen Production by Biomass Gasification in Supercritical Water," *Energy Procedia*, vol. 69, pp. 444–450, 2015.
- [31] Z. Hou and D. Zheng, "Solar utility and renewability evaluation for biodiesel production process," *Appl. Therm. Eng.*, vol. 29, no. 14–15, pp. 3169–3174, 2009.
- [32] A. Nzihou, G. Flamant, and B. Stanmore, "Synthetic fuels from biomass using concentrated solar energy - A review," *Energy*, vol. 42, no. 1, pp. 121–131, 2012.
- [33] F. Manenti, A. R. Leon-Garzon, Z. Ravaghi-Ardebili, and C. Pirola, "Assessing thermal energy storage technologies of concentrating solar plants for the direct coupling with chemical processes. The case of solar-driven biomass gasification," *Energy*, vol. 75, pp. 45–52, 2014.
- [34] K. M. Powell, K. Rashid, K. Ellingwood, J. Tuttle, and B. D. Iverson, "Hybrid concentrated solar thermal power systems: A review," *Renew. Sustain. Energy Rev.*, vol. 80, no. January, pp. 215–237, 2017.
- [35] L. M. Halabi and S. Mekhilef, "Flexible hybrid renewable energy system design for a typical remote village located in tropical climate," *J. Clean. Prod.*, vol. 177, pp. 908–924, 2018.
- [36] R. Meenal *et al.*, "Weather Forecasting for Renewable Energy System: A Review," *Arch. Comput. Methods Eng.*, no. 0123456789, 2022.
- [37] A. H. Elsheikh, S. W. Sharshir, M. Abd Elaziz, A. E. Kabeel, W. Guilan, and Z. Haiou, "Modeling of solar energy systems using artificial neural network: A comprehensive review," *Sol. Energy*, vol. 180, no. October 2018, pp. 622–639, 2019.
- [38] P. Malik, A. Gehlot, R. Singh, L. R. Gupta, and A. K. Thakur, "A Review on ANN Based Model for Solar Radiation and Wind Speed Prediction with Real-Time Data," *Arch. Comput. Methods Eng.*, no. 0123456789, 2022.
- [39] S. Pereira, E. F. M. Abreu, M. Iakunin, A. Cavaco, R. Salgado, and P. Canhoto, "Method for solar

resource assessment using numerical weather prediction and artificial neural network models based on typical meteorological data: Application to the south of Portugal,” *Sol. Energy*, vol. 236, no. January, pp. 225–238, 2022.

- [40] F. Rodríguez, A. Fleetwood, A. Galarza, and L. Fontán, “Predicting solar energy generation through artificial neural networks using weather forecasts for microgrid control,” *Renew. Energy*, vol. 126, pp. 855–864, 2018.
- [41] S. Kuravi, J. Trahan, D. Y. Goswami, M. M. Rahman, and E. K. Stefanakos, “Thermal energy storage technologies and systems for concentrating solar power plants,” *Prog. Energy Combust. Sci.*, vol. 39, no. 4, pp. 285–319, 2013.
- [42] K. Mohammadi, M. Saghafifar, K. Ellingwood, and K. Powell, “Hybrid concentrated solar power (CSP)-desalination systems: A review,” *Desalination*, vol. 468, no. May, p. 114083, 2019.
- [43] H. L. Zhang, J. Baeyens, J. Degrève, and G. Cacères, “Concentrated solar power plants: Review and design methodology,” *Renew. Sustain. Energy Rev.*, vol. 22, pp. 466–481, 2013.
- [44] R. Kunwer, S. Pandey, and G. Pandey, “Technical Challenges and Their Solutions for Integration of Sensible Thermal Energy Storage with Concentrated Solar Power Applications—a Review,” *Process Integr. Optim. Sustain.*, no. 0123456789, 2022.
- [45] M. Van Den Broek, N. Berghout, and E. S. Rubin, “The potential of renewables versus natural gas with CO₂ capture and storage for power generation under CO₂ constraints,” *Renew. Sustain. Energy Rev.*, vol. 49, pp. 1296–1322, 2015.
- [46] M. J. Ghadi, L. Li, J. Zhan, L. Chen, Q. Huang, and C. Li, “A Review on the Development of Concentrated Solar Power and its Integration in Coal-Fired Power Plants*,” *2019 IEEE PES Innov. Smart Grid Technol. Asia, ISGT 2019*, pp. 1106–1111, 2019.
- [47] “largest CSP plant.” [Online]. Available: <http://torresolenergy.com/en/gemasolar/>.
- [48] X. Xu, K. Vignarooban, B. Xu, K. Hsu, and A. M. Kannan, “Prospects and problems of concentrating solar power technologies for power generation in the desert regions,” *Renew. Sustain. Energy Rev.*, vol. 53, pp. 1106–1131, 2016.
- [49] Estela and A. T. Kearney, “Solar Thermal Electricity 2025,” *Clean Electr. Demand Attractive STE Cost ...*, no. June, p. 52, 2010.
- [50] D. Barlev, R. Vidu, and P. Stroeve, “Innovation in concentrated solar power,” *Sol. Energy Mater. Sol. Cells*, vol. 95, no. 10, pp. 2703–2725, 2011.
- [51] V. Badescu *et al.*, “Computing global and diffuse solar hourly irradiation on clear sky. Review and testing of 54 models,” *Renew. Sustain. Energy Rev.*, vol. 16, no. 3, pp. 1636–1656, 2012.

- [52] P. Kuchhal, A. Kumar, and P. Upadhyay, "Opportunities and challenges of solar thermal technologies in the Indian context," no. May, 2022.
- [53] D. B. E. of hourly averaged solar irradiation: evaluation of models. B. services engineering research and technology. 2010 F.-25. Tham Y, Muneer T, "Estimation of hourly averaged solar irradiation: evaluation of models."
- [54] IEA, "Solutions for a low-carbon energy future," *Int. Energy Agency*, vol. 1, pp. 1–35, 2011.
- [55] G. Iaquaniello, A. Salladini, A. Mari, A. A. Mabrouk, and H. E. S. Fath, "Concentrating solar power (CSP) system integrated with MED-RO hybrid desalination," *Desalination*, vol. 336, no. 1, pp. 121–128, 2014.
- [56] C. Mao, Y. Feng, X. Wang, and G. Ren, "Review on research achievements of biogas from anaerobic digestion," *Renew. Sustain. Energy Rev.*, vol. 45, pp. 540–555, 2015.
- [57] K. C. Surendra, D. Takara, A. G. Hashimoto, and S. K. Khanal, "Biogas as a sustainable energy source for developing countries: Opportunities and challenges," *Renew. Sustain. Energy Rev.*, vol. 31, pp. 846–859, 2014.
- [58] M. Heiker, M. Kraume, A. Mertins, T. Wawer, and S. Rosenberger, "Biogas plants in renewable energy systems—a systematic review of modeling approaches of biogas production," *Appl. Sci.*, vol. 11, no. 8, 2021.
- [59] K. C. Surendra, D. Takara, A. G. Hashimoto, and S. K. Khanal, "Biogas as a sustainable energy source for developing countries: Opportunities and challenges," *Renew. Sustain. Energy Rev.*, vol. 31, pp. 846–859, 2014.
- [60] J. Dahlin, C. Herbes, and M. Nelles, "Biogas digestate marketing: Qualitative insights into the supply side," *Resour. Conserv. Recycl.*, vol. 104, pp. 152–161, 2015.
- [61] K. Hagos, J. Zong, D. Li, C. Liu, and X. Lu, "Anaerobic co-digestion process for biogas production: Progress, challenges and perspectives," *Renew. Sustain. Energy Rev.*, vol. 76, no. March 2016, pp. 1485–1496, 2017.
- [62] D. Li, Y. Ran, L. Chen, Q. Cao, Z. Li, and X. Liu, "Instability diagnosis and syntrophic acetate oxidation during thermophilic digestion of vegetable waste," *Water Res.*, vol. 139, pp. 263–271, 2018.
- [63] H. B. Nielsen and I. Angelidaki, "Congestion of manure and industrial organic waste at centralized biogas plants: Process imbalances and limitations," *Water Sci. Technol.*, vol. 58, no. 7, pp. 1521–1528, 2008.
- [64] C. Emte and T. Borges, "First commercial CSP-Biomass Hybrid Power Plant in Spain."
- [65] H. Liu, Y. Shao, and J. Li, "A biomass-fired micro-scale CHP system with organic Rankine cycle (ORC)

- Thermodynamic modelling studies," *Biomass and Bioenergy*, vol. 35, no. 9, pp. 3985–3994, 2011.
- [66] J. Servert, G. San Miguel, and D. López, "Hybrid solar - Biomass plants for power generation; technical and economic assessment," *Glob. Nest J.*, vol. 13, no. 3, pp. 266–276, 2011.
- [67] Z. Bai, Q. Liu, J. Lei, X. Wang, J. Sun, and H. Jin, "Thermodynamic evaluation of a novel solar-biomass hybrid power generation system," *Energy Convers. Manag.*, vol. 142, pp. 296–306, 2017.
- [68] R. Bet Sarkis and V. Zare, "Proposal and analysis of two novel integrated configurations for hybrid solar-biomass power generation systems: Thermodynamic and economic evaluation," *Energy Convers. Manag.*, vol. 160, no. January, pp. 411–425, 2018.
- [69] J. H. Peterseim, U. Hellwig, A. Tadros, and S. White, "Hybridisation optimization of concentrating solar thermal and biomass power generation facilities," *Sol. Energy*, vol. 99, pp. 203–214, 2014.
- [70] M. R. Gomaa, R. J. Mustafa, and N. Al-Dmour, "Solar thermochemical conversion of carbonaceous materials into syngas by Co-Gasification," *J. Clean. Prod.*, vol. 248, 2020.
- [71] N. Ghaffour, J. Bundschuh, H. Mahmoudi, and M. F. A. Goosen, "Renewable energy-driven desalination technologies: A comprehensive review on challenges and potential applications of integrated systems," *Desalination*, vol. 356, pp. 94–114, 2015.
- [72] R. Borsani and S. Rebagliati, "Fundamentals and costing of MSF desalination plants and comparison with other technologies," *Desalination*, vol. 182, no. 1–3, pp. 29–37, 2005.
- [73] N. Ghaffour, V. K. Reddy, and M. Abu-Arabi, "Technology development and application of solar energy in desalination: MEDRC contribution," *Renew. Sustain. Energy Rev.*, vol. 15, no. 9, pp. 4410–4415, 2011.
- [74] N. Ghaffour, T. M. Missimer, and G. L. Amy, "Technical review and evaluation of the economics of water desalination: Current and future challenges for better water supply sustainability," *Desalination*, vol. 309, no. 2013, pp. 197–207, 2013.
- [75] F. E. Ahmed, R. Hashaikeh, and N. Hilal, "Solar powered desalination – Technology, energy and future outlook," *Desalination*, vol. 453, no. October 2018, pp. 54–76, 2019.
- [76] F. Banat, N. Jwaied, M. Rommel, J. Koschikowski, and M. Wieghaus, "Desalination by a 'compact SMADES' autonomous solarpowered membrane distillation unit," *Desalination*, vol. 217, no. 1–3, pp. 29–37, 2007.
- [77] A. Cipollina, M. G. Di Sparti, A. Tamburini, and G. Micale, "Development of a Membrane Distillation module for solar energy seawater desalination," *Chem. Eng. Res. Des.*, vol. 90, no. 12, pp. 2101–2121, 2012.
- [78] G. Zaragoza, A. Ruiz-Aguirre, and E. Guillén-Burrieza, "Efficiency in the use of solar thermal energy

- of small membrane desalination systems for decentralized water production," *Appl. Energy*, vol. 130, pp. 491–499, 2014.
- [79] N. Riaz *et al.*, "A review of recent advances in adsorption desalination technologies," *Int. Commun. Heat Mass Transf.*, vol. 128, no. September, p. 105594, 2021.
- [80] W. S. Hua, H. J. Xu, and W. H. Xie, "Review on adsorption materials and system configurations of the adsorption desalination applications," *Appl. Therm. Eng.*, vol. 204, no. October 2021, 2022.
- [81] F. E. Ahmed, B. S. Lalia, R. Hashaikeh, and N. Hilal, "Alternative heating techniques in membrane distillation: A review," *Desalination*, vol. 496, no. July, p. 114713, 2020.
- [82] J. Ravi *et al.*, "Polymeric membranes for desalination using membrane distillation: A review," *Desalination*, vol. 490, no. May, p. 114530, 2020.
- [83] M. Qasim, I. U. Samad, N. A. Darwish, and N. Hilal, "Comprehensive review of membrane design and synthesis for membrane distillation," *Desalination*, vol. 518, no. August, p. 115168, 2021.
- [84] K. Choon, K. Thu, Y. Kim, A. Chakraborty, and G. Amy, "Adsorption desalination : An emerging low-cost thermal desalination method," *DES*, vol. 308, pp. 161–179, 2013.
- [85] M. Ghazy, A. A. Askalany, E. M. M. Ibrahim, A. S. A. Mohamed, E. S. Ali, and R. AL-Dadah, "Solar powered adsorption desalination system employing CPO-27(Ni)," *J. Energy Storage*, vol. 53, no. March, p. 105174, 2022.
- [86] A. Narasimhan, R. Kamal, and E. Almatrafi, "Novel synergetic integration of supercritical carbon dioxide Brayton cycle and adsorption desalination," *Energy*, vol. 238, 2022.
- [87] A. Desalination, "Adsorption Desalination and Cooling Systems : Advances in," pp. 1–6, 2022.
- [88] N. Ghaffour, S. Lattemann, T. Missimer, K. C. Ng, S. Sinha, and G. Amy, "Renewable energy-driven innovative energy-efficient desalination technologies," *Appl. Energy*, vol. 136, pp. 1155–1165, 2014.
- [89] K. Thu, Y. D. Kim, G. Amy, W. G. Chun, and K. C. Ng, "A hybrid multi-effect distillation and adsorption cycle," *Appl. Energy*, vol. 104, pp. 810–821, 2013.
- [90] K. C. Ng, K. Thu, Y. Kim, A. Chakraborty, and G. Amy, "Adsorption desalination: An emerging low-cost thermal desalination method," *Desalination*, vol. 308, pp. 161–179, 2013.
- [91] D. González, J. Amigo, and F. Suárez, "Membrane distillation: Perspectives for sustainable and improved desalination," *Renew. Sustain. Energy Rev.*, vol. 80, no. March, pp. 238–259, 2017.
- [92] M. F. A. Goosen, H. Mahmoudi, and N. Ghaffour, "Today's and future challenges in applications of renewable energy technologies for desalination," *Crit. Rev. Environ. Sci. Technol.*, vol. 44, no. 9, pp. 929–999, 2014.

- [93] Y. D. Kim, K. Thu, N. Ghaffour, and K. Choon Ng, "Performance investigation of a solar-assisted direct contact membrane distillation system," *J. Memb. Sci.*, vol. 427, pp. 345–364, 2013.
- [94] R. B. Saffarini, E. K. Summers, H. A. Arafat, and J. H. Lienhard V, "Economic evaluation of stand-alone solar powered membrane distillation systems," *Desalination*, vol. 299, pp. 55–62, 2012.
- [95] W. M. R. for the D. of D. P. by R. E. P. for R. E. for W. P. through D. F. V. 2010 J. 1. Papapetrou M, Biercamp C, *Roadmap for the Development of Desalination Powered by Renewable Energy: Promotion for Renewable Energy for Water Production through Desalination*. .
- [96] M. Badami and M. Mura, "Preliminary design and controlling strategies of a small-scale wood waste Rankine Cycle (RC) with a reciprocating steam engine (SE)," *Energy*, vol. 34, no. 9, pp. 1315–1324, 2009.
- [97] X. Li, B. Xu, H. Tian, and G. Shu, "Towards a novel holistic design of organic Rankine cycle (ORC) systems operating under heat source fluctuations and intermittency," *Renew. Sustain. Energy Rev.*, vol. 147, no. October 2020, p. 111207, 2021.
- [98] S. Quoilin, M. Orosz, H. Hemond, and V. Lemort, "Performance and design optimization of a low-cost solar organic Rankine cycle for remote power generation," *Sol. Energy*, vol. 85, no. 5, pp. 955–966, 2011.
- [99] A. M. Delgado-Torres and L. García-Rodríguez, "Analysis and optimization of the low-temperature solar organic Rankine cycle (ORC)," *Energy Convers. Manag.*, vol. 51, no. 12, pp. 2846–2856, 2010.
- [100] U. Drescher and D. Brüggemann, "Fluid selection for the Organic Rankine Cycle (ORC) in biomass power and heat plants," *Appl. Therm. Eng.*, vol. 27, no. 1, pp. 223–228, 2007.
- [101] M. J. Proctor, W. Yu, R. D. Kirkpatrick, and B. R. Young, "Dynamic modelling and validation of a commercial scale geothermal organic rankine cycle power plant," *Geothermics*, vol. 61, pp. 63–74, 2016.
- [102] V. Maizza and A. Maizza, "Unconventional working fluids in organic Rankine-cycles for waste energy recovery systems," *Appl. Therm. Eng.*, vol. 21, no. 3, pp. 381–390, 2001.
- [103] E. H. Wang, H. G. Zhang, Y. Zhao, B. Y. Fan, Y. T. Wu, and Q. H. Mu, "Performance analysis of a novel system combining a dual loop organic Rankine cycle (ORC) with a gasoline engine," *Energy*, vol. 43, no. 1, pp. 385–395, 2012.
- [104] P. J. Mago, A. Hueffed, and L. M. Chamra, "Analysis and optimization of the use of CHP-ORC systems for small commercial buildings," *Energy Build.*, vol. 42, no. 9, pp. 1491–1498, 2010.
- [105] F. Fang, L. Wei, J. Liu, J. Zhang, and G. Hou, "Complementary configuration and operation of a CCHP-ORC system," *Energy*, vol. 46, no. 1, pp. 211–220, 2012.

- [106] B. Peñate and L. García-Rodríguez, "Seawater reverse osmosis desalination driven by a solar Organic Rankine Cycle: Design and technology assessment for medium capacity range," *Desalination*, vol. 284, pp. 86–91, 2012.
- [107] M. Chys, M. van den Broek, B. Vanslambrouck, and M. De Paepe, "Potential of zeotropic mixtures as working fluids in organic Rankine cycles," *Energy*, vol. 44, no. 1, pp. 623–632, 2012.
- [108] B. M. F. of engineering thermodynamics. J. W. & S. 2010 D. 7. Moran MJ, Shapiro HN, Boettner DD, *Fundamentals of engineering thermodynamics*. .
- [109] A. Giuffrida, "Modelling the performance of a scroll expander for small organic Rankine cycles when changing the working fluid," *Appl. Therm. Eng.*, vol. 70, no. 1, pp. 1040–1049, 2014.
- [110] P. Bombarda, C. Invernizzi, and M. Gaia, "Performance Analysis of OTEC Plants With Multilevel Organic Rankine Cycle and Solar Hybridization," *J. Eng. Gas Turbines Power*, vol. 135, no. 4, p. 042302, 2013.
- [111] S. Quoilin, M. Van Den Broek, S. Declaye, P. Dewallef, and V. Lemort, "Techno-economic survey of organic rankine cycle (ORC) systems," *Renew. Sustain. Energy Rev.*, vol. 22, pp. 168–186, 2013.
- [112] D. P. M. O. R. cycle as efficient alternative to steam cycle for small scale power generation. H. 2011. 2011 J. 11. Vankeirsbilck I, Vanslambrouck B, Gusev S, "Organic Rankine cycle as efficient alternative to steam cycle for small scale power generation."
- [113] B. F. Tchanche, G. Lambrinos, A. Frangoudakis, and G. Papadakis, "Low-grade heat conversion into power using organic Rankine cycles - A review of various applications," *Renew. Sustain. Energy Rev.*, vol. 15, no. 8, pp. 3963–3979, 2011.
- [114] U. D. of E. 2008. BCS I. Waste heat recovery: technology and opportunities in US Industry. Industrial technologies program, "Waste heat recovery: technology and opportunities."
- [115] 1997. 105. United Nations Environment Program (UNEP), Montreal Protocol on Substances that Deplete the Ozone Layer, Final Act, United Nations, New York, "Montreal Protocol on Substances that Deplete the Ozone Layer."
- [116] G. D. Hayman and R. G. Derwent, "Atmospheric chemical reactivity and ozone-forming potentials of potential CFC replacements," *Environ. Sci. Technol.*, vol. 31, no. 2, pp. 327–336, 1997.
- [117] J. Sarkar and S. Bhattacharyya, "Application of graphene and graphene-based materials in clean energy-related devices Minghui," *Arch. Thermodyn.*, vol. 33, no. 4, pp. 23–40, 2012.
- [118] W. T. Tsai, H. P. Chen, and W. Y. Hsien, "A review of uses, environmental hazards and recovery/recycle technologies of perfluorocarbons (PFCs) emissions from the semiconductor manufacturing processes," *J. Loss Prev. Process Ind.*, vol. 15, no. 2, pp. 65–75, 2002.

- [119] S. K. . Hung, T.C.; Shai, T.Y.; Wang, "A review of organic Rankine cycles (ORCs) for the recovery of low-grade waste heat: Hung, T.C.; Shai, T.Y.; Wang, S.K. *Energy*, 1997, 22, (7), 661–667," *Fuel Energy Abstr.*, vol. 39, no. 2, pp. 151-, 1998.
- [120] K. Rahbar, S. Mahmoud, R. K. Al-Dadah, and N. Moazami, "Parametric analysis and optimization of a small-scale radial turbine for Organic Rankine Cycle," *Energy*, vol. 83, pp. 696–711, 2015.
- [121] B. T. Liu, K. H. Chien, and C. C. Wang, "Effect of working fluids on organic Rankine cycle for waste heat recovery," *Energy*, vol. 29, no. 8, pp. 1207–1217, 2004.
- [122] J. Bao and L. Zhao, "A review of working fluid and expander selections for organic Rankine cycle," *Renew. Sustain. Energy Rev.*, vol. 24, pp. 325–342, 2013.
- [123] B. F. Tchanche, G. Lambrinos, A. Frangoudakis, and G. Papadakis, "Low-grade heat conversion into power using organic Rankine cycles - A review of various applications," *Renew. Sustain. Energy Rev.*, vol. 15, no. 8, pp. 3963–3979, 2011.
- [124] A. Energy, M. Engineering, B. Mk, G. Britain, and W. Rankine-cycle, "Q oNo ," *Appl. Energy*, vol. 21, pp. 1–42, 1985.
- [125] A. Schuster, S. Karellas, E. Kakaras, and H. Spliethoff, "Energetic and economic investigation of Organic Rankine Cycle applications," *Appl. Therm. Eng.*, vol. 29, no. 8–9, pp. 1809–1817, 2009.
- [126] R. Rayegan and Y. X. Tao, "A procedure to select working fluids for Solar Organic Rankine Cycles (ORCs)," *Renew. Energy*, vol. 36, no. 2, pp. 659–670, 2011.
- [127] S. Quoilin, S. Declaye, B. F. Tchanche, and V. Lemort, "Thermo-economic optimization of waste heat recovery Organic Rankine Cycles," *Appl. Therm. Eng.*, vol. 31, no. 14–15, pp. 2885–2893, 2011.
- [128] B. F. Tchanche, M. Pétrissans, and G. Papadakis, "Heat resources and organic Rankine cycle machines," *Renew. Sustain. Energy Rev.*, vol. 39, pp. 1185–1199, 2014.
- [129] A. Zourellis, B. Perers, J. Donneborg, and J. Matoricz, "Optimizing Efficiency of Biomass - Fired Organic Rankine Cycle with Concentrated Solar Power in Denmark," *Energy Procedia*, vol. 149, pp. 420–426, 2018.
- [130] S. Karellas and K. Braimakis, "Energy-exergy analysis and economic investigation of a cogeneration and trigeneration ORC-VCC hybrid system utilizing biomass fuel and solar power," *Energy Convers. Manag.*, vol. 107, pp. 103–113, 2016.
- [131] B. Patel, N. B. Desai, and S. S. Kachhwaha, "Thermo-economic analysis of solar-biomass organic Rankine cycle powered cascaded vapor compression-absorption system," *Sol. Energy*, vol. 157, no. March, pp. 920–933, 2017.
- [132] C. Yue, B. Zhu, and B. Wang, "Thermodynamic analysis for the closed solar biomass drying system

- with a bottom ORC heat recovery,” *Energy Procedia*, vol. 142, pp. 117–124, 2017.
- [133] A. M. Pantaleo, S. M. Camporeale, A. Sorrentino, A. Miliozzi, N. Shah, and C. N. Markides, “Solar/biomass hybrid cycles with thermal storage and bottoming ORC: System integration and economic analysis,” *Energy Procedia*, vol. 129, no. 0, pp. 724–731, 2017.
- [134] A. M. Pantaleo, S. M. Camporeale, A. Miliozzi, V. Russo, N. Shah, and C. N. Markides, “Novel hybrid CSP-biomass CHP for flexible generation : Thermo-economic analysis and profitability assessment,” *Appl. Energy*, vol. 204, pp. 994–1006, 2017.
- [135] E. A. Bui *et al.*, “Parametric multi-objective optimization of an Organic Rankine Cycle with thermal energy storage for distributed generation,” *Energy Procedia*, vol. 126, pp. 429–436, 2017.
- [136] A. M. Pantaleo *et al.*, “Hybrid solar-biomass combined Brayton / organic Rankine-cycle plants integrated with thermal storage : Techno-economic feasibility in selected Mediterranean areas,” *Renew. Energy*, vol. 147, pp. 2913–2931, 2020.
- [137] E. Bellos, L. Vellios, I. C. Theodosiou, and C. Tzivanidis, “Investigation of a solar-biomass polygeneration system,” *Energy Convers. Manag.*, vol. 173, no. August, pp. 283–295, 2018.
- [138] P. Morrone, A. Algieri, and T. Castiglione, “Hybridisation of biomass and concentrated solar power systems in transcritical organic Rankine cycles: A micro combined heat and power application,” *Energy Convers. Manag.*, vol. 180, no. July 2018, pp. 757–768, 2019.
- [139] J. Soares and A. C. Oliveira, “Numerical simulation of a hybrid concentrated solar power / biomass mini power plant,” vol. 111, pp. 1378–1386, 2017.
- [140] A. M. Delgado-Torres and L. García-Rodríguez, “Preliminary assessment of solar organic Rankine cycles for driving a desalination system,” *Desalination*, vol. 216, no. 1–3, pp. 252–275, 2007.
- [141] A. M. Delgado-Torres and L. García-Rodríguez, “Comparison of solar technologies for driving a desalination system by means of an organic Rankine cycle,” *Desalination*, vol. 216, no. 1–3, pp. 276–291, 2007.
- [142] A. M. Delgado-Torres, L. García-Rodríguez, and V. J. Romero-Ternero, “Preliminary design of a solar thermal-powered seawater reverse osmosis system,” *Desalination*, vol. 216, no. 1–3, pp. 292–305, 2007.
- [143] J. C. Bruno, J. López-Villada, E. Letelier, S. Romera, and A. Coronas, “Modelling and optimisation of solar organic rankine cycle engines for reverse osmosis desalination,” *Appl. Therm. Eng.*, vol. 28, no. 17–18, pp. 2212–2226, 2008.
- [144] A. S. Nafey and M. A. Sharaf, “Combined solar organic Rankine cycle with reverse osmosis desalination process : Energy , exergy , and cost evaluations,” *Renew. Energy*, vol. 35, no. 11, pp.

2571–2580, 2010.

- [145] M. Borunda, O. A. Jaramillo, R. Dorantes, and A. Reyes, "Organic Rankine Cycle coupling with a Parabolic Trough Solar Power Plant for cogeneration and industrial processes," *Renew. Energy*, vol. 86, pp. 651–663, 2016.
- [146] A. H. Mosaffa, Z. Ghaffarpour, and L. Garousi Farshi, "Thermoeconomic assessment of a novel integrated CHP system incorporating solar energy based biogas-steam reformer with methanol and hydrogen production," *Sol. Energy*, vol. 178, no. September 2018, pp. 1–16, 2019.
- [147] A. M. Pantaleo *et al.*, "Thermo-economic Assessment of an Externally Fired Hybrid CSP/biomass Gas Turbine and Organic Rankine Combined Cycle," *Energy Procedia*, vol. 105, pp. 174–181, 2017.
- [148] J. Freeman, K. Hellgardt, and C. N. Markides, "An assessment of solar-powered organic Rankine cycle systems for combined heating and power in UK domestic applications," *Appl. Energy*, vol. 138, pp. 605–620, 2015.
- [149] M. Rady, A. Amin, and M. Ahmed, "Conceptual design of small scale multi-generation concentrated solar plant for a medical center in Egypt," *Energy Procedia*, vol. 83, pp. 289–298, 2015.
- [150] M. Ibarra, A. Rovira, D. C. Alarcón-Padilla, G. Zaragoza, and J. Blanco, "Performance of a 5 kWe solar-only organic Rankine unit coupled to a reverse osmosis plant," *Energy Procedia*, vol. 49, pp. 2251–2260, 2014.
- [151] D. J. Sargent, "Comparison of artificial neural networks with other statistical approaches: Results from medical data sets," *Cancer*, vol. 91, no. 8 SUPPL., pp. 1636–1642, 2001.
- [152] R. Siddaiah and R. P. Saini, "A review on planning, configurations, modeling and optimization techniques of hybrid renewable energy systems for off grid applications," *Renew. Sustain. Energy Rev.*, vol. 58, pp. 376–396, 2016.
- [153] C. Ter Chang, "Multi-choice goal programming model for the optimal location of renewable energy facilities," *Renew. Sustain. Energy Rev.*, vol. 41, pp. 379–389, 2015.
- [154] B. Das and A. Kumar, "A NLP approach to optimally size an energy storage system for proper utilization of renewable energy sources," *Procedia Comput. Sci.*, vol. 125, pp. 483–491, 2018.
- [155] M. Vaccari, G. M. Mancuso, J. Riccardi, M. Cantù, and G. Pannocchia, "A Sequential Linear Programming algorithm for economic optimization of Hybrid Renewable Energy Systems," *J. Process Control*, vol. 74, pp. 189–201, 2019.
- [156] N. Wu and H. Wang, "Deep learning adaptive dynamic programming for real time energy management and control strategy of micro-grid," *J. Clean. Prod.*, vol. 204, pp. 1169–1177, 2018.
- [157] R. Wang, G. Li, M. Ming, G. Wu, and L. Wang, "An efficient multi-objective model and algorithm for

- sizing a stand-alone hybrid renewable energy system,” *Energy*, vol. 141, pp. 2288–2299, 2017.
- [158] L. Moretti, M. Astolfi, C. Vergara, E. Macchi, J. I. Pérez-Arriaga, and G. Manzolini, “A design and dispatch optimization algorithm based on mixed integer linear programming for rural electrification,” *Appl. Energy*, vol. 233–234, no. June 2018, pp. 1104–1121, 2019.
- [159] A. Kamjoo, A. Maheri, A. M. Dizqah, and G. A. Putrus, “Multi-objective design under uncertainties of hybrid renewable energy system using NSGA-II and chance constrained programming,” *Int. J. Electr. Power Energy Syst.*, vol. 74, pp. 187–194, 2016.
- [160] W. Zhang, A. Maleki, M. A. Rosen, and J. Liu, “Sizing a stand-alone solar-wind-hydrogen energy system using weather forecasting and a hybrid search optimization algorithm,” *Energy Convers. Manag.*, vol. 180, no. November 2018, pp. 609–621, 2019.
- [161] A. Giallanza, M. Porretto, G. L. Puma, and G. Marannano, “A sizing approach for stand-alone hybrid photovoltaic-wind-battery systems: A Sicilian case study,” *J. Clean. Prod.*, vol. 199, pp. 817–830, 2018.
- [162] A. Askarzadeh and L. dos Santos Coelho, “A novel framework for optimization of a grid independent hybrid renewable energy system: A case study of Iran,” *Sol. Energy*, vol. 112, pp. 383–396, 2015.
- [163] A. Madhlopa, D. Sparks, S. Keen, M. Moorlach, P. Krog, and T. Dlamini, “Optimization of a PV-wind hybrid system under limited water resources,” *Renew. Sustain. Energy Rev.*, vol. 47, pp. 324–331, 2015.
- [164] C. E. C. Nogueira *et al.*, “Sizing and simulation of a photovoltaic-wind energy system using batteries, applied for a small rural property located in the south of Brazil,” *Renew. Sustain. Energy Rev.*, vol. 29, pp. 151–157, 2014.
- [165] A. R. Starke, J. M. Cardemil, R. Escobar, and S. Colle, “Multi-objective optimization of hybrid CSP+PV system using genetic algorithm,” *Energy*, vol. 147, pp. 490–503, 2018.
- [166] G. Zhang, B. Wu, A. Maleki, and W. Zhang, “Simulated annealing-chaotic search algorithm based optimization of reverse osmosis hybrid desalination system driven by wind and solar energies,” *Sol. Energy*, vol. 173, no. April, pp. 964–975, 2018.
- [167] W. Zhang, A. Maleki, M. A. Rosen, and J. Liu, “Optimization with a simulated annealing algorithm of a hybrid system for renewable energy including battery and hydrogen storage,” *Energy*, vol. 163, pp. 191–207, 2018.
- [168] N. Ghorbani, A. Kasaeian, A. Toopshekan, L. Bahrami, and A. Maghami, “Optimizing a hybrid wind-PV-battery system using GA-PSO and MOPSO for reducing cost and increasing reliability,” *Energy*, vol. 154, pp. 581–591, 2018.

- [169] S. Sanajaoba and E. Fernandez, "Maiden application of Cuckoo Search algorithm for optimal sizing of a remote hybrid renewable energy System," *Renew. Energy*, vol. 96, pp. 1–10, 2016.
- [170] A. Maleki and A. Askarzadeh, "Artificial bee swarm optimization for optimum sizing of a stand-alone PV/WT/FC hybrid system considering LPSP concept," *Sol. Energy*, vol. 107, pp. 227–235, 2014.
- [171] K. H. Chang and G. Lin, "Optimal design of hybrid renewable energy systems using simulation optimization," *Simul. Model. Pract. Theory*, vol. 52, pp. 40–51, 2015.
- [172] S. Rehman and M. Mohandes, "Artificial neural network estimation of global solar radiation using air temperature and relative humidity," *Energy Policy*, vol. 36, no. 2, pp. 571–576, 2008.
- [173] S. Kalogirou, S. Michaelides, and F. Tymvios, "Prediction of Maximum Solar Radiation using Artificial Neural Networks," *World Renew. Energy Congr. VII (WREC 2002)*, no. Wrec, pp. 1–5, 2002.
- [174] H. A. Yavasoglu, Y. E. Tetik, and H. G. Ozcan, "Neural network-based energy management of multi-source (battery/UC/FC) powered electric vehicle," *Int. J. Energy Res.*, vol. 44, no. 15, pp. 12416–12429, 2020.
- [175] K. S. Garud, S. Jayaraj, and M. Y. Lee, "A review on modeling of solar photovoltaic systems using artificial neural networks, fuzzy logic, genetic algorithm and hybrid models," *Int. J. Energy Res.*, vol. 45, no. 1, pp. 6–35, 2021.
- [176] Z. Guo, W. Zhao, H. Lu, and J. Wang, "Multi-step forecasting for wind speed using a modified EMD-based artificial neural network model," *Renew. Energy*, vol. 37, no. 1, pp. 241–249, 2012.
- [177] H. Salem, H. Pharma, E. Abdelhafez, M. A. Hamdan, E. Abdelhafez, and O. Ghnaimat, "Prediction of Hourly Solar Radiation in Amman Jordan by Using Artificial Neural Networks," *Int. J. Therm. Environ. Eng.*, vol. 14, no. 2, pp. 103–108, 2017.
- [178] A. Moghaddamnia, R. Remesan, M. H. Kashani, M. Mohammadi, D. Han, and J. Piri, "Comparison of LLR, MLP, Elman, NNARX and ANFIS Models-with a case study in solar radiation estimation," *J. Atmos. Solar-Terrestrial Phys.*, vol. 71, no. 8–9, pp. 975–982, 2009.
- [179] A. Sözen, T. Menlik, and S. Ünvar, "Determination of efficiency of flat-plate solar collectors using neural network approach," *Expert Syst. Appl.*, vol. 35, no. 4, pp. 1533–1539, 2008.
- [180] A. Sfetsos and A. H. Coonick, "Univariate and multivariate forecasting of hourly solar radiation with artificial intelligence techniques," *Sol. Energy*, vol. 68, no. 2, pp. 169–178, 2000.
- [181] M. Ozgoren, M. Bilgili, and B. Sahin, "Estimation of global solar radiation using ANN over Turkey," *Expert Syst. Appl.*, vol. 39, no. 5, pp. 5043–5051, 2012.
- [182] A. Rahimikhoob, "Estimating global solar radiation using artificial neural network and air temperature data in a semi-arid environment," *Renew. Energy*, vol. 35, no. 9, pp. 2131–2135, 2010.

- [183] L. T. Wong and W. K. Chow, "Solar radiation model," *Appl. Energy*, vol. 69, no. 3, pp. 191–224, 2001.
- [184] D. R. Myers, "Solar radiation modeling and measurements for renewable energy applications: data and model quality," *Energy*, vol. 30, no. 9, pp. 1517–1531, 2005.
- [185] S. Bhardwaj *et al.*, "Estimation of solar radiation using a combination of Hidden Markov Model and generalized Fuzzy model," *Sol. Energy*, vol. 93, pp. 43–54, 2013.
- [186] S. A. Kalogirou, "Artificial neural networks in renewable energy systems applications: A review," *Renew. Sustain. Energy Rev.*, vol. 5, no. 4, pp. 373–401, 2000.
- [187] A. Mellit, S. A. Kalogirou, L. Hontoria, and S. Shaari, "Artificial intelligence techniques for sizing photovoltaic systems: A review," *Renew. Sustain. Energy Rev.*, vol. 13, no. 2, pp. 406–419, 2009.
- [188] A. Mellit and A. M. Pavan, "A 24-h forecast of solar irradiance using artificial neural network: Application for performance prediction of a grid-connected PV plant at Trieste, Italy," *Sol. Energy*, vol. 84, no. 5, pp. 807–821, 2010.
- [189] Z. Wang, F. Wang, and S. Su, "Solar irradiance short-term prediction model based on BP neural network," *Energy Procedia*, vol. 12, pp. 488–494, 2011.
- [190] S. Alam, S. C. Kaushik, and S. N. Garg, "Assessment of diffuse solar energy under general sky condition using artificial neural network," *Appl. Energy*, vol. 86, no. 4, pp. 554–564, 2009.
- [191] G. López, F. J. Batlles, and J. Tovar-Pescador, "Selection of input parameters to model direct solar irradiance by using artificial neural networks," *Energy*, vol. 30, no. 9 SPEC. ISS., pp. 1675–1684, 2005.
- [192] J. L. Bosch, G. López, and F. J. Batlles, "Daily solar irradiation estimation over a mountainous area using artificial neural networks," *Renew. Energy*, vol. 33, no. 7, pp. 1622–1628, 2008.
- [193] C. S. Yang X-y, Xiao Y, "Wind speed and generated power forecasting in wind farm.," *Proc. CSEE*, no. 25(11), pp. 1–5, 2005.
- [194] F. Alharbi and D. Csala, "Saudi Arabia's solar and wind energy penetration: Future performance and requirements," *Energies*, vol. 13, no. 3, 2020.
- [195] M. Marciukaitis, V. Katinas, and A. Kavaliauskas, "Wind power usage and prediction prospects in Lithuania," *Renew. Sustain. Energy Rev.*, vol. 12, no. 1, pp. 265–277, 2008.
- [196] M. A. Mohandes and S. Rehman, "A NEURAL NETWORKS APPROACH FOR WIND SPEED PREDICTION," pp. 345–354, 1998.
- [197] P. Flores, A. Tapia, and G. Tapia, "Application of a control algorithm for wind speed prediction and active power generation," *Renew. Energy*, vol. 30, no. 4, pp. 523–536, 2005.
- [198] W. Mandal, Paras, Zareipour, Hamidreza, D. Rosehart, "Forecasting aggregated wind power

- production of multiple wind farms using hybrid wavelet-PSO-NNs," *Int. J. Energy Res.*, vol. 38, pp. 1654–1666, 2014.
- [199] M. Carolin Mabel and E. Fernandez, "Analysis of wind power generation and prediction using ANN: A case study," *Renew. Energy*, vol. 33, no. 5, pp. 986–992, 2008.
- [200] S. Li, "Wind Power Prediction Using Recurrent Multilayer Perceptron Neural Networks," in *2003 IEEE Power Engineering Society General Meeting, Conference Proceedings*, 2003, vol. 4, pp. 2325–2330.
- [201] T. G. Barbounis and J. B. Theocharis, "Locally recurrent neural networks for long-term wind speed and power prediction," *Neurocomputing*, vol. 69, no. 4–6, pp. 466–496, 2006.
- [202] G. H. Riahy and M. Abedi, "Short term wind speed forecasting for wind turbine applications using linear prediction method," *Renew. Energy*, vol. 33, no. 1, pp. 35–41, 2008.
- [203] S. Yayla and E. Harmanci, "Estimation of target station data using satellite data and deep learning algorithms," *Int. J. Energy Res.*, vol. 45, no. 1, pp. 961–974, 2021.
- [204] P. A. Adedeji, S. A. Akinlabi, N. Madushele, and O. O. Olatunji, "Hybrid neurofuzzy wind power forecast and wind turbine location for embedded generation," *Int. J. Energy Res.*, vol. 45, no. 1, pp. 413–428, 2021.
- [205] A. Gastli and Y. Charabi, "Solar electricity prospects in Oman using GIS-based solar radiation maps," *Renew. Sustain. Energy Rev.*, vol. 14, no. 2, pp. 790–797, 2010.
- [206] O. A. Marzouk *et al.*, "Proposed 2MW Wind Turbine for Use in the Governorate of Dhofar at the Sultanate of Oman To cite this article :," vol. 7, no. 2, pp. 20–28, 2019.
- [207] "Rural Area Electricity Company. 2017. 'Rural Area Electricity Company (RAECO)'. Sultanate of Oman. Annual Report 2017."
- [208] E. Coyle, "A case study of the Omani electricity network and readiness for solar energy integration," vol. 5, no. 1, pp. 0–8, 2017.
- [209] "Climatestotravel.com. 2020. Oman Climate: Average Weather, Temperature, Precipitation, Best Time. [online] Available at: <<https://www.climatestotravel.com/climate/oman>> [Accessed 17 April 2020]."
- [210] E. S. Hrayshat, "Off-grid hybrid wind – diesel power plant for application in remote Jordanian settlements," pp. 425–436, 2009.
- [211] E. Cadenas and W. Rivera, "Short term wind speed forecasting in La Venta , Oaxaca , Me using artificial neural networks," vol. 34, pp. 274–278, 2009.
- [212] X. Xue, "Prediction of daily diffuse solar radiation using artificial neural networks," *Int. J. Hydrogen*

Energy, vol. 42, no. 47, pp. 28214–28221, 2017.

- [213] A. K. Yadav and S. S. Chandel, “Solar radiation prediction using Artificial Neural Network techniques: A review,” *Renew. Sustain. Energy Rev.*, vol. 33, pp. 772–781, 2014.
- [214] P. Ramasamy, S. S. Chandel, and A. K. Yadav, “Wind speed prediction in the mountainous region of India using an artificial neural network model,” *Renew. Energy*, vol. 80, no. March 2014, pp. 338–347, 2015.
- [215] A. Omar, A. Nashed, Q. Li, G. Leslie, and R. A. Taylor, “Pathways for integrated concentrated solar power - Desalination : A critical review,” *Renew. Sustain. Energy Rev.*, vol. 119, no. May 2019, p. 109609, 2020.
- [216] M. F. A. Goosen, H. Mahmoudi, and N. Ghaffour, “Today ’ s and future challenges in applications of renewable energy technologies for desalination Critical Reviews in Environmental Science and Technology Today ’ s and Future Challenges in Applications of Renewable Energy Technologies for Desalination,” no. August 2013, 2020.
- [217] A. Alkudhiri, N. Darwish, and N. Hilal, “Membrane distillation : A comprehensive review,” *DES*, vol. 287, pp. 2–18, 2012.
- [218] T. Sachdev, V. Kumar, and A. Kr, “Solar desalination system integrated to use waste heat of air conditioners for continuous output : suitable for coastal areas,” vol. 174, pp. 1–10, 2020.
- [219] E. Guillén-burrieza *et al.*, “Experimental analysis of an air gap membrane distillation solar desalination pilot system,” vol. 379, pp. 386–396, 2011.
- [220] T. Chen and C. Ho, “Immediate assisted solar direct contact membrane distillation in saline water desalination,” *J. Memb. Sci.*, vol. 358, no. 1–2, pp. 122–130, 2010.
- [221] F. Banat, N. Jwaied, M. Rommel, and J. Koschikowski, “Performance evaluation of the ‘ large SMADES ’ autonomous desalination solar-driven membrane distillation plant in Aqaba , Jordan,” vol. 217, pp. 17–28, 2007.
- [222] J. Lee, W. Kim, J. Choi, N. Gha, and Y. Kim, “Dynamic solar-powered multi-stage direct contact membrane distillation system : Concept design , modeling and simulation,” vol. 435, no. April 2017, pp. 278–292, 2018.
- [223] G. Li and L. Lu, “Modeling and performance analysis of a fully solar-powered stand-alone sweeping gas membrane distillation desalination system for island and coastal households,” *Energy Convers. Manag.*, vol. 205, no. July 2019, p. 112375, 2020.
- [224] S. T. Bouguecha, S. E. Aly, M. H. Al-beirutty, M. M. Hamdi, and A. Boubakri, “Solar driven DCMD : Performance evaluation and thermal energy efficiency Chemical Engineering Research and Design

- Solar driven DCMD : Performance evaluation and," *Chem. Eng. Res. Des.*, vol. 100, no. May, pp. 331–340, 2015.
- [225] L. Zhang and G. Li, "Energy and economic analysis of a hollow fiber membrane-based desalination system driven by solar energy," *DES*, vol. 404, pp. 200–214, 2017.
- [226] S. Pramanik and R. V Ravikrishna, "A review of concentrated solar power hybrid technologies," *Appl. Therm. Eng.*, vol. 127, pp. 602–637, 2017.
- [227] M. Petrollese and D. Cocco, "Techno-economic assessment of hybrid CSP-biogas power plants," *Renew. Energy*, vol. 155, pp. 420–431, 2020.
- [228] G. Zhang, Y. Li, Y. J. Dai, and R. Z. Wang, "Design and analysis of a biogas production system utilizing residual energy for a hybrid CSP and biogas power plant," vol. 109, pp. 423–431, 2016.
- [229] R. Sterrer, S. Schidler, O. Schwandt, P. Franz, and A. Hammerschmid, "Theoretical analysis of the combination of CSP with a biomass CHP-plant using ORC-technology in Central Europe," *Energy Procedia*, vol. 49, pp. 1218–1227, 2014.
- [230] N. S. Suresh, N. C. Thirumalai, and S. Dasappa, "Modeling and analysis of solar thermal and biomass hybrid power plants," *Appl. Therm. Eng.*, vol. 160, no. July, p. 114121, 2019.
- [231] P. Morrone, A. Algieri, and T. Castiglione, "Hybridisation of biomass and concentrated solar power systems in transcritical organic Rankine cycles : A micro combined heat and power application," *Energy Convers. Manag.*, vol. 180, no. July 2018, pp. 757–768, 2019.
- [232] SEPCO, "SEPCO Annual Report 2012," p. 64, 2012.
- [233] T. S. website. [Online]. A. [Http://www.solargis.com](http://www.solargis.com), "www.solargis.com," p. 45354766, 2019.
- [234] H. Price *et al.*, "Advances in parabolic trough solar power technology," *J. Sol. Energy Eng. Trans. ASME*, vol. 124, no. 2, pp. 109–125, 2002.
- [235] M. A. Sharaf Eldean and H. E. Fath, "Exergy and thermo-economic analysis of solar thermal cycles powered multi-stage flash desalination process," *Desalin. Water Treat.*, vol. 51, no. 40–42, pp. 7361–7378, 2013.
- [236] H. Auracher, "Thermal design and optimization: Adrian Bejan, George Tsatsaronis and Michael Moran John Wiley & Sons, Inc. (1996) 542 pp., \$64.95, ISBN 0-471-58467-3," *Int. J. Refrig.*, vol. 19, no. 7, p. 482, 1996.
- [237] E. H. El-Dessouky HT, "Fundamentals of Salt Water Desalination," *Fundamentals of Salt Water Desalination*. 2002.
- [238] M. A. Sharaf, A. S. Nafey, and L. García-Rodríguez, "Exergy and thermo-economic analyses of a combined solar organic cycle with multi effect distillation (MED) desalination process,"

Desalination, vol. 272, no. 1–3, pp. 135–147, 2011.

- [239] V. T. Shahu and S. B. Thombre, “Air gap membrane distillation: A review,” *J. Renew. Sustain. Energy*, vol. 11, no. 4, 2019.
- [240] H. Guo, H. M. Ali, and A. Hassanzadeh, “Simulation study of flat-sheet air gap membrane distillation modules coupled with an evaporative crystallizer for zero liquid discharge water desalination,” *Appl. Therm. Eng.*, vol. 108, pp. 486–501, 2016.
- [241] A. T. Servi *et al.*, “A systematic study of the impact of hydrophobicity on the wetting of MD membranes,” *J. Memb. Sci.*, vol. 520, pp. 850–859, 2016.
- [242] R. S and Z. H, “Modelisation of Membrane Distillation: Mass and Heat Transfer in Air Gap Membrane Distillation,” *J. Membr. Sci. Technol.*, vol. 6, no. 2, 2016.
- [243] D. Winter *et al.*, “Comparative analysis of full-scale membrane distillation contactors - methods and modules,” *J. Memb. Sci.*, vol. 524, no. December 2016, pp. 758–771, 2017.
- [244] A. Criscuoli and E. Drioli, “Energetic and exergetic analysis of an integrated membrane desalination system,” *Desalination*, vol. 124, no. 1–3, pp. 243–249, 1999.
- [245] E. Drioli, E. Curcio, G. Di Profio, F. Macedonio, and A. Criscuoli, “Integrating membrane contactors technology and pressure-driven membrane operations for seawater desalination: Energy, exergy and costs analysis,” *Chem. Eng. Res. Des.*, vol. 84, no. 3 A, pp. 209–220, 2006.
- [246] F. Macedonio and E. Drioli, “An exergetic analysis of a membrane desalination system,” *Desalination*, vol. 261, no. 3, pp. 293–299, 2010.
- [247] F. Banat and N. Jwaied, “Exergy analysis of desalination by solar-powered membrane distillation units,” vol. 230, pp. 27–40, 2008.
- [248] D. A. B. Karki and P. J. N. S. M. S. Bajgain, *As Renewable Source of Energy in Nepal*. 2005.
- [249] *Design of Biogas Plant, Bio-gas Project, LGED: Preparing this training material all the important information have been collected from the booklets & research materials of Biogas Training Center (BRC) Chendu, Sichuan, China.* .
- [250] A. M. Alklaibi and N. Lior, “pc,” vol. 171, pp. 111–131, 2004.
- [251] N. G. Voros, C. T. Kiranoudis, and Z. B. Maroulis, “Solar energy exploitation for reverse osmosis desalination plants,” vol. 115, pp. 83–101, 1998.
- [252] L. Jarrar, O. Ayadi, and J. Al Asfar, “Techno-economic Aspects of Electricity Generation from a Farm Based Biogas Plant,” pp. 476–492, 2020.
- [253] A. Marni Sandid, M. Bassyouni, D. Nehari, and Y. Elhenawy, “Experimental and simulation study of multichannel air gap membrane distillation process with two types of solar collectors,” *Energy*

Convers. Manag., vol. 243, p. 114431, 2021.

- [254] F. A. Banat and J. Simandl, "Desalination by Membrane Distillation: A Parametric Study," *Sep. Sci. Technol.*, vol. 33, no. 2, pp. 201–226, 1998.
- [255] M. C. García-Payo, M. A. Izquierdo-Gil, and C. Fernández-Pineda, "Air gap membrane distillation of aqueous alcohol solutions," *J. Memb. Sci.*, vol. 169, no. 1, pp. 61–80, 2000.
- [256] A. M. Soliman *et al.*, "A new system design of using solar dish-hydro combined with reverse osmosis for sewage water treatment: Case study Al-Marj, Libya," *Desalin. Water Treat.*, vol. 193, no. July, pp. 189–211, 2020.
- [257] M. A. Sharaf Eldean and A. M. Soliman, "A novel study of using oil refinery plants waste gases for thermal desalination and electric power generation: Energy, exergy & cost evaluations," *Appl. Energy*, vol. 195, pp. 453–477, 2017.
- [258] B. Shboul *et al.*, "A new ANN model for hourly solar radiation and wind speed prediction: A case study over the north & south of the Arabian Peninsula," *Sustain. Energy Technol. Assessments*, vol. 46, no. April, p. 101248, 2021.
- [259] I. AL-Arfi *et al.*, "Thermo-economic and design analysis of a solar thermal power combined with anaerobic biogas for the air gap membrane distillation process," *Energy Convers. Manag.*, vol. 257, no. November 2021, p. 115407, 2022.
- [260] K. Elsaid, E. Taha Sayed, B. A. A. Yousef, M. Kamal Hussien Rabaia, M. Ali Abdelkareem, and A. G. Olabi, "Recent progress on the utilization of waste heat for desalination: A review," *Energy Convers. Manag.*, vol. 221, no. July, p. 113105, 2020.
- [261] S. Mirjalili, S. Saremi, S. M. Mirjalili, and L. D. S. Coelho, "Multi-objective grey wolf optimizer: A novel algorithm for multi-criterion optimization," *Expert Syst. Appl.*, vol. 47, pp. 106–119, 2016.
- [262] L. G. Acuña, R. V. Padilla, and A. S. Mercado, "Measuring reliability of hybrid photovoltaic-wind energy systems: A new indicator," *Renew. Energy*, vol. 106, pp. 68–77, 2017.
- [263] Y. Yang, S. Guo, D. Liu, R. Li, and Y. Chu, "Operation optimization strategy for wind-concentrated solar power hybrid power generation system," *Energy Convers. Manag.*, vol. 160, no. December 2017, pp. 243–250, 2018.
- [264] Z. Ding, H. Hou, G. Yu, E. Hu, L. Duan, and J. Zhao, "Performance analysis of a wind-solar hybrid power generation system," *Energy Convers. Manag.*, vol. 181, no. November 2018, pp. 223–234, 2019.
- [265] E. Keyif, M. Hornung, and W. Zhu, "Optimal configurations and operations of concentrating solar power plants under new market trends," *Appl. Energy*, vol. 270, no. May, p. 115080, 2020.

- [266] J. Guo and X. Huai, "Multi-parameter optimization design of parabolic trough solar receiver," *Appl. Therm. Eng.*, vol. 98, pp. 73–79, 2016.
- [267] S. Toghyani, E. Baniasadi, and E. Afshari, "Thermodynamic analysis and optimization of an integrated Rankine power cycle and nano-fluid based parabolic trough solar collector," *Energy Convers. Manag.*, vol. 121, pp. 93–104, 2016.
- [268] S. Rajanna and R. P. Saini, "Optimal modeling of solar/biogas/biomass based IRE system for a remote area electrification," pp. 1–5, 2015.
- [269] A. Chauhan and R. P. Saini, "Discrete harmony search based size optimization of Integrated Renewable Energy System for remote rural areas of Uttarakhand state in India," *Renew. Energy*, vol. 94, pp. 587–604, 2016.
- [270] A. Chauhan and R. P. Saini, "Techno-economic optimization based approach for energy management of a stand-alone integrated renewable energy system for remote areas of India," *Energy*, vol. 94, pp. 138–156, 2016.
- [271] L. Olatomiwa, S. Mekhilef, A. S. N. Huda, and K. Sanusi, "Techno-economic analysis of hybrid PV–diesel–battery and PV–wind–diesel–battery power systems for mobile BTS: The way forward for rural development," *Energy Sci. Eng.*, vol. 3, no. 4, pp. 271–285, 2015.
- [272] L. Olatomiwa, R. Blanchard, S. Mekhilef, and D. Akinyele, "Hybrid renewable energy supply for rural healthcare facilities: An approach to quality healthcare delivery," *Sustain. Energy Technol. Assessments*, vol. 30, no. February, pp. 121–138, 2018.
- [273] M. A. Mohamed, A. M. Eltamaly, and A. I. Alolah, "PSO-based smart grid application for sizing and optimization of hybrid renewable energy systems," *PLoS One*, vol. 11, no. 8, pp. 1–22, 2016.
- [274] M. Colakoglu and A. Durmayaz, "Energy, exergy and environmental-based design and multiobjective optimization of a novel solar-driven multi-generation system," *Energy Convers. Manag.*, vol. 227, no. July 2020, p. 113603, 2021.
- [275] K. Wang, M. J. Li, J. Q. Guo, P. Li, and Z. Bin Liu, "A systematic comparison of different S-CO₂ Brayton cycle layouts based on multi-objective optimization for applications in solar power tower plants," *Appl. Energy*, vol. 212, no. December 2017, pp. 109–121, 2018.
- [276] R. Bravo, C. Ortiz, R. Chacartegui, and D. Friedrich, "Multi-objective optimisation and guidelines for the design of dispatchable hybrid solar power plants with thermochemical energy storage," *Appl. Energy*, vol. 282, no. PB, p. 116257, 2021.
- [277] H. Liu, R. Zhai, J. Fu, Y. Wang, and Y. Yang, "Optimization study of thermal-storage PV-CSP integrated system based on GA-PSO algorithm," *Sol. Energy*, vol. 184, no. December 2018, pp. 391–409, 2019.

- [278] Y. Cao, H. A. Dhahad, H. Togun, A. E. Anqi, N. Farouk, and B. Farhang, "A novel hybrid biomass-solar driven triple combined power cycle integrated with hydrogen production: Multi-objective optimization based on power cost and CO₂ emission," *Energy Convers. Manag.*, vol. 234, no. February, p. 113910, 2021.
- [279] J. Mahmoudimehr and P. Sebghati, "A novel multi-objective Dynamic Programming optimization method: Performance management of a solar thermal power plant as a case study," *Energy*, vol. 168, pp. 796–814, 2019.
- [280] I. Siksnelyte, E. K. Zavadskas, D. Streimikiene, and D. Sharma, "An overview of multi-criteria decision-making methods in dealing with sustainable energy development issues," *Energies*, vol. 11, no. 10, 2018.
- [281] A. Kumar *et al.*, "A review of multi criteria decision making (MCDM) towards sustainable renewable energy development," *Renew. Sustain. Energy Rev.*, vol. 69, no. June 2016, pp. 596–609, 2017.
- [282] T. L. Saaty, "Decision making — the Analytic Hierarchy and Network Processes (AHP/ANP)," *J. Syst. Sci. Syst. Eng.*, vol. 13, no. 1, pp. 1–35, 2004.
- [283] A. Ishizaka and A. Labib, "Analytic Hierarchy Process and Expert Choice: Benefits and limitations," *OR Insight*, vol. 22, no. 4, pp. 201–220, 2009.
- [284] Shahroodi Kambiz, A. Keramatpanah, S. Amini, E. Shiri, and . M. N., "Application of Analytical Hierarchy Process (AHP) Technique To Evaluate and Selecting Suppliers in an Effective Supply Chain," *Kuwait Chapter Arab. J. Bus. Manag. Rev.*, vol. 1, no. 8, pp. 1–14, 2012.
- [285] R. Wang, Z. Zhou, H. Ishibuchi, T. Liao, and T. Zhang, "Localized Weighted Sum Method for Many-Objective Optimization," *IEEE Trans. Evol. Comput.*, vol. 22, no. 1, pp. 3–18, 2018.
- [286] J.- August, I. No, S. K. Misra, and A. Ray, "Comparative Study on Different Multi-Criteria Decision Making Tools in Software project selection scenario," *Int. J. Adv. Res. Comput. Sci.*, vol. 3, no. 4, pp. 172–178, 2012.
- [287] D. Jato-Espino, E. Castillo-Lopez, J. Rodriguez-Hernandez, and J. C. Canteras-Jordana, "A review of application of multi-criteria decision making methods in construction," *Autom. Constr.*, vol. 45, pp. 151–162, 2014.
- [288] H. S. Shih, H. J. Shyr, and E. S. Lee, "An extension of TOPSIS for group decision making," *Math. Comput. Model.*, vol. 45, no. 7–8, pp. 801–813, 2007.
- [289] F. E. Boran, S. Genç, M. Kurt, and D. Akay, "A multi-criteria intuitionistic fuzzy group decision making for supplier selection with TOPSIS method," *Expert Syst. Appl.*, vol. 36, no. 8, pp. 11363–11368, 2009.

- [290] D. Diakoulaki, G. Mavrotas, and L. Papayannakis, "Determining objective weights in multiple criteria problems: The critic method," *Comput. Oper. Res.*, vol. 22, no. 7, pp. 763–770, 1995.
- [291] A. Tuş and E. Aytaç Adalı, "The new combination with CRITIC and WASPAS methods for the time and attendance software selection problem," *Opsearch*, vol. 56, no. 2, pp. 528–538, 2019.
- [292] K. Deb, A. Pratap, S. Agarwal, and T. Meyarivan, "A fast and elitist multiobjective genetic algorithm: NSGA-II," *IEEE Trans. Evol. Comput.*, vol. 6, no. 2, pp. 182–197, 2002.
- [293] G. R. Timilsina, L. Kurdgelashvili, and P. A. Narbel, "Solar energy: Markets, economics and policies," *Renew. Sustain. Energy Rev.*, vol. 16, no. 1, pp. 449–465, 2012.